# The role of African horse sickness virus non-structural protein NS4 in virulence and host immunity

**by**

**Gayle Victoria Wall**

Submitted in partial fulfilment of the requirements for the degree

***Philosophiae Doctor***

In the Faculty of Natural & Agricultural Sciences

University of Pretoria

Pretoria

January 2022

**DECLARATION**

I, Gayle Victoria Wall declare that the thesis, which I hereby submit for the degree *Philosophiae Doctor* at the University of Pretoria, is my own work and has not previously been submitted by me for a degree at this or any other tertiary institution.

SIGNATURE: 

DATE: 14 January 2022

**ACKNOWLEDGEMENTS**

I would like to express my sincere thanks to the following people and institutions:

My supervisor, Prof. Vida van Staden, thank you for the opportunity to do this study in your research group. Being your student has been an honour. Your encouragement, patience and kindness know no bounds and your unwavering belief in me has always inspired me to give my all.

My co-supervisor, Prof. Christiaan Potgieter, thank you for sharing your expertise with me. I have learnt so much from you during this study.

The University of Pretoria, the Poliomyelitis Research Foundation, the National Research Foundation, the Genomics Research Institute and Deltamune (Pty) Ltd for financial support.

Prof. Jacques Theron, thank you for your advice and for always taking a keen interest in my work.

Deltamune (Pty) Ltd, the Centre for High Performance Computing (Cape Town), the University of Pretoria's Laboratory for Microscopy and Microanalysis, Centre for Bioinformatics and Computational Biology, DNA Sanger sequencing facility, ACGT Microarray Facility and Ion Torrent Sequencing Facility for the use of their facilities.

Erna van Wilpe, thank you for assistance with confocal microscopy and Renate Zipfel, Gladys Shabangu and Dr Nicky Olivier for technical support and helpful advice. Arrie Klopper, Sandra van Wyngaardt and Ntutu Letseka for technical assistance.

Ying Li, Dr Noel Chen, Prof. Fourie Joubert, Alisa Postma, Dr Charles Hefer, Prof. Eshchar Mizrachi, Dr Erik Visser and Dr Lizahn Zwart for assisting me with the analysis of the transcriptome data.

All researchers and staff at Deltamune (Pty) Ltd, especially Isabel Wright, Dr Carin Barnardo, Jacky Welgemoed, Leoni Smit and Shirley Smith for assisting me with the embryonated chicken egg model and other experiments. Thank you too for your encouragement and continued interest in this study.

The students in Prof. Jacques Theron and Dr Pontsho Moela's research groups for your assistance in the lab.

Adrene Laubscher, for your encouragement and advice, and for all the laughs we have shared over a cup of coffee.

The students, past and present, of the Orbivirus Research Group, especially Dr Shareen Boughan, Dr Linda Ferreira-Venter, Litia Yssel and Ané Pieters, for assistance in the lab, and for the fun times on campus and at conferences. Shareen, your motivation and support during the last stretch in particular was much appreciated.

My dear friends and family, your endless patience, support, and encouragement has meant the world to me and has inspired me throughout this study. I would especially like to thank:
My grandmothers, Marjorie Howard and Erica Neilson, as well as my late grandfather Albert Neilson, for always asking how my work was progressing.
Estée, Pieter and Carissa Jansen van Rensburg, Leriché, Kobus, Lukke and Joa Lourens, and Daniell Humphries. Thank you for your constant love and moral support, and for always showing an interest in my work.
Jeanne-Marie Hickley, Lee-Ann Lamb, Johann de Beer, Tessa Rossi, Zelda van Heerden, Miné Pretorius, Dr Eudri Venter, Dr Letrisha Padayachee and Dr Shani Bekker. Johann, thanks also to you and Jason for helping me with anything laptop related. Shani, Eudri and Letrisha, thank you for the fruitful discussions we have had over the years, Eudri for your help with confocal microscopy and Letrisha, for your much appreciated assistance with the chicken embryos.

Chrizelda Humphries, I will be forever grateful to you for encouraging me on a daily basis, and for the kindness and love with which you welcomed me into your home and family.

Lastly, to my parents, Glynis Wall, and Grant Wall, thank you for affording me every opportunity throughout my life. Without that, and your belief in me, this would not have been possible. Thank you for your unconditional love, support, and patience. I am blessed to have you as my parents.

**RESEARCH OUTPUTS**

**1. Publication**

Wall, G.V., Wright, I.M., Barnardo, C., Erasmus, B.J., van Staden, V., Potgieter, A.C., 2021. African horse sickness virus NS4 protein is an important virulence factor and interferes with JAK-STAT signaling during viral infection. Virus Research 298, 198407. https://doi.org/10.1016/j.virusres.2021.198407

**2. International conferences**

Gayle Wall, Christiaan Potgieter, Fourie Joubert and Vida van Staden (2018) African horse sickness virus non-structural protein NS4 suppresses host innate immunity. 13th International dsRNA Virus Symposium, Houffalize, Belgium, 24 – 28 September 2018.
Shotgun presentation.

G.V. Wall, A.C. Potgieter, V. van Staden (2020) African horse sickness virus NS4 is an important virulence factor in horses and suppresses host innate immunity. International Veterinary Vaccinology Network Conference 2020, Hanoi, Vietnam, 16 – 18 March 2020.
Abstract accepted for poster presentation.
Conference cancelled due to COVID-19 pandemic.

**3. National conferences**

Gayle Wall, Christiaan Potgieter, Fourie Joubert and Vida van Staden (2017) African horse sickness virus non-structural protein NS4 suppresses host innate immunity. 2017 Genomics Research Institute (GRI) Symposium, University of Pretoria, South Africa, 10 November 2017.
Oral presentation.

Gayle Wall, Christiaan Potgieter, Fourie Joubert and Vida van Staden (2018) African horse sickness virus non-structural protein NS4 suppresses the host immune response. SASBi/SAGS 2018, Golden Gate Resort, Free State, South Africa, 16 – 18 October 2018.
Poster presentation.

G.V. Wall, A.C. Potgieter, V. van Staden (2019) AHSV non-structural protein NS4 interferes with JAK-STAT signaling and suppresses host innate immunity. Proceedings of the Microscopy Society of Southern Africa, Volume 48, page 7, ISSN 0250-0418 : ISBN 978-0-6398435-0-6.
Oral presentation.
Awarded The Scientific Group Award for Best Presentation: Confocal Microscopy.

S. Boughan, G.V. Wall, A.C. Potgieter, V. van Staden (2019) Colocalisation of African horse sickness virus non-structural protein NS4 with cellular and viral proteins. Proceedings of the Microscopy Society of Southern Africa, Volume 48, page 12, ISSN 0250-0418 : ISBN 978-0-6398435-0-6.

# SUMMARY

## The role of African horse sickness virus non-structural protein NS4 in virulence and host immunity

by

Gayle Victoria Wall

Supervisor: Prof. V van Staden
Department of Biochemistry, Genetics and Microbiology
University of Pretoria

Co-supervisor: Prof. A C Potgieter
Deltamune (Pty) Ltd, Moraine House – The Braes, 193 Bryanston Drive, Bryanston, Gauteng, 2191, South Africa
Department of Biochemistry, Focus Area for Human Metabolomics, North-West University, Potchefstroom, South Africa

For the degree *Philosophiae Doctor*

African horse sickness virus (AHSV) causes African horse sickness (AHS), a highly infectious vector-borne disease that impacts significantly on animal health. A live-attenuated vaccine is currently used to control AHS but has many associated risks and problems. Little is known about the function of the recently identified fourth AHSV non-structural protein, NS4. AHSV NS4 exists as one of three variants: NS4-I, NS4-II or NLS-NS4-II and whilst orbiviruses replicate exclusively in the cytoplasm, the NS4 proteins of AHSV and the related bluetongue virus (BTV) are nucleocytoplasmic and bind dsDNA. BTV NS4 is an interferon antagonist and virulence factor, and its early expression and localisation to the plasma membrane suggest possible roles in virus entry and/or exit. AHSV NS4 may have an analogous role to BTV NS4. This study aimed to investigate the role of AHSV NS4 in virus virulence and host immunity, to increase our understanding of the function of NS4.

The interaction (if any) of NS4 with mitochondria and other AHSV non-structural proteins associated with virus entry and exit was investigated. Overall, limited colocalisation with NS4 was observed at the perimeter of NS1 tubule bundles, NS2 viral inclusion bodies (VIBs) and perinuclear NS3. No NS4 was observed in the matrix of VIBs, and NS4 did not colocalise with NS3/A at the plasma membrane. Therefore, AHSV NS4 is unlikely to be involved in virus assembly or exit. Some limited colocalisation of NS4 was observed at the

perimeter of mitochondria clusters. Hence it is possible that NS4 associates with the outer mitochondrial membrane, perhaps interfering with RIG-I-like receptor signalling in innate immunity.

To further understand the role of NS4 in virus replication, virulence and pathogenesis, reverse genetics was used to generate AHSV NS4 knockout and reassortant viruses based on virulent AHSV5 (expressing NS4-II) and attenuated AHSV4LP (expressing NS4-I). *In vitro* assays showed the expression and intracellular localisation of NS4 is dependent on Seg-9, not the backbone into which it is incorporated. This segment encodes both VP6 and NS4, therefore this could be due to one, or both, of the proteins. It was also shown that NS4-II, and/or VP6 encoded by AHSV5 Seg-9 ($S9_5$), may give AHSV a replication advantage in BSR cells.

All reverse genetics-derived viruses were injected into embryonated chicken eggs (ECEs), and virulence and pathogenesis were compared to wild-type viruses. Viruses containing $S9_5$ (NS4-II) remained virulent whereas those lacking NS4 expression were attenuated, suggesting that NS4-II is a virulence factor in ECEs. Vaccine trials undertaken at Deltamune (Pty) Ltd established that rAHSV5 (NS4-II) was virulent in horses, and that the same virus with NS4 knocked out (rAHSV5minNS4) was attenuated. Comparing the transcriptional response in a subset of these horses suggested that the absence of NS4 allows the host to launch an earlier innate immune response. Further investigations indicated that the NS4 protein interfered with the nuclear accumulation of STAT1 during JAK-STAT signalling.

This study highlights the importance of AHSV NS4 in virulence, and suggests a mechanism of immune system evasion by AHSV.

# TABLE OF CONTENTS

# CHAPTER 1

## LITERATURE REVIEW

## 1.1. INTRODUCTION

African horse sickness virus (AHSV) causes African horse sickness (AHS), a highly infectious vector-borne and economically important viral disease of *Equidae.* The virus is endemic to sub-Saharan Africa and possibly even Yemen in the Arabian Peninsula, but has extended as far as India, Pakistan and in recent years Thailand and certain parts of Europe. The focus of this study was on AHSV NS4, the recently described fourth non-structural protein of AHSV and its role in the viral replication cycle and virus-host interactions. This literature review gives an overview of orbivirus disease and epidemiology, followed by a discussion of orbivirus molecular biology and the role of each protein in the replication cycle. The focus then shifts to both AHSV and bluetongue virus (BTV) NS4, followed by a discussion of host immunity and how viruses evade the host immune system.

## 1.2. ORBIVIRUS DISEASE AND EPIDEMIOLOGY

The arbovirus AHSV belongs to the *Orbivirus* genus (family *Reoviridae*) and is closely related to BTV, the orbivirus prototype species. To date, 9 serotypes of AHSV (Howell, 1962) and at least 27 serotypes of BTV (Zientara *et al.*, 2014; Maclachlan *et al.*, 2019) have been identified. Several new BTV types have been observed but have yet to be assigned a numerical serotype designation (Maclachlan *et al.*, 2019; Ries *et al.*, 2021). AHSV has a dual life cycle, infecting and replicating in both insect and mammalian cells. Zebras are considered the natural reservoir of the virus, while horses are most susceptible to the disease. As such they are the most severely affected and often exhibit a mortality rate of as high as 90% (Mellor and Hamblin, 2004). Upon infection of the mammalian host, AHSV multiplies in the lymph nodes prior to the dissemination of the virus throughout the body via the circulatory system. This is followed by infection of the target organs and cells (heart, lungs, spleen, lymphoid tissues and certain endothelial cells), in which secondary viraemia occurs (Mellor and Hamblin, 2004; Clift *et al.*, 2009; Clift and Penrith, 2010). Microvascular endothelial cells and monocyte-macrophages are the main target cells for virus replication (Clift and Penrith, 2010). There are four forms of the disease AHS, each ranging in severity (Erasmus, 1973). Horse sickness fever is the mildest form, with the pulmonary form causing the most deaths among infected animals with a mortality rate often exceeding 95% (Mellor and Hamblin, 2004). The other two forms are the mixed form and the cardiac/subacute form. As a result of the severity of AHS, the disease has joined bluetongue as an Office International des Epizooties (OIE)-listed disease (OIE, 2011).

Although the first reference to AHSV was made in 1327 and concerned an epidemic in Yemen at that time, the virus is thought to have originated in Africa (Mellor and Hamblin, 2004; Dennis *et al.*, 2019). The first major southern African outbreak of AHS occurred in 1719 and killed over 1 700 animals. Since then, several outbreaks of the disease have been reported in the region, with the outbreak of 1854-1855 being the most severe, killing some 70 000 horses, which at the time made up about 40% of the entire horse population of the Cape of Good Hope (Coetzer and Guthrie, 2004; Mellor and Hamblin, 2004; Zientara *et al.*, 2015;

Carpenter *et al.*, 2017). AHS is rarely found in the Western Cape with only four confirmed outbreaks of AHS occurring between 1950 and 2006 (in 1967, 1990, 1999 and 2004) (Venter *et al.*, 2006). Every summer South Africa sees outbreaks across the country, except in the AHS-free zone which was implemented in 1997. Outbreaks within this zone have occurred in 1999, 2004, 2011, 2013, 2014 and 2016 (Zientara *et al.*, 2015; Grewar *et al.*, 2019). The 1999 and 2004 outbreaks led to a two-year suspension on the export of horses costing the industry about R50 million (US$ 8.2 million) per annum (Venter *et al.*, 2006).

Serotypes 1 through 8 of AHSV are usually only found within regions of sub-Saharan Africa, whereas serotype 9 has been responsible for many of the outbreaks outside of the African continent (Hazrati, 1967; Zientara *et al.*, 2015; Carpenter *et al.*, 2017). The exceptions of this were the Spanish-Portuguese outbreaks of 1987-1990 which were due to serotype 4, as well as the occurrence of serotype 2 in Nigeria (2006, the first incidence of AHSV2 in the northern hemisphere), Ethiopia (2007) and Senegal (2007), serotype 6 in Ethiopia (2003) and serotype 7 in Senegal (2007) (Fasina *et al.*, 2008; Maclachlan and Guthrie, 2010; Zientara *et al.*, 2015). In 2020, the first incidence of AHSV1 outside of Africa caused an outbreak in Thailand, the first in South East Asia (King *et al.*, 2020; Lu *et al.*, 2020; Toh *et al.*, 2021).

Both AHSV and BTV are transmitted by certain species of the *Culicoides* biting midge, haematophagous insects that are potent vectors of arboviruses (Mellor *et al.*, 2000). The presence of competent vector species influences the geographical distribution and seasonal incidence of AHSV (Mellor *et al.*, 2000; Venter *et al.*, 2000). Thus, the epidemiology of *Culicoides*-borne viral diseases are strongly linked to the vast population sizes of *Culicoides*, their means of dispersal as well as altitude, climate and weather (Mellor *et al.*, 2000; Verhoef *et al.*, 2014). Two species of *Culicoides*, namely *C. imicola* and *C. bolitinos,* have been implicated in the transmission of both BTV and AHSV in southern Africa specifically (Mellor *et al.*, 2000; Venter *et al.*, 2000; Verhoef *et al.*, 2014), with *C. bolitinos* appearing to be the major vector in certain high-lying regions of South Africa (Meiswinkel *et al.*, 2000; Riddin *et al.*, 2019). The most important species worldwide however is *C. imicola,* an Afro-Asiatic midge that is the most widespread of the *Culicoides* species, stretching throughout Africa, South East Asia, the Middle East and certain parts of Europe (Mellor *et al.*, 2000; Mellor and Hamblin, 2004; Carpenter *et al.*, 2017).

The current northward expansion of *C. imicola* as well as the ability of AHSV to overwinter in southern Spain, Portugal and Morocco, and perhaps the Eastern Cape of South Africa, highlights the possibility of outbreaks of AHSV similar to those of BTV in recent years whereby at least eight serotypes of BTV spread across Europe (Mellor and Hamblin, 2004; Gould and Higgs, 2009; Maclachlan and Guthrie, 2010; Carpenter *et al.*, 2017; Riddin *et al.*, 2019). The emergence of several new BTV serotypes, as well as a serotype of the related epizootic haemorrhagic disease virus (EHDV) in certain parts of North and South America led to concerns over future and more extensive outbreaks of BTV in those areas (Gibbs *et al.*, 2008; Maclachlan and Guthrie,

2010). Novel BTV serotypes have also been found in Israel and Australia, and BTV8 emerged in Belgium, France, Luxembourg, Germany and the Netherlands (August 2006), and the United Kingdom (September 2007) and could be indicative of a changing epidemiology of the virus (Gibbs *et al.*, 2008; Gould and Higgs, 2009; Maclachlan and Guthrie, 2010). Rather than *C. imicola* or *C. bolitinos*, *C. pulicaris* and *C. obsoletus* were implicated in outbreaks of BTV in western Europe and Great Britain. Recent outbreaks of BTV have indicated that once these viruses reach North Africa they can spread readily throughout the Mediterranean basin (Maclachlan and Guthrie, 2010).

The increased incidence of both BTV and AHSV in recent years may in part be due to climate change (Mellor *et al.*, 2000) and international trade, with global warming extending the distribution of *C. imicola* extensively in Europe (Mellor *et al.*, 2000; Tabachnick and Day, 2013). This may be due to increased temperatures creating more favourable breeding grounds for arthropods such as the *Culicoides* species which is known to thrive in warmer, wet environments (Mellor and Hamblin, 2004). Although outbreaks of AHS occur every year in South Africa, major outbreaks tend to occur every 10-15 years and may coincide with the warm (El Niño) phase of the El Niño/Southern Oscillation (ENSO) (Carpenter *et al.*, 2017). The effect of climate change is however, a complicated one, as it will almost certainly continue to cause social and economic changes throughout the world which may in turn affect the transmission of insect-transmitted diseases (Maclachlan, 2010; Tabachnick and Day, 2013).

### 1.3. PREVENTION AND CONTROL MEASURES

There is no cure, nor is there a specific form of treatment for AHS, apart from rest, good husbandry and interventions targeting symptomatic relief (Mellor and Hamblin, 2004; Dennis *et al.*, 2019). Therefore, several control measures exist to try and prevent or reduce the incidence and spread of disease. Restricting the movement of equids prevents infected animals from initiating new sites of infection in areas that were previously infection-free (Mellor and Hamblin, 2004; Zientara *et al.*, 2015) and was employed by the government of Thailand to control the potential further spread of AHSV during the recent outbreak (Lu *et al.*, 2020).

AHSV is non-contagious and can only be spread via the bites of infected vectors, therefore, other control measures centre around the insect vector (Mellor and Hamblin, 2004). Vector control itself can be addressed in a number of ways, with the main goal to reduce the number of potentially infecting bites and render an epidemic unsustainable (Mellor and Hamblin, 2004). Biting midges such as *C. imicola* are exophilic therefore the nocturnal stabling of horses may reduce the rate of biting and likelihood of infection (Barnard, 1997; Meiswinkel *et al.*, 2000). This strategy may not, however, be effective for other *Culicoides* species, such as *C. bolitinos*, especially in areas where the latter is more abundant. The closing of doors and gauzing of windows reduces the number of both species entering stables (Meiswinkel *et al.*, 2000). Due to the abundant

populations of *Culicoides* and their vast sizes, trying to identify and destroy, as well the attempt to apply insecticides and larvicides proves difficult in vector control strategies (Mellor and Hamblin, 2004).

The most important form of prevention and control is vaccination. Early vaccines were attenuated by multiple passages in adult mice brain (Alexander *et al.*, 1936). While somewhat effective, extensive passage in adult mouse brain caused the strains to become neurotropic, causing encephalitis and blindness in people who inhaled the freeze-dried viruses and occasionally resulted in serious side-effects in horses, donkeys and guinea pigs (Erasmus, 1963; van der Meyden *et al.*, 1992). The original serotype 4 (Vryheid) vaccine strain gave poor immunogenicity (Howell, 1963) and was therefore excluded from the mouse brain vaccine. These problems were addressed by passaging virulent strains in baby hamster kidney (BHK) cells, in that way obtaining attenuated strains that were no longer neurotropic (Erasmus, 1973). This significantly advanced the development of live-attenuated vaccine (LAV) strains and forms the basis of the vaccine currently available from Onderstepoort Biological Products [(OBP), Onderstepoort, South Africa]. The first serotype to be introduced to the mouse brain vaccine was AHSV4LP (Erasmus, 1973) and the rest of the serotypes were attenuated in the same way and introduced over a number of years until all neurotropic strains had been replaced. Horses are sequentially immunised with cocktails of different AHSV serotypes contained in two polyvalent vials containing serotypes 1, 3 and 4 (vial 1) and serotypes 2, 6, 7 and 8 (vial 2) (Mellor and Hamblin, 2004). Although serotype 5 was included in the original cocktail, it caused reversion to virulence of serotype 4 and was therefore removed (Dr BJ Erasmus, personal communication). AHSV9 is not included as it is rare in the southern African region (Mellor and Hamblin, 2004; Zientara *et al.*, 2015). Protection against serotypes 5 and 9 is provided by cross-protection of serotypes 8 and 6 respectively (von Teichman *et al.*, 2010). Animals are vaccinated twice in the first and second years of life, and annually thereafter. This vaccine has greatly reduced the impact of AHS but outbreaks of the disease still occur (Mellor and Hamblin, 2004). Monovalent attenuated AHSV9 has been used as a vaccine in West Africa, where this was the only serotype in circulation at the time (Mellor and Hamblin, 2004; Zientara *et al.*, 2015). Additionally, monovalent vaccines against serotypes 4 or 9 have been used successfully outside of sub-Saharan Africa on their own or in combination with other control measures to eradicate AHSV during several outbreaks (Mellor and Hamblin, 2004).

Despite the success of LAVs, there are still concerns regarding their use. These include the possibility of reversion to virulence and reassortment between vaccine strains and field strains (Weyer *et al.*, 2016; Grewar *et al.*, 2019). Live vaccines may also be teratogenic and as a result are not recommended for use in pregnant mares (Mellor and Hamblin, 2004; Zientara *et al.*, 2015; Carpenter *et al.*, 2017). There is also the possibility that the vector may acquire and disseminate vaccine strains in nature (MacLachlan *et al.*, 2007; Carpenter *et al.*, 2017). Furthermore, the LAV developed by OBP is not licensed in the European Union and require multiple inoculations for animals to become fully protected (Mellor and Hamblin, 2004; Dennis *et al.*, 2019; van Rijn

*et al.*, 2020). Another limitation with LAVs is the inability to differentiate infected from vaccinated animals (DIVA). Being able to differentiate vaccine-induced immunity from that caused by natural infection is important for the early detection of disease during an outbreak (Dennis *et al.*, 2019). Additionally, DIVA is important for the export of horses and for those taking part in international events.

A range of new generation vaccines, such as inactivated, sub-unit or recombinant vaccines, have been developed to address the limitations associated with LAVs. Ideally vaccines should be safe, efficacious, DIVA compliant, cost effective to produce and induce long-lasting immunity to all AHSV serotypes. Additionally, there should be no possibility of reassortment or reversion to virulence (Dennis *et al.*, 2019; van Rijn, 2019). The use of inactivated vaccines has not proved feasible as they are expensive to produce and require multiple inoculations to reach full immunity (Zientara *et al.*, 2015). A recent study investigated the safety and efficacy of an inactivated AHSV vaccine that was formulated with different adjuvants (van Rijn *et al.*, 2020). Unfortunately, the vaccine resulted in partial protection and is not suitable as an emergency vaccine. Also, better adjuvants are needed in order to increase protection without causing inflammation in vaccinated horses (van Rijn *et al.*, 2020).

A recombinant canarypox virus vector (BTV-CP) co-expressing BTV VP2 and VP5 induces high levels of protection in sheep. Sheep immunised with this recombinant vaccine developed high titres of virus-specific neutralising antibodies and were resistant to challenge with a field strain of BTV17 (Boone *et al.*, 2007). Humoral and cellular immune responses are essential for resistance to primary infections, but virus-specific neutralising antibodies are important in the case of reinfection with AHSV (MacLachlan *et al.*, 2007). Such a recombinant canarypox virus vectored vaccine has also been developed for AHSV (ALVAC-AHSV) (Guthrie *et al.*, 2009). This vaccine also co-expresses VP2 and VP5 of AHSV4 and provides protective immunisation of horses. Both vaccines appear to circumvent some of the problems associated with live-attenuated vaccines (Boone *et al.*, 2007; Guthrie *et al.*, 2009).

Sub-unit vaccines using baculovirus expressed AHSV VP2 on its own or with VP5 and/or VP7 induce protective immunity (Martinez-Torrecuadrada *et al.*, 1996; Roy *et al.*, 1996; Kanai *et al.*, 2014). Although such vaccines are DIVA compliant, they are not feasible for large-scale production due to the high costs required to culture insect cells (Dennis *et al.*, 2019). Virus-like particles (VLPs) are a specific class of sub-unit vaccine that form from the self-assembly of viral structural proteins (Noad and Roy, 2003). VLPs resemble the particles formed during infection but do not contain the virus genome or any of the non-structural proteins. Therefore, they are non-replicating, pose no risk of reversion to virulence, nor of segment reassortment and are DIVA compliant (Noad and Roy, 2003; Kushnir *et al.*, 2012; Dennis *et al.*, 2019). Recently, advances have been made with regard to producing AHSV VLPs in plants (Dennis *et al.*, 2018a; Dennis *et al.*, 2018b; Rutkowska *et al.*, 2019).

Currently, the use of reverse genetics systems is giving promising results in vaccine development and allows for the generation of synthetic viruses that are engineered by design so that specific genetic changes can be made and then assessed (van Rijn, 2019; Calvo-Pinilla *et al.*, 2020; Roy, 2020b). Using reverse genetics Entry Competent Replication Abortive (ECRA), previously referred to as Disabled Infectious Single Cycle (DISC), vaccines have been made to lack a functional VP6 and therefore cannot replicate (Lulla *et al.*, 2016; Lulla *et al.*, 2017; Sullivan *et al.*, 2021). Alternatively, Disabled Infectious Single Animal (DISA) vaccine strains have been made to lack NS3/NS3A (van de Water *et al.*, 2015; van Rijn *et al.*, 2018). These viruses are thus able to infect host cells but cannot egress, resulting in localised infection and no viraemia. Both ECRA and DISA vaccine candidates are DIVA compliant. Reverse genetics has also been used to generate reassortant strains of AHSV for all nine serotypes by exchanging genome segment 2 (van de Water *et al.*, 2015). It however appeared that exchanging only one protein did not yield vaccine strains that replicated efficiently. Rather, exchange of between two to five segments was required to generate ECRA for all nine serotypes (van de Water *et al.*, 2015). Reverse genetics allows for the rapid generation of vaccines that offer immunogenicity and safety levels that are better than alternative methods such as attenuated or recombinant vaccines (Roy, 2020b).

The control measures targeted at the vector are not sufficient to prevent the disease, and the only vaccines commercially available are live-attenuated vaccines that are not registered in Europe (Mellor and Hamblin, 2004). Thus, there is a need for improved vector control measures, surveillance systems and efficacious, inactivated vaccines, a goal of much research over the past few decades. Efficacious vaccines are crucial to the control of infectious diseases of horses worldwide and to the safe international movement of horses (MacLachlan *et al.*, 2007).

In order to better understand viral disease, it is important to have some insight into the genome and virion structural organisation.

### 1.4. ORBIVIRUS GENOME AND VIRION STRUCTURAL ORGANISATION

Both AHSV and BTV are non-enveloped viruses that have a double-stranded RNA (dsRNA) genome housed in a double-layered protein capsid (Els and Verwoerd, 1969; Verwoerd, 1969; Oellermann, 1970; Oellermann *et al.*, 1970; Verwoerd *et al.*, 1972). This dsRNA genome is composed of 10 segments (Oellermann, 1970; Verwoerd *et al.*, 1970; Bremer, 1976) that encode seven structural proteins (VP1-VP7) as well as four non-structural proteins NS1, NS2, NS3/A and NS4 (Table 1.1). All segments encode one protein, except for segment 9 (Seg-9) which encodes both VP6 and NS4 from two out-of-phase overlapping reading frames (Firth, 2008; Belhouchet *et al.*, 2010; Belhouchet *et al.*, 2011; Ratinier *et al.*, 2011), and Seg-10 which encodes both NS3 and NS3A from two in-phase overlapping open reading frames (van Staden and Huismans, 1991).

An alternative open reading frame (ORF) has been discovered in Seg-10 of both BTV and AHSV (Stewart *et al.*, 2015). In BTV this ORF appears to encode a protein that is 59 amino acids in length and localises to the nucleolus when expressed via a transient expression system (Stewart *et al.*, 2015).

**Table 1.1.** The 10 AHSV genome segments and the proteins they encode.

| Genome segment | Encoded protein(s) | Protein size (kDa) | Reference |
|---|---|---|---|
| Seg-1 | VP1 | 150 | Vreede and Huismans (1998) |
| Seg-2 | VP2 | 123 | Potgieter *et al.* (2003) |
| Seg-3 | VP3 | 103 | Maree *et al.* (1998) |
| Seg-4 | VP4 | 76 | Mizukoshi *et al.* (1993) |
| Seg-5 | NS1 | 63 | Mizukoshi *et al.* (1992) |
| Seg-6 | VP5 | 57 | du Plessis and Nel (1997) |
| Seg-7 | VP7 | 38 | Maree *et al.* (1998) |
| Seg-8 | NS2 | 41 | van Staden *et al.* (1991) |
| Seg-9 | VP6<br>NS4 | 38<br>20-30 | Turnbull *et al.* (1996)<br>Boughan *et al.* (2020) |
| Seg-10 | NS3<br>NS3A | 24<br>23 | van Staden and Huismans (1991) |

The structure of the AHSV virion is shown in Figure 1.1. The dsRNA genomes of orbiviruses are enclosed in icosahedral cores surrounded by a diffuse outer capsid layer. The minor structural proteins VP1, VP4 and VP6 form the enzymatic machinery of the orbivirus core, with VP1 representing the RNA polymerase, VP4 the capping enzyme and VP6 the viral helicase (Urakawa *et al.*, 1989; Stauber *et al.*, 1997; Ramadevi *et al.*, 1998). These three proteins, as well as the dsRNA genome, are encapsidated by two concentric layers of the major structural proteins VP3 and VP7 to form the viral core, an impressive viral transcription machine.

The organisation of the VP3 and VP7 layers of the core was revealed in 1998, when the BTV core was solved at high resolution by Grimes *et al*. (1998). At the time, the BTV core was the largest molecular structure to be solved at such high resolution (Grimes *et al.*, 1998). Years later, the architecture of an AHSV4 reference strain was determined using cryo-electron microscopy and three-dimensional image reconstruction (Manole *et al.*, 2012). Both the BTV and the AHSV VP3 scaffolds are composed of 120 copies of VP3 (Prasad *et al.*, 1992; Manole *et al.*, 2012). VP1, VP4 and VP6 attach to the inner layer of VP3 on the 5-fold axis, and are surrounded by dsRNA (Manole *et al.*, 2012). Also, like what is observed with BTV, the AHSV core is completed by the addition of 260 almost identical trimers of VP7 arranged on a T=13 icosahedral lattice (Prasad *et al.*, 1992; Grimes *et al.*, 1998; Manole *et al.*, 2012).

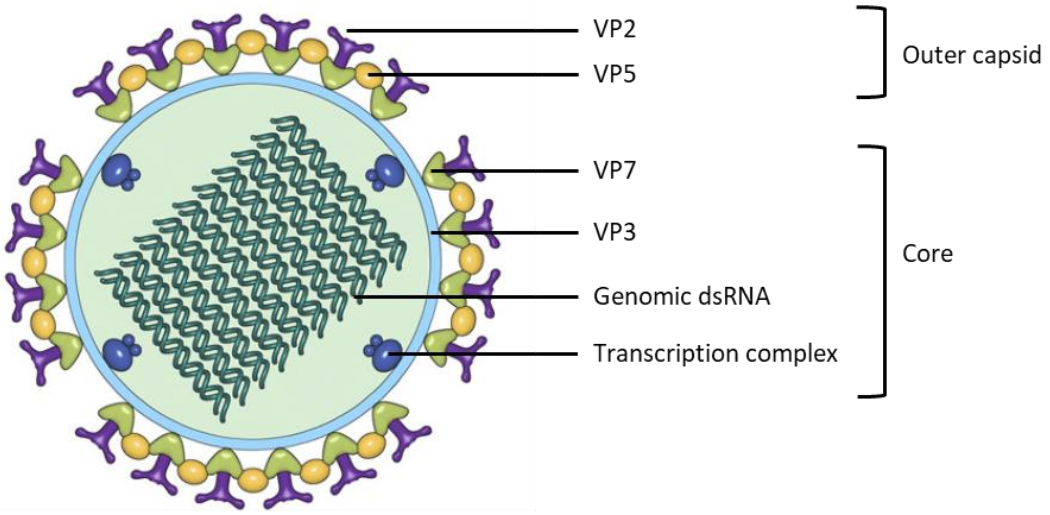


**Figure 1.1. Structure of the AHSV virion.** The minor structural proteins VP1, VP4 and VP6 form the transcription complex, which, together with the dsRNA genome, is encapsidated by VP3 and VP7 to form the viral core. VP5 and VP2 form the outer capsid. (From Manole *et al.* 2012, reproduced with permission from the American Society for Microbiology).

Major structural proteins VP2 and VP5 form the outer capsid of the intact virion (Figure 1.1). Two distinct motifs are present in the organisation of the outer capsid, namely globular motifs (representing VP5 trimers) that are interspersed between propeller-shaped triskelion motifs, representing VP2 trimers (Hewat *et al.*, 1992, 1994; Hassan *et al.*, 2001; Nason *et al.*, 2004; Manole *et al.*, 2012; Zhang *et al.*, 2016). BTV VP5 consists of three domains: dagger, unfurling and anchoring (Zhang *et al.*, 2016). The dagger domain is located in the N-terminus and interacts with VP7 through charge complementarity and hydrophobic interactions. Notably, this domain is found in the space between two adjacent VP7 trimers so that it is hidden from the surface of the virion (Zhang *et al.*, 2016; Xia *et al.*, 2021). AHSV VP5 is found between peripentonal VP2 molecules as well as around VP7 on the 3-fold axis (Manole *et al.*, 2012).

The structure of the BTV VP2 triskelion is such that each monomer consists of four domains: hub, hairpin, body and external tip (Zhang *et al.*, 2016). Each trimer, formed by the trimerisation of the hub domains of three VP2 monomers, attaches to four VP7 trimers. One interaction is via the hub domain of the VP2 trimer and the remaining three are through the body domains of three monomers. AHSV VP2 differs from that of BTV VP2 in that additional densities are found in the hub and tip domains (Manole *et al.*, 2012). Furthermore, AHSV VP2 has a “plug” at the 5-fold axis, something that is also not observed with BTV VP2 (Manole *et al.*, 2012).

VP2 and VP5 tend to form stronger interactions with VP7 than they do with one another, with VP5-VP7 interactions appearing stronger than VP2-VP7 interactions (Nason *et al.*, 2004; Zhang *et al.*, 2016). These interactions allow outer capsid proteins to be easily removed from the virion during uncoating, either due to weak VP2-VP5 interactions, or due to its interactions with the VP7 layer being weaker interactions than VP5-

VP7 interactions (Nason *et al.*, 2004). These observations are consistent with previous observations showing that VP2 can dissociate from virions without the removal of VP5 (Verwoerd *et al.*, 1972; Huismans *et al.*, 1987c).

Thus, each viral component is important for orbivirus structural organisation with each also having functional significance in the viral replication cycle, knowledge of which is important if one is to understand and study the control of disease.

## 1.5. ORBIVIRUS REPLICATION CYCLE

An overview of the orbivirus replication cycle is shown in Figure 1.2 and is similar for BTV and AHSV.

### 1.5.1. Viral adhesion, entry and uncoating

Virus entry into a host cell requires a number of steps culminating in the release of the viral genome into the cytosol (Forzan *et al.*, 2004). In general, this takes place by cell attachment, followed by the host cell inducing virus uptake (Patel and Roy, 2014). In the case of most animal viruses this requires the recognition by viral attachment proteins of cellular receptors (which are likely to be glycoproteins) on the surface of the cell, in addition to their association with various coreceptors prior to virus entry (Hassan and Roy, 1999).

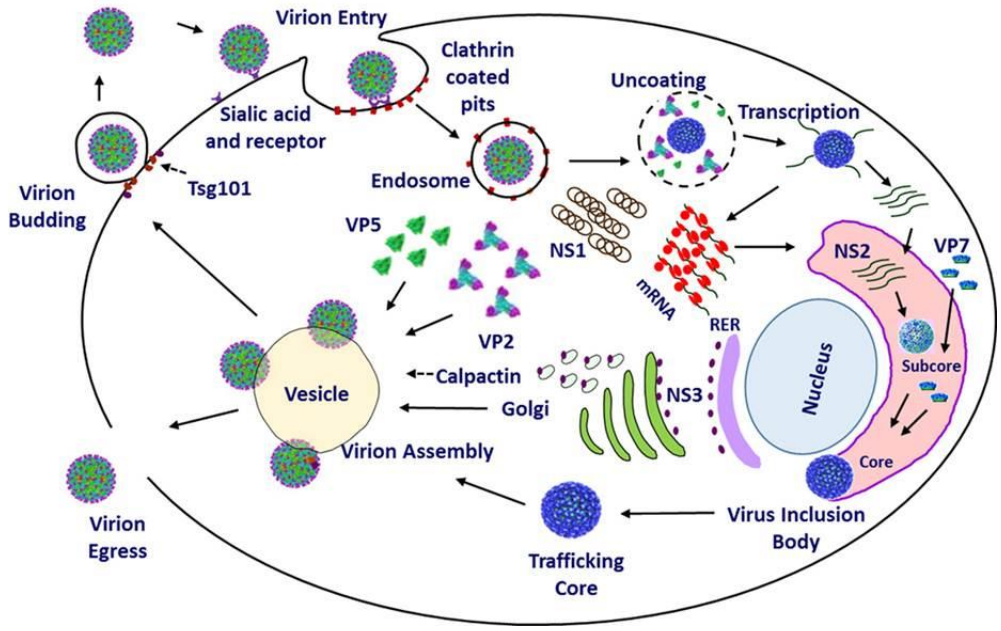


**Figure 1.2. Diagram representing an overview of the BTV replication cycle.** Virus adsorption occurs via VP2 binding to sialic acid and a receptor on the host cell surface. This is followed by entry into the cell via varying mechanisms depending on the virus serotype or cell type in question. The virion is then trafficked to the endosome in which uncoating takes place. The transcriptionally active core is released into the cytosol where viral transcription and translation take place leading to cellular morphogenesis by the non-structural proteins. NS1 forms tubules and NS2 forms the viral inclusion body (VIB) in which virus assembly takes place, after which VP2 and VP5 are added to form a complete virion. Egress of the mature virion follows via Tsg101 and NS3 mediated budding or via lysis of the host cell membrane. (From Patel and Roy 2014, reproduced with permission from Elsevier).

The outermost capsid protein, VP2, is involved in viral attachment and entry into the cell (Hassan and Roy, 1999). This protein appears to have two sites for plasma membrane binding, an inner sialic acid-binding site on the hub domain and an outer site on the tip domains (Zhang *et al.*, 2010). The sialic acid interaction is not sufficient for cell entry and instead facilitates infection by stabilising the interaction of projections in the tip domains with a coreceptor on the cell surface (Zhang *et al.*, 2010). Suggestions have been made that VP7 may also mediate attachment and entry into the cell, perhaps due to it being the most exposed of the two core proteins (Mertens *et al.*, 1996; Xu *et al.*, 1997).

AHSV uses a dynamin-dependent macropinocytosis as the primary pathway to enter BSR cells (Vermaak *et al.*, 2016). BTV was previously thought to enter the cell via clathrin-mediated endocytosis (Eaton *et al.*, 1990; Forzan *et al.*, 2007) but it has recently been shown to also enter the cell via a clathrin-independent, actin- and dynamin-dependent mechanism resembling macropinocytosis (Gold *et al.*, 2010; Stevens *et al.*, 2019). It appears that the mechanism of entry favoured by the virus depends on the serotype or cell line in question. For example, in the studies mentioned above, Forzan *et al.* (2007) focused on the entry of BTV-10 into Vero and HeLa cells, whereas the study done by Gold *et al*. (2010) focused on BTV-1 entry into BHK cells. Stevens *et al.* (2019) used bovine foetal aorta endothelial (BFAE) cells derived from the host. BTV is also infectious in at least three different forms, each of which may favour a different cell entry mechanism (Mertens *et al.*, 1996; Gold *et al.*, 2010). The core particle is infectious in *C. variipennis* cells as well as in KC cells (a *Culicoides*-derived cell line) but is not infectious in mammalian cells. This observation alludes to differences between mammalian and insect cells with regard to the route of infection as well as the mechanism of cellular entry used by the virus (Grimes *et al.*, 1995). This is particularly important when one considers that the virus is vector-borne, as such needing a way in which to enter the insect cell. In addition to the importance of endocytosis, or the preferred mechanism of entry into a cell, entry into an acidic environment is also essential for successful viral infection (Forzan *et al.*, 2007; Zhang *et al.*, 2010; Vermaak *et al.*, 2016).

After VP2 has recognised cellular receptors and the virion has entered the cell it is delivered to an endosome, the type of which depends on the serotype and cell line (Forzan *et al.*, 2007). Virions are delivered to early-endosomes, as in the case of BTV10 infection (Vero and HeLa cells) or late endosomes/lysosomes, as is the case in BTV1 infection (BHK cells) (Forzan *et al.*, 2007; Gold *et al.*, 2010). An essential step in the replication cycle takes place while the virion is in endosome, namely virus uncoating – the separation of the VP2/VP5 outer capsid from the inner core (Forzan *et al.*, 2007). At low pH, the VP5 trimer undergoes conformational changes in which it transforms into an elongated shape with a stalk protruding out of the viral core (Xia *et al.*, 2021). A surface loop of the anchoring domain of each monomer also undergoes changes, transforming into a β-hairpin which anchors VP5 to the core by inserting into a crevice formed between adjacent VP7 timers (Zhang *et al.*, 2016; Xia *et al.*, 2021). These changes are accompanied by the movement of two VP7

trimers toward the fivefold axis. Together, these changes weaken the interactions between VP2 and VP5, leading to the detachment of VP2. VP5 then inserts the stalk tip (R250-K260) into the endosomal membrane. Thereafter, the dagger domain and the WHXL motif are brought to the membrane to create a single pore at the site of stalk-membrane interaction. This pore gradually increases in size due to the participation of VP5 trimers and the detachment of VP5 that is already interacting with the membrane so that the core can be released without disrupting the entire endosomal membrane (Forzan *et al.*, 2007; Xia *et al.*, 2021).

Once the endosomal membrane has been destabilised, VP5 is retained in the endosome while the transcriptionally active core is released into the cytosol, where it initiates transcription and viral protein synthesis (Huismans *et al.*, 1987b; Eaton *et al.*, 1990; Forzan *et al.*, 2007; Xia *et al.*, 2021).

### 1.5.2. Viral genome transcription, translation, and replication

Orbiviruses make use of their own enzymatic machinery for viral transcription. Thus, viral transcription takes place by the minor structural proteins VP1, VP4 and VP6 enclosed in the viral core. A further reason for transcription to take place in the core is that it may prevent the host cell from eliciting an immune response against the dsRNA (Eaton *et al.*, 1990; Diprose *et al.*, 2002; Dennis *et al.*, 2019). In addition to this, the BTV core binds dsRNA, perhaps in an effort to prevent the dsRNA released from damaged particles from eliciting a host response (Diprose *et al.*, 2002).

As the viral helicase, VP6 unwinds the dsRNA after which the negative strand is used as a template for the transcription of positive sense single-stranded (ss) messenger RNA (mRNA) by VP1, which is then capped and methylated by VP4, before extrusion into the cytoplasm (Urakawa *et al.*, 1989; Stauber *et al.*, 1997; Ramadevi *et al.*, 1998). VP1-VP4 interactions appear to be rather stable and may be necessary for the capping of the mRNA by VP4. Once in the cytoplasm, the mRNAs can be translated into the seven structural and four non-structural proteins using host cell machinery.

VP1 is also involved in the synthesis of dsRNA genome segments from plus-strand RNA templates by acting as a replicase (Urakawa *et al.*, 1989; Boyce *et al.*, 2004). Thus, in addition to being templates for the translation of viral proteins, the extruded single-stranded mRNAs also serve as templates for negative strand synthesis, resulting in progeny dsRNA genome segments, and the subsequent incorporation of the full dsRNA genome into the core of the newly formed virion (Grimes *et al.*, 1998; Dennis *et al.*, 2019).

### 1.5.3. Viral assembly

AHSV and BTV assembly takes place in perinuclear viral inclusion bodies (VIBs) after which the newly synthesised particles are released into the surrounding cytoplasm of the infected cell (Eaton *et al.*, 1987; Brookes *et al.*, 1993; Uitenweerde *et al.*, 1995). NS2 forms a large component of VIBs (Huismans *et al.*, 1987a).

This phosphorylated protein is able to bind ssRNA (Huismans *et al.*, 1987a; Thomas *et al.*, 1990) and is involved in the recruitment of newly transcribed mRNA to VIBs (Lymperopoulos *et al.*, 2003) prior to interactions with VP1, VP4 and VP6 within the VIB matrix and subsequent encapsidation by VP3 (Huismans *et al.*, 1987a; Roy, 2005). VP6 binds ssRNA, and interacts with VP3, and is essential for the recruitment and packing thereof (Matsuo *et al.*, 2018; Sung *et al.*, 2019).

All seven structural proteins are involved in virion assembly. The core proteins VP3 and VP7 are located in the VIB matrix, and the outer capsid proteins VP2 and VP5 are located at the periphery of the VIB (Roy, 2005). It is believed that BTV core assembly starts with the assembly of the VP3 layer followed by the attachment of a VP1/VP4 flower-shaped structure to the underside of the VP3 layer, so that both proteins come into contact with VP3 (Nason *et al.*, 2004; Roy, 2005). The viral genome then wraps itself around the VP1/VP4 complex, with which VP6 may be associated as the VP3 subcore assembles. The assembly of the core is then completed by the association of 260 VP7 trimers with the VP3 layer via hydrophobic residues on the flat underside of the trimers (Grimes *et al.*, 1998). Although the connections between the top and bottom domains of both BTV and AHSV VP7 trimers are quite weak (Basak *et al.*, 1996), the interactions between the monomers are extensive, leading to robust trimeric building blocks (Grimes *et al.*, 1995). Two models for the incorporation of VP7 into the core particle have been suggested. The first suggests that preformed hexamers of VP7 bind around the initial trimer at a single nucleation site. The other suggests that multiple nucleation sites may be present leading to strong interactions between VP7 trimers and the VP3 scaffold. Weaker interactions then fill in the gaps between the two (Limn and Roy, 2003). Interestingly, the majority of AHSV VP7 expressed in a cell self-assembles into flat, hexagonal crystals, the function of which is unknown. These crystals are unique to AHSV and assemble independently of other viral proteins or intracellular trafficking pathways (Bekker *et al.*, 2014).

Once the core has been assembled, the outer capsid proteins VP2 and VP5 attach to the VP7 layer to form an intact virion, after which the virions are no longer transcriptionally active (Roy, 2005; Dennis *et al.*, 2019). The newly formed intact virions are then ready for release from the host cell.

### 1.5.4. Virus release

Orbiviruses have had to adopt mechanisms of virus egress that are somewhat different to those used by enveloped viruses. This is so as they are non-enveloped and lack the glycosylated proteins used by enveloped viruses in viral egress. AHSV and BTV make use of two processes for release, non-lytic and lytic. Non-lytic processes involved budding through the plasma membrane as single particles or as multiple particles enclosed in vesicular structures and lytic processes involve release via cell lysis (Roy, 2020a). Non-structural protein NS3/NS3A plays an important role in virus release and is localised in the plasma membrane, especially at sites of viral egress, as well as in intracellular smooth surface vesicles (Hyatt *et al.*, 1991; Stoltz *et al.*, 1996;

Ferreira-Venter *et al.*, 2019). NS3 is also found at the periphery of VIBs, suggesting that it may play a role in the transport of virions in the maturation process (Mohl *et al.*, 2020).

Non-lytic processes occur mainly early on in infection and the viral particles acquire a temporary membrane and bud through the plasma membrane (Eaton *et al.*, 1990; Roy, 2001). BTV virions can also transit through multivesicular bodies to lysosomes from which they are released at the cell membrane as extracellular vesicles (Labadie *et al.*, 2020). Non-lytic release is mediated by NS3 and is dependent on multiple functional domains (Hyatt *et al.*, 1993; Wirblich *et al.*, 2006; Ferreira-Venter *et al.*, 2019; Labadie *et al.*, 2019). It was previously suggested that NS3/NS3A may take advantage of the host cell's exocytotic pathway to facilitate the non-lytic release of virus particles from insect cells, by forming a complex (at its N-terminal) with cellular protein S100A10/p11, the calpactin light chain of the Annexin II complex involved in exocytosis (Beaton *et al.*, 2002). This study also illustrated that NS3/NS3A interacts with VP2 at its C-terminal. It has subsequently been shown with the use of a reverse genetics system that NS3, but not NS3A, is required for assembly and virus trafficking in mammalian cells, but both are required in insect cells, thereby indicating a possible explanation for the expression of both proteins in orbiviruses (Celma and Roy, 2011). This NS3-S100A10/p11 complex may form part of a larger active but non-lytic, egression process by acting as a bridge between virus particles and the host cell's export machinery (Patel and Roy, 2014).

As infection progresses virus particles can be released from the cell through a disrupted plasma membrane, in a so-called lytic fashion (Hyatt *et al.*, 1989; Eaton *et al.*, 1990; Labadie *et al.*, 2020). BTV-induced apoptosis and the activation of the proinflammatory response play a key role in lytic release from infected cells (Labadie *et al.*, 2020; Roy, 2020a). Also, AHSV NS3 can act as a viroporin by altering membrane permeability and as such facilitate virus release and total virus yield (Meiring *et al.*, 2009). A difference exists between AHSV-infected mammalian and insect cells, in that mammalian cells exhibit morphological changes that eventually result in cell death, whereas no observable cytopathic effect (CPE) has been observed in infected insect cells (Martin *et al.*, 1998; Wirblich *et al.*, 2006). A cellular defence mechanism has recently been proposed for the facilitation of non-lytic viral release of AHSV in insect cells (Venter *et al.*, 2014). Large vesicle-like structures containing viral material, including viral particles were observed merging with the plasma membrane to release their contents, and in so doing facilitated non-lytic release in insect cells (Venter *et al.*, 2014).

### 1.6. NON-STRUCTURAL PROTEIN NS4

Several years ago a bioinformatic analysis of Seg-9 revealed that the VP6 cistron of most orbiviruses contains an additional out-of-phase overlapping ORF (Firth, 2008; Belhouchet *et al.*, 2010). This ORF was found in all analysed Seg-9 sequences of both insect-borne and tick-borne orbiviruses with mammalian hosts (Firth, 2008; Belhouchet *et al.*, 2010), except for Saint Croix River virus (SCRV) (Firth, 2008). SCRV has not been shown to have a known vertebrate host, and could therefore be considered a true 'tick-virus' (Belhouchet *et*

*al.*, 2010). This newly discovered ORF on Seg-9 was initially named ORFX (BTV) (Firth, 2008) and ORF-2 [Great Island virus (GIV)] (Belhouchet *et al.*, 2010), but its designation was later changed to NS4 when subsequent studies showed that it encoded a protein of non-structural nature in both BTV (insect-borne) and GIV (tick-borne) infected cells (Belhouchet *et al.*, 2011). Due to the mostly strong Kozak context of the AUG-initiated ORF of NS4 (Firth, 2008; Belhouchet *et al.*, 2010) it is possible that the protein may be translated by leaky scanning (Firth, 2008). For leaky scanning the optimal conditions include the first AUG in a weak Kozak context and the second AUG in a strong Kozak context. Some orbiviruses (including BTV) have additional AUG codons between the VP6 initiation codon and the presumed NS4 initiation codon, suggesting that mechanisms other than leaky scanning may be at play in order to bypass the intermediate AUG codons (Belhouchet *et al.*, 2011).

Bioinformatics showed that the amino acid identity of NS4 ranged between 5 and 50% within orbiviruses, with the highest identity detected between BTV and EDHV (50%). BTV NS4 contains a coiled-coil domain between amino acid residues 27 and 77, and AHSV NS4 contains coiled-coil domains between amino acids 5 and 85 and 110-140. Nuclear localisation signals (NLSs) were predicted in the NS4 proteins of Peruvian horse sickness virus (PHSV), Yunnan orbivirus (YUOV), EHDV and GIV which showed overlapping, single and bipartite NLSs respectively, as well as in BTV and AHSV NS4, which showed single and three potential overlapping NLSs respectively (Belhouchet *et al.*, 2011). Two putative alpha helices were identified in BTV NS4, one of which contains a conserved leucine zipper domain (Ratinier *et al.*, 2011). AHSV NS4 showed strong relatedness with domain of unknown function (DUF) domains that have helical structures known to be involved in nucleic acid binding and/or modification while BTV NS4 shows relatedness (over amino acids 14-54) to a DUF domain belonging to the MetJ/Arc repressor superfamily, which is known to have a characteristic DNA-binding motif.

The initial work done on BTV NS4 showed that NS4 is produced in BTV1 and BTV8 infected insect and mammalian cells (Belhouchet *et al.*, 2011; Ratinier *et al.*, 2011). Immunofluorescence microscopy of infected cells showed that NS4 forms fine aggregates in the cytoplasm and nucleus of both BTV8- and GIV-infected cells as early as 4 hours post infection (hpi) (Belhouchet *et al.*, 2011) and NS4 was detected as early as 2 hpi in BFAE cells infected with BTV1 (Ratinier *et al.*, 2011). By 24 hpi NS4 was also observed as small aggregates in the nucleus, consistent with the identification of nuclear localisation signals in the BTV8 and GIV NS4 sequences, and at 72 hpi, NS4 localised to the cell membrane (Belhouchet *et al.*, 2011). Consistent with bioinformatic analyses showing similarities between NS4 and lipid-associated domains, NS4 was also observed to colocalise with lipid droplets of 0.7 to 1 µm in diameter in the cytoplasm (Belhouchet *et al.*, 2011).

*In vitro* nucleic acid binding assays showed that GIV NS4 protects dsRNA from cleavage by Dicer and RNase III endoribonucleases (Belhouchet *et al.*, 2011), consistent with previous analyses showing the presence of dsRNA-binding domains (Belhouchet *et al.*, 2010). BTV NS4 however, does not protect dsRNA from cleavage by Dicer or RNAse III (Belhouchet *et al.*, 2011). This is due to a dsRNA-binding domain that is present in GIV NS4 but absent from BTV NS4. Both GIV and BTV NS4 did not protect ssRNA or ssDNA from degradation by RNase A or nuclease S1 respectively, whereas both GIV and BTV NS4 are able to bind to and at least partially protect dsDNA from degradation by DNase I (Belhouchet *et al.*, 2011).

Ratinier *et al.* (2011) used a reverse genetics system to investigate the role of NS4 in BTV viral replication. Results showed that NS4 is not needed for BTV replication *in vivo* and *in vitro* in both insect and mammalian cells. Furthermore, it does not affect virulence in murine models of bluetongue infection (Ratinier *et al.*, 2011). The high conservation of the NS4 reading frame in Seg-9 in BTV and related orbiviruses (Firth, 2008) indicated that in some way it must be essential for the maintenance of BTV in nature (Ratinier *et al.*, 2011). Interestingly, this was indeed shown to be the case with NS4 conferring a replication advantage to BTV8, but not to BTV1, in mammalian cells in an interferon (IFN)-induced state (Ratinier *et al.*, 2011). The authors postulated that NS4 may play an important role in virus-host interactions, especially interactions involving the host immune response. Using an NS4 deletion mutant, BTV8ΔNS4, work done by the same group showed that BTV NS4 modulates the IFN-response by downregulating mRNA levels of IFN-I and interferon stimulated genes (ISGs) and downregulating the activities of certain promoters (Ratinier *et al.*, 2016). NS4 is not required for BTV replication in insect cells, mammalian cells, or type I IFN receptor$^{-/-}$ (IFNAR$^{-/-}$) mice (Ratinier *et al.*, 2016). It does, however, confer a replication advantage to BTV in mammalian cells in an IFN-induced state as well as *in vivo* in the host (Ratinier *et al.*, 2011; Ratinier *et al.*, 2016). BTV NS4 was therefore concluded to be an IFN antagonist and a key virulence factor in the host (Ratinier *et al.*, 2016).

*In silico* analysis of AHSV Seg-9 sequences showed that the ORF encoding the putative NS4 protein was present in addition to the VP6 ORF in all nine serotypes (Zwart *et al.*, 2015). The sequences clustered into two groups based on the length and nucleotide alignment of the full-length Seg-9 sequence and therefore included both the VP6 and the NS4 ORFs. Higher levels of sequence identity were observed within clades than between clades, with only 52% identity between the NS4 amino acid sequences of Clade I and Clade II (Zwart *et al.*, 2015). The Clade I ORF is 435 nucleotides in length and encodes NS4-I (145 aa). Clade II is slightly longer at 465 nucleotides and encodes NS4-II (155 aa). Most of the putative AHSV NS4 proteins lacked the NLSs that had previously been predicted by Belhouchet *et al.* (2011) and those that did contain them belonged to Clade II (Zwart *et al.*, 2015).

Western blot analyses showed that the AHSV NS4 proteins expressed by Clades I and II were slightly larger than the size (17 kDa) predicted by Belhouchet *et al.* (2011) at 20 kDa and 23 kDa respectively (Zwart *et al.*,

2015). Both proteins were found in the nucleus and cytoplasm of AHSV-infected cells, often as early as 3 hpi. By 12 hpi and up to 48 hpi small punctate to stellate foci were observed in the nucleus of infected cells and the protein was distributed homogenously throughout the cytoplasm of infected cells. Although AHSV NS4 formed punctate foci in nuclei, resembling those of BTV NS4 (Belhouchet *et al.*, 2011; Ratinier *et al.*, 2011), AHSV NS4 does not localise to the nucleolus. The labelling of fibrillarin became weaker over time (Zwart *et al.*, 2015), as was reported for BTV (Belhouchet *et al.*, 2011), and was proposed to result from viral induced apoptosis in the nucleus. Unlike BTV and GIV NS4 (Belhouchet *et al.*, 2011), AHSV NS4 does not localise to the plasma membrane nor does it localise to lipid droplets (Zwart *et al.*, 2015). Nuclear and cytoplasmic patterns of intracellular localisation were also observed in post-mortem tissue of AHSV-infected horses, specifically microvascular endothelial, mononuclear phagocytes, and stellate-shaped cells in the spleen. AHSV NS4 was also shown to bind to dsDNA but not dsRNA.

A study in our laboratory that was done in parallel to the work presented in this thesis confirmed that all AHSV reference and field strains tested (18 strains in total) express either NS4-I or NS4-II, or a subtype of NS4-II that contained an NLS and was termed NLS-NS4-II (Figure 1.3) (Boughan *et al.*, 2020). Both NS4-I and NS4-II were confirmed to be nucleocytoplasmic proteins. NS4-I displayed a higher proportion of the total protein localising to the nucleus and NS4-II had a stronger cytoplasmic presence, while NLS-NS4-II had a homogenous cytoplasmic distribution plus formed distinct nuclear foci in AHSV-infected cells. Colocalisation analyses showed that NS4 colocalised with promyelocytic leukemia nuclear bodies (PML-NBs), suggesting a role for AHSV NS4 in antagonising the antiviral response (Boughan *et al.*, 2020).

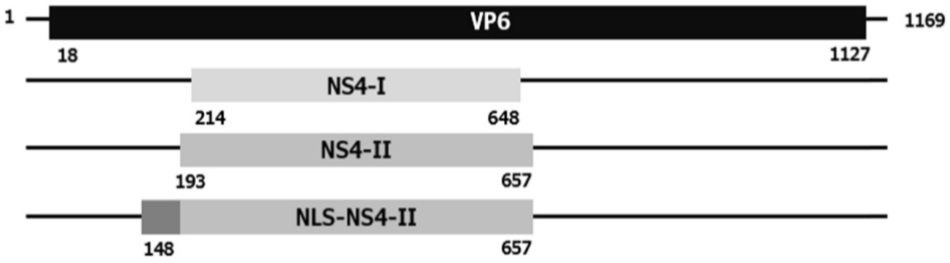


**Figure 1.3. Schematic representation of the VP6 and NS4-I, NS4-II and NLS-NS4-II ORFs on Seg-9. T**he dark grey block on NLS-NS4-II represents the NLS. The numbers indicate the beginning and end of each ORF on Seg-9, sizes in base pairs. (From Boughan *et al.* 2020, reproduced with permission from the Microbiology Society).

A recent study by Li *et al.* (2021) showed that both the NS3 and NS4 proteins of BTV1 target the SH2 domain of signal transducer and activator of transcription 1 (STAT1) and inhibit its phosphorylation, heterodimerisation and nuclear translocation. In so doing, this inhibits the activation of downstream genes of the Janus kinase-signal transducers and activators of transcription (JAK-STAT) signalling pathway and reveals a new way in which BTV can evade host innate immunity.

## 1.7. HOST IMMUNITY

The immune system has evolved to detect and defend multicellular organisms from invading pathogens such as viruses, bacteria, fungi or parasites (Kindt *et al.*, 2007; Goubau *et al.*, 2014; Chow *et al.*, 2015). Protection by the immune system can be divided into two activities, namely recognition and response (Kindt *et al.*, 2007). Recognition involves distinguishing self from non-self which is important as the immune system can be a potent aggressor when it fails to act, or when it turns on the host. The immune system can detect molecular patterns found on groups of common pathogens but it is also able to detect subtle differences between one pathogen and another (Kindt *et al.*, 2007). The initial recognition event triggers effector responses that ultimately eliminate or neutralise the pathogen. Some responses may even induce a memory response, in which there is a faster and heightened immune response upon later infection.

The immune system is composed of two main branches, namely the innate immune response and the adaptive immune response. These two branches collaborate to protect the host from foreign pathogens. The first line of defence against invading pathogens that have passed the barriers that protect the host (e.g. the skin and mucosal membranes) is the innate immune response (Kindt *et al.*, 2007; Chow *et al.*, 2015; Kell and Gale, 2015) and will be the focus here.

### 1.7.1. The innate immune response

The innate immune response includes molecular and cellular mechanisms that are deployed before infection, and prevents infection at the outset, or eliminates it within hours of exposure. Although the recognition elements of the innate immune response are able to distinguish between self and pathogens, they are unable to distinguish between one pathogen and another (Kindt *et al.*, 2007). An important innate defence mechanism is phagocytosis, a form of endocytosis, which is carried out by cells such as monocytes, neutrophils and macrophages. In phagocytosis the membrane of a cell surrounds extracellular particulate material that may include whole pathogens, in order to ingest it (Kindt *et al.*, 2007).

Central to the innate immune response, triggered by exposure to for example dsRNA viruses (Figure 1.4), is the production of inflammatory cytokines and interferons (Chow *et al.*, 2015). Interferons (IFNs) are soluble proteins that are produced by virus-infected cells and have the ability to bind to cells near the site of infection and initiate a generalised antiviral state (Goodbourn *et al.*, 2000; Samuel, 2001; Kindt *et al.*, 2007). Therefore, the IFN response consists of cells that produce IFN and cells that respond to IFN (Samuel, 2001). So-called antiviral immunity is initiated upon host recognition of viral products, such as proteins, protein or lipid complexes and viral nucleic acid via distinct non-self molecular patterns known as pathogen-associated molecular patterns (PAMPs) (Chow *et al.*, 2015; Kell and Gale, 2015). PAMPs accumulate at various sites during infection, including the cell surface, free in the cytosol or in endosomal compartments. Pathogen recognition receptors (PRRs) are host cell-associated proteins that recognise these foreign PAMPs (Kell and

Gale, 2015). PRRs can be classified into several groups including: Toll-like receptors (TLRs), retinoic acid inducible gene-I (RIG-I) like receptors (RLRs), nucleotide oligomerization domain-like receptors (NLRs), non-RLR DEXD/H-box helicases and cytosolic DNA sensors (Rojas *et al.*, 2021). There are three major IFN-inducing PRRs in mammals, namely TLRs, RLRs and cGAMP synthase-stimulator of interferon genes (cGAS-STING).

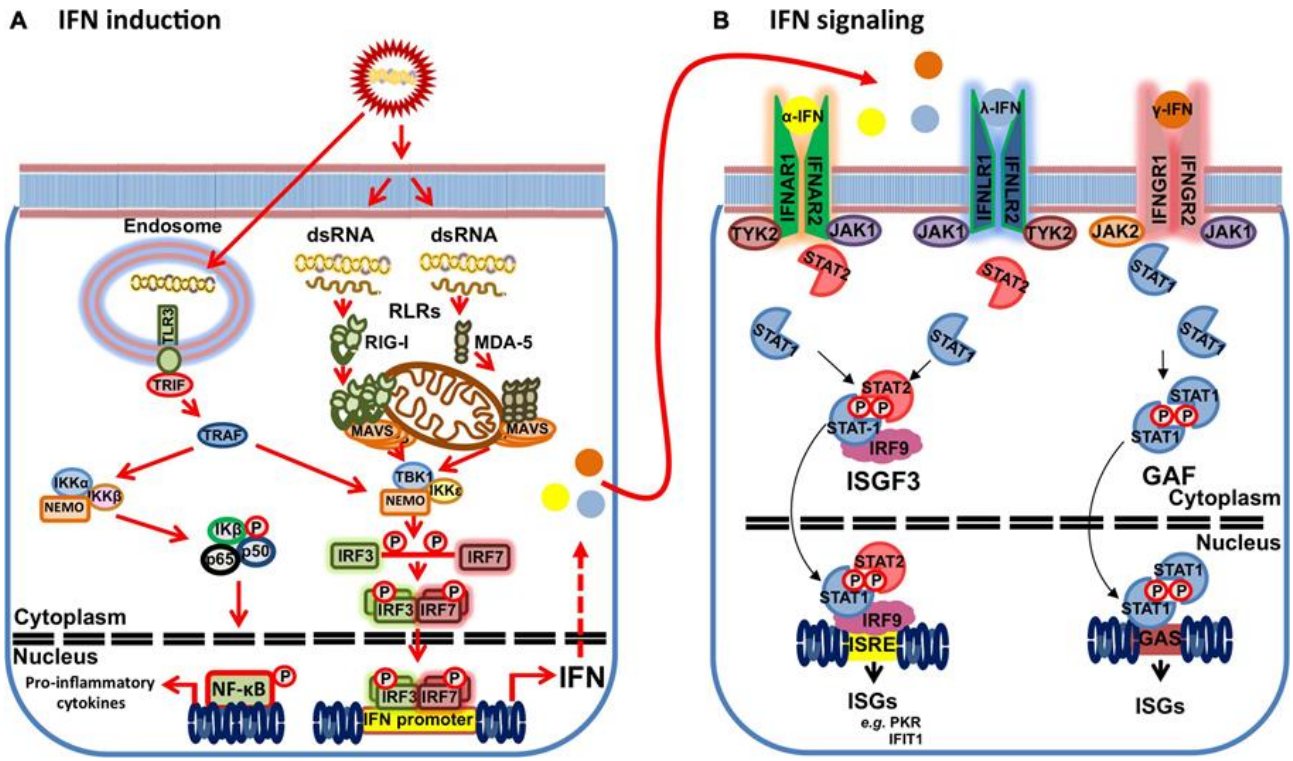


**Figure 1.4. IFN response to dsRNA viruses.** (A) dsRNA is recognised by TLR or the RLRs, RIG-I and MDA5 which initiates a cascade of events leading to the production of proinflammatory cytokines and IFN. (B) The newly produced IFN activates the JAK-STAT signalling pathway which culminates in the expression of hundreds of ISGs. [From Rojas *et al.* 2021, reproduced with permission from Frontiers under the terms of the Creative Commons Attribution License (CC BY), Copyright© 2021 Rojas, Avia, Martin and Sevilla].

TLRs are transmembrane proteins, several of which recognise nucleic acids and consequently play an important role in antiviral defence (Muzio and Mantovani, 2000; Chow *et al.*, 2015). TLRs are located in compartments where viral genomes can be exposed, such as in endolysosomes after the endocytosis of viral particles (Figure 1.4) (Chow *et al.*, 2015). In order to prevent the detection of host nucleic acids, TLRs are restricted to endolysosomal compartments by a process mediated by UNC93B1, a multipass membrane protein located in the endoplasmic reticulum (ER) (Chow *et al.*, 2015). The TLR family is vast, with 13 paralogous TLRs found in mouse and humans combined (10 in human and 12 in mice) and all TLRs observed to date contain leucine-rich repeats (LRRs), and a single intracellular Toll/interleukin-1 (IL-1) receptor (TIR) domain, homologous to the intracellular domain of IL-1 receptor family members (Muzio and Mantovani, 2000; Moresco *et al.*, 2011; Chow *et al.*, 2015). In order to prevent autoimmunity TLR3, 7, 8 and 9 undergo proteolysis by various proteases as they pass through acidic endosomal compartments. Downstream

signalling cannot take place until after this proteolysis, therefore TLRs that remain inactivated until they reach their proper destination reduces the risk of autoimmunity (Chow *et al.*, 2015).

Mammalian TLR3 recognises dsRNA in an endosome and signals through its adaptor protein Toll/IL-1R domain-containing adaptor inducing IFN-β (TRIF) to activate tumour necrosis factor receptor-associated factors (TRAF). TRAF promotes the activation of the IKK complex [composed of IκB kinase α (IKKα), IKKβ, and nuclear factor kappa B (NF-κB) essential modulator (NEMO)] that activates NF-κB and the transcription of pro-inflammatory cytokines in the nucleus (Figure 1.4) (Alexopoulou *et al.*, 2001; Rojas *et al.*, 2021). TLR7 and TLR8 recognise viral ssRNA and TLR9 recognises DNA containing unmethylated CpG motifs, which are common in some viral as well as non-viral pathogens (Moresco *et al.*, 2011; Chow *et al.*, 2015).

dsRNA viruses such as BTV and AHSV are sensed predominantly by RLRs (Rojas *et al.*, 2021) which include RIG-I, melanoma differentiation-associated gene 5 (MDA5) and laboratory of genetics and physiology gene 2 (LGP2). Within mammalian cells, this family plays an important role in the recognition of viruses across genera and families, often by acting as sensors of RNA viruses and promoting the recognition of some DNA viruses and both RIG-I and MDA5 are essential for interferon induction (Habjan *et al.*, 2008; Kell and Gale, 2015; Liu *et al.*, 2015). TLRs only survey the extracellular space and are only expressed in a limited number of cell types, whereas the PRRs RIG-I and MDA5 are ubiquitously expressed (Chow *et al.*, 2015; Rojas *et al.*, 2021). RIG-I specifically is expressed in most cells of the body, albeit at a low level, and its abundance increases in the presence of IFN.

These RLRs are cytoplasmic helicases and contain a DExD/H-box helicase domain and a C-terminal domain known as the repressor domain (RD), and both RIG-I and MDA5 contain N-terminal tandem caspase activation and recruitment domains (CARDs) that function in signalling (Chow *et al.*, 2015; Kell and Gale, 2015). The prediction of RIG-I binding sequences and stimulatory RNA motifs based on structure and sequence remains challenging. Over the years there have been several characteristics that appear to influence the recognition and level of specificity with which RIG-I recognises PAMP RNA ligands. These include sequence composition, PAMP motif length, ss or dsRNA, and the presence of a 5’ cap versus an exposed 5’ triphosphate (5’ppp). The ideal PAMP RNA ligands for RIG-I, however, appear to be dsRNA of < 300 bp with blunt ends containing a 5’ppp moiety. The minimal length is as short as 10 bp as long as there are no mismatches near the blunt end (Goubau *et al.*, 2014; Chow *et al.*, 2015; Kell and Gale, 2015). There are however other RNA structures that can be involved in RIG-I activation such as a poly(U/UC) tract, 3’-monophosphates, AU-rich regions and 5’pp (Goubau *et al.*, 2014; Liu *et al.*, 2015). There is also evidence suggesting that a stretch of dsRNA near the 5’ ppp end in conjunction with a free 5’ppp end, bind to distinct sites on RIG-I and define a PAMP that is sufficiently recognised by RIG-I, leading to the induction of IFN (Schmidt *et al.*, 2009). Unpaired 5’ppps such

as those found in arenavirus dsRNA panhandle structures are however not recognised by RIG-I (Marq *et al.*, 2010). In contrast to RIG-I, MDA5 binds to 5'ppp and 5'pp on long dsRNA molecules (Chow *et al.*, 2015).

Both RIG-I and MDA5 (Figure 1.4) are activated upon detection of viral RNA, causing the liberation of CARDs (Rojas *et al.*, 2021). The released CARDs are then able to interact with the CARD found on the mitochondrial antiviral signalling proteins (MAVS) which are located on the mitochondria, peroxisomes and mitochondria-associated ER membranes (MAM). MAVS then recruit TRAF which promotes the formation of the TANK binding kinase 1 (TBK1) complex consisting of TBK1, IKKε and NEMO which then mediates the phosphorylation and homodimerization of interferon regulatory factors (IRF) 3 and 7 (Kell and Gale, 2015; Rojas *et al.*, 2021). IRF3, IRF7 and NF-κB then translocate from the cytoplasm to the nucleus where they induce the transcription of IFN-I (Figure 1.4) (Kell and Gale, 2015).

The newly expressed IFN bind to IFN receptors on the plasma membrane and initiate the JAK-STAT signalling pathway and the transcription of ISGs (Figure 1.4) (Samuel, 2001; Rojas *et al.*, 2021), whose products have many actions including antiviral and immunomodulatory actions that create a general antiviral state in the infected cell and surrounding tissue, effectively reducing or restricting viral replication and the cell-to-cell spread of infection (Kell and Gale, 2015).

The last major PRR of mammals is the cGAS-STING pathway. STING is localised on the membrane of the endoplasmic reticulum and is an innate immune sensor of cyclic dinucleotides (Burdette *et al.*, 2011) and regulates the induction of type I IFN (Shu *et al.*, 2012). While RLRs detect viral RNA and induce an IFN response, STING coordinates the IFN I response to viral DNA (Chow *et al.*, 2015). Theoretically, all microorganisms that carry DNA into the cytoplasm should be able to initiate the cGAS-STING pathway (Sun *et al.*, 2013). Host DNA should not be located in the cytoplasm of uninfected cells, thus any cytoplasmic DNA detected by the PRR cGAS is most likely of viral origin (Chow *et al.*, 2015). This transmembrane protein is located on the ER-membrane (Ishikawa and Barber, 2008; Ishikawa *et al.*, 2009) and is activated by the cytoplasmic protein cGAS (Sun *et al.*, 2013). Upon binding DNA, cGAS synthesises the cyclic dinucleotide cGAMP from both ATP and GTP (Sun *et al.*, 2013; Wu *et al.*, 2013). cGAMP functions as a secondary messenger and binds to and activates STING, thereby promoting IFN expression to a level comparable to that induced by MAVS and higher than the level of induction caused by several putative DNA sensors (DAI, IFI16 and DDX41) (Sun *et al.*, 2013; Wu *et al.*, 2013). Some bacteria also produce cyclic dinucleotides that can activate STING (Burdette *et al.*, 2011) but cGAMP binds STING at a higher affinity due to its non-canonical 2'-5' phosphodiester linkage (Chow *et al.*, 2015).

As reviewed by Chow *et al*. (2015), the cGAS-STING pathway appears to be regulated by proteins involved in the autophagy pathway. Once STING has bound to dinucleotides it relocates from the ER to the Golgi

apparatus via a mechanism that is dependent on VPS34, a class III PI3K that is involved in the regulation of many pathways. STING then leaves the Golgi apparatus and associates with TBK1 on vesicles to activate the downstream transcription factor, IFN-regulatory factor 3 (IRF3) and NF-κB (Ishikawa and Barber, 2008). These then enter the nucleus and induce interferon and other cytokine production (Wu *et al.*, 2013).

Interestingly, it appears that although cGAS is not activated by ds- or ssRNA it may play a role in the control of RNA virus replication (Chow *et al.*, 2015). This mechanism of control would not be a direct one in which cGAS would recognise and bind to RNA. Rather it appears that this control is linked to the observation that cells deficient of cGAS exhibit lower basal levels of ISGs, which may allow for a viral replication advantage. The host may not recover from this, even if IFN responses are initiated later in infection.

### 1.7.2. The adaptive immune response

In contrast to the innate immune response, the adaptive immune response is able to distinguish between one pathogen and another (Kindt *et al.*, 2007). Contingent on innate immunity (Iwasaki and Medzhitov, 2015), adaptive immunity is the second line of defence and begins a few days after infection, focusing on eliminating pathogens that evade the innate immune response, or continue in spite of it. This response adapts to recognise, eliminate and remember pathogens, eventually leading to memory (Bonilla and Oettgen, 2010). Unlike innate immune responses with PRRs, adaptive responses are not the same in all organisms of a species but rather are tailored to specific antigenic challenges (Kindt *et al.*, 2007).

There are two main branches of the adaptive immune response, namely humoral and cell-mediated immunity and both are required for a full immune response. The cells involved in adaptive immunity are B lymphocytes which are produced in the bone marrow and T lymphocytes which are produced in the thymus. These lymphocytes then leave these primary lymphoid organs and move to secondary lymphoid organs which include the lymph nodes and the spleen (Bonilla and Oettgen, 2010).

Humoral immunity is the branch of the adaptive immune system in which immunity is mediated by antibodies contained in the host (Kindt *et al.*, 2007). Upon leaving the bone marrow, B-lymphocytes express unique antigen-binding receptors (B-cell receptors) on their membranes, and as such are membrane-bound antibodies. The binding of a matching antigen to the antibody of a naïve B-cell causes the cell to divide rapidly with the progeny differentiating into memory B cells and effector B cells referred to as plasma cells (Kindt *et al.*, 2007). Memory B cells express the same membrane-bound antibody as the parent cell and plasma cells express the same antibody but in a form that can be readily secreted. These secreted antibodies are the major effector molecules of humoral immunity. Antigen coated with antibody can then be eliminated in a number of ways such as ingestion by phagocytic cells, and when on the surface of microorganisms, the initiation of the complement system.

Cell-mediated immunity involves T lymphocytes. As they mature, these cells produce T-cell receptors (TCRs) on their membranes (Kindt *et al.*, 2007). These serve as antigen-binding molecules of cell-mediated immunity. Two subpopulations of T cells exist, namely T helper (TH) and T cytotoxic (TC) cells. Cells with the membrane glycoprotein CD4 on their surface (CD4+) function as TH cells (Bonilla and Oettgen, 2010) and those with CD8 (CD8+) function as TC cells. T regulatory (Treg) cells carry CD4 on their surface but can be distinguished from the other types of T cells by cell surface markers associated with the cells stage of activation.

Unlike the membrane bound antibodies of B cells, TCRs recognise antigens that are bound to cell membrane proteins called major histocompatibility complex (MHC) molecules, and not to free antigens (Maggioni and Braakman, 2005; Kindt *et al.*, 2007). There are to major types of these polymorphic glycoproteins found on cell membranes. MHC class I molecules are expressed by almost all nucleated cells, whereas MHC class II molecules are only expressed by antigen-presenting cells (APCs) which include macrophages, B lymphocytes and dendritic cells. APCs internalise the antigen and then present part of the antigen on the membrane bound to an MHC class I molecule. CD4+ cells only recognise antigen bound to MHC class II molecules on APCs and CD8+ cells only recognise antigen bound to MHC class I molecule (Bonilla and Oettgen, 2010). A TH cell becomes activated after it has recognised and bound an antigen-MHC class II complex, causing it to undergo metabolic transformation and secrete various cytokines. These cytokines are essential for the activation of both humoral and cell-mediated immunity. They activate TC cells, B cells, macrophages, phagocytic cells and other cells involved in the immune response (Kindt *et al.*, 2007). The type of cytokine produced affects the type of immune response seen. At times TC cells can be induced to change into cytotoxic T lymphocytes that exhibit cytotoxic activity and can monitor host cells, killing those that display foreign antigens, such as those that are virus infected.

### 1.8. VIRAL EVASION OF THE IMMUNE SYSTEM

In order for successful infection, viruses need to produce as many viral particles as possible but as discussed above, once inside the cell they are exposed to a number of innate and adaptive responses that are bent on their destruction. Thus, the outcome of infection rests on the ability of the immune system to resist the viral offense and rid the cell of infection (Maggioni and Braakman, 2005; Kindt *et al.*, 2007). The immune system has evolved to counter viral infections but it is not always a match for the infecting virus as viruses are able to evolve at a more rapid pace than the immune system and they are also able to evade the host immune system in a variety of ways (Maggioni and Braakman, 2005).

Some viruses manage to evade the immune system by constantly changing their antigens (Maggioni and Braakman, 2005). Such antigenic variation is the main strategy used by enveloped viruses to mask their highly

immunogenic envelope glycoproteins from the immune system by high levels of variation in the antigenic regions. Inhibition of antigen presentation by infected cells is another way of evading the immune system. This mechanism is used by herpes simplex virus (HSV). HSV-1 and HSV-2 express ICP47, an intermediate-early protein that inhibits the human transporter molecule needed for antigen processing and prevents peptide translocation into the ER (Hill *et al.*, 1995; Kindt *et al.*, 2007). This blocks antigen delivery to MHC class I receptors on HSV-infected cells, in turn preventing antigen delivery to $CD8^+$ T cells. This causes the trapping of empty MHC class I molecules in the ER, effectively shutting down a $CD8^+$ T cell response to HSV-infected cells. Other viruses have been shown to down-regulate MHC class I expression shortly after infection. Adenoviruses and cytomegalovirus (CMV), for example reduce the surface expression of these molecules thereby inhibiting antigenic presentation to $CD8^+$ T cells (Lorenzo *et al.*, 2001; Kindt *et al.*, 2007). The human immunodeficiency virus Nef protein downregulates MHC class I molecules (Lorenzo *et al.*, 2001).

RNA viruses are more susceptible to genetic variation than DNA viruses due to their lack of a proof-reader for replication. This allows such viruses to mutate rapidly and more frequently than DNA viruses and allows such viruses to use mutation as a means to escape the immune system (Alcami and Koszinowski, 2000). Recombination, whereby genetic material is exchanged with related viral or cellular sequences, is common in certain positive-stranded RNA viruses and reassortment is common in viruses with a segmented genome (Maggioni and Braakman, 2005), both making it easier for a virus to evade the immune system.

Due to its importance in innate immunity and the development of an antiviral state, the IFN response is targeted by many viruses. There are several ways in which the IFN response is targeted and some viruses make use of multiple strategies (Beachboard and Horner, 2016; Nelemans and Kikkert, 2019). As such many viruses encode IFN antagonists that function in evading the IFN response.

Evading detection by PRRs is one way of evading innate immunity (Beachboard and Horner, 2016). Dengue virus for example, conceals viral RNA in the intracellular membrane to keep it away from RIG-I and MDA5 detection, which results in poor induction of IFN (Uchida *et al.*, 2014). To limit their PAMP exposure, some viruses, such as arenavirus, make use of a “prime and realign” mechanism to initiate genome synthesis (Marq *et al.*, 2010). The result of this is that 5’pppG is found as an unpaired nucleotide, as opposed to blunt ends, when the complementary genome ends have annealed to form a dsRNA panhandle. RIG-I favours blunt ends; therefore, arenavirus dsRNA panhandle structures are poor PAMPs, and go undetected by cytoplasmic PRRs, thereby clearly reducing the ability of dsRNA to induce IFN. Two mismatches in some arenavirus genome segments may also limit their recognition as PAMPs (Marq *et al.*, 2010). RIG-I is a major PRR for the genome of most negative-sense RNA viruses, including both segmented and non-segmented negative-sense RNA viruses. Some negative strand viruses generate 5’ monophosphate genome ends to avoid the activation of the IFN system (Habjan *et al.*, 2008). RNA isolated from particles of the highly virulent Ebola virus, Nipah

virus, Lassa virus and Rift Valley fever virus strongly activate the IFN-β promoter and it was shown that this induction required RIG-I not MDA5, as well as the 5'ppp group. In contrast to this however, genomic RNAs of Crimean-Congo haemorrhagic fever virus (CCHFV), Borna disease virus and Hantaan virus did not induce IFN. It was shown that this was due to the post-transcriptional removal of the 5'ppp in a process that differs between viruses. Thus, as a consequence of this, RIG-I is not able to bind RNAs of these viruses and the IFN response is not induced (Habjan *et al.*, 2008).

Viruses also target adaptor proteins such as MAVS and the kinases IKKε and TBK1 which act as signal transducers from MAVS or STING, an example of which is Ebola virus protein VP35 (Prins *et al.*, 2009). The inhibition of these kinases prevents their interactions with IRF3 and IRF7, also resulting in poor induction of IFN.

Viruses have been shown to block IFN-induced transcriptional responses and inhibit the activation of IFN effector pathways. This is done mainly by blocking or inhibiting the action of PKR, the phosphorylation of eIF-2α and the RNase L system that may degrade viral RNA (Alcami and Koszinowski, 2000; Beachboard and Horner, 2016). Respiratory syncytial virus (RSV) reduces the phosphorylation of eIF-2α by sequestering PKR away from eIF-2α and binding it to the RSV N protein (Groskreutz *et al.*, 2010). This, in conjunction with an increased association of the phosphatase PP2A with eIF-2α after PKR activation leads to limited phosphorylation of eIF-2α and continued translation of cellular and viral proteins (Groskreutz *et al.*, 2010). IFN-inducible genes are significantly downregulated by human papillomavirus (HPV) infection (Chang and Laimins, 2000). Influenza A virus (IAV) NS1 is the protein largely responsible for the ability of the virus to inhibit IFN production (Krug, 2015). There are, however, functional differences between the NS1 proteins of different strains. IAV NS1 acts in one of two ways to carry this out. Firstly, it can inhibit the activation of IRF3 and IFN transcription and secondly, it can inhibit the processing of IFN pre-mRNAs. NS1 also inhibits PKR (Krug, 2015). Mouse CMV encoded M27 (a STAT2 antagonist) reduces IFN-I responses in myeloid dendritic cells, whereas in macrophages M27, and yet to be identified evasins, inhibit the induction of IFN-I responses (Döring *et al.*, 2014).

Another way of counteracting IFN-mediated innate immunity is by disrupting the normal functioning of the JAK-STAT signalling pathway (Fleming, 2016). For example, many viral proteins can 1) prevent the nuclear translocation of STAT1/2, 2) prevent the phosphorylation of STAT1/2 or 3) promote the nuclear export of STAT1/2 (Melén *et al.*, 2004; Ashour *et al.*, 2009; Mazzon *et al.*, 2009; Fros *et al.*, 2010; Röthlisberger *et al.*, 2010; Fros *et al.*, 2013; Goertz *et al.*, 2018; Feng *et al.*, 2019). It is also possible for viruses to inhibit nuclear translocation after STAT has already been activated and bound to importin-α, as is the case in rotavirus infection (Holloway *et al.*, 2009; Holloway *et al.*, 2014).

BTV uses multiple proteins in its evasion of the host innate immunity (Rojas *et al.*, 2021). BTV NS4 is an IFN-antagonist (Ratinier *et al.*, 2016), and also works together with NS3 to inhibit the JAK-STAT signalling pathway by blocking the phosphorylation and nuclear translocation of STAT1 early in infection, or by downregulating the expression of JAK1 and TYK2 later in the infection cycle (Doceul *et al.*, 2014; Li *et al.*, 2021). It also appears that VP3 associates with MAVS and interferes with RIG-I-like signalling (Pourcelot *et al.*, 2021).

Less is known about the antiviral defence mechanisms of AHSV. Indirect evidence for type I IFN involvement in the control of AHSV infection was suggested by de la Grandière *et al.* (2014) and recent papers have shown that several AHSV4 antigens induce cytotoxic T cell responses *in vitro* (Faber *et al.*, 2016) and that virulent and attenuated AHSV strains differ in their ability to interfere with the host innate immune response (Faber *et al.*, 2021; Faber *et al.*, 2022). The molecular mechanisms and viral proteins involved in this are unknown.

### 1.9. CONCLUDING REMARKS

When this study was initiated, very little information regarding NS4 was available and most of the research that existed had been done on BTV NS4. BTV NS4 is found in the nucleus and cytoplasm of infected cells and is also found in the nucleolus. This, as well as its ability to bind dsDNA, suggested a possible role for the protein in nuclear virus host-interactions. Due to its early expression and localisation to the plasma membrane it was suggested that BTV NS4 may play a role in virus entry and/or exit. It was subsequently shown that BTV NS4 is an interferon antagonist and virulence factor in the host but there is still a knowledge gap regarding the mechanisms used by AHSV to evade the immune system. Like BTV NS4, the AHSV NS4 ORF is conserved across all serotypes, and the expressed protein localises to both the nucleus and cytoplasm of infected cells and binds dsDNA. Therefore, it is possible that AHSV NS4 has similar functions to its BTV counterpart.

### 1.10. AIM AND OBJECTIVES OF THIS STUDY

The aim of this study was to investigate the role of AHSV NS4 in virulence and host immunity.

To this end, the objectives of this study were to:

1. Assess the intracellular colocalisation of AHSV NS4 with other AHSV non-structural proteins and/or host organelles during the AHSV replication cycle.
    - Infect cells with three different AHSV strains each expressing one of the forms of AHSV NS4 and process for immunofluorescence and confocal laser scanning microscopy by performing dual labelling for NS4 and NS1, NS2 or NS3/A. Stain mitochondria and label for NS4.
    - Perform colocalisation analyses on the resulting micrographs using the appropriate software programs.

2. Determine the effect of AHSV NS4 knockout and reassortant viruses on the *in vitro* viral phenotype.
   - Generate AHSV NS4 knockout and reassortant viruses using reverse genetics and compare to wild-type viruses by assessing the expression and intracellular localisation of NS4 in cell culture.
   - Compare the replication kinetics of all reverse genetics-derived viruses to wild-type viruses in cell culture.

3. Determine the effect of AHSV NS4 on virulence using an embryonated chicken egg model.
   - Infect embryonated chicken eggs with each of the reverse genetics-derived viruses generated under objective 2 and compare virulence and pathogenesis to that of the wild-type viruses.

4. Investigate the effect of AHSV NS4 on the host transcriptional response to see if the protein plays a role in the host immune response.
   - Use RNA sequencing to compare the transcriptional response of genes related to innate immunity in horses following inoculation with the recombinant virulent wild-type virus rAHSV5 or the NS4 knockdown strain rAHSV5minNS4.
   - Use interferon treatment and confocal laser scanning microscopy to determine if AHSV NS4 affects the innate immune response by interfering with the JAK-STAT signalling pathway.

# CHAPTER 2

## INVESTIGATING THE COLOCALISATION OF NS4 WITH OTHER AHSV NON-STRUCTURAL PROTEINS AND MITOCHONDRIA

## 2.1. INTRODUCTION

Four non-structural proteins are expressed by AHSV and BTV during infection, and play key roles in the viral replication cycle. NS1, which at 63 kDa is the largest of the non-structural proteins, is encoded by Seg-5 and NS2 (41 kDa) is encoded by Seg-8. NS3 and NS3A (24 and 23 kDa respectively) are encoded from in-frame overlapping reading frames on Seg-10 (van Staden and Huismans, 1991) and NS4 is encoded by Seg-9, which also encodes VP6 in a different reading frame (Firth, 2008; Belhouchet *et al.*, 2010; Belhouchet *et al.*, 2011; Ratinier *et al.*, 2011).

One of the hallmarks of orbivirus infection is the presence of hollow tubular structures in infected cells. These structures are formed by the self-assembly of NS1, and are commonly referred to as tubules (Huismans and Els, 1979; Maree and Huismans, 1997). Although the function of AHSV NS1 remains unclear, BTV NS1, including the non-tubular form of NS1, is a positive regulator of viral protein synthesis (Boyce *et al.*, 2012; Kerviel *et al.*, 2019) and may play a role in virus egress, cellular pathogenesis and morphogenesis of BTV (Owens *et al.*, 2004). BTV NS1 localises to the centrosomal regions of a cell and may therefore also be involved in the disruption of the centrosome as has been observed in BTV-infected mammalian cells, in this way disrupting the cell cycle (Shaw *et al.*, 2013). Although predominantly cytoplasmic, AHSV NS1 has also been observed in the nucleus of infected cells (Venter *et al.*, 2014; Ferreira-Venter *et al.*, 2019).

NS2 is highly expressed in AHSV- and BTV-infected cells and leads to the formation of cytoplasmic VIBs (Thomas *et al.*, 1990; Uitenweerde *et al.*, 1995). These dense structures are the sites of viral replication and virus assembly (Brookes *et al.*, 1993; Kar *et al.*, 2007) and can form in the absence of other viral proteins (Uitenweerde *et al.*, 1995). This phosphorylated protein binds ssRNA (Huismans *et al.*, 1987a; Thomas *et al.*, 1990) and recruits newly transcribed viral mRNA (Lymperopoulos *et al.*, 2003) and the viral proteins needed for core particle assembly (Kar *et al.*, 2007). Due to its ability to bind BTV mRNA over non-specific RNA, NS2 is able to retain viral mRNA within VIBs where they can be used for viral replication and assembly (Modrof *et al.*, 2005). BTV particles are assembled and released from the periphery of VIBs rather than the matrix (Brookes *et al.*, 1993).

NS3 and NS3A are synthesised in equimolar amounts within infected mammalian cells (van Staden *et al.*, 1995) and are involved in viral trafficking and release (Beaton *et al.*, 2002; Celma and Roy, 2009; Meiring *et al.*, 2009; Celma and Roy, 2011; Ferreira-Venter *et al.*, 2019). Release can take place in one of two ways: budding through the plasma membrane (Eaton *et al.*, 1990; Roy, 2001) or via lytic release through a disrupted plasma membrane (Hyatt *et al.*, 1989; Eaton *et al.*, 1990). Non-lytic release is more common in insect cells, whereas lytic release is more common in mammalian cells were observable CPE is observed (Venter *et al.*, 2014). NS3/NS3A is localised in the plasma membrane, especially at sites of viral release, as well as in intracellular smooth surface vesicles (Hyatt *et al.*, 1991; Stoltz *et al.*, 1996). It has previously been suggested

that NS1 may be involved in the transport of mature virus particles from VIBs to the cell membrane where NS3 is involved in virus release (Maree and Huismans, 1997). A study by Owens *et al.* (2004) suggested that the ratio of NS1 tubules to NS3 protein levels in BTV-infected cells is involved in the shift of lytic release of viral progeny to budding. When NS3 levels are low compared to NS1 tubule levels an accumulation of progeny virus occurs in the cytoplasm, leading to lysis and cell death. When NS3 levels are higher, NS3-directed budding of progeny virus is observed (Owens *et al.*, 2004). In addition to its other functions, BTV NS3 also acts as an IFN antagonist (Chauveau *et al.*, 2013).

NS4 is the smallest protein of the AHSV proteins, and its function in the viral replication cycle remains unclear. BTV NS4 is highly conserved across all serotypes (Ratinier *et al.*, 2011), however two clades of AHSV NS4 exist, *i.e.* NS4-I and NS4-II, with only 52% amino acid (aa) identity between the clades (Zwart *et al.*, 2015). NS4-II is larger (154 aa) than NS4-I (144 aa), with several strains in clade II encoding a longer version of NS4-II containing a 15 aa N-terminal NLS (Zwart *et al.*, 2015) hence termed NLS-NS4-II. The AHSV NS4 protein has been observed in the nucleus and cytoplasm of infected mammalian cells, something that is unusual for a dsRNA virus that replicates exclusively in the cytoplasm (Zwart *et al.*, 2015). The NS4 proteins of both AHSV and BTV bind dsDNA, but not dsRNA, suggesting a role for NS4 in nuclear virus-host interactions (Belhouchet *et al.*, 2011; Zwart *et al.*, 2015). Whilst BTV NS4 is also present in the cytoplasm and nucleus, it shows an intranuclear nucleolar localisation (Belhouchet *et al.*, 2011; Ratinier *et al.*, 2011) not observed for AHSV NS4 (Zwart *et al.*, 2015).

BTV NS4 modulates the IFN-response by downregulating mRNA levels of IFN-I and ISGs and downregulating the activities of certain promoters (Ratinier *et al.*, 2016). NS4 is not required for BTV replication in insect cells, mammalian cells, or IFNAR$^{-/-}$ mice (Ratinier *et al.*, 2016). It does, however, confer a replication advantage to BTV in mammalian cells in an IFN-induced state as well as *in vivo* in the host (Ratinier *et al.*, 2011; Ratinier *et al.*, 2016). BTV NS4 was therefore concluded to be an IFN antagonist and a key virulence factor in the host (Ratinier *et al.*, 2016).

Mitochondria are cytoplasmic organelles involved in a wide variety of cellular processes including programmed cell death and the generation of ATP (West *et al.*, 2011). Recent evidence shows that these organelles are also involved in innate immunity and can regulate antiviral signalling (West *et al.*, 2011). Innate immunity is the first line of defense against an invading pathogen, and is initiated when viral dsRNA or ssRNA is recognized by host PRRs (Kell and Gale, 2015), ultimately leading to the production of type I IFN α and β (Randall and Goodbourn, 2008). Several families of PRRs exist, for example TLRs which are membrane-bound, and RLRs which are cytoplasmic. The RLR receptor family includes RIG-I, MDA5 and LGP2. Within innate immunity, mitochondria appear to be involved mainly in RLR signalling, antibacterial immunity and sterile inflammation (West *et al.*, 2011).

The RLR MAVS protein is located on the outer mitochondrial membrane (West *et al.*, 2011; Weinberg *et al.*, 2015), peroxisomes and MAMs (Chow *et al.*, 2015). Interestingly, these membranes are exploited by various RNA viruses for their replication. MAVS are essential for RLR-mediated antiviral immunity to be activated correctly (Weinberg *et al.*, 2015). Upon the recognition of viral RNA, RIG-I and MDA5 interact with MAVS via mutual CARDs (Weinberg *et al.*, 2015), an interaction that is essential for downstream NF-κB and IFN signalling for type I IFN and pro-inflammatory cytokine production (Soubannier and McBride, 2009; West *et al.*, 2011; Weinberg *et al.*, 2015). Mitochondrial MAVS induce type I and type III IFN, whereas peroxisomal MAVS only induce type III (Chow *et al.*, 2015; Weinberg *et al.*, 2015). Several non-structural proteins have been shown to disrupt mitochondrial dynamics. For example, Zika virus non-structural protein 4A (NS4A) blocks the CARD of MAVS, essentially blocking the accessibility of MAVS to RLRs, leading to a way of evading the host immune system (Ma *et al.*, 2018). Rotavirus non-structural protein 1 (NSP1) controls host innate immunity in a variety of ways, one of which is by attenuating MAVS in infected cells, thereby disrupting antiviral signalling (Nandi *et al.*, 2014).

In addition to the roles already found for BTV NS4, several additional roles for NS4 have been suggested in the literature. Its early expression suggests that it may be involved in the early stages of the infection cycle (Belhouchet *et al.*, 2011; Ratinier *et al.*, 2011). BTV NS4 appears to have a structural relatedness to nucleic acid binding proteins that contain coiled-coils or helical structures and are associated with the ER or cell membranes. In particular, BTV NS4 shows strong relatedness to fzo-mitofusin protein which has the mammalian homologues mitofusin 1 (MFN1) and mitofusin 2 (MFN2) (Santel and Fuller, 2001; Eura *et al.*, 2003). These proteins are transmembrane GTPases with a coiled-coil structure (Hales and Fuller, 1997; Koshiba *et al.*, 2004) and are involved in mitochondrial membrane fusion. MFN2 causes the tethering of mitochondria to the ER (de Brito and Scorrano, 2008) and can also cause the clustering of active mitochondria at the perinuclear region (Rojo *et al.*, 2002). Based on its relatedness to fzo-mitofusin, it is possible that NS4 localises to mitochondria. Colocalisation with mitochondria would also suggest a possible role for NS4 in innate immunity (West *et al.*, 2011). Due it its similarities to ER-, lipid-, or membrane associated proteins and its localisation to the plasma membrane late in infection (Belhouchet *et al.*, 2011) BTV NS4 was also suggested to be involved in virus exit, perhaps in association with NS1 and NS3.

Interactions between proteins, and between proteins and organelles, is common in infected cells. Therefore, the aim of this chapter was to determine whether AHSV NS4 colocalises with NS1, NS2, NS3/A or mitochondria. In order to do this, BSR-T7/5 cells were infected with three different AHSV strains and processed for immunofluorescence and confocal laser scanning microscopy (CLSM). The three strains were selected on the basis that each one expresses one of the three forms of NS4, *i.e.,* NS4-I (AHSV4 Field), NS4-II (AHSV1 Field) or NLS-NS4-II (AHSV8 Field) and are therefore representative of all AHSV NS4 variants.

Colocalisation analyses were then performed on the resulting micrographs. Colocalisation of AHSV NS4 with NS1 and/or NS3 would indicate a possible role for NS4 in virus release, while colocalisation with NS2 would indicate a possible role in virus replication and assembly. Colocalisation with mitochondria would indicate a possible role in immunity or that NS4 may act as a transmembrane GTPase and compete against MFN2.

## 2.2. MATERIALS AND METHODS

### 2.2.1. Cells

BSR-T7/5 cells, BSR cells that constitutively express T7 polymerase, were obtained from Prof. AC Potgieter [Deltamune (Pty) Ltd] and used with permission from Ulla Buchholz (Department of Clinical Virology, Federal Research Center for Virus Diseases of Animals, Tubingen, Germany) (Buchholz *et al.*, 1999). The cells were maintained as monolayers in Modified Eagle's Medium with Earle's Balanced Salt Solution (EBSS) and 2.0 mM L-glutamine (MEM, HyClone™), supplemented with 1% non-essential amino acids (NEAA, Sigma-Aldrich®), 5% foetal bovine serum (FBS, Gibco®), 1.2% Fungizone (Sigma-Aldrich®) and 1% Penicillin and Streptomycin (Pen/Strep, Lonza) at 37°C, with carbon dioxide ($CO_2$) and 90% humidity. Geneticin (1 mg/ml, Invitrogen™) was added every third passage. *Spodoptera frugiperda* (Sf9) cells (ATCC CRL-1711) were maintained in suspension cultures or grown as monolayers in TC-100 medium (Lonza) supplemented with 10% FBS, Fungizone (50 mg/l), 1% Pluronic (Sigma-Aldrich®), and 1% Pen/Strep at 28°C.

### 2.2.2. Viruses and titre determination

The viruses used are listed in Table 2.1. The viruses or the components needed for their rescue were received from Prof. AC Potgieter at Deltamune (Pty) Ltd. The plasmid-based reverse genetics protocol for AHSV described by Boughan *et al.* (2020) was used to rescue these viruses. This requires the simultaneous transfection of ten transcription plasmids and six expression plasmids into BSR-T7/5 cells. In the transcription plasmids, complementary DNA (cDNA) of each of the 10 complete AHSV segments of a particular strain was cloned into vector pSMART-T7 in which cDNA is flanked by the phage T7 promoter at the 5' end and a HDV ribozyme at the 3' end. The six expression plasmids contain the ORFs for AHSV VP1, VP3, VP4, VP6, VP7 and NS2 under control of the CMV promoter. The ORFs in the expression plasmids were optimised for expression in Syrian golden hamster cells (BHK and BSR cells). All transcription and expression plasmids used here, were designed by Prof. AC Potgieter at Deltamune (Pty) Ltd and ordered from GenScript Corporation. The expression vector phCMV dream was a kind gift from Prof. PA van Rijn, Wageningen Bioveterinary Research, the Netherlands. The same expression plasmids were used for the rescue of all viruses and mutants and contained the ORFs of AHSV5 (HS 30/62).

**Table 2.1.** Viruses used in Chapter 2, and the type of NS4 protein expressed by each.

| Virus | | Isolate name | NS4 type | GenBank accession number for Seg-9 |
|---|---|---|---|---|
| rAHSV4LP | Rescued by RG | - | NS4-I | KM820857 |
| rAHSV4LPminNS4 | Rescued by RG | - | - | - |
| rAHSV5 | Rescued by RG | - | NS4-II | KM886352 |
| rAHSV5minNS4 | Rescued by RG | - | - | - |
| AHSV4F | Field strain | DM10/14 | NS4-I | MN625129 |
| AHSV1F | Field strain | DM21/11 | NS4-II | MN625126 |
| AHSV8F | Field strain | DM5/15 | NLS-NS4-II | MN625133 |

RG = reverse genetics.

For the rescue of recombinant virulent AHSV5, the cDNA in the transcription plasmids correspond to the sequences of the virulent OIE reference strain of AHSV5 [HS 30/62 – also called Fourie (FR)] as published in Potgieter *et al.* (2015). The rescue of this virus has also been described by Boughan *et al.* (2020). Here, the recombinant virulent virus is referred to as rAHSV5, but it is the same virus as rFR described in the patent of Potgieter *et al.* (2017).

For rescue of recombinant attenuated AHSV4, the cDNA in the transcription plasmids correspond to the sequences of the attenuated strain of AHSV4 which is used as a vaccine in South Africa. This virus was attenuated from the OIE reference strain of AHSV4 (HS 32/62), by 10 passages in suckling mice, 10 passages in BHK cells and selection of viruses which display a large plaque phenotype in Vero cells (Erasmus, 1973). The rescue of the same virus has been published by van de Water *et al*. (2015) in which it was called AHSV4LP. Therefore, in this study the virus will be referred to as rAHSV4LP. The sequences used are reported in the same paper.

rAHSV4LPminNS4 was rescued using the AHSV4LP Seg9minNS4 plasmid with nucleotide substitutions T215C, T260C, T296C, T395C, T440C, T443C, T446C, T458C, T620C and T638C to the wild-type Seg-9 sequence (synthesised by GenScript Corporation) resulting in the M1T, M16T, M28T, M61T, M76T, M77T, M78T, M82T, M136T and M142T in the NS4 ORF. rAHSV5minNS4 was rescued using the AHSV5 Seg9minNS4 plasmid including nucleotide substitutions T194C, T197C, T305C, T377C, T401C, T449C, T452C, T455C, T467C and A551G (synthesised by GenScript Corporation) resulting in the M1T, M2T, M38T, M62T, M70T, M86T, M87T, M88T, M92T, N120S in the NS4 ORF.

Briefly, BSR-T7/5 cells were seeded in T25 cell culture flasks ($1x10^7$ cells). When confluent, the cells were rinsed twice with 5 ml 1 x PBS, followed by the addition of 3 ml Opti-MEM™ I Reduced Serum Medium (Gibco™) and incubation at 37°C, with $CO_2$ and 90% humidity. Each transfection reaction was prepared in a round bottom tube. In tube 1, a 5 µg equimolar mix of expression plasmids was combined with a 5 µg

equimolar mix of transcription plasmids and diluted in 250 µl Opti-MEM™. Alternatively, a ratio of 3 µg expression plasmids to 7 µg transcription plasmids was used. In tube 2, 25 µl of Lipofectamine 2000 (LF2000, Thermo Scientific™) was diluted in 250 µl Opti-MEM™. Each tube was mixed by hand and the tubes were left at RT for 5 min. The contents of tube 1 were then added to the contents of tube 2 in one motion and mixed gently by hand or using a vortex. The tube was then tapped once on the surface of the laminar flow cabinet and incubated at RT for 30 min. The resulting transfection mixture was added directly to the cells containing Opti-MEM™ in a dropwise manner and the flask was incubated for 24 h at 37°C, with $CO_2$ and 90% humidity. The medium in the flask was then replaced with fresh complete DMEM and harvesting of the virus was done when 100% CPE was observed.

The remaining viruses were AHSV field strains from the Deltamune collection: AHSV4 Field (AHSV4F) expressing NS4-I, AHSV1 Field (AHSV1F) expressing NS4-II and AHSV8 Field (AHSV8F) expressing NLS-NS4-II. To obtain fresh viral stocks of each virus, BSR-T7/5 cells ($3.0x10^7$ cells) were infected at a multiplicity of infection (MOI) of 0.1, followed by harvesting the supernatant when total CPE was seen. The supernatant was stored at 4°C. Virus titres were determined by endpoint dilution in BSR-T7/5 cells and expressed as $TCID_{50}$/ml (50% tissue infective dose per millilitre) (Reed and Muench, 1938) and converted to pfu/ml (plaque forming units per millilitre) by multiplying by 0.7.

Additionally, a recombinant baculovirus, BacNS1, expressing wild type AHSV6 NS1 (Lacheiner, 2006) was used to purify NS1 for injection into rabbits (Section 2.4). This virus, and its titre, was obtained from Dr L Zwart (University of Pretoria).

### 2.2.3. Harvesting infected BSR-T7/5 cells for protein expression analysis

Monolayers of BSR-T7/5 cells ($3.8x10^6$ cells) were infected with AHSV at an MOI of 0.1 and incubated at 37°C for 24 hours (h). Thereafter, cells were harvested via low-speed centrifugation at 1 500 x g for 10 minutes (min). The pellet was rinsed twice with 1 x phosphate buffered saline (PBS, 137 mM NaCl, 2.7 mM KCl, 4.3 mM Na2HPO4.2H2O, 1.4 mM KH2PO4, pH 7.3) at low-speed centrifugation (800 x g, 5 min) and then resuspended in 100 µl lysis buffer [0.5% Triton-X 100, 0.15 M STE (0.01 M Tris, 0.001 M EDTA, 0.15 M NaCl)] with a 22G needle. The resuspended pellet was incubated at 4°C for 30 min and stored at -20°C for analysis via Western blot.

### 2.2.4. Generation of anti-NS1 and anti-NS4 sera

To prepare AHSV NS1 for injection into rabbits, Sf9 cells ($1x10^7$ cells) were infected with BacNS1 at an MOI of 7.5 followed by incubation at 28˚C for 72 h. Thereafter, cells were scraped off the bottom of the flask and collected via centrifugation at 800 x g for 5 min at 4˚C. Cells were rinsed with 1 x PBS, then resuspended in 1 ml 0.15 M STE and dounce homogenised. Nuclei were pelleted out via low-speed centrifugation at 166 x g

for 5 min and the supernatant was retained and loaded onto a 40% (w/v) sucrose cushion and centrifuged at 30 000 revolutions per minute (rpm) for 90 min at 4°C in a Beckman Coulter OptimaTM L-80 Ultracentrifuge (SW55Ti rotor). The supernatant was discarded, and the pellet resuspended in 100 µl 1 x PBS. A small volume was used to confirm protein recovery of particulate protein via SDS-PAGE and Western blot analysis (Section 2.2.7) and the remainder was stored at 4°C until injected into rabbits at Deltamune Pty (Ltd). The NS1 antigen was prepared in Montanide™ ISA 70 adjuvant (Seppic, France) according to the manufacturer's instructions. Two rabbits (45B and 786) were injected intramuscularly with 20 µg antigen, followed by a boost (20 µg) on day 21. Both rabbits were anaesthetised with Dormitol®/Ketamine and bled out of the heart. This was done with Deltamune Ethical Committee (DEC) approval number O-15-17. Anti-NS4 sera obtained from blood derived from chickens (R121, R130 and R145), rabbits (O2A and E3F) and a horse were obtained from Deltamune (Pty) Ltd. These were produced against bacterially expressed and purified full length AHSV NS4-II protein with DEC approval number O-15-17 or PD-15-18.

### 2.2.5. Antibodies

Table 2.2 shows the complete list of antibodies that were used in Chapter 2. Some were available for use at the beginning of the study, some were acquired commercially, and several were raised at the animal facilities of Deltamune (Pty) Ltd specifically for this and other studies.

**Table 2.2.** Primary and secondary antibodies used in this study.

| | Name | Biological Source | Species reactivity | Dilution for Western blot | Dilution for IF | Details |
|---|---|---|---|---|---|---|
| **Primary antibodies** | Anti-NS1 | Mouse | | 1:80 | - | AHSV NS1 specific monoclonal antibody (Eurofins Technologies Ingenasa). |
| | Anti-NS1(786) | Rabbit | | 1:100 | 1:500 | Baculovirus expressed AHSV NS1 was prepared by GV Wall (Section 2.2.4.) and antibodies raised in rabbits at Deltamune (Pty) Ltd. |
| | Anti-NS2 | Rabbit | | 1:100 | 1:500 | Bled from rabbits injected with recombinant baculovirus expressed AHSV NS2 (Uitenweerde *et al.*, 1995). |
| | Anti-NS3 | Rabbit | | - | 1:500 | Bacterially expressed AHSV NS3 was prepared by Dr L Ferreira-Venter and antibodies raised in rabbits at Deltamune (Pty) Ltd (Ferreira-Venter *et al.*, 2019). |
| | Anti-NS4(GS) | Rabbit | | 1:100 | 1:100 | Produced in rabbits using a mixture of two NS4 antigenic peptides as the immunogen (GenScript) (Zwart *et al.*, 2015). |
| | Anti-NS4(E3F) | Rabbit | | 1:100 | 1:100 | Produced in rabbits against bacterially expressed and purified full length AHSV NS4-II protein at Deltamune (Pty) Ltd. |
| | Anti-NS4(Ch)* | Chicken | | 1:100 | 1:100 | Produced in chickens against bacterially expressed and purified full length AHSV NS4-II protein at Deltamune (Pty) Ltd. |
| | Anti-NS4(Horse) | Horse | | 1:100 | - | Produced in a horse against bacterially expressed and purified full length AHSV NS4-II protein at Deltamune (Pty) Ltd. |
| **Secondary antibodies** | Goat anti-rabbit HRP | Goat | Rabbit | 1:5 000 | - | Goat anti-rabbit IgG (H + L), HRP conjugate (Invitrogen™, A16110). |
| | Goat anti-chicken HRP | Goat | Chicken | 1:5 000 | - | Goat anti-chicken IgY (H + L), HRP conjugate, affinity purified (Invitrogen™, A16054). |
| | Goat anti-rabbit AF 633 | Goat | Rabbit | - | 1:500 | Alexa Fluor® 633-conjugated goat anti-rabbit IgG (H+L) (Invitrogen™, A21070) |
| | Goat anti-rabbit AF 488 | Goat | Rabbit | - | 1:250 | Alexa Fluor® 488-conjugated goat anti-rabbit IgG (H+L) (Invitrogen™, A11034) |
| | Goat anti-chicken AF 488 | Goat | Chicken | - | 1:2 000 | Alexa Fluor® 488-conjugated goat anti-chicken IgY (H+L) (Invitrogen™, A11039) |

IF = immunofluorescence, GS = GenScript, Ch = Chicken, HRP = horse radish peroxidase, AF = Alexa Fluor®.
*Antibody that was preabsorbed.

### 2.2.6. Preabsorption of anti-NS4(Ch)

The NS4 antibody raised in chicken R121 (Table 2.2) was preabsorbed for use in immunofluorescence and confocal microscopy. One 75 $cm^2$ flask seeded with $3.0x10^7$ BSR-T7/5 cells was incubated at 37°C for 24 h after which cells were collected by low-speed centrifugation (800 x g for 5 min) and resuspended in 0.5 ml 1% blocking solution (1% milk powder in 1 X PBS). Thereafter, cells were lysed via passage through a 22G

needle, and 1% blocking solution and undiluted serum were added to the cell lysate to make a final dilution of 1:100. This was incubated with gentle agitation at room temperature (RT) for 3 h followed by centrifugation at 1 500 x g for 10 min. The supernatant was stored at -20°C for future use.

### 2.2.7. Sodium dodecyl sulphate-polyacrylamide gel electrophoresis (SDS-PAGE)

SDS-PAGE was done under denaturing conditions using 12% (NS1, NS2 or NS3) or 15% (NS4) separating gels (12% or 15 % polyacrylamide, 0.375 M Tris-HCl pH 8.8, 0.1% SDS) and 5% stacking (5% polyacrylamide, 0.125 M Tris-HCl, pH 6.8, 0.1% SDS) gels. Both the separating and stacking gel layers were prepared from 30% acrylamide, 0.8% bisacrylamide (Merck) and polymerised by adding 0.008% (v/v) N,N,N',N' tetramethylethylene diamine (TEMED, Sigma-Aldrich®) and 0.08% (m/v) ammonium persulphate (Roche Applied Science). Samples were resuspended in 3 x protein solvent buffer (PSB, 0.188 mM Tris-HCl pH=6.8; 6% SDS; 30% glycerol; 15% 2-mercaptoethanol; 0.005% bromophenol blue) followed by further denaturation of the samples by heating to 95°C for 3 min. Electrophoresis was done at 130 V for 2-2.5 h in 1 x Tris-Glycine-SDS (TGS, 25 mM Tris-HCl pH 8.3, 192 mM glycine, 0.1% SDS) buffer. Proteins were visualised by staining the gels in Coomassie Brilliant Blue staining solution (0.125% Coomassie Blue, 50% methanol, 10% acetic acid) for 30 min at RT followed by destaining in 5% methanol, 5% acetic acid at RT overnight.

### 2.2.8. Western blot analysis

Proteins that had been separated by SDS-PAGE were transferred to a nitrocellulose membrane (Amersham™ Hybond™ C extra or Amersham™ Protran® nitrocellulose membrane, GE Healthcare) at 100 V for 1 h in the presence of Towbin's transfer buffer (25 mM Tris, 192 mM glycine, 20% methanol, pH 8.3). Membranes were then blocked with 1% (w/v) skimmed (nonfat) milk powder in 1 x PBS for 30 min to 1 h, followed by overnight incubation (with gentle agitation) with the appropriate primary antibody (Table 2.2) diluted in 1% blocking solution. Membranes were subsequently washed three times with wash buffer (0.05% Tween-20 in 1 x PBS, 5 min) and incubated with the appropriate secondary antibody (Table 2.2) or protein A horseradish peroxidase (HRP) conjugate (Calbiochem®, 1:10 000) or recombinant protein G-HRP (Invitrogen™, 10-1223, 1:5 000) for 1 h at RT. This was followed by washing three times with wash buffer and rinsing once with 1 x PBS before transferring the membranes to an enzyme-substrate solution consisting of 60 mg 4-chloro-1-napthol in 20 ml ice-cold methanol, mixed with 60 µl hydrogen peroxide in 100 ml 1 x PBS directly before use. Membranes were incubated at RT until bands became visible followed by rinsing with $dH_2O$ to stop the detection reaction.

### 2.2.9. Immunofluorescence and confocal microscopy

BSR-T7/5 cells grown on sterile coverslips in 24-well plates were infected at an MOI of 0.1-1 . Cells were rinsed with 1 x PBS at 24 hpi, and fixed with 4% paraformaldehyde (PFA, Sigma-Aldrich®) for 30 min at RT. The cells were then permeabilized with 0.2% Triton X-100 (TX-100) for 10 min at RT and blocked using 5%

blocking solution (5% milk powder in 1 x PBS). Primary antibody labelling was done with the appropriate antibody (Table 2.2) diluted in 1% blocking solution and left overnight at 4°C. Cells were washed three times with wash buffer, followed by secondary antibody (Table 2.2) labelling for 1 h at RT. In the case of dual labelling, both primary antibodies were diluted in 1% blocking solution and added at the same time and the same was done for the secondary antibodies. Excess antibody was washed off with wash buffer and two rinses of 1 x PBS and nuclei were stained with 10 µg/µl 4',6-diamidino-2-phenylindole (DAPI, Roche Applied Science) for 10 min at RT. The cells were rinsed a final time with 1 x PBS and the coverslips mounted onto glass slides using VECTASHIELD Mounting Medium (Vector Laboratories). All slides were viewed using a Zeiss Zeiss LSM 510 Meta Confocal Laser Scanning Microscope (CLSM) or a Zeiss LSM 880 CLSM coupled to an Airyscan detector.

### 2.2.10. MitoTracker® staining

The staining of mitochondria followed by NS4 labelling required modifications to the manufacturer's instructions. Cells were infected as above, and at 24 hpi cells were rinsed once with 1 x PBS after which 1000 nM MitoTracker® stain (MitoTracker® Deep Red FM, Invitrogen™) diluted in 1 x PBS was added to the coverslip. Coverslips were incubated at 37°C with $CO_2$ and 90% humidity for 45 min. The stain was rinsed off with 1 x PBS and the cells fixed with 4% PFA for 30 min at RT. The cells were rinsed twice with 1 x PBS and then permeabilised with ice-cold acetone for 5 min. Thereafter, cells were rinsed twice with 1 x PBS. NS4 labelling and DAPI staining were done as above from the blocking step onward (Section 2.2.9). Slides were viewed with a Zeiss LSM 510 Meta CLSM or a Zeiss LSM 880 CLSM coupled to an Airyscan detector.

### 2.2.11. Colocalisation analysis

Colocalisation analyses were done using the Fiji (ImageJ, version 1.52h) or Zeiss ZEN 3.3 (Blue edition, ©Carl Zeiss Microscopy GmbH) software packages. Fiji was used to compare pixels in one channel (green) with the corresponding pixels in the second channel (red). Colocalised pixels would appear yellow. A threshold of 38-50 for hue was used to represent yellow. Colocalised pixels were then indicated in white in the merged image generated by the software. Alternatively, the JACoP plugin (Bolte and Cordelieres, 2006) was used to calculate the Pearson's correlation coefficient. For fluorescence intensity profiles, a line was drawn across a region of interest using ZEN software and fluorescence intensity plots obtained. Graphs were redrawn in Microsoft Excel for presentation purposes. Non-random colocalisation occurs when the profiles of both channels show the same pattern at the same place.

## 2.3. RESULTS

### 2.3.1. Producing anti-NS1 serum in rabbits and testing of all primary antibodies

The aim of this section was to investigate the colocalisation of NS4 with AHSV NS1, NS2 and NS3 and mitochondria via immunofluorescence and confocal microscopy. Thus, reliable antibodies against each non-structural protein were needed. At the beginning of this study verified antibodies against NS2 and NS3 were available for use, both of which were raised in rabbits (Table 2.2). In addition to this, a commercially acquired rabbit antibody, designated anti-NS4(GS) (Zwart *et al.*, 2015) and a small quantity of a commercially acquired antibody directed against NS1 were available. There was a need for an additional antibody directed against NS1.

As the sera against the other non-structural proteins were raised in rabbits, it was decided to also raise a new anti-NS1 antibody in rabbit. To this end, Sf9 cells were infected with BacNS1 after which NS1 was purified through a sucrose cushion. To confirm that NS1 had been recovered, SDS-PAGE was performed (Figure 2.1A). Although multiple bands were observed on the SDS-PAGE gel, a predominant band corresponding to the size of NS1 was observed. As this antibody was not to be used in baculovirus-infected cells, it was anticipated that the low level of background proteins present in the sample would not influence the reliability of the resulting antibody. The bulk of the recovered protein was injected into rabbits at Deltamune (Pty) Ltd. Serum from two different rabbits was obtained and both were tested via Western blot analysis of BSR-T7/5 cells infected with rAHSV4LP or rAHSV5 (Table 2.1). Figure 2.1B shows that while both batches of anti-NS1 detected the protein (~63 kDa), batch 786 gave a stronger signal on a Western blot and was therefore chosen for downstream analyses. The anti-NS2 serum was also tested via Western blotting on BSR-T7/5 cells infected with rAHSV4LP or rAHSV5 and showed good labelling of NS2 (~41 kDa, Figure 2.1C). Anti-NS3 was confirmed to be specific for AHSV NS3 (Ferreira-Venter *et al.*, 2019). Therefore, these antibodies were successfully detecting NS1, NS2 and NS3 via Western blot.

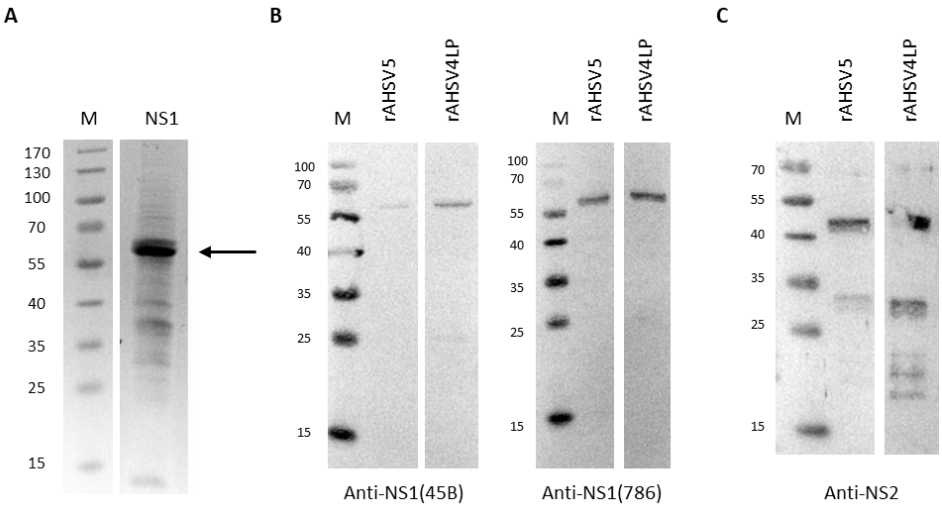


**Figure 2.1. NS1 purification and testing of anti-NS1 and anti-NS2 specificity.** Sf9 cells were infected with BacNS1, harvested at 72 hpi, and NS1 purified using a sucrose cushion and analysed via SDS-PAGE (A). The position of NS1 is indicated by the arrow. The specificity of the anti-NS1(45B) and anti-NS1(786) sera generated in rabbits at Deltamune (Pty) Ltd and anti-NS2 were determined by infecting BSR-T7/5 cells with rAHSV5 or rAHSV4LP and assaying the whole cell lysates for the presence of NS1 (B) or NS2 (C). M = PageRuler™ Prestained Protein Ladder, sizes of molecular weight markers are indicated on the left (kDa).

Western blotting of BSR-T7/5 cells infected with rAHSV4LP, rAHSV4LPminNS4, rAHSV5 or rAHSV5minNS4 were used to test all antibodies directed against NS4. rAHSV4LP expresses NS4-I, which is ~20 kDa in size, and rAHSV5 expresses the larger NS4-II (~23 kDa). The minNS4 variants were engineered to lack NS4 expression and were used to determine if the anti-NS4 sera were specific for NS4. The commercially acquired antibody designated anti-NS4(GS) (Table 2.2) was used to confirm whether the viruses were expressing NS4. As seen in Figure 2.2A, bands corresponding to the sizes of NS4-I and NS4-II were observed. No bands were detected in the lysates of cells infected with rAHSV4LPminNS4 or rAHSV5minNS4, as expected. In order to do dual labelling of NS1, NS2 and NS3 with NS4, it was necessary to have an anti-NS4 antibody raised in an organism other than rabbit. Thus, anti-NS4 sera raised in one horse horses and three chickens (Table 2.2) were tested. All sera detected both forms of NS4 (Figure 2.2B and C), but the horse serum showed more background labelling than what was observed for the chicken sera. Anti-NS4(ChR121) showed low levels of background whilst still detecting both types of NS4 and was therefore chosen for dual labelling. Analysis of anti-NS4 sera from two rabbits, O2A and E3F, showed that both sera detected NS4 and that E3F gave less background than O2A (Figure 2.2D). This antibody could be used to detect NS4 in conjunction with the staining of mitochondria using MitoTracker®. All NS4 antibodies were raised against mixture of two NS4 antigenic peptides or full length AHSV NS4-II, therefore it is possible that NS4-II was detected better than NS4-I due to better recognition of the epitopes on NS4-II.

The following antibodies were subsequently tested in immunofluorescence and CLSM: anti-NS1(786), anti-NS2, anti-NS3, anti-NS4(ChR121) and anti-NS4(E3F). In all cases cells were grown on glass coverslips, infected with rAHSV5 or rAHSV5minNS4 and processed for CLSM at 24 hpi. Some optimisation of antibody dilution

was done (not shown) and only the final dilutions are shown here. The anti-NS1, anti-NS2 and anti-NS3 antibodies gave little to no background labelling in confocal microscopy and detected the relevant protein's localisation accurately (Figure 2.3). The tubule bundles characteristic of AHSV NS1 expression were observed in infected cells, as were the viral inclusion bodies characteristic of NS2. Perinuclear staining (typical of ER/Golgi localisation) and well as some staining on the plasma membrane was observed in the case of labelling for NS3.

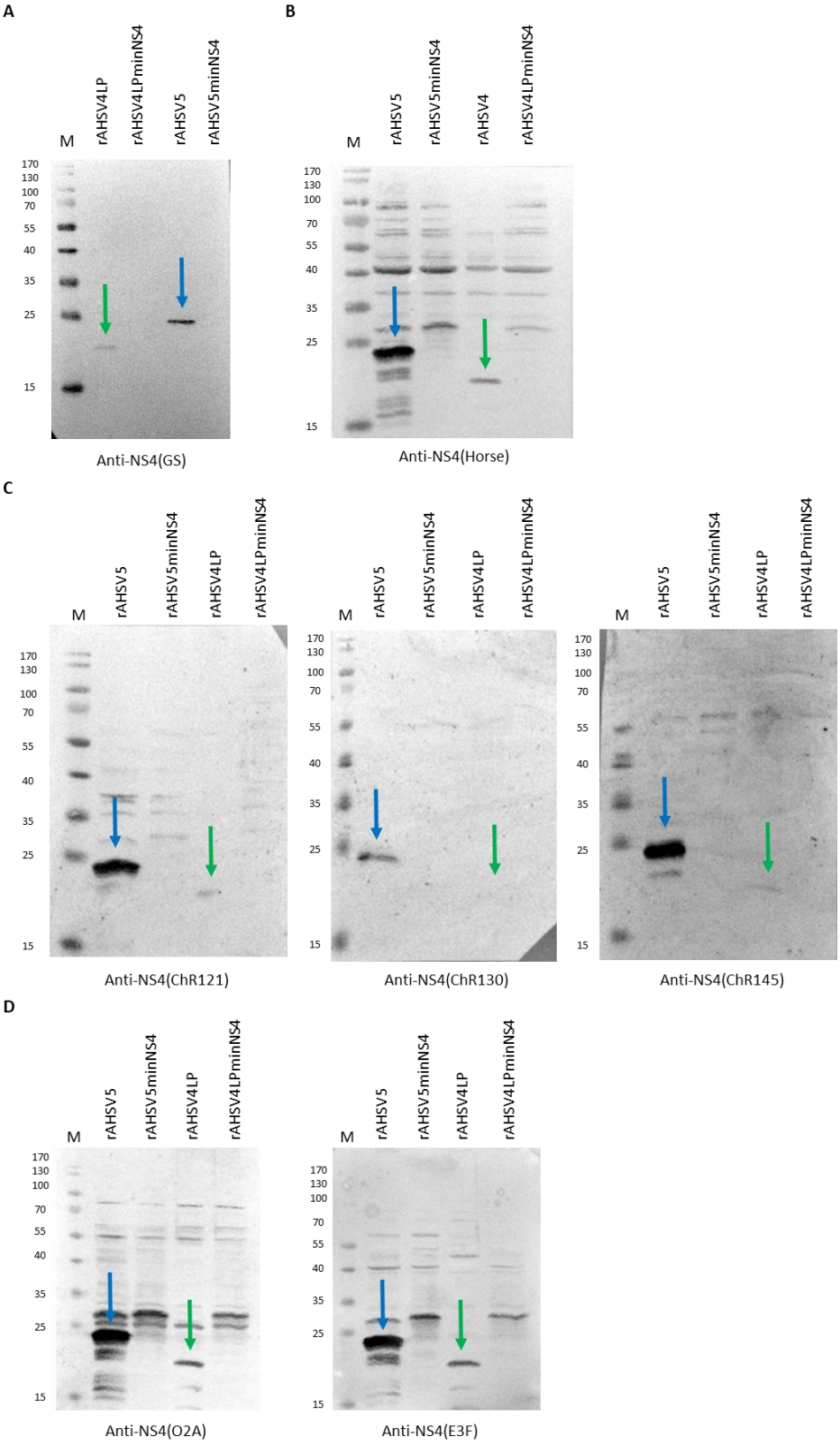


**Figure 2.2. Western blot analysis of anti-NS4 antibodies.** BSR-T7/5 cells infected with rAHSV4LP, rAHSV4LPminNS4, rAHSV5 or rAHSV5minNS4 were harvested and whole cell lysates separated by SDS-PAGE. Membranes were labelled with anti-NS4(GS) (A), anti-NS4(Horse) (B), anti-NS4(ChR121), anti-NS4(ChR130) or anti-NS4(ChR145) (C) or anti-NS4(O2A) or anti-NS4(E3F) (D). The green arrow indicates the position of NS4-I (~20 kDa) and the blue arrow indicates NS4-II (~23 kDa). M = PageRuler$^{TM}$ Prestained Protein Ladder, sizes of molecular weight markers are indicated on the left (kDa).

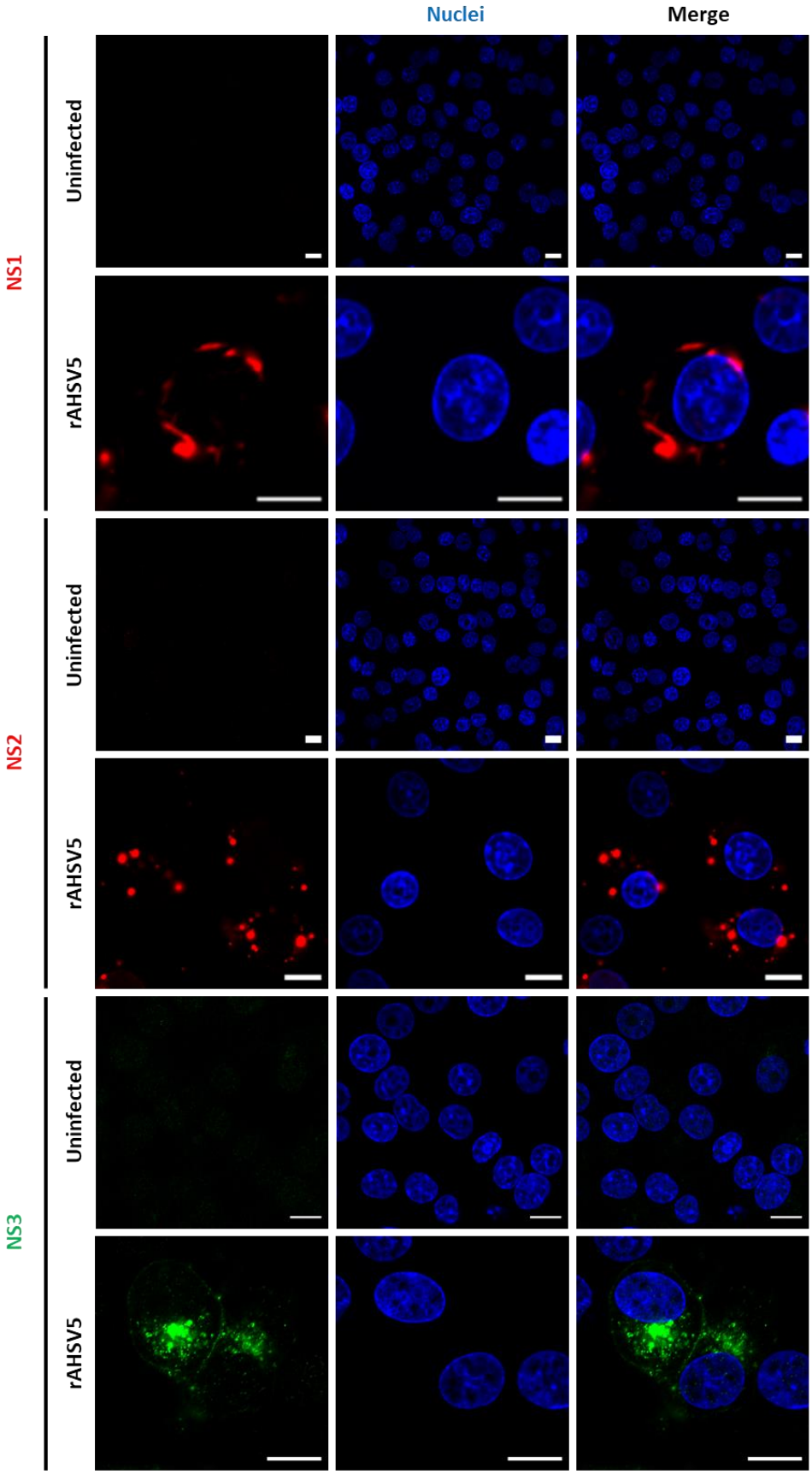


**Figure 2.3. Preliminary analyses of primary antibodies directed against NS1, NS2 and NS3.** BSR-T7/5 cells were mock infected or infected with rAHSV5 and processed for immunofluorescence and CLSM using anti-NS1(786), anti-NS2 or anti-NS3 primary antibodies and AF 633 conjugated goat anti-rabbit IgG (red) or AF 488 conjugated goat anti-rabbit IgG (green) secondary antibodies. Nuclei were stained with DAPI. Scale bar = 10 µm.

Next, the anti-NS4(E3F) and anti-NS4(ChR121) antibodies were tested. The anti-NS4(ChR121) antibody displayed some cellular background (not shown) and was therefore preabsorbed with a BSR-T7/5 cell extract prior to further use. NS4 showed a homogeneous, predominantly cytoplasmic distribution with weaker labelling also observed throughout the nucleus of infected BSR-T7/5 cells (Figure 2.4). This corresponded to the profile described previously for all AHSV strains expressing NS4-II (Boughan *et al.*, 2020). The same pattern was observed at a low intensity in some cells infected with rAHSV5minNS4. This suggested some low-level expression of NS4 by rAHSV5minNS4 that was not detected via Western blot, likely due to that procedure not being as sensitive as CLSM. This problem was addressed in Chapter 3.

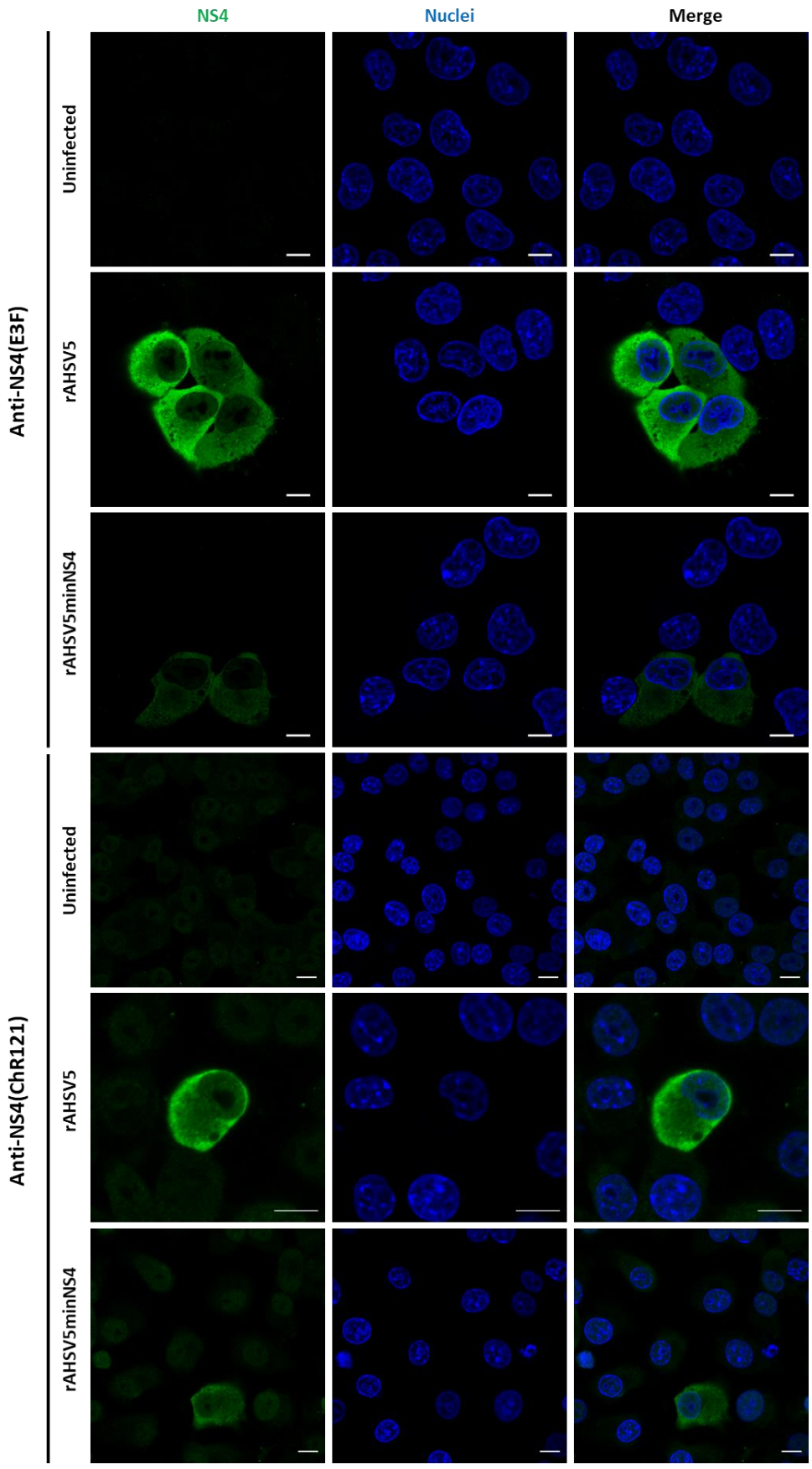


**Figure 2.4. Preliminary analyses of the anti-NS4 primary antibodies raised in rabbit and chicken.** BSR-T7/5 cells were mock infected or infected with rAHSV5 and processed for immunofluorescence and CLSM using anti-NS4(E3F) or anti-NS4(ChR121) primary antibodies and AF 488 conjugated goat anti-rabbit IgG or AF 488 conjugated goat anti-chicken IgY secondary antibodies. Nuclei were stained with DAPI. Scale bars = 10 µm.

Based on these results, all antibodies were deemed suitable for use in downstream analyses.

### 2.3.2. MitoTracker® staining of mitochondria

The staining of mitochondria was done with MitoTracker® Deep Red FM. This mitochondrial stain was chosen as it labels active mitochondria, can passively diffuse through the plasma membrane and is retained after fixation. It is also suitable for use in multicolour experiments, due to its red fluorescence being distant from green fluorescence in the colour spectrum thereby minimising the chances of bleed through. This required some optimisation in order to obtain clear staining of the organelle in BSR-T7/5 cells. Shown here are the optimised conditions of staining with 1000 nM MitoTracker®, followed by fixation with 4% PFA and permeabilisation with ice-cold acetone (Figure 2.5). This resulted in good staining of the organelles and as expected mitochondria were observed in the cytoplasm and were not present in the perinuclear area.

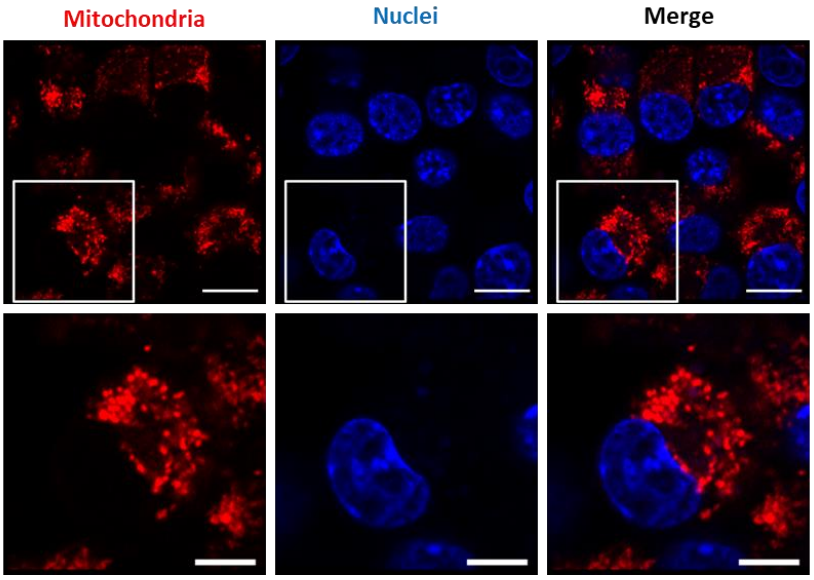


**Figure 2.5. Optimisation of MitoTracker® staining.** Uninfected BSR-T7/5 cells were stained with 1000 nM MitoTracker® diluted in 1 X PBS before fixation with 4% PFA and permeabilisation with ice-cold acetone. The area demarcated by the white block is enlarged in the row beneath. Nuclei were stained with DAPI. Scale bars = 10 µm, row 1; 5 µm, row 2.

### 2.3.3. Expression and intracellular localisation of NS4 in AHSV4F-, AHSV1F- and AHSV8F-infected cells

The AHSV field strains of serotypes 1, 4 and 8 were chosen for use in the colocalisation analyses as they are representative of all three types of NS4. AHSV4F expresses NS4-I, AHSV1F expresses NS4-II and AHSV8F expresses NLS-NS4-II (Table 2.1) (Boughan *et al.*, 2020). To confirm that the viruses were expressing the correct type of NS4, BSR-T7/5 cells were infected with each of the field strains and processed for Western blot analysis with anti-NS4(GS). As expected AHSV1F expressed a protein of ~23 kDa in size, corresponding to NS4-II and AHSV4F expressed a protein of ~20 kDa in size, corresponding to NS4-I (Figure 2.6A). Two bands of ~30 kDa and ~23 kDa were observed in the case of AHSV8F infection. The larger band represents full length NLS-NS4-II and the smaller band is thought to represent NS4-II due to downstream translation initiation of

the in-frame NS4-II start codon (Boughan *et al.*, 2020). The extra bands observed in the case of AHSV4F and AHSV8F were observed as a result of over-development of the membrane.

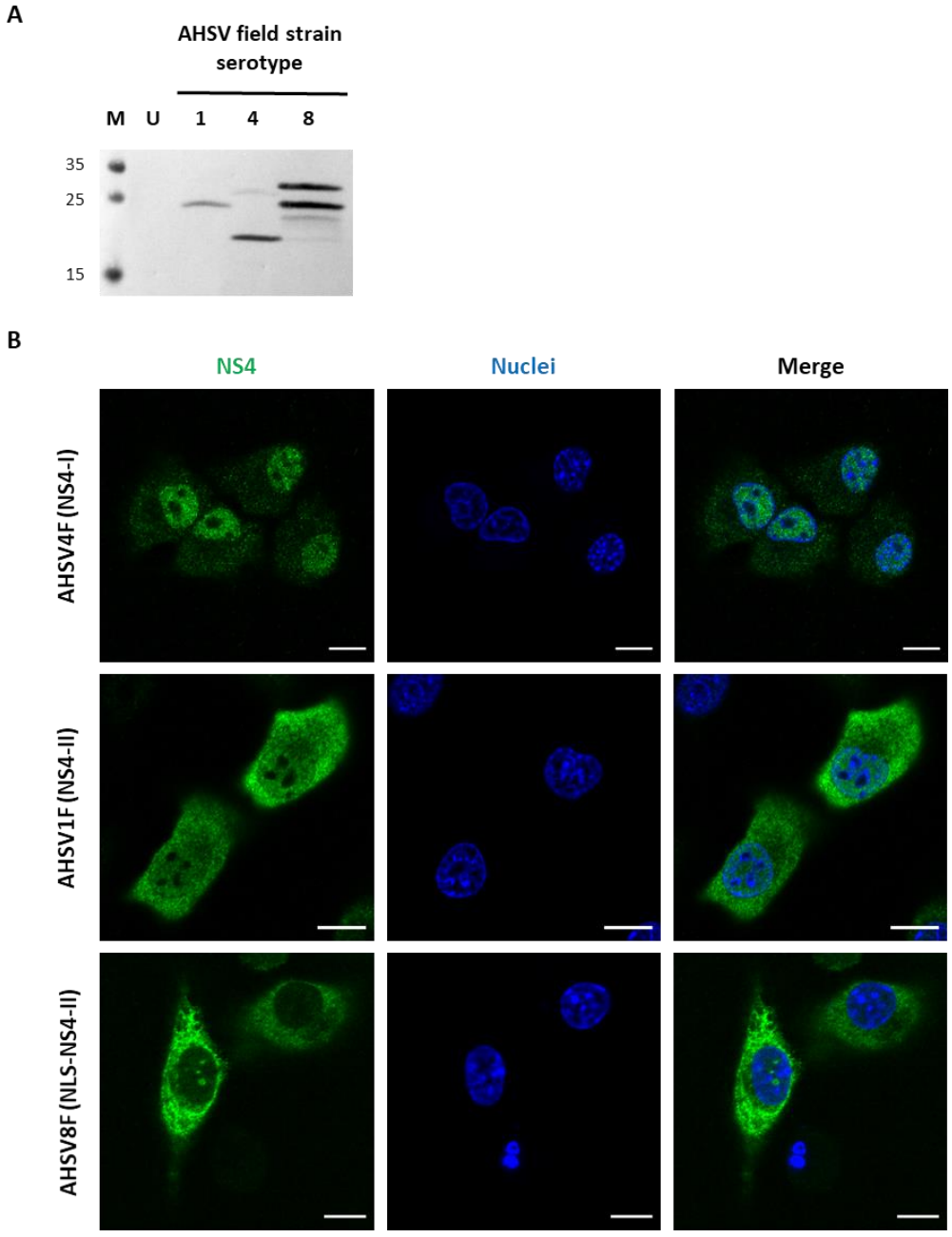


**Figure 2.6. NS4 expression and intracellular localisation in AHSV4F-, AHSV1F- and AHSV8F-infected BSR-T7/5 cells.** (A) BSR-T7/5 cells were infected with AHSV4F, AHSV1F or AHSV8F and at 24 hpi were harvested for Western blot analysis using anti-NS4(GS) and protein A HRP conjugate. M = PageRuler™ Prestained Protein Ladder, sizes of molecular weight markers are indicated on the left (kDa). (B) BSR-T7/5 cells were infected with AHSV4F, AHSV1F or AHSV8F and at 24 hpi were processed for immunofluorescence and CLSM using anti-NS4(ChR121) primary and AF 488 conjugated goat anti-chicken IgY secondary antibodies. Nuclei were stained with DAPI. Scale bars = 10 µm.

The intracellular localisation patterns of each NS4 type were then investigated via immunofluorescence and CLSM. BSR-T7/5 cells were seeded on sterile coverslips, infected with AHSV4F, AHSV1F or AHSV8F and processed for CLSM at 24 hpi using anti-NS4(Ch121) primary and AF 488 conjugated goat anti-chicken IgY

secondary antibodies. As expected, NS4-I displayed a predominantly nuclear localisation pattern in AHSV4F-infected cells (Figure 2.6B). NS4-II was found homogenously in the nucleus and cytoplasm and confirming what was seen previously, NLS-NS4-II showed a homogenous cytoplasmic signal accompanied by distinct foci within the nucleus of some cells (Boughan *et al.*, 2020). Therefore, infection with each field strain gave the expected expression and intracellular localisation pattern of NS4 and confirmed that they were indeed representative of each NS4 type.

### 2.3.4. Colocalisation analyses of NS4 with different non-structural proteins and mitochondria

Next, colocalisation analyses were done on BSR-T7/5 cells infected with AHSV4F, AHSV1F or AHSV8F in order to investigate whether AHSV NS4 colocalises with the other AHSV non-structural proteins or with mitochondria.

#### 2.3.4.1. NS1 and NS4

Firstly, it was investigated whether NS4 colocalises with non-structural protein NS1. This protein forms distinct tubules approximately 23 nm in diameter and up to 4 µm in length within infected cells (Huismans and Els, 1979; Maree and Huismans, 1997) and are viewed as tubule arrays/bundles with CLSM, rather than as the individual NS1 tubules that can be observed via transmission electron microscopy (TEM) (Ferreira-Venter *et al.*, 2019).

In this section, the green channel represents NS4, and the red channel represents NS1. Using ZEN software, uninfected cells were used to determine the baseline fluorescence intensity signal for each channel (Figure 2.7A) and served as the control. The fluorescence intensities of both channels were measured along the line drawn in the micrograph and the resulting plot is shown in Figure 2.7A. The profiles of both channels were essentially straight lines at a value of 10 000 on the y-axis. Therefore, the baseline for all remaining graphs was set at 10 000 on the y-axis and any deviations from this were considered positive signal.

NS1 was detected in the nucleus and cytoplasm of AHSV4F-infected cells. In most cases, NS4-I colocalised with NS1 at one or more point along the length of tubule bundles found in the nucleus. This is shown in Figure 2.7B where a line was drawn across the width of a tubule. In this instance, the red and green fluorescence profiles peak at the same place, indicating non-random colocalisation. The same was observed in the cytoplasm (Figure 2.7C). Of the three types of NS4, NS4-I is often difficult to detect. This was the case here and at times the signal was rather grainy, therefore Fiji was used to confirm what was obtained using ZEN. The merged images were compared and the colocalised pixels were indicated in white in Figure 2.7B and C. Colocalised pixels were observed on the perimeter of NS1 bundles in both images, confirming what was observed using ZEN software. Although only one fluorescence intensity profile was shown per image the data obtained from Fiji (white pixels) show that overall, there is limited colocalisation of NS4-I and NS1.

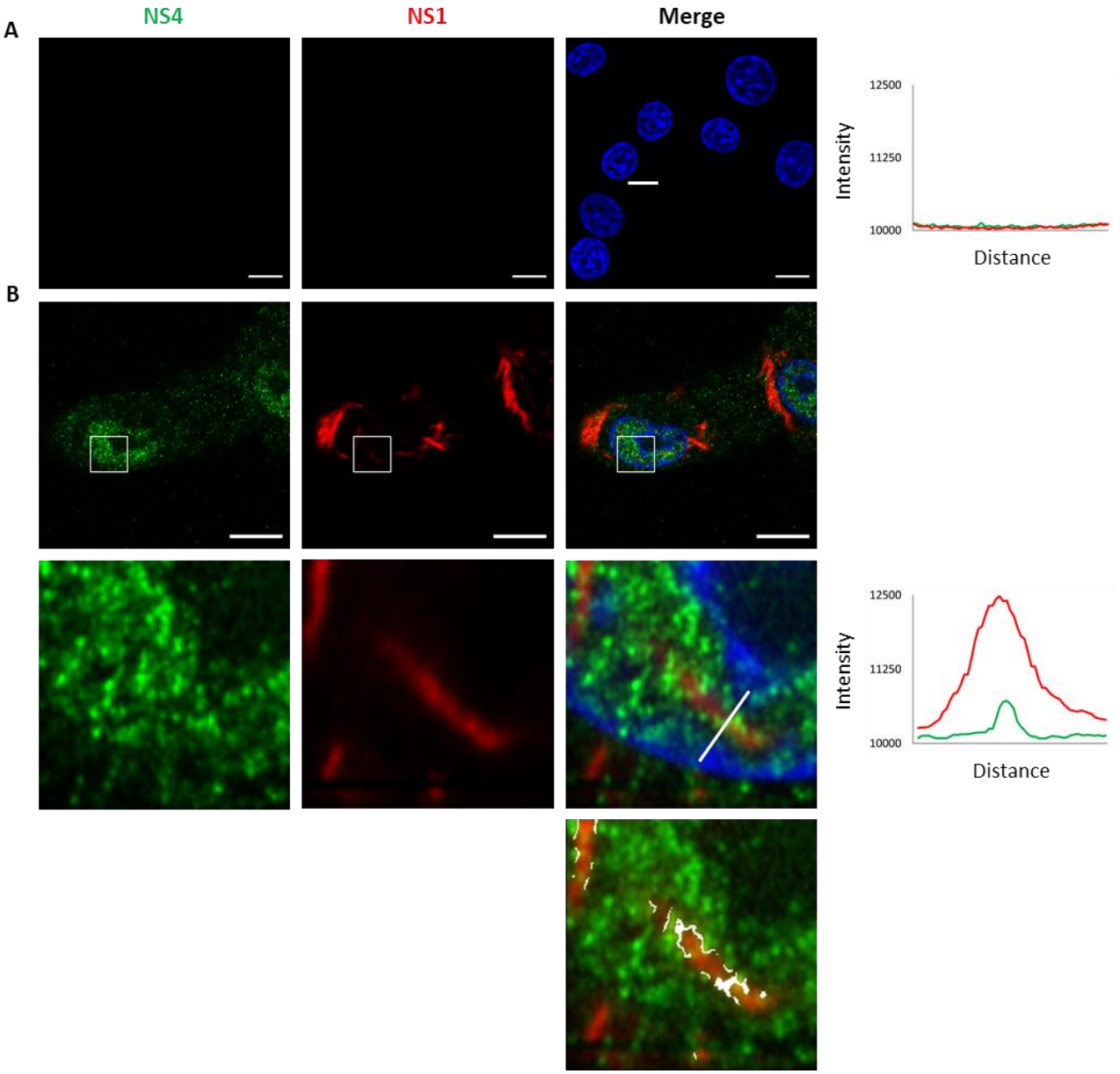

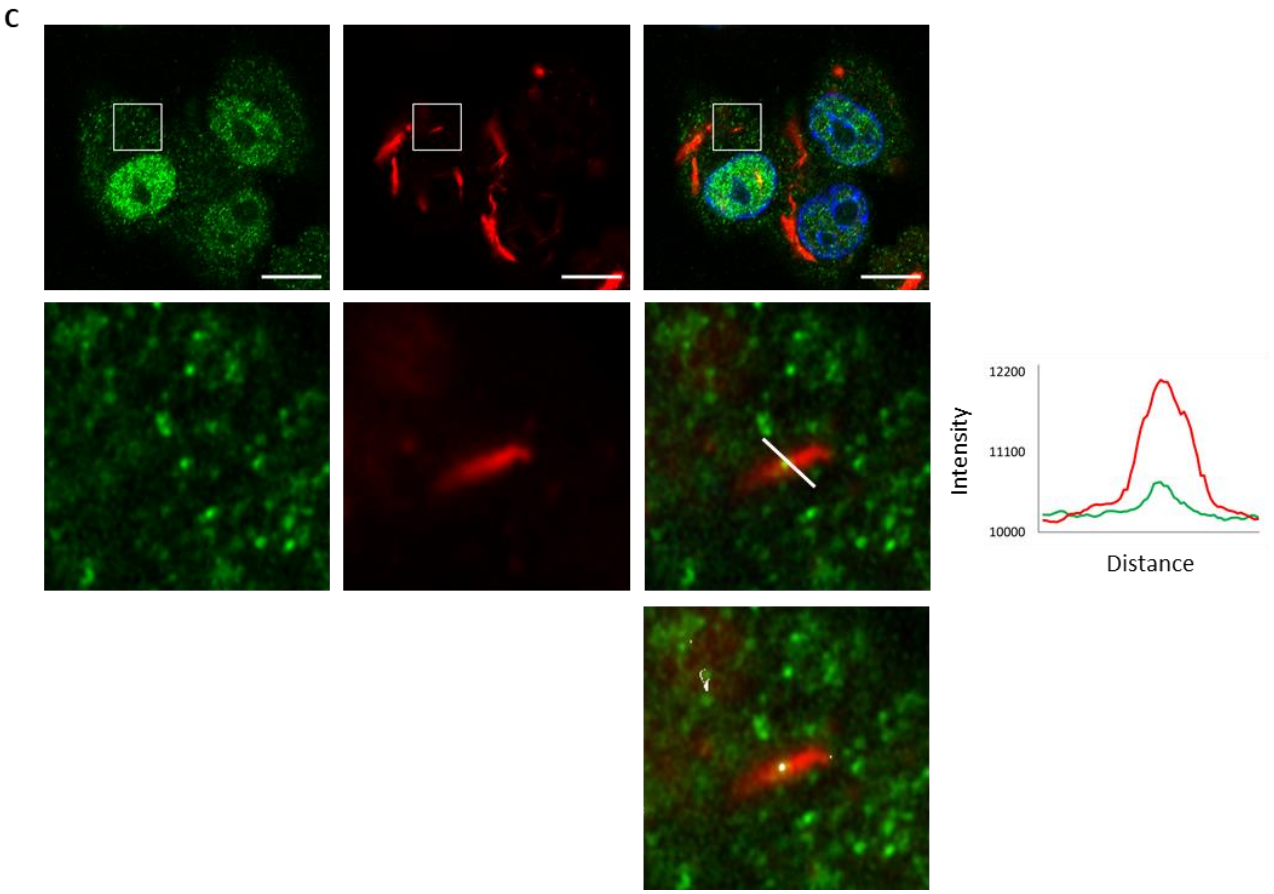


**Figure 2.7. NS4-I shows limited colocalisation with NS1 tubule bundles.** BSR-T7/5 cells were left uninfected (A) or infected with AHSV4F (B and C), which expresses NS4-I, and dual labelled with anti-NS4(ChR121) and anti-NS1(786) at 24 hpi. Secondary labelling was done with AF 488 conjugated goat anti-chicken IgY and AF 633 conjugated goat anti-rabbit IgG. (B) NS1 in the nucleus. (C) NS1 in the cytoplasm. Each second row in B and C shows an enlargement of the demarcated areas in the micrographs in the previous row. Fluorescence intensity plots were generated by measuring the fluorescence intensity of each channel along the white line drawn in the merged images. Each third row in B and C shows colocalised pixels (white) as determined by Fiji. Nuclei were stained with DAPI. Scale bars = 10 µm.

Next, AHSV1F-infected cells were investigated. This virus expresses NS4-II, which is found homogenously throughout the nucleus and cytoplasm of infected cells and was observed in Figure 2.8. Once again, NS1 tubule bundles were found in the nucleus and cytoplasm of infected cells. Very little colocalisation of nuclear NS1 and NS4-II was indicated by the fluorescence intensity profile in Figure 2.8A. Although some NS1-NS4 colocalisation was observed in the cytoplasm (Figure 2.8B), majority of cells resulted in a negligible result for the intensity profile of the green channel (Figure 2.8C). This was contradictory to what was observed with the eye and may have been due to the intensity of the red fluorescence influencing the results. Therefore, Fiji was used to analyse the data. Colocalised pixels were found at the perimeter of NS1 bundles in all three images (Figure 2.8).

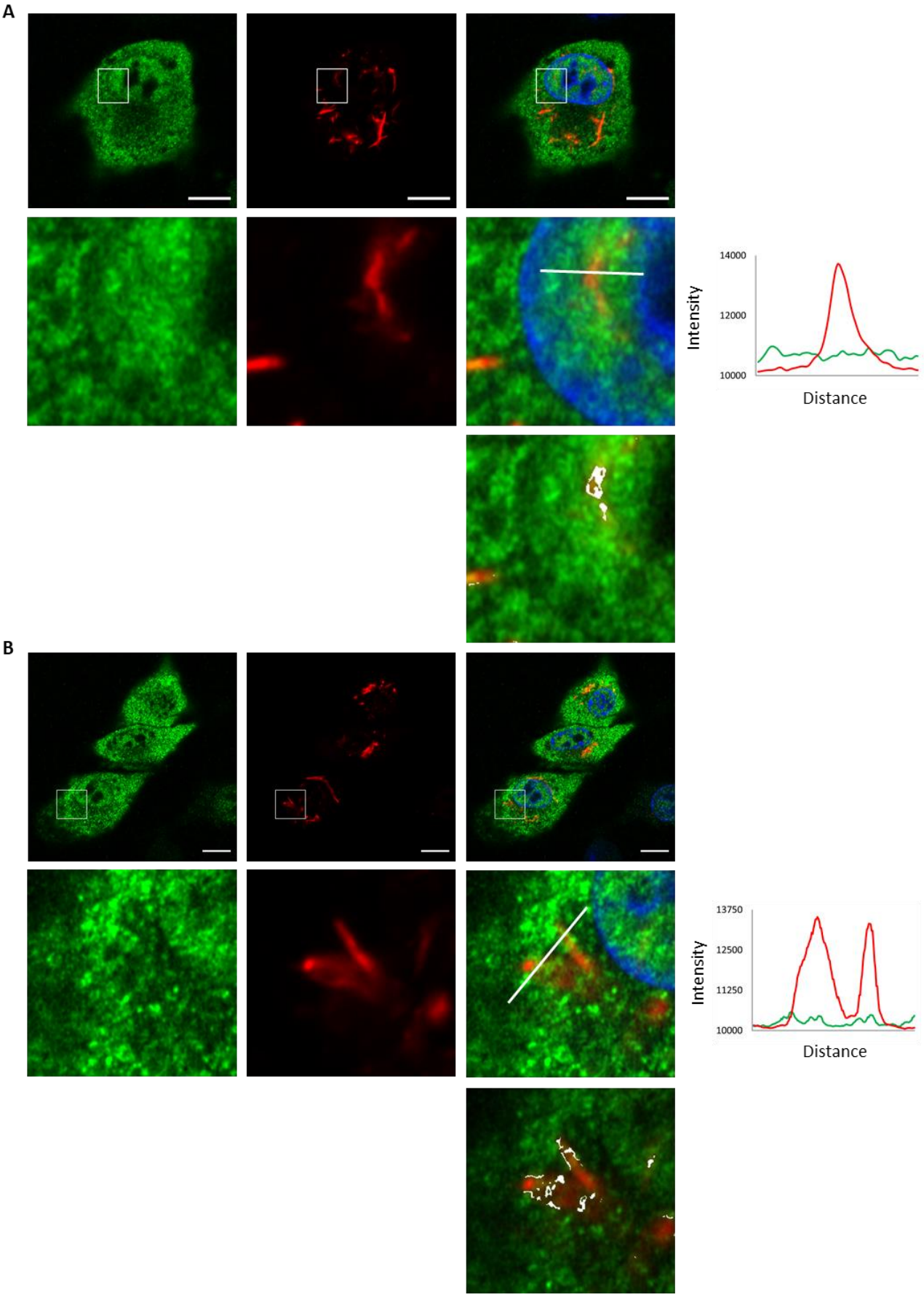

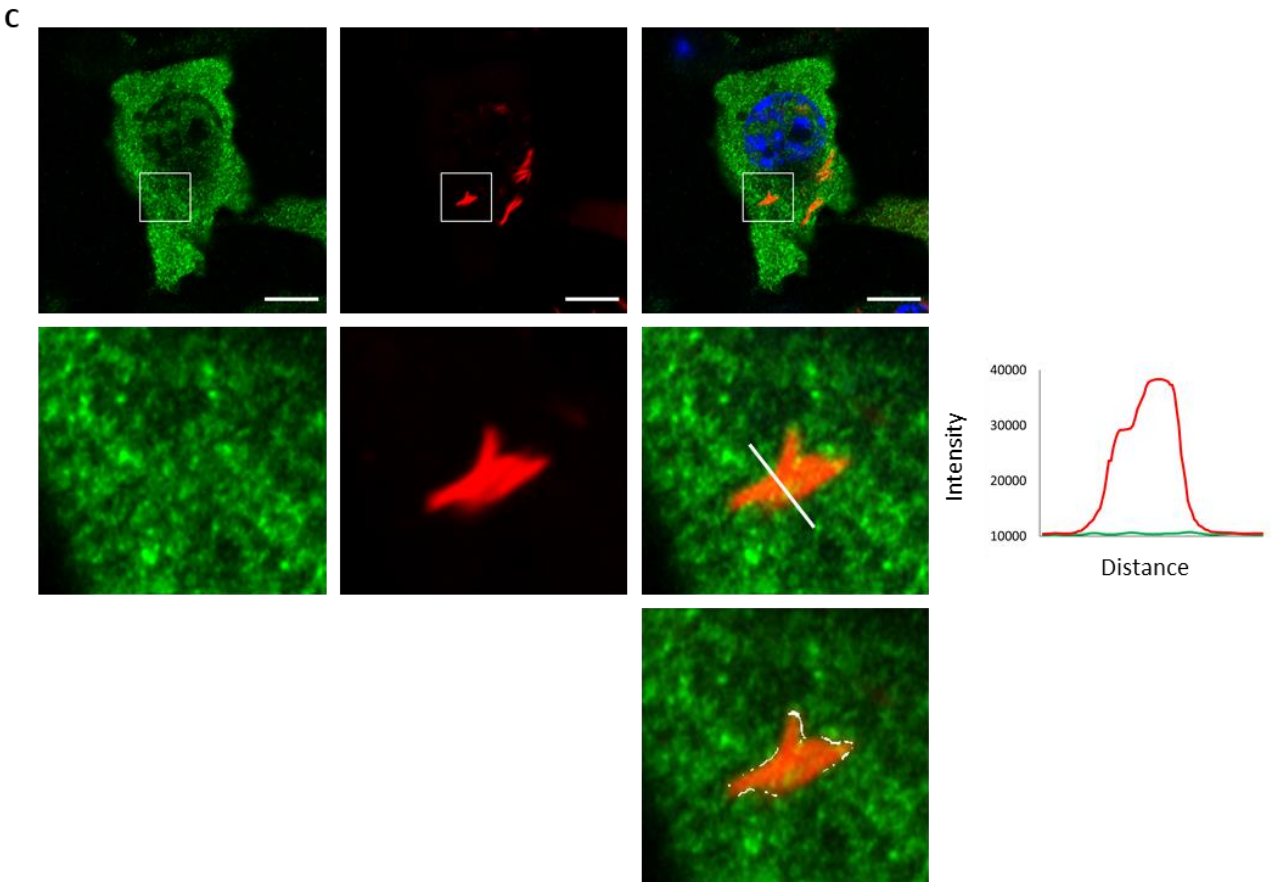


**Figure 2.8. NS4-II shows partial colocalisation with the perimeter of NS1 tubule bundles.** BSR-T7/5 cells were infected with AHSV1F, which expresses NS4-II, and dual labelled with anti-NS4(ChR121) and anti-NS1(786) at 24 hpi. Secondary labelling was done with AF 488 conjugated goat anti-chicken IgY and AF 633 conjugated goat anti-rabbit IgG. (A) NS1 in the nucleus. (B and C) NS1 in the cytoplasm. Each second row in A-C shows an enlargement of the demarcated areas in the micrographs in the previous row. Fluorescence intensity plots were generated by measuring the fluorescence intensity of each channel along the white line drawn in the merged images. Each third row in A-C shows colocalised pixels (white) as determined by Fiji. Nuclei were stained with DAPI. Scale bars = 10 µm.

AHSV8F expresses NLS-NS4-II, which is found homogenously in the cytoplasm and as foci in the nucleus. Although some foci showed colocalisation with NS1 tubules in the nucleus (Figure 2.9A) the majority were found located near NS1 tubules but not always in direct contact with them (Figure 2.9B). This was confirmed using Fiji (third row of Figure 2.9A and B). Several tubules were located in the nucleus in the absence of NLS-NS4-II foci. In these cases, ZEN showed that most did not colocalise with NLS-NS4-II (Figure 2.9C), whereas Fiji indicated some colocalisation at one point along the tubule (white in third row, Figure 2.9C). NLS-NS4-II colocalised with NS1 at some points in the cytoplasm (Figure 2.9D and E) and in most cases showed slight elevation of NLS-NS4-II (green) at NS1 tubule bundles, an observation that was confirmed by Fiji (white pixels in third row, Figure 2.9C, D and E).

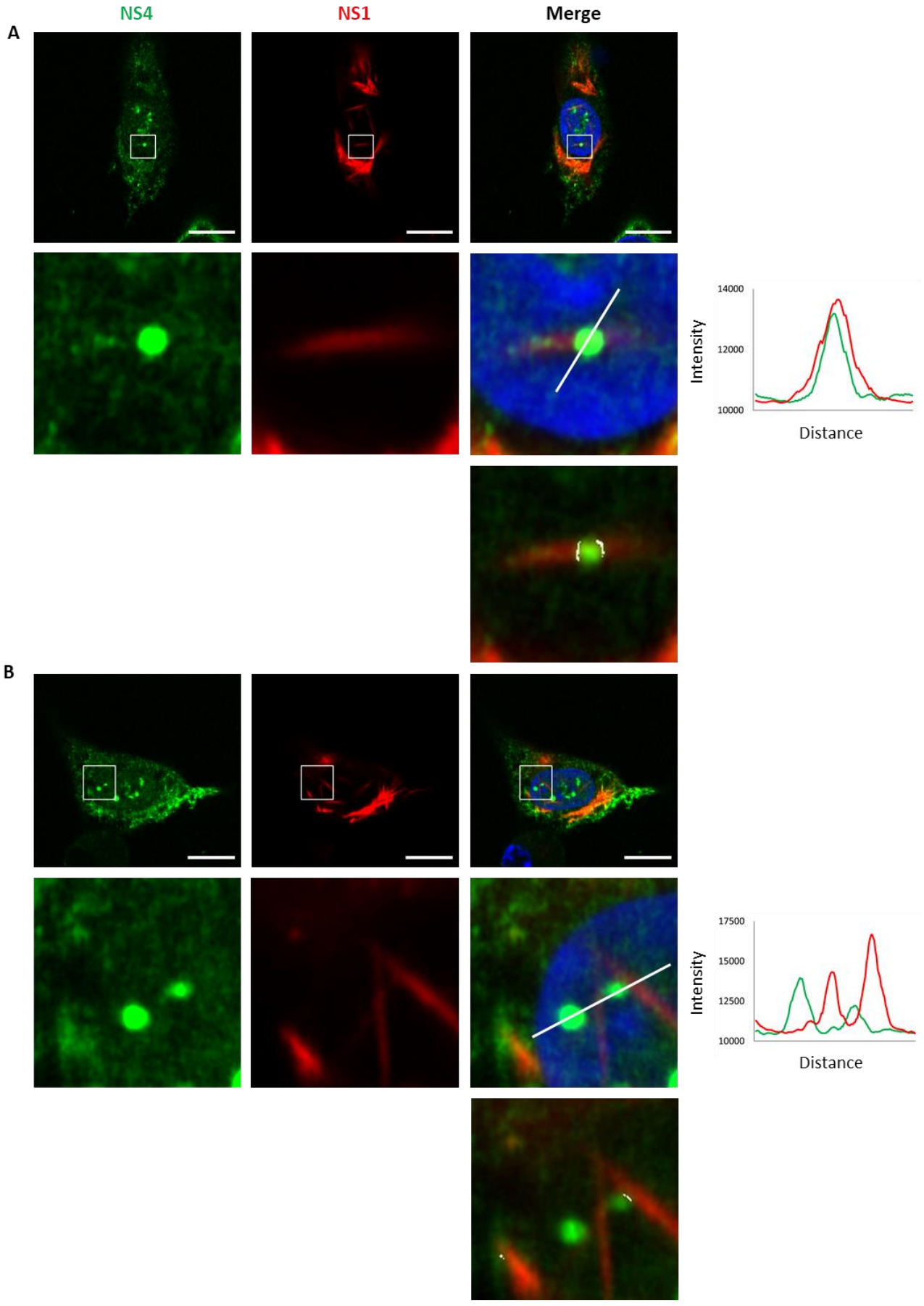

C

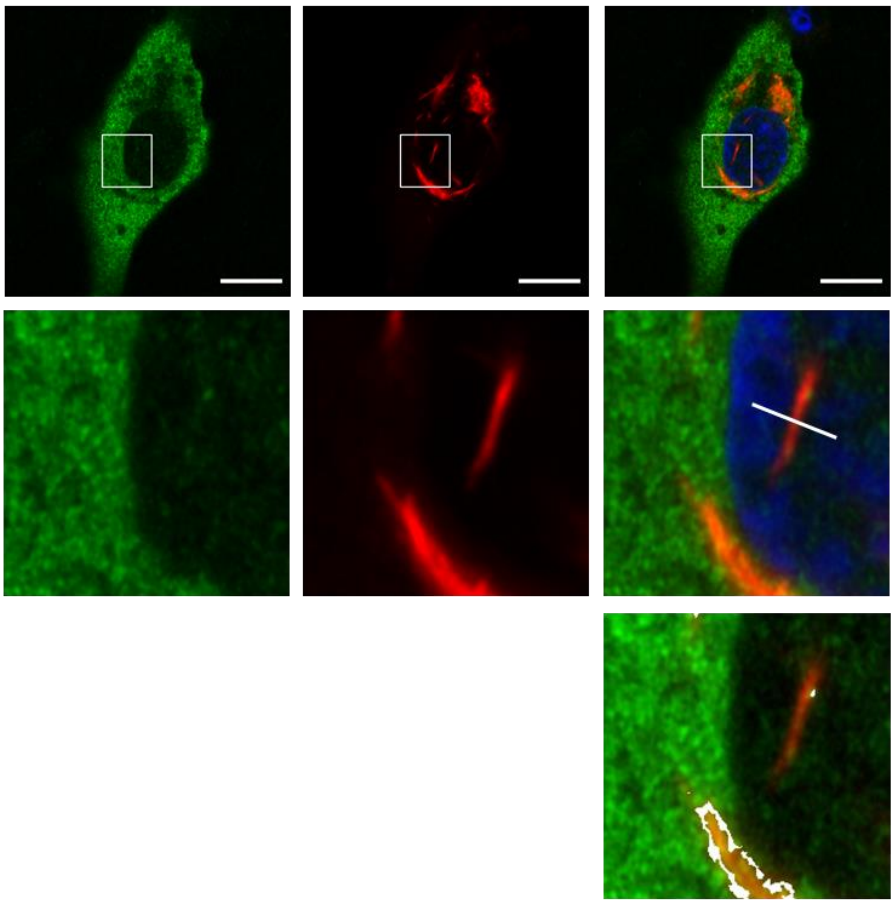

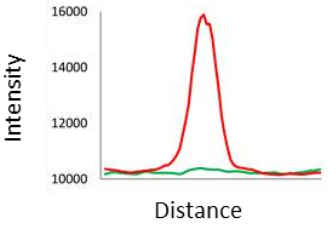


D

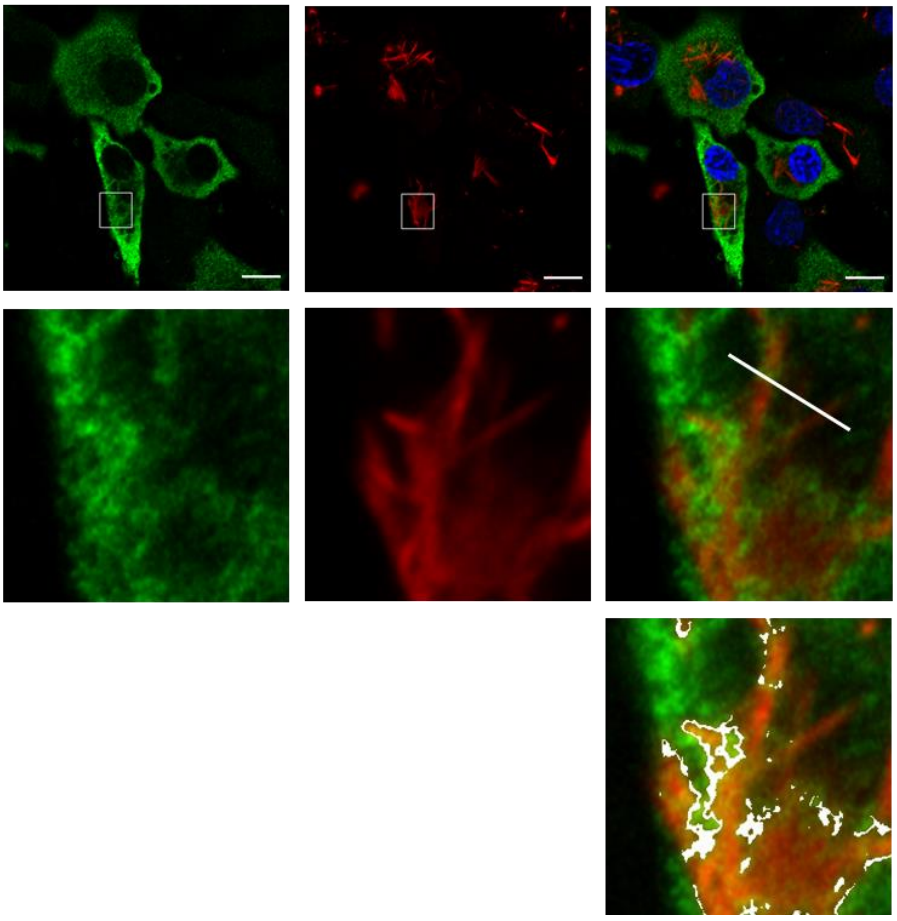

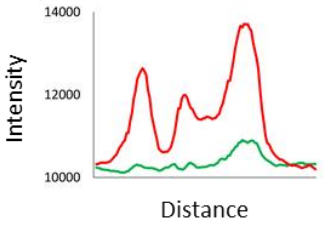

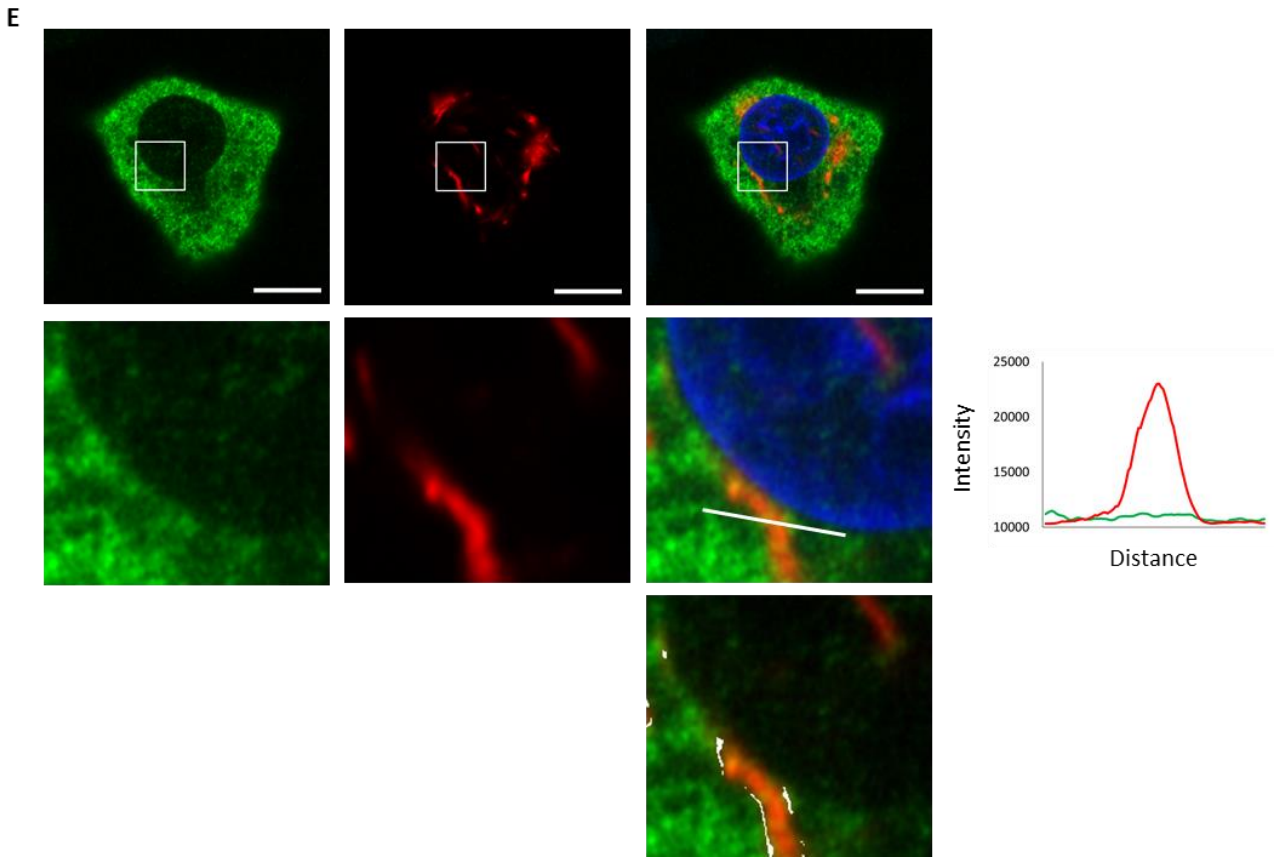


**Figure 2.9. NLS-NS4-II shows partial colocalisation with the perimeter of NS1 tubule bundles.** BSR-T7/5 cells were infected with AHSV8F, which expresses NLS-NS4-II, and dual labelled with anti-NS4(ChR121) and anti-NS1(786) at 24 hpi. Secondary labelling was done with AF 488 conjugated goat anti-chicken IgY and AF 633 conjugated goat anti-rabbit IgG. (A-C) NS1 in the nucleus. (D-E) NS1 in the cytoplasm. Each second row in A-E shows an enlargement of the demarcated areas in the micrographs in the previous row. Fluorescence intensity plots were generated by measuring the fluorescence intensity of each channel along the white line drawn in the merged images. Each third row in A-E shows colocalised pixels (white) as determined by Fiji. Nuclei were stained with DAPI. Scale bars = 10 µm.

Therefore, all three types of NS4 show limited partial colocalisation with NS1 at the periphery of NS1 tubule bundles.

### 2.3.4.2. NS2 and NS4

Next it was investigated if NS4 colocalises with non-structural protein NS2, which forms distinct VIBs in infected cells (Thomas *et al.*, 1990; Uitenweerde *et al.*, 1995). As with NS1, uninfected cells were used as a control (Figure 2.10A). The fluorescence profiles along the line drawn in the merged image shows essentially straight lines at a value of 10 000 on the y-axis. Therefore, any deviation from the baseline of 10 000 on the y-axis was once again considered positive signal.

The micrographs shown in Figure 2.10 are representative of what was observed in AHSV4F (NS4-I) infected cells. Smaller VIBS show homogenous NS2 staining throughout the structure, as seen in Figure 2.10B. This is

visualised as a single red peak on a fluorescence intensity plot. In contrast, larger VIBs often appeared “ring-like” when viewed with a confocal microscope (Figure 2.10C and D). In such cases there is a stronger NS2 signal toward the periphery of the VIB and lower signal toward the interior. This is visualised as two red peaks separated by a dip on the fluorescence intensity plots (Figure 2.10C and D). It is possible that the density of a VIB does not allow the primary and secondary antibodies to penetrate the matrix, leading to this somewhat “ring-like” shape (Yssel, 2020).

As expected, no NS2 was observed in the nucleus therefore no colocalisation of NS4-I with NS2 was observed in the nucleus of infected cells (not shown). Figure 2.10B shows two peaks of green (NS4-I) within the red (NS2) peak. This was observed for the majority of VIBs analysed and indicates colocalisation at those points on the periphery of a VIB. In some cases, no colocalisation was observed between NS4-I and ring-like VIBs (Figure 2.10C), as indicated by the flat green line and no colocalised pixels being detected by Fiji. In most cases however, some colocalisation was observed at the periphery of a VIB (Figure 2.10D). This was shown by the increase in green signal shown in the intensity plot as well as when comparing pixels between the two channels (white in third row, Figure 2.10D). This confirms that some colocalisation of NS4-I with VIBs occurs at the periphery of the VIBs.

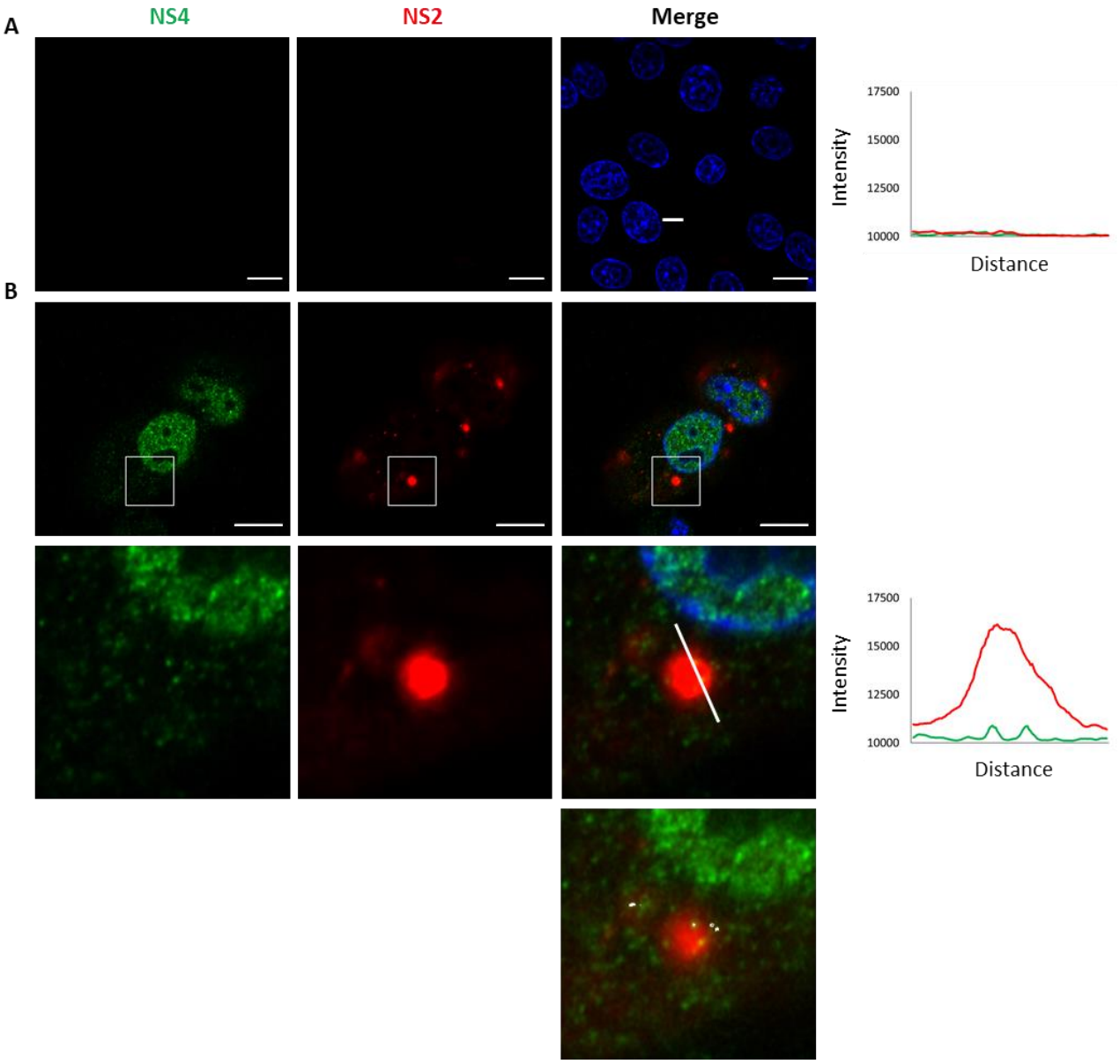

C

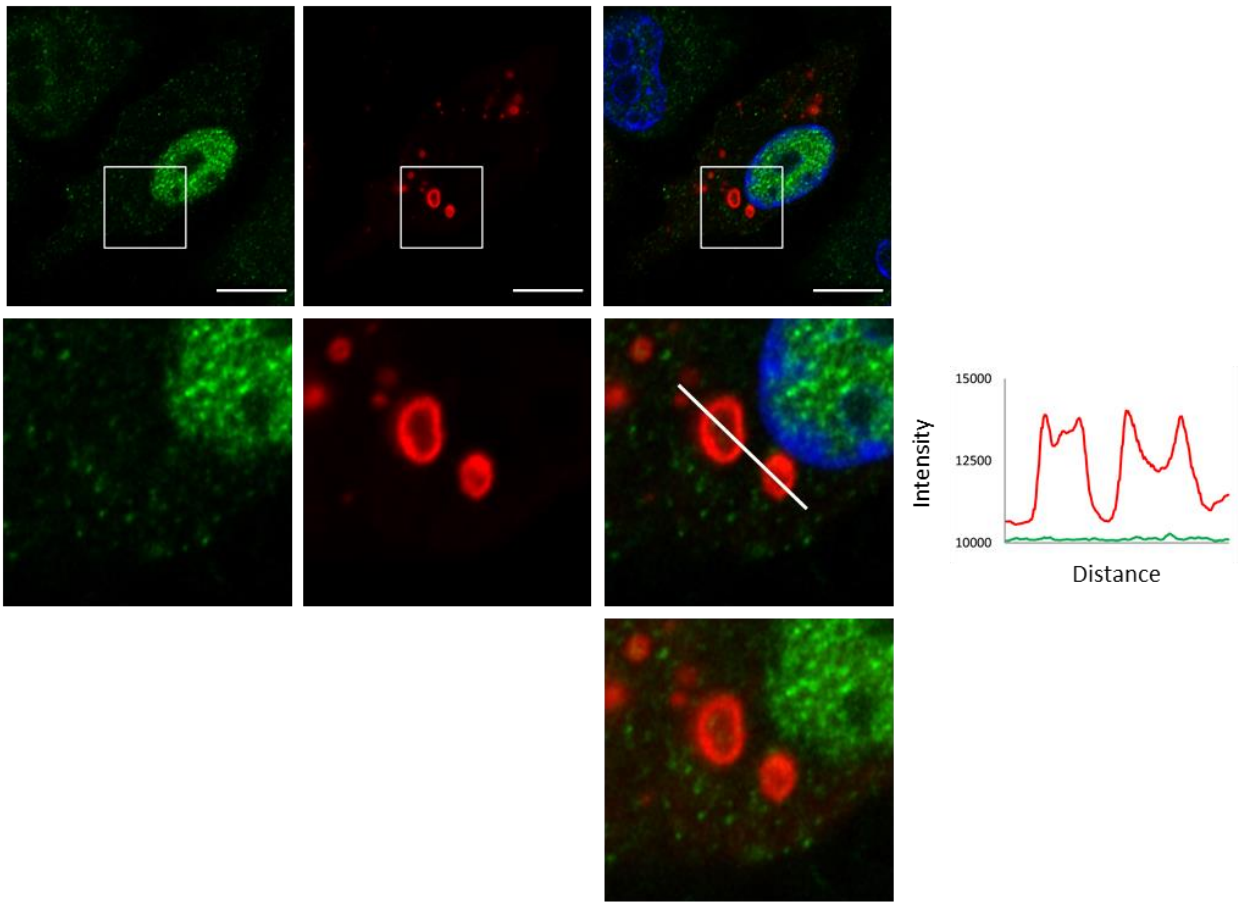


D

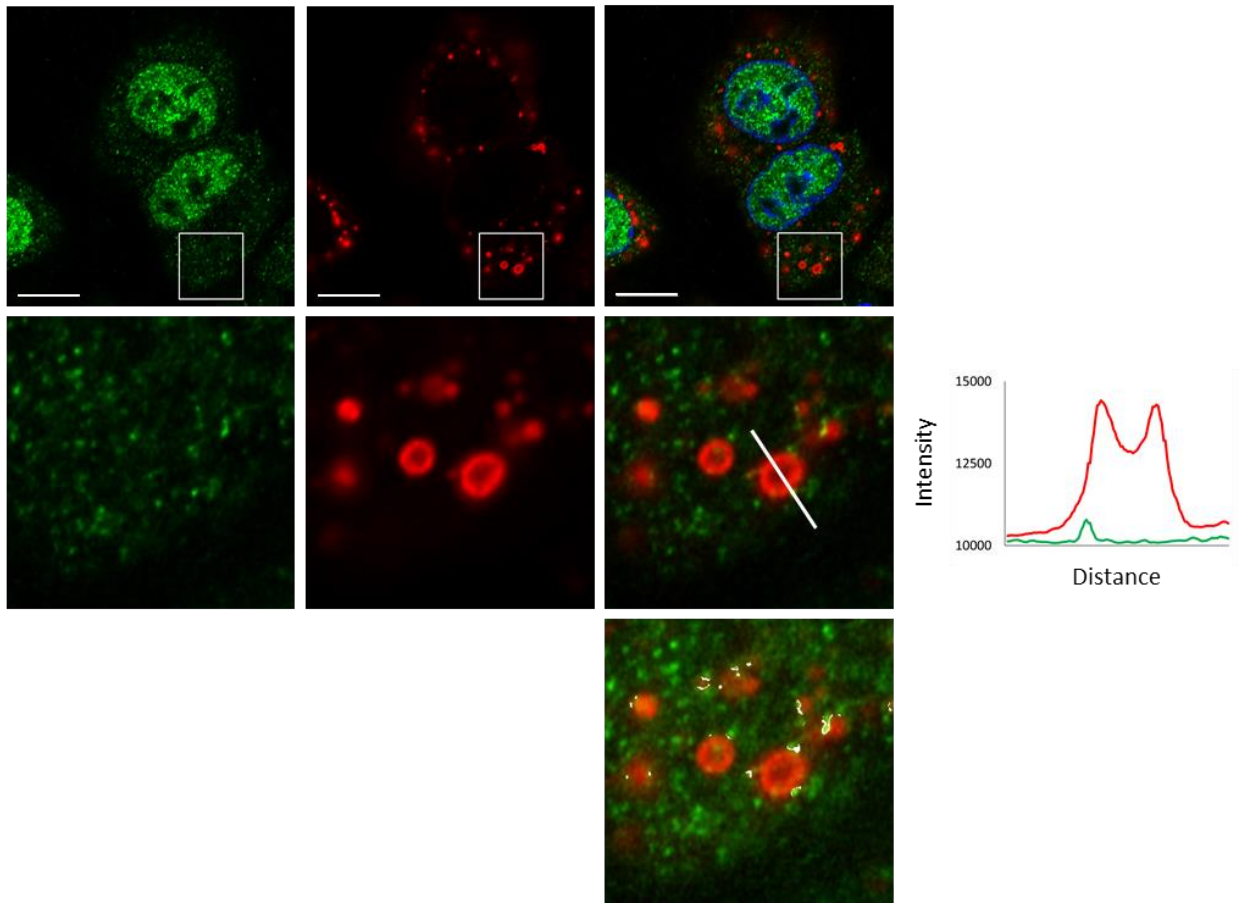

**Figure 2.10. NS4-I shows limited colocalisation with the periphery of VIBs.** BSR-T7/5 cells were left uninfected (A) or infected with AHSV4F (B, C and D), which expresses NS4-I, and dual labelled with anti-NS4(ChR121) and anti-NS2 at 24 hpi. Secondary labelling was done with AF 488 conjugated goat anti-chicken IgY and AF 633 conjugated goat anti-rabbit IgG. Each second row in B-D shows an enlargement of the demarcated areas in the micrographs in the previous row. Fluorescence intensity plots were generated by measuring the fluorescence intensity of each channel along the white line drawn in the merged images. Each third row in B-D shows colocalised pixels (white) as determined by Fiji. Nuclei were stained with DAPI. Scale bars = 10 µm.

Figure 2.11 shows the results obtained for cells infected with AHSV1F which expresses NS4-II. As with NS4-I, no colocalisation was observed in the nucleus (not shown). Figure 2.11A shows an increase in the intensity of the green signal toward the outskirts of the red signal, showing that NS4-II colocalises with the periphery of VIBs. This was confirmed by comparing the pixels in both channels using Fiji. Figure 2.11B shows that at times, the intensity of the red channel was such that it overpowered the green, making any changes in intensity of the green channel appear slight on the intensity profile plots. Comparing the pixels of both channels using Fiji showed that there was some colocalisation of NS4-II with the periphery of VIBs, even though this was hard to see in the profile plots. Also seen here was the absence of green signal at the sites of VIBs.

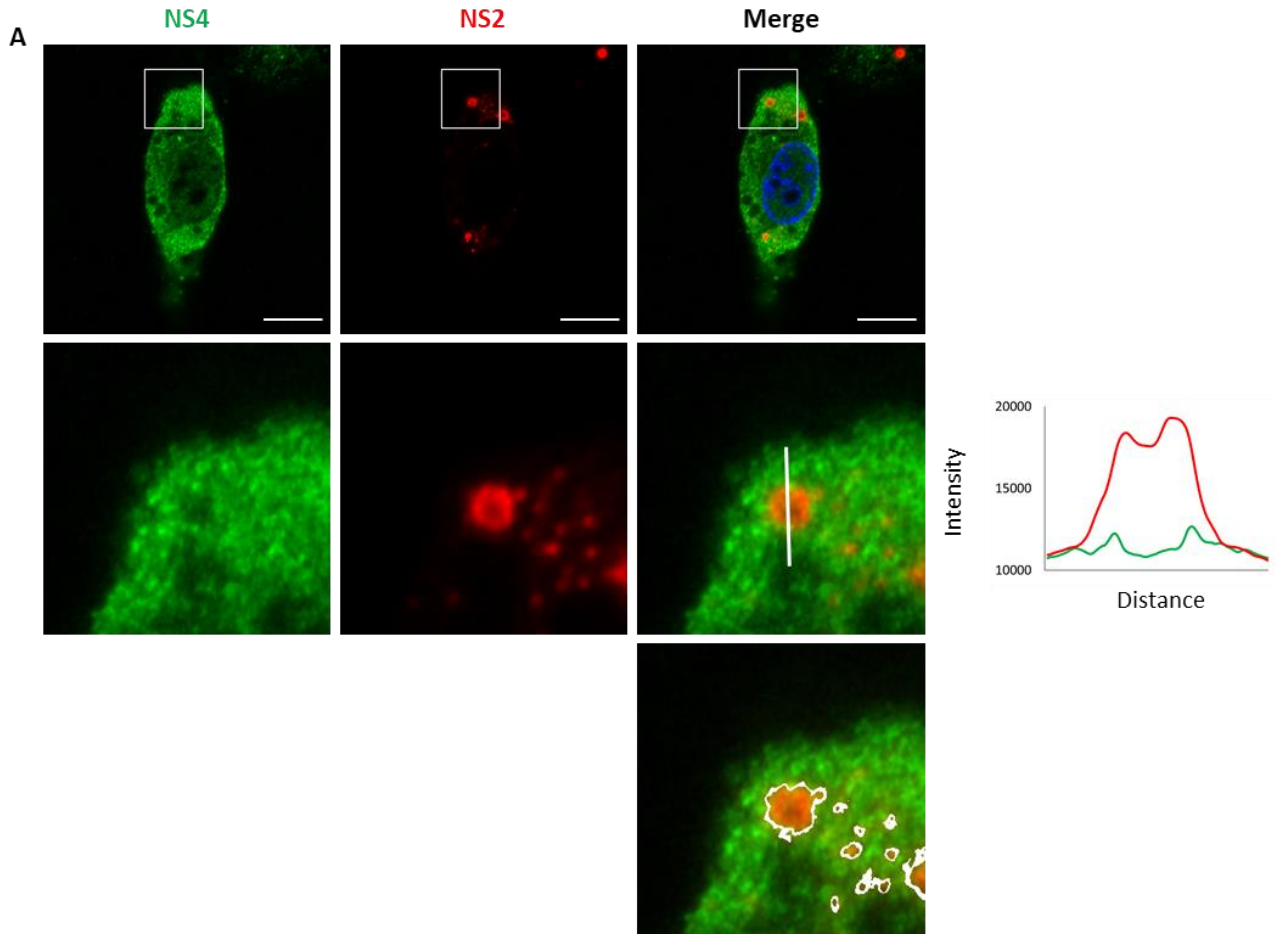

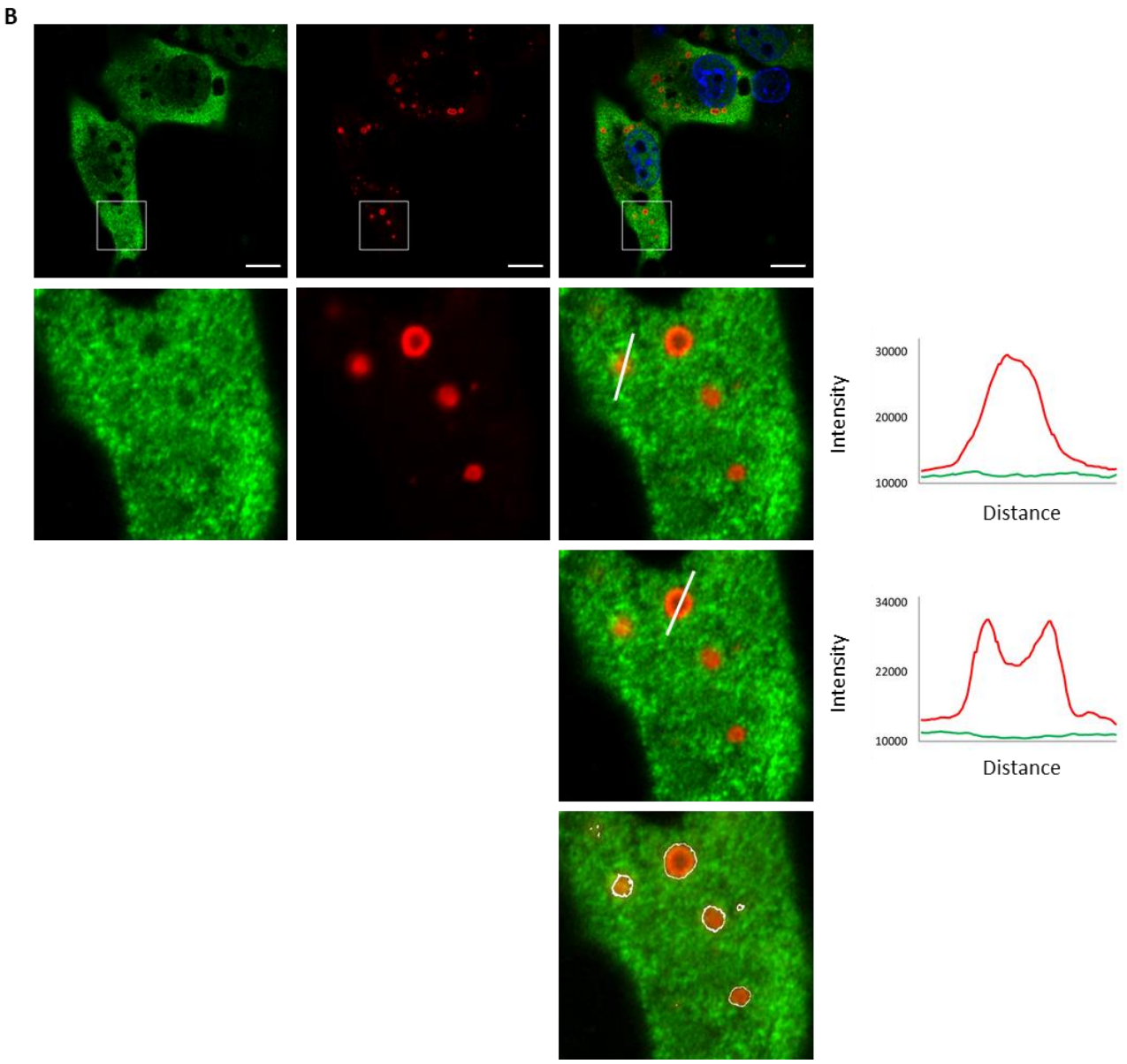


**Figure 2.11. NS4-II colocalises with the periphery of VIBs.** BSR-T7/5 cells were infected with AHSV1F, which expresses NS4-II, and dual labelled with anti-NS4(ChR121) and anti-NS2 at 24 hpi. Secondary labelling was done with AF 488 conjugated goat anti-chicken IgY and AF 633 conjugated goat anti-rabbit IgG. (A) Large VIB observed as a ring-like structure. (B) Small VIB observed as a solid structure or as a ring-like structure. Each second row in A and B shows an enlargement of the demarcated areas in the micrographs in the previous row. Fluorescence intensity plots were generated by measuring the fluorescence intensity of each channel along the white line drawn in the merged images. Each third row in A and B shows colocalised pixels (white) as determined by Fiji. Nuclei were stained with DAPI. Scale bars = 10 µm.

The results obtained from AHSV8F-infected cells are shown in Figure 2.12. The nuclear foci formed by NLS-NS4-II (green) did not colocalise with NS2 (Figure 2.12A). Within the cytoplasm two scenarios were observed, either no colocalisation was suggested by the fluorescence intensity plots (Figure 2.12B) or colocalisation was observed at the periphery of VIBs as seen in the plot in Figure 2.12C. Fiji however confirmed that there was some colocalisation at the periphery of VIBs. Even more prominent in AHSV8F-infected cells were the areas within the cytoplasm that showed no green signal at the sites of VIBs (Figure 2.12B and C).

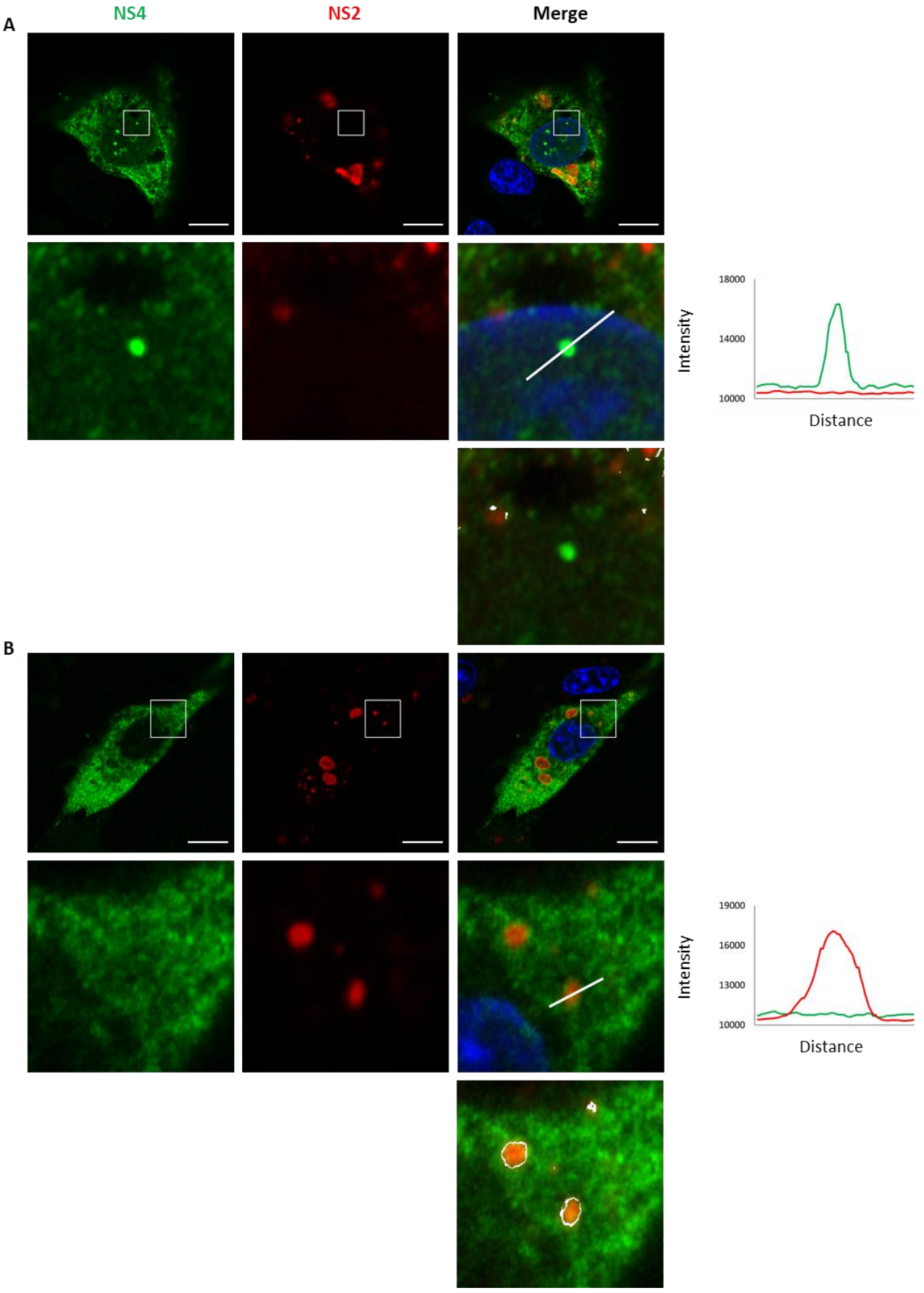

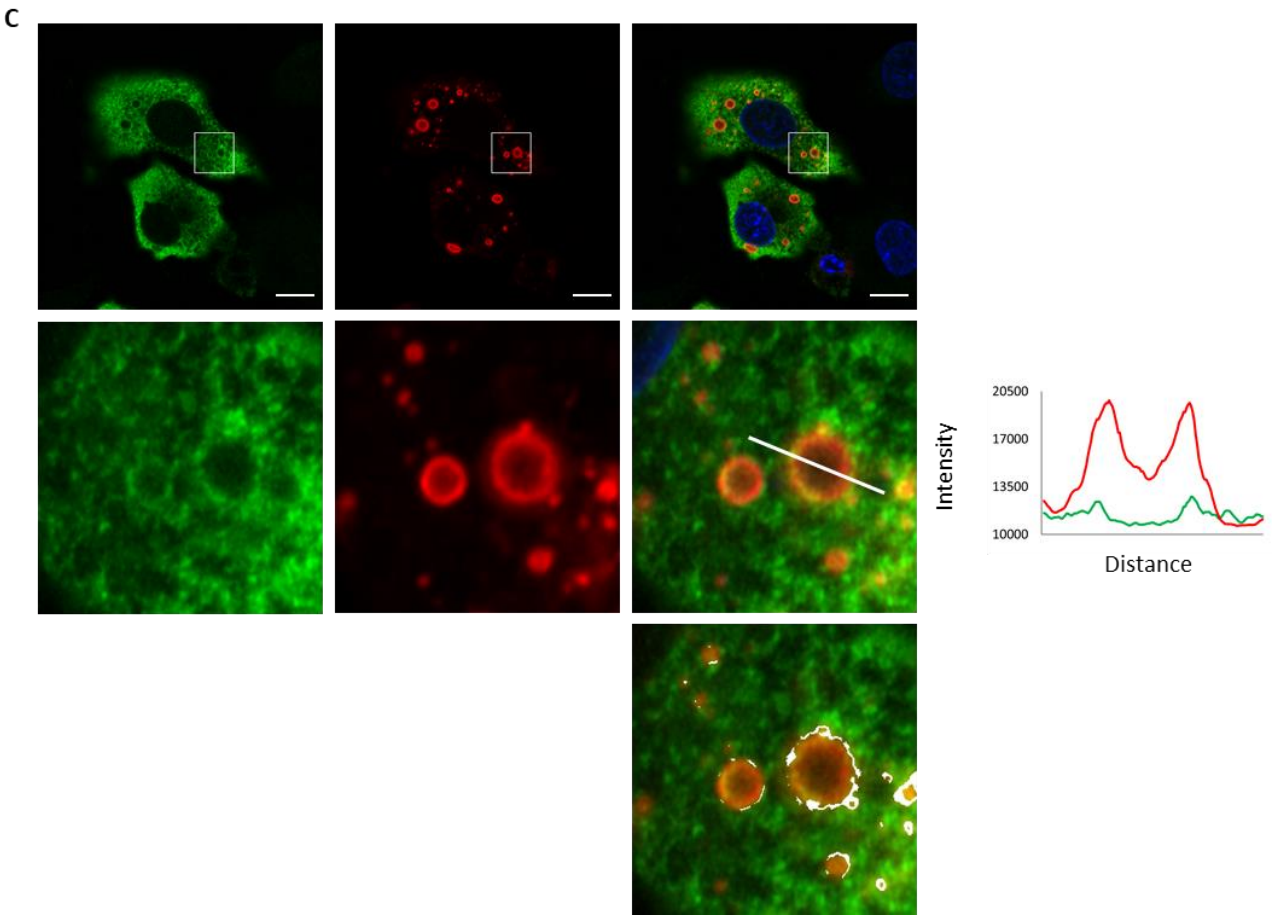


**Figure 2.12. Cytoplasmic NLS-NS4-II colocalises with the periphery of VIBs.** BSR-T7/5 cells were infected with AHSV8F, which expresses NLS-NS4-II, and dual labelled with anti-NS4(ChR121) and anti-NS2 at 24 hpi. Secondary labelling was done with AF 488 conjugated goat anti-chicken IgY and AF 633 conjugated goat anti-rabbit IgG. (A) Nuclear NLS-NS4-II focus. (B) Small VIBs observed as solid structures. (C) Large VIBs observed as ring-like structures. Each second row in A-C shows an enlargement of the demarcated areas in the micrographs in the previous row. Fluorescence intensity plots were generated by measuring the fluorescence intensity of each channel along the white line drawn in the merged images. Each third row in A-C shows colocalised pixels (white) as determined by Fiji. Nuclei were stained with DAPI. Scale bars = 10 µm.

Therefore, partial colocalisation of all three types of NS4 was observed at the periphery of VIBs and was clearer in AHSV1F- and AHSV8F-infected cells compared to AHSV4F-infected cells.

#### 2.3.4.3. NS3 and NS4

The last of the non-structural proteins to be investigated was NS3. Unlike NS1 and NS2, this protein does not self-assemble into distinct structures in infected cells. Therefore, the JACoP plugin in Fiji was used to give the Pearson's coefficient in addition to what had been done with NS1 and NS2. Pearson's coefficient can range from -1 to 1, with 1 indicating complete positive colocalisation, -1 indicating complete negative colocalisation and 0 indicating no colocalisation (Bolte and Cordelieres, 2006). Uninfected cells displayed the same fluorescence intensity profiles as those seen in the controls of the previous sections (Figure 2.13A). Therefore, the baseline was set to 10 000 in this section too.

As expected, no colocalisation was observed in the nucleus of AHSV4F-infected cells (not shown). Fluorescence intensity profiles showed some peaks of NS4-I (green) where there was NS3, typically toward the edges of what represented the perinuclear NS3 (Figure 2.13B and C). Fiji also indicated that very few pixels were colocalised in the images, and when present they were located toward the outside of perinuclear NS3. This was confirmed by Pearson's coefficients of -0.313 and 0.046 for the images in Figure 2.13B and C respectively. Overall, the results for AHSV4F-infected cells suggest that while some NS4-I may be found directly next to NS3, majority is not and there is essentially no colocalisation between the two proteins.

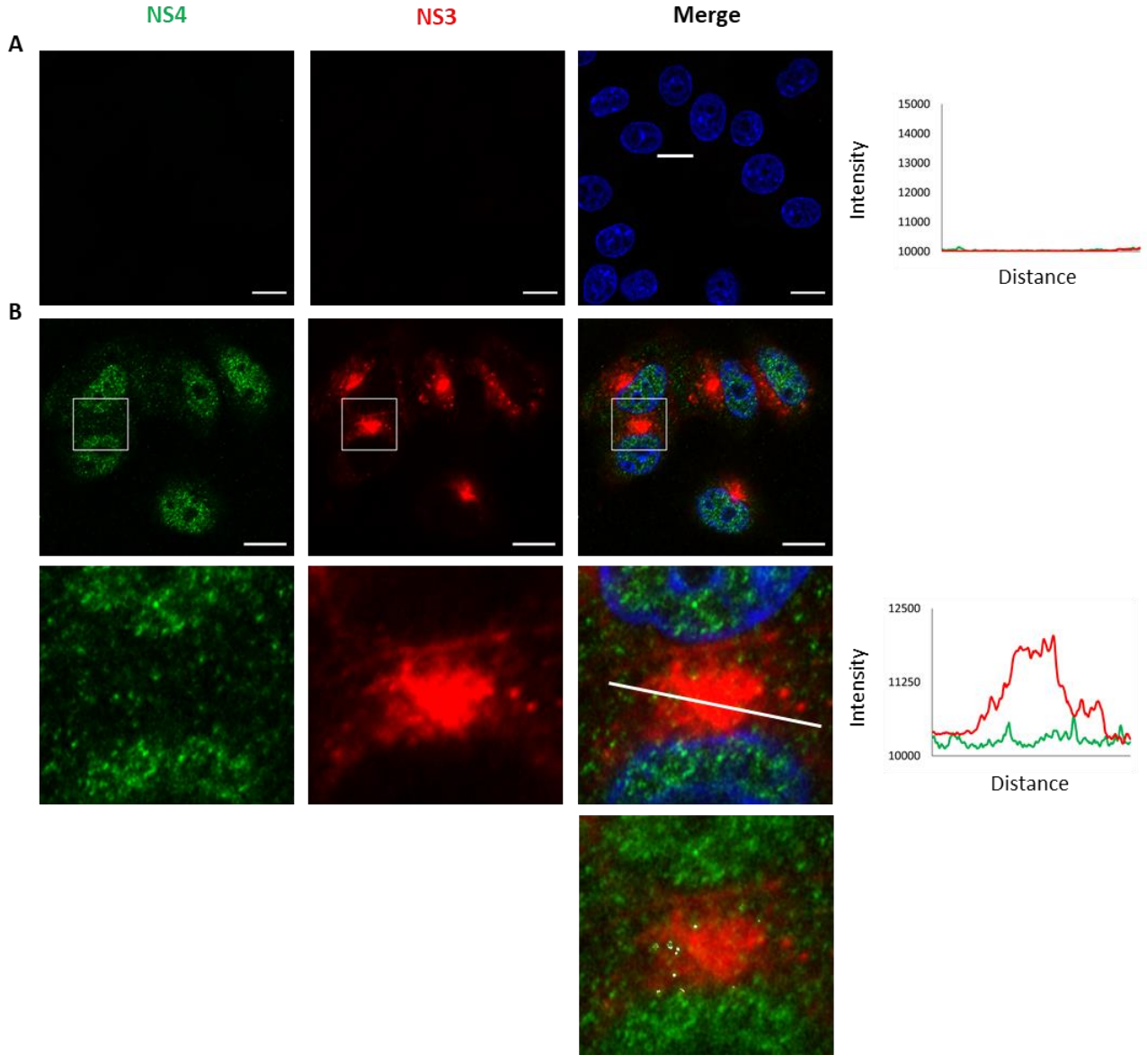

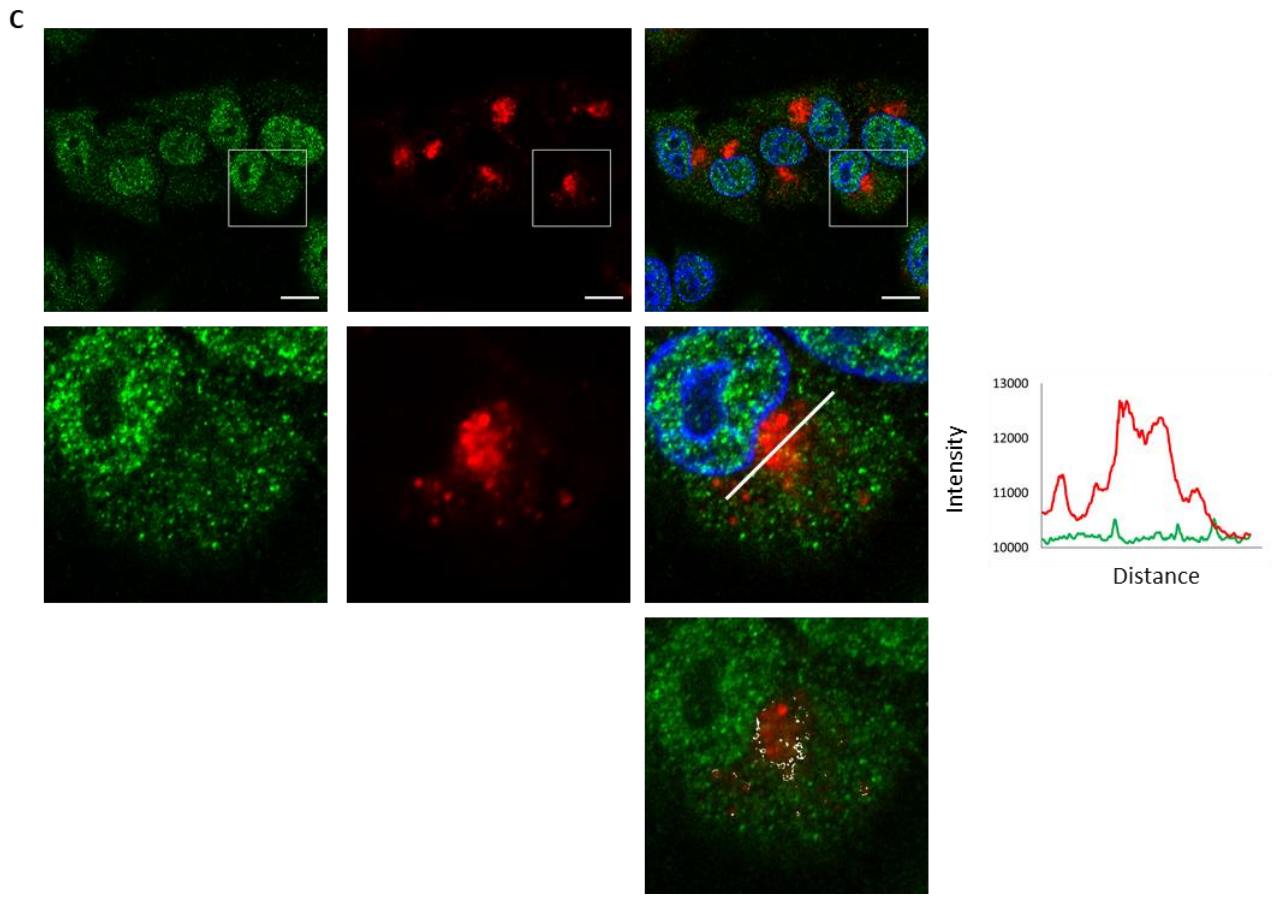


**Figure 2.13. NS4-I does not colocalise with NS3.** BSR-T7/5 cells were left uninfected (A) or infected with AHSV4F (B and C), which expresses NS4-I, and dual labelled with anti-NS4(ChR121) and anti-NS3 at 24 hpi. Secondary labelling was done with AF 488 conjugated goat anti-chicken IgY and AF 633 conjugated goat anti-rabbit IgG. Each second row in B-D shows an enlargement of the demarcated areas in the micrographs in the previous row. Fluorescence intensity plots were generated by measuring the fluorescence intensity of each channel along the white line drawn in the merged images. Each third row in B-D shows colocalised pixels (white) as determined by Fiji. Nuclei were stained with DAPI. Scale bars = 10 µm.

The fluorescence intensity plots in Figure 2.14 show several peaks of the NS4-II signal (green) that correspond to, or lie next to, peaks in the NS3 channel (red). In addition to this Fiji showed colocalised pixels (white) toward the outside of perinuclear NS3. The Pearson's coefficient for enlarged image in Figure 2.14A was -0.320, indicating negative colocalisation overall for this image. The Pearson's coefficient of the enlarged image in Figure 2.14B was 0.139. These results indicate that while some colocalisation was observed, overall, there is very little colocalisation between NS4-II and NS3. Rather, NS4-II is found surrounding NS3.

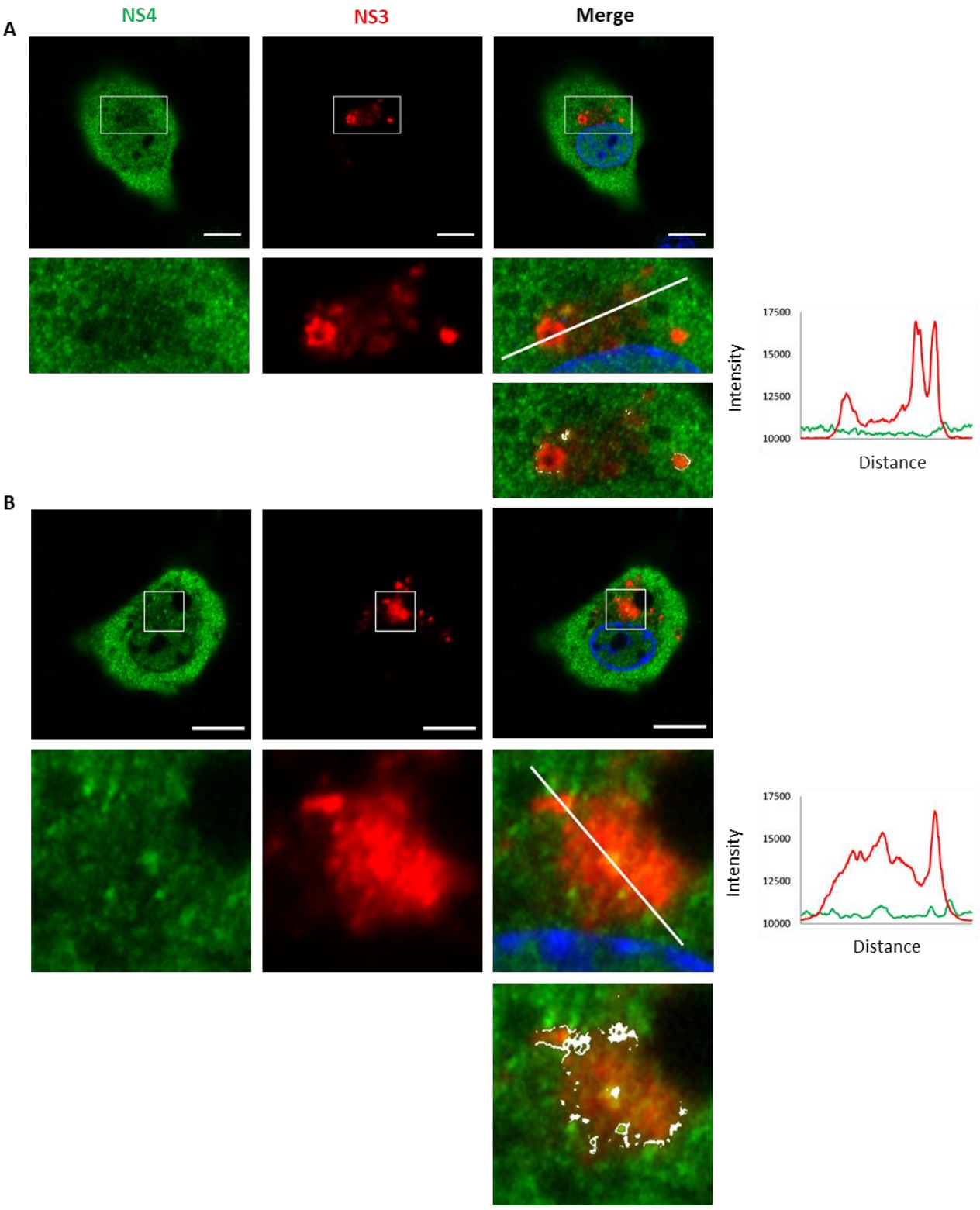


**Figure 2.14. NS4-II partially colocalises with the outside of perinuclear NS3.** BSR-T7/5 cells were infected with AHSV1F (B and C), which expresses NS4-II, and dual labelled with anti-NS4(ChR121) and anti-NS3 at 24 hpi. Secondary labelling was done with AF 488 conjugated goat anti-chicken IgY and AF 633 conjugated goat anti-rabbit IgG. Each second row in A and B shows an enlargement of the demarcated areas in the micrographs in the previous row. Fluorescence intensity plots were generated by measuring the fluorescence intensity of each channel along the white line drawn in the merged images. Each third row in A and B shows colocalised pixels (white) as determined by Fiji. Nuclei were stained with DAPI. Scale bars = 10 µm.

The fluorescence intensity profile in Figure 2.15A shows that nuclear NLS-NS4-II foci did not colocalise with NS3. Several pixels located in the cytoplasm however appeared to colocalise, as seen in the image obtained by Fiji. When looking at the perinuclear distribution of NS3, it was seen that NLS-NS4-II showed a fluorescence intensity profile like that observed in Figure 2.14A. It was however more pronounced in this instance, with the level of NLS-NS4-II signal (green) decreasing where the signal of NS3 increases and vice versa, indicating that NLS-NS4-II is located on the outside of NS3 perinuclear regions. More evidence of this is the apparent lack of signal in the green channel at the site of NS3 (Figure 2.15B). The white pixels in the images obtained by Fiji show some colocalisation at the edges of perinuclear NS3 (Figure 2.15B). On the outskirts of the cell, NS3 is located on the plasma membrane, with NLS-NS4-II located adjacent to it toward the inside of the cell (Figure 2.15C). As seen in the plot, there is some overlap between the two channels at this point. Fiji confirmed this, with some colocalised pixels being seen along the plasma membrane. Also, seen in this image is confirmation that some NLS-NS4-II colocalises with the edges of perinuclear NS3. The Pearson's coefficients for the enlarged images in Figure 2.15 were 0.033, 0.141 and 0.386 respectively, confirming that the images in Figure 2.15A had the least amount of colocalised pixels and the image in Figure 2.15C had the most.

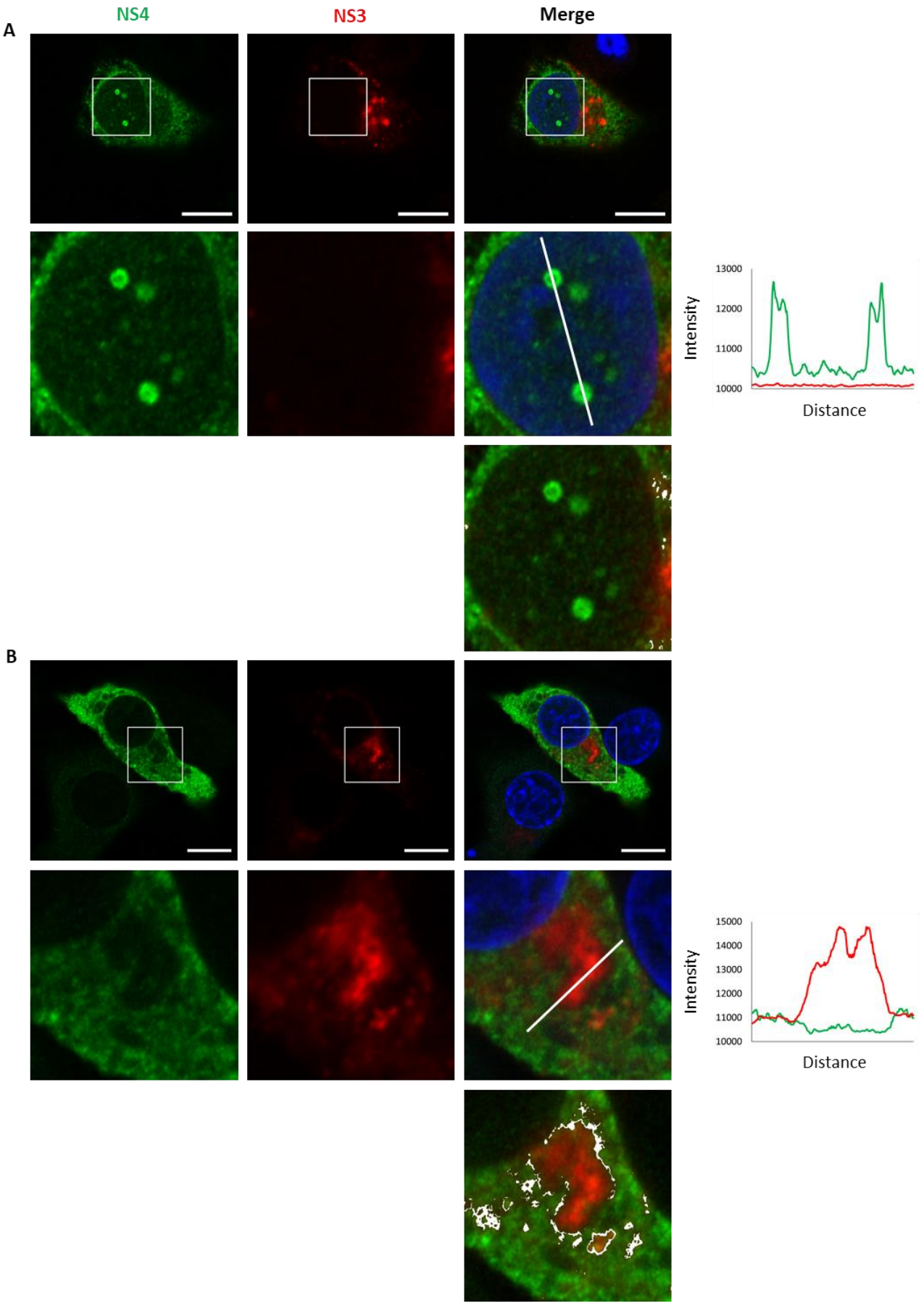

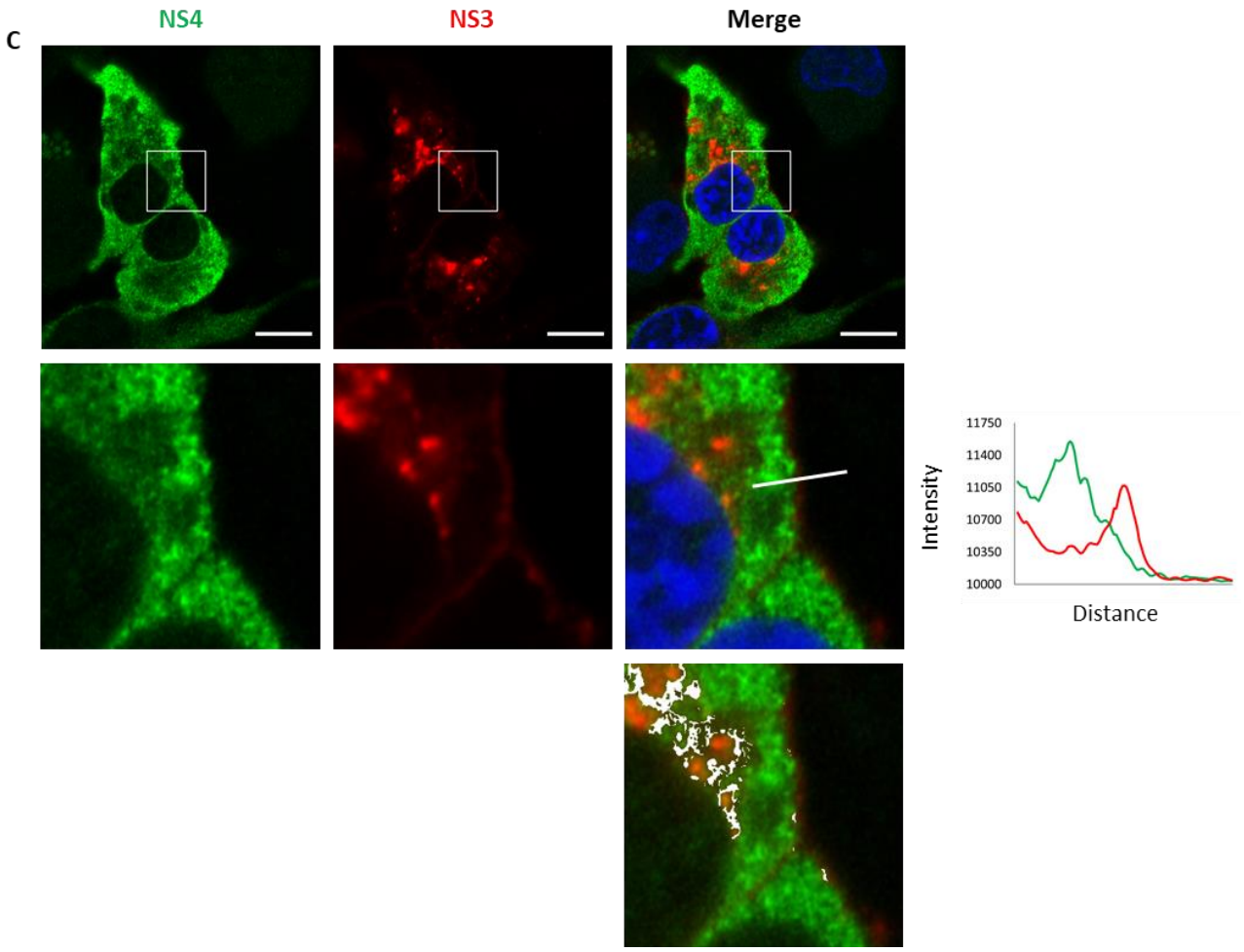


**Figure 2.15. Cytoplasmic NLS-NS4-II surrounds, and partially colocalises with, NS3.** BSR-T7/5 cells were infected with AHSV8F, which expresses NLS-NS4-II, and dual labelled with anti-NS4(ChR121) and anti-NS3 at 24 hpi. Secondary labelling was done with AF 488 conjugated goat anti-chicken IgY and AF 633 conjugated goat anti-rabbit IgG. (A) NLS-NS4-II foci in the nucleus. (B) perinuclear NS3 and (C) perinuclear NS3 and NS3 located at the plasma membrane. Each second row in A-C shows an enlargement of the demarcated areas in the micrographs in the previous row. Fluorescence intensity plots were generated by measuring the fluorescence intensity of each channel along the white line drawn in the merged images. Each third row in A-C shows colocalised pixels (white) as determined by Fiji. Nuclei were stained with DAPI. Scale bars = 10 µm.

Therefore, overall NS4 partially colocalises with the perimeter of perinuclear NS3 and does not colocalise with NS3 at the plasma membrane.

### 2.3.4.3. Mitochondria and NS4

Lastly, staining with MitoTracker™ was used to see if AHSV NS4 colocalises with mitochondria. BSR-T7/5 cells were infected with AHSV4F, AHSV1F or AHSV8F and at 24 hpi were stained with MitoTracker™ and processed for immunofluorescence and CLSM using ant-NS4(E3F) and AF 488 conjugated goat anti-rabbit IgG (Table 2.2). Super-resolution images were taken as above, and the resulting micrographs were used for colocalisation analyses.

The micrographs in Figure 2.16A show that no NS4 was observed in uninfected cells (green channel), with mitochondria (red channel) showing the same cytoplasmic distribution observed in Figure 2.5. The fluorescence intensity plot generated along the line in the merged image confirmed that no NS4 was present in uninfected cells and showed a clear signal for mitochondria in red.

Figure 2.16B shows a line drawn through the nucleus and cytoplasm of a cell infected with AHSV4F. No colocalisation of NS4-I and mitochondria was observed in the nucleus. The micrographs show that NS4-I was found homogenously in the nucleus and the cytoplasm, with more being observed in the nucleus. This was confirmed by the fluorescence intensity plot with a higher intensity of green (NS4-I) being observed in the nucleus than in the cytoplasm. The mitochondria observed in the cytoplasm (red) were represented by the increase in profile of the red line in the plot. No distinctive pattern between the red and green was observed and indicated that although both were found in the same area, they were not colocalising. This was confirmed using Fiji as no white pixels were observed and a Pearson's coefficient of -0.542 was obtained. In some instances, a drop in fluorescence of the green channel (NS4-I) was observed where mitochondria were located in the cytoplasm (red, Figure 2.16C). This suggested that NS4-I surrounds mitochondria rather than being colocalised with the organelles. A Pearson's coefficient of 0.048 and very few areas of colocalised pixels showed that while some colocalisation was observed, it was practically negligible.

No colocalisation was observed in the nucleus in cells infected with AHSV1F (not shown). The fluorescence intensity plots in Figure 2.17 show that the peaks of NS4-II and mitochondria did not occur at the same place but were lying next to one another, suggesting that NS4-II was found on the outside of the organelles. This was also observed using Fiji, with colocalised pixels, indicated in white, being observed on the outside of mitochondria. The Pearson's coefficients were 0.273 and 0.185 respectively for the images in Figure 2.17.

NLS-NS4-II also appears to be found on the outside of mitochondria (Figure 2.18). In Figure 2.18A the perinunclear area in the cytoplasm where mitochondria are located appears dimmer in the green channel. This is echoed in the fluorescence intensity plot wherein the green channel dips where the red channel increases. A few peaks toward the edges of this coincide, indicating some colocalisation. This was confirmed by Fiji, with some colocalised pixels being observed on the outside of the group of mitochondria. The overall Pearson's coefficient for the image was -0.342 even though some colocalisation was observed. A similar situation was observed in Figure 2.18B, where red increased, green decreased and vice versa. A few peaks overlapped and were observed as white pixels by Fiji, with a Pearson's coefficient of 0.153 obtained for this image.

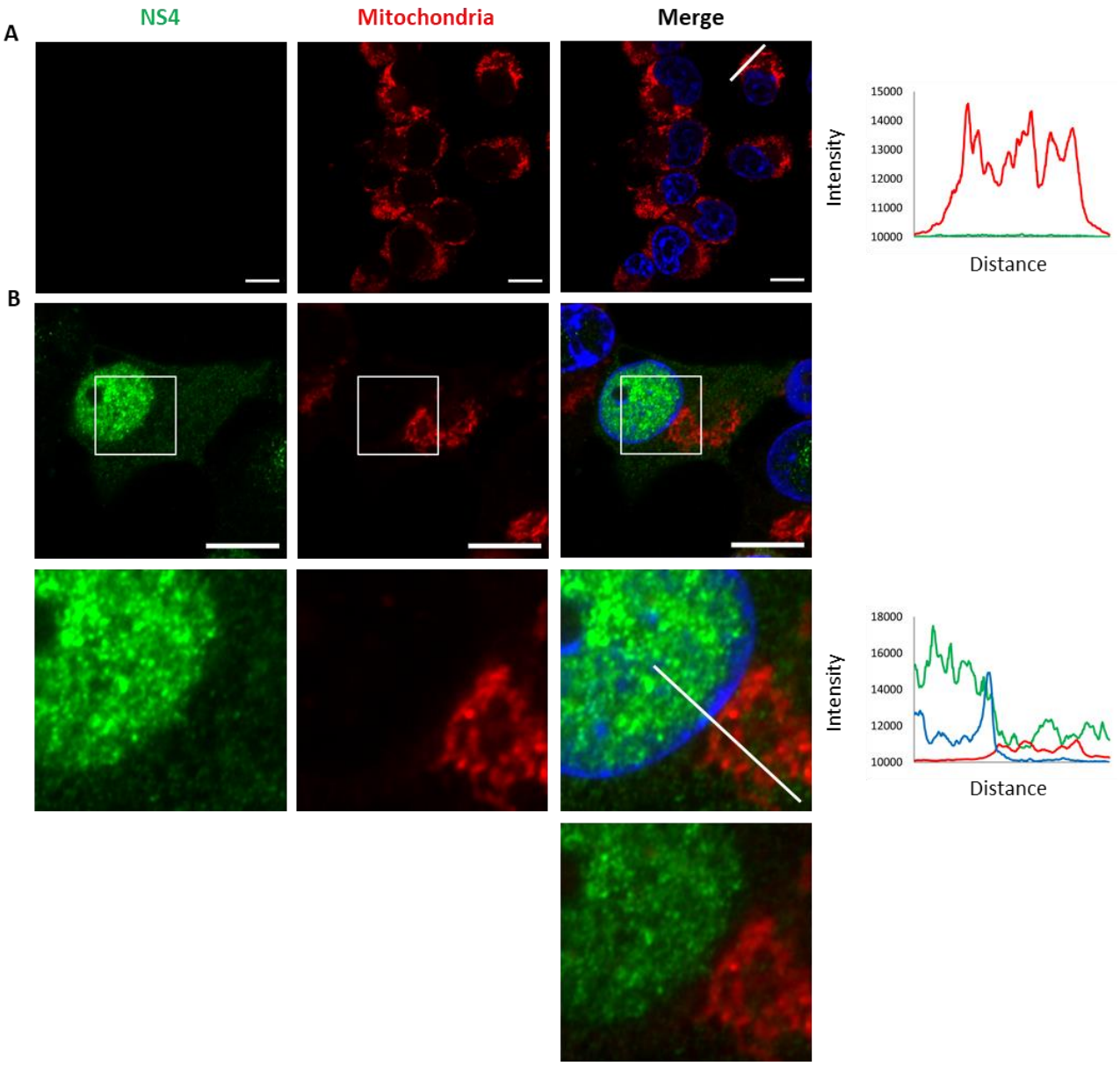

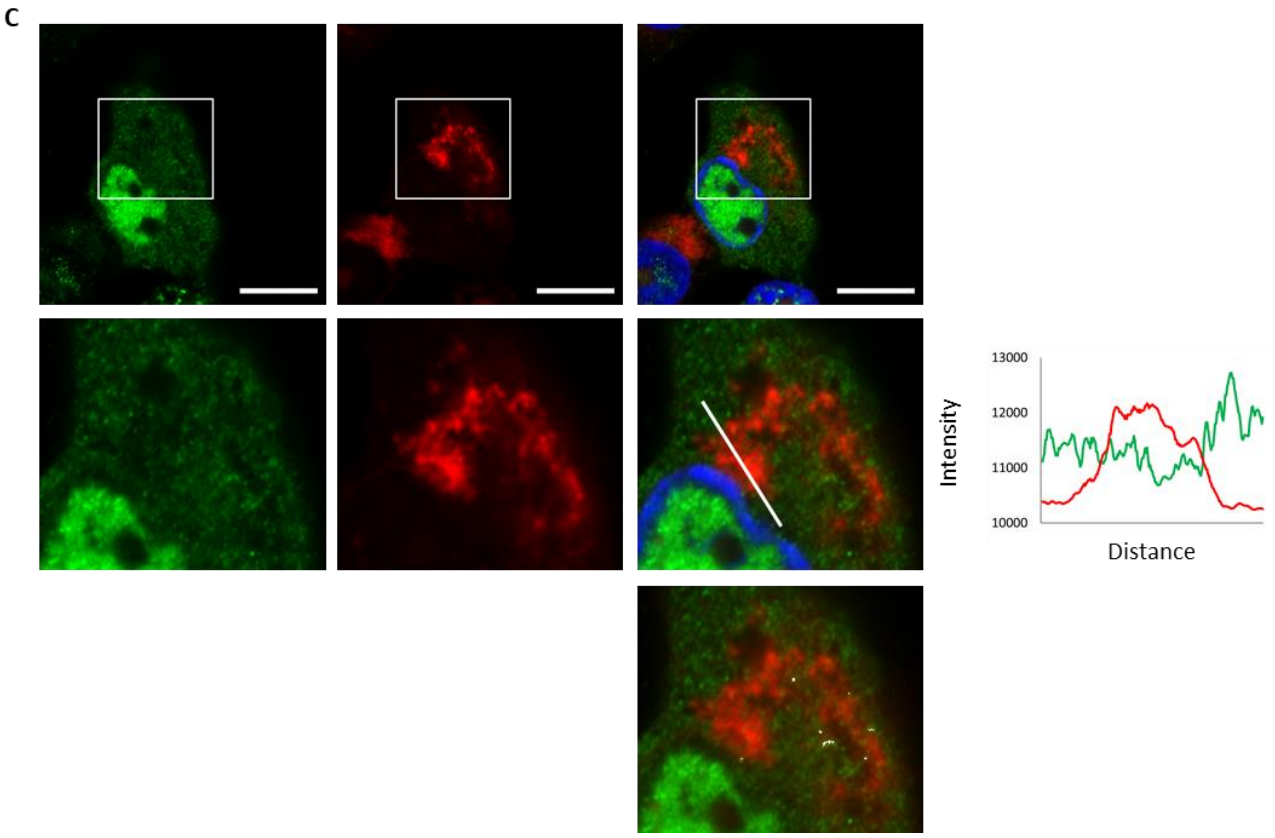


**Figure 2.16. NS4-I does not colocalise with mitochondria.** BSR-T7/5 cells were left uninfected (A) or were infected with AHSV4F (B and C), which expresses NS4-I, and at 24 hpi were stained with MitoTracker™ and processed for immunofluorescence and CLSM using anti-NS4(E3F) and AF 488 conjugated goat anti-rabbit IgG. Each second row in B and C shows an enlargement of the demarcated areas in the micrographs in the previous row. Fluorescence intensity plots were generated by measuring the fluorescence intensity of each channel along the white line drawn in the merged images. Each third row in B and C shows colocalised pixels (white) as determined by Fiji. Nuclei were stained with DAPI. Scale bars = 10 µm.

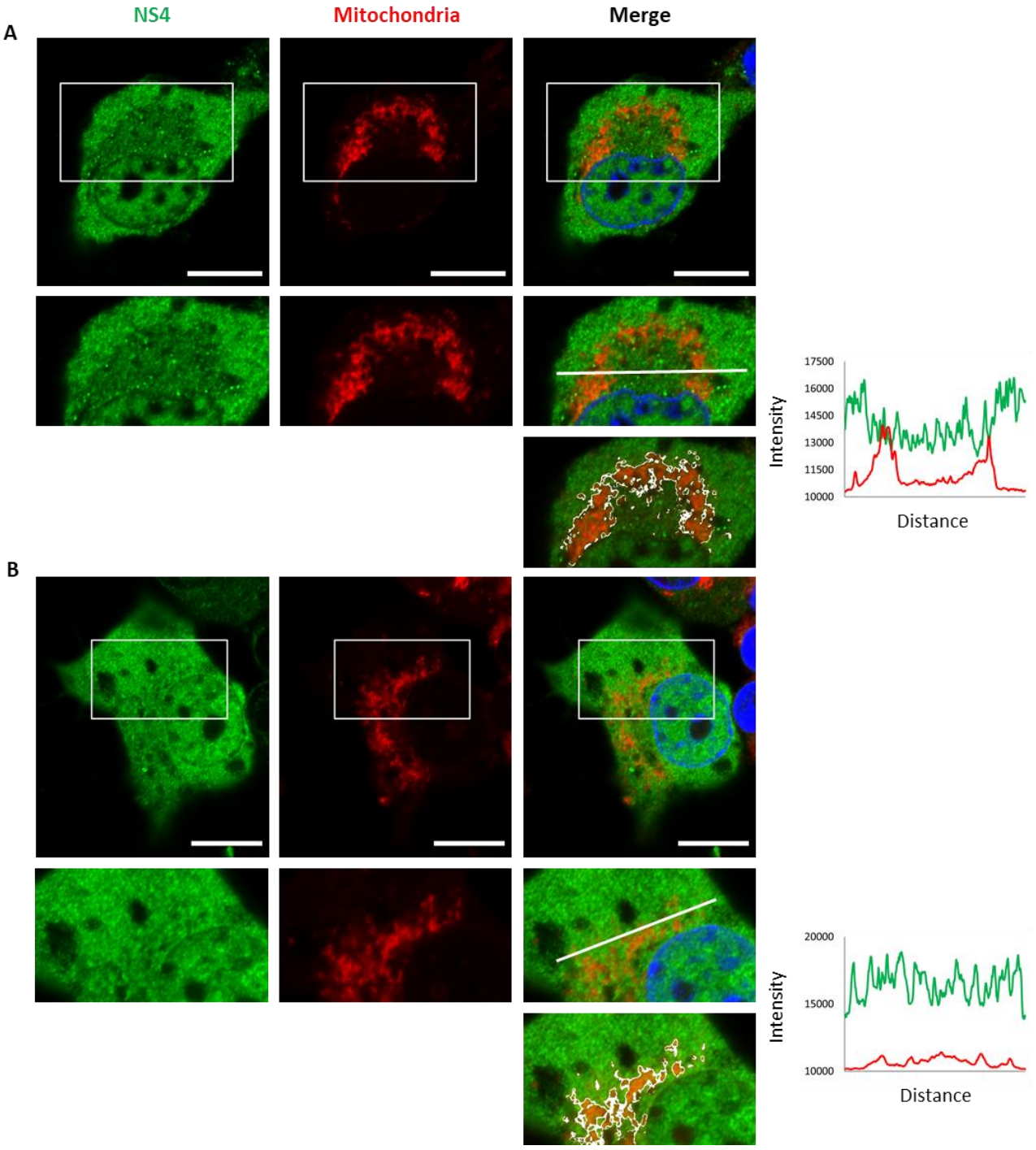


**Figure 2.17. NS4-II surrounds, and shows partial colocalisation with, mitochondria in infected cells.** BSR-T7/5 cells were infected with AHSV1F, which expresses NS4-II, and at 24 hpi were stained with MitoTracker™ and processed for immunofluorescence and CLSM using anti-NS4(E3F) and AF 488 conjugated goat anti-rabbit IgG. (A) Mitochondria leaving a gap on the perinuclear region and (B) evenly distributed mitochondria. Each second row in A and B shows an enlargement of the demarcated areas in the micrographs in the previous row. Fluorescence intensity plots were generated by measuring the fluorescence intensity of each channel along the white line drawn in the merged images. Each third row in A and B shows colocalised pixels (white) as determined by Fiji. Nuclei were stained with DAPI. Scale bars = 10 µm.

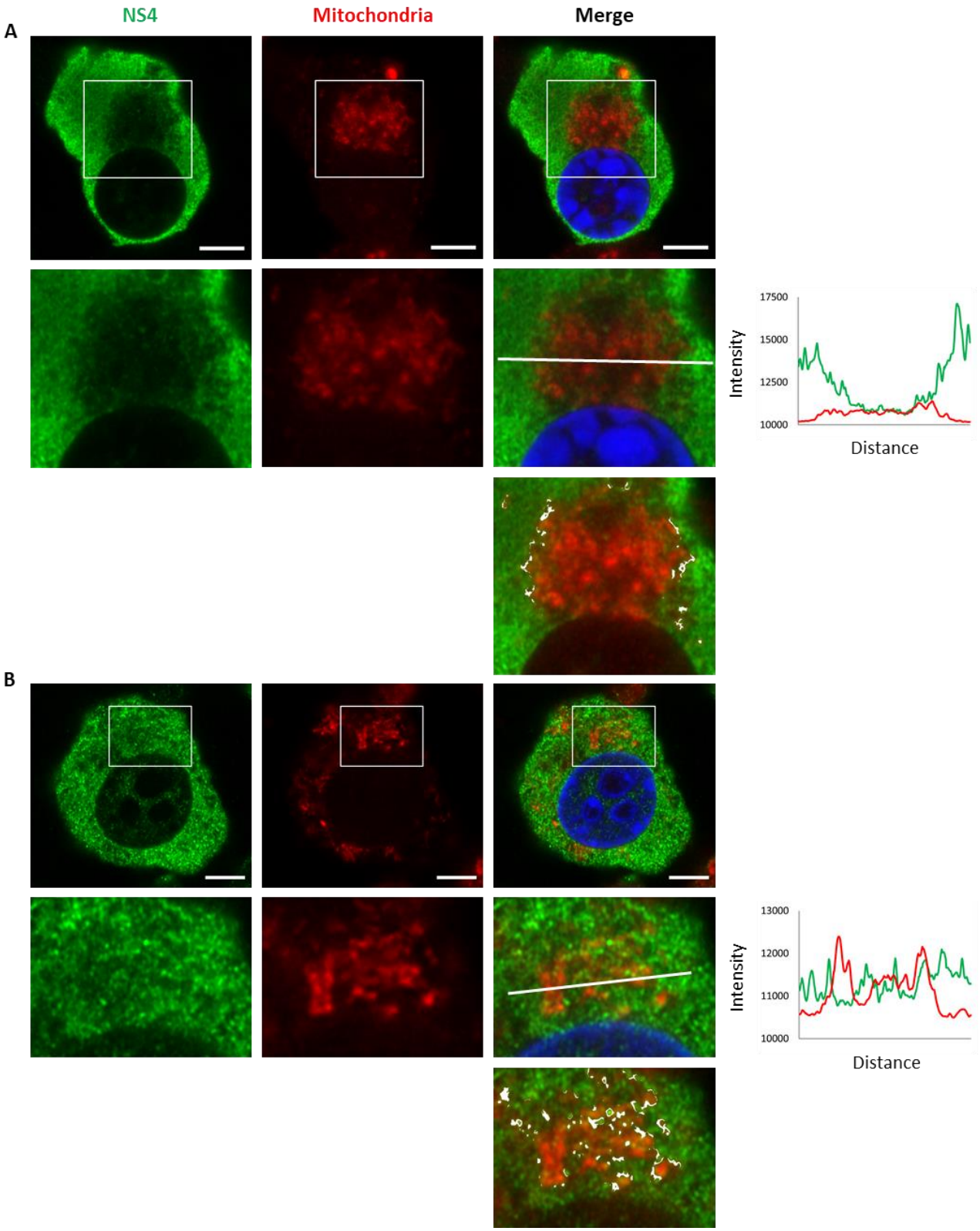


**Figure 2.18. Cytoplasmic NLS-NS4-II surrounds, and shows partial colocalisation with, mitochondria in infected cells.** BSR-T7/5 cells were infected with AHSV8F, which expresses NLS-NS4-II, and at 24 hpi were stained with MitoTracker™ and processed for immunofluorescence and CLSM using anti-NS4(E3F) and AF 488 conjugated goat anti-rabbit IgG. (A) NLS-NS4-II dipped in intensity in the areas in which mitochondria were found and appeared lighter in the green channel at that location. (B) NLS-NS4-II increased in intensity when mitochondria decreased in intensity and vice versa. Each second row in A and B shows an enlargement of the demarcated areas in the micrographs in the previous row. Fluorescence intensity plots were generated by measuring the fluorescence

intensity of each channel along the white line drawn in the merged images. Each third row in A and B shows colocalised pixels (white) as determined by Fiji. Nuclei were stained with DAPI. Scale bars = 10 µm.

These results show that, overall, NS4 surrounds mitochondria in the cytoplasm and at times shows limited partial colocalisation.

## 2.4. DISCUSSION

Non-structural protein NS4 was identified within the last decade, and most of the research done to date has focused on BTV NS4. While some functions have been assigned to BTV NS4, the role of AHSV NS4 in the viral replication cycle and pathogenesis remains largely unknown. NS4 is one of four non-structural proteins expressed by BTV and AHSV. BTV NS1 is a positive regulator of protein synthesis, NS2 forms VIBs which are the sites for viral replication and assembly, and NS3/A is involved in virus trafficking and release. While BTV is the prototype virus within the orbiviruses, AHSV and BTV are different in many aspects. Therefore, research done on BTV NS4 can be used to suggest similar functions for its AHSV counterpart but should not be extrapolated without doing separate investigations into AHSV NS4. This chapter aimed to investigate the colocalisation of AHSV NS4 with NS1, NS2, NS3/A and mitochondria in the hopes of gaining some insight into the role of the protein during virus replication and immunity. Furthermore, interactions with the other non-structural proteins would suggest that AHSV NS4 may be able to influence virulence by regulating viral protein synthesis, affecting viral assembly, and/or affecting virus exit. This was done using immunofluorescence and confocal microscopy, followed by colocalisation analyses on the resulting micrographs. Colocalisation analyses are a good starting point when investigating protein-protein, or protein-organelle, interactions as the results indicate if potential interactions exist. Further experimentation using the yeast two-hybrid system, co-immunoprecipitation or pull-down assays for example can then be done to validate possible interactions. The field strains AHSV4F, AHSV1F and AHSV8F were used in the colocalisation analyses done here as they express NS4-I, NS4-II and NLS-NS4-II respectively and therefore represent all three forms of AHSV NS4 (Boughan *et al.*, 2020).

The tubules characteristic of NS1 (Huismans and Els, 1979; Maree and Huismans, 1997) were observed in cells infected with all three AHSV field strains, as were the VIBs characteristic of NS2 (Thomas *et al.*, 1990; Uitenweerde *et al.*, 1995). NS3 was confirmed to localise to perinuclear areas and the plasma membrane as expected (Hyatt *et al.*, 1991; Stoltz *et al.*, 1996; Ferreira-Venter *et al.*, 2019; Kundlacz *et al.*, 2019). The same patterns of NS4 distribution observed by Boughan *et al.* (2020) were observed here. NS4-I (AHSV4F) was found in the nucleus and cytoplasm of infected cells with the majority localising to the nucleus. NS4-II (AHSV1F) was distributed homogenously throughout the nucleus and cytoplasm, with more being observed in the cytoplasm, and NLS-NS4-II (AHSV8F) formed distinct foci in the nucleus and was homogenously located in the cytoplasm. This confirmed that AHSV NS4 displays three different patterns in infected cells, and apart from NLS-NS4-II foci, NS4 does not form any distinct structures within infected cells. As expected, mitochondria were observed in the cytoplasm of uninfected and infected BSR-T7/5 cells.

Whilst optimising NS4 labelling, homogenous staining of NS4-II was observed in the cytoplasm and nucleus of rAHSV5minNS4-infected cells. It was an unexpected observation, as this virus was designed to lack NS4 expression. No bands corresponding to NS4-II were observed via Western blot of rAHSV5minNS4-infected

cells, probably due to this technique not being as sensitive as CLSM. This low level of expression was observed using two different combinations of antibodies produced in different organisms, and was therefore not due to the antibodies themselves. This issue was addressed further in Chapter 3.

Colocalisation analyses involve comparing pixels in one channel (green) with those located in the same place in a second channel (red). Colocalisation is visualised as yellow pixels in the merged image and can be visualised with the naked eye in cases of strong colocalisation. For example, in a study by Mohl *et al.* (2020), BTV outer capsid protein VP5 colocalised with VIBs and appeared yellow in the merged image. Similarly, NS3 was found to colocalise with the periphery of VIBs (Mohl *et al.*, 2020). In a recent example involving AHSV, a mutant form of AHSV NS3 formed thin fibres that colocalised with NS1 tubules. These structures appeared yellow in the merged image and had a Pearson's R value of 0.616 ± 0.077 indicating relatively strong correlation between the two proteins (Ferreira-Venter *et al.*, 2019). Several studies also show the use of fluorescence intensity profiles in colocalisation analyses (Holloway *et al.*, 2015; Buttafuoco *et al.*, 2020). Of particular interest, Boughan *et al.* (2020) showed that AHSV NS4 colocalises with promyelocytic leukemia nuclear bodies (PML-NBs) using colocalisation analyses with fluorescence intensity plots. In such studies, the profiles of both channels peak at the same place when there is colocalisation. Many studies involving colocalisation occur in the literature and what becomes apparent is that in instances of high levels of colocalisation the proteins/structures being compared display the same shape or localisation pattern in the cell.

The advantage of using more than one method to investigate colocalisation was illustrated when looking at possible interactions between NS4-II and cytoplasmic NS1 tubule bundles. ZEN showed little to no evidence of fluorescence in the green channel, whereas Fiji showed that several areas on the outside of tubule bundles colocalised with NS4-II. In instances such as this, the sheer intensity of fluorescence in the red channel overpowered that of the green channel. If one lowered the maximum value on the y-axis, peaks in green fluorescence could be observed. Overall, limited colocalisation between NS1 and all forms of NS4 was observed on the periphery of NS1 tubule bundles.

It was recently shown that all forms of AHSV NS4 colocalise with PML-NBs within the nucleus (Boughan et al., 2020). Also observed in that study was the colocalisation of NS1 with PML-NBs. Here, limited colocalisation between all forms of NS4 and NS1 was observed in the nucleus. One of the roles of PML-NBs in the cell is involvement in antiviral defense via activation of innate immunity, and many viruses have evolved antagonistic effector proteins that modify PML-NBs, thereby disabling host cell intrinsic defences (Scherer and Stamminger, 2016). It is possible that NS4, in connection with NS1, is one such antagonistic protein.

The formation of cytoplasmic replication factories is an integral part of the viral replication cycle. Within rotavirus infection these factories are termed viroplasms and are formed by NSP2 and NSP5. Reovirus viral factories (VFs) are formed by non-structural protein µNS, while BTV and AHSV VIBs are formed by non-structural protein NS2. The matrix of VIBs is known to contain the structural proteins VP1, VP4 and VP6, which form the viral transcription complex (Modrof *et al.*, 2005), as well as virus particles (Brookes *et al.*, 1993). Small foci of core protein VP7 associate with VIBs in AHSV-infected cells and represent the small amount of VP7 that is available for the formation of the core particle during virus assembly in VIBs (Bekker *et al.*, 2014). In the case of BTV, VP7 only colocalises to VIBs in the presence of VP3 (Kar *et al.*, 2007). Outer capsid protein VP5 associates with transcriptionally active cores in VIBs and at the later stages of infection non-structural protein NS3 relocalises to the periphery of VIBs (Mohl *et al.*, 2020). It is possible that the association of VP5 and NS3 with VIBs play a role in virus maturation and virus egress via the exocytosis at the plasma membrane (Mohl *et al.*, 2020). Colocalisation analyses were used in the above-mentioned studies and proteins that are found in the matrix of virus factories display obvious signs of colocalisation when viewing the micrographs of individual channels. For example, BTV VP6 and VP5 showed a similar shape and overall localisation pattern as entire VIBs in a study by Mohl *et al.* (2020). When these channels were merged, colocalisation was observed throughout the VIBs, including in the matrix. Similar observations are seen in studies involving rotavirus viroplasms and reovirus viral factories (Broering *et al.*, 2004; Papa *et al.*, 2019; Buttafuoco *et al.*, 2020; Crawford *et al.*, 2020). This was not observed here, therefore AHSV NS4 was not observed in the matrix of VIBs. Rather, limited colocalisation was observed between NS4 and the periphery of VIBs, an observation that was more obvious in the cases of NS4-II and NLS-NS4-II, perhaps due to better recognition of the epitopes on these NS4 proteins by the anti-NS4 antibody. It is possible that NS4 gets trapped in the periphery of VIBs during their formation or during the recruitment of the viral mRNA and viral proteins needed for assembly.

BTV NS3 colocalises with the ER and with the Golgi apparatus (Han and Harty, 2004; Labadie *et al.*, 2019) and has also recently been shown to colocalise with the phosphorylated forms of STAT1 and STAT2 (pSTAT1 and pSTAT2) in BTV1 infected cells (Li *et al.*, 2021). Similar to what was described above for proteins located in the matrix of VIBs, NS3 showed the same pattern of intracellular localisation as that of the protein (pSTAT1/pSTAT2) or organelle (ER, Golgi) with which it was being compared (Li *et al.*, 2021). This further indicated that strong colocalisation would be apparent to the naked eye if it existed and limited colocalisation would be detectable using software. Overall, little to no colocalisation between NS3 and NS4-I was observed here, visually or with the use of software. NS4-II and NLS-NS4-II however, showed some colocalisation on the periphery of perinuclear NS3 and NLS-NS4-II was flanked by NS3 at the plasma membrane.

Mitochondria were often seen flanking the perinuclear area, an area occupied by cellular organelles such as the Golgi apparatus. While mitochondria have a somewhat characteristic structure, they are pleomorphic

structures that vary in their morphology, density and location (Dempsey 1956; Soubannier and McBride, 2009) and are under the influence of metabolic and cellular signals. The position of mitochondria can be influenced by developmental stage, physiological context and the need to supply ATP where it is needed (McBride *et al.*, 2006; Trevisan *et al.*, 2018). Several non-structural proteins colocalise with mitochondria and cause intrinsic apoptosis. As mitochondria are an integral part of many cell signalling cascades, such as immunity and cellular proliferation (McBride *et al.*, 2006; Soubannier and McBride, 2009; Wisnovsky *et al.*, 2016) this can lead to the complete collapse of infected cells. CCHFV non-structural protein NSs induces apoptosis by triggering the extrinsic and the intrinsic apoptotic pathways by colocalising in mitochondria and disrupting membrane potential (Barnwal *et al.*, 2016). This permeabilisation of the mitochondria leads to the activation of caspases that lead to apoptosis. Several Hepatitis C virus (HCV) non-structural proteins colocalise with mitochondria. Non-structural protein 4A (NS4A) of HCV genotype 1a alters the distribution of mitochondria and causes intrinsic mitochondria-mediated apoptosis through the release of cytochrome c in to the cytoplasm and the activation of caspase-3 (Nomura-Takigawa *et al.*, 2006). NS4A of HCV genotype 3a has the same properties on its own, or in complex with NS3 (Javed and Manzoor, 2018) and HCV NS5A depolarises mitochondria leading to mitochondria fragmentation and mitophagy (Jassey *et al.*, 2019).

Here, no colocalisation between NS4-I and mitochondria was observed, and NS4-II and NLS-NS4-II showed some colocalisation at the periphery of the organelles. Also observed was that there appeared to be fewer mitochondria in infected cells compared to uninfected cells. AHSV infection causes the depolarisation of mammalian cell mitochondrial membranes, leading to the activation of caspase-3 and intrinsic apoptosis (Stassen *et al.*, 2012). Its similarity to membrane-associated proteins and its localisation at the periphery of mitochondria, suggest that AHSV NS4 may play a role in the induction of intrinsic apoptosis caused by AHSV infection. It is also possible that like BTV VP3, NS4 associates with MAVS on the outer mitochondrial membrane, thereby interfering with RIG-I-like signalling (Pourcelot *et al.*, 2021). The intrinsic apoptosis caused by AHSV infection would account for fewer mitochondria being observed in infected cells as MitoTracker® stains active mitochondria.

Literature suggests that true colocalisation or high levels of colocalisation between two proteins or a protein and an organelle are obvious both when analysing the micrographs visually and with the use of software. Therefore, while some overlap between NS4 and the perimeter of NS1 tubule bundles, NS2 VIBs, perinuclear NS3 and mitochondria was observed in this chapter it was limited and overall, very little colocalisation was present despite the literature suggesting possible interactions of NS4 with the other AHSV non-structural proteins and mitochondria. While it is possible that some interactions may occur, the level of colocalisation is too low to warrant further investigations and was most likely observed due to chance based on the proximity of the proteins and organelles in the cell.

# CHAPTER 3

## INVESTIGATING THE ROLE OF AHSV NS4 ON THE VIRAL PHENOTYPE, AND ON VIRULENCE IN AN EMBRYONATED CHICKEN EGG MODEL

## 3.1. INTRODUCTION

Viral infections are characterised by virulence and pathogenesis. Virulence refers to the virus and its ability to cause disease within the host, and pathogenesis refers to the development of disease in the host and is the result of the interplay of many factors unique to the virus, the species and the individual host (Heise and Virgin, 2013). Attenuation refers to a virus becoming less virulent. As such an attenuated virus is one that replicates but causes no disease or very mild disease in the host. The viral molecular determinants and exact interplay between virulence and pathogenesis with regard to AHSV infection is largely unknown.

After a susceptible host has been bitten by an AHSV-infected *Culicoides* midge, the virus moves toward regional lymph nodes in which initial replication occurs. Virus particles then disseminate in the blood (primary viraemia) allowing the virus to move throughout the body of the infected horse (Mellor and Hamblin, 2004; Zientara *et al.*, 2015; Dennis *et al.*, 2019). The virus subsequently infects a number of target organs including the heart, lungs, spleen and lymphoid tissues giving rise to secondary viraemia, the duration of which is variable (Erasmus, 1973; Mellor and Hamblin, 2004; Clift and Penrith, 2010). Microvascular endothelial cells and monocyte–macrophages are the main target cells for virus replication (Brown *et al.*, 1994; Wohlsein *et al.*, 1997; Wohlsein *et al.*, 1998; Clift and Penrith, 2010).

Although the level of AHSV replication is relatively low in these organs, AHSV causes severe damage to the microvascular endothelial cells. This is the major cause of the lesions typically observed in the more severe forms of AHS, and is dependent on the organ and type of blood vessel and independent of the form of AHS (Gomez-Villamandos *et al.*, 1999). Microvascular damage is characterised by loss of electron density of the cytoplasm, loss of endothelial cells and disruption to intercellular junctions (Laegreid *et al.*, 1992; Gomez-Villamandos *et al.*, 1999; Mellor and Hamblin, 2004). This causes an increase in permeability of capillary walls, resulting in oedema, haemorrhaging and microthromboses of the lung and myocardium in particular (Gomez-Villamandos *et al.*, 1999; Zientara *et al.*, 2015; Dennis *et al.*, 2019).

AHS manifests as one of four forms. Horse sickness fever is the mildest form of the disease and has an incubation period of 4-14 days. It is characterised by mild to moderate fever that is often more pronounced in the afternoon (Erasmus, 1973; Burrage and Laegreid, 1994). No mortality is observed with this form of AHS (Mellor and Hamblin, 2004). The cardiac (or subacute) form has a mortality rate between 50 and 70% and clinical signs include fever and subcutaneous oedema of the head, neck and chest. Also common is the presence of a gelatinous exudate in the subcutaneous, subfascial, subserous and intermuscular tissues and lymph nodes (Erasmus, 1973; Mellor and Hamblin, 2004). Petechial haemorrhaging can occur in the eyes, with some ecchymotic haemorrhages on the tongue (Erasmus, 1973; Mellor and Hamblin, 2004). Hydropericardium is also a characteristic lesion of this form of disease and death occurs within 4-8 days after the onset of clinical lesions (Erasmus, 1973; Burrage and Laegreid, 1994). The pulmonary (or peracute) form

develops rapidly and is the most severe form of AHS, showing mortality rates upward of 95% (Erasmus, 1973). The most common lesions associated with this form of disease are fever and pulmonary (including alveolar and interstitial) oedema that may be associated with pleural effusion (Burrage and Laegreid, 1994; Mellor and Hamblin, 2004). Subpleural and interlobular tissues may also become infiltrated with yellow gelatinous exudate with the bronchial tree filled with a surfactant, stabilised froth (Mellor and Hamblin, 2004). In this form the infected horse dies from asphyxia (Erasmus, 1973). The mixed form is the most prevalent form of the disease, and infected horses present with lesions common to both the cardiac and pulmonary forms of AHS. The incubation period rate is intermediate between the cardiac and pulmonary forms of the disease and the mortality rate is approximately 70% (Burrage and Laegreid, 1994; Mellor and Hamblin, 2004). Direct microvascular damage causing increased vascular permeability is thought to play more of a role in the pathogenesis of oedema in the cardiac (subacute) and mixed forms of AHS than heart failure (Erasmus, 1973; Clift and Penrith, 2010).

Although the nine serotypes of AHSV have the same target cells (Clift and Penrith, 2010) each serotype displays varying clinical lesions in different horses (Laegreid *et al.*, 1993). Virulence is complex and multifactorial, with factors such as the efficiency of replication, tropism, the ability of the virus to infect susceptible cells, evade the immune system, and cause tissue damage, are all thought to influence virus virulence (Heise and Virgin, 2013). It also appears that certain viral proteins play a role in orbivirus virulence. In particular it has been suggested that some of the major candidates are the proteins encoded by the more variable genome segments such VP2 and VP5 (involved in entry) and NS3/NS3A (involved in exit) (O'Hara *et al.*, 1998; Huismans *et al.*, 2004; Coetzee *et al.*, 2012).

A study done in the 1970s linked plaque morphology to virulence, with large plaques in Vero cells associated with attenuated AHSV4 (Erasmus, 1973). A recent study showed that outer capsid protein VP2 is responsible for plaque morphology, in particular one amino acid that increases the hydrophilicity of VP2 in large plaque strains (Schade-Weskott *et al.*, 2018). This agrees with a previous BTV8 study showing that incorporating a so-called “large plaque” Seg-2 into a small plaque virus causes a change in plaque phenotype from small to large (Janowicz *et al.*, 2015). This study also showed that mutations to VP2 and NS3 reduce the virulence of BTV in IFNAR$^{-/-}$ mice but do not cause complete attenuation. Full attenuation was achieved by mutating VP2 in combination with VP1, VP6 or NS3 (Janowicz *et al.*, 2015). Furthermore, BTV8 with a high passage number required at least 5 genome segments from the same virus with a low passage number for a full reversion to virulence. Thus, VP2 and NS3 are the major determinants of BTV8 pathogenesis but structural proteins VP1, VP4, VP5, VP6 and VP7 also play a role, showing that multiple genome segments determine BTV virulence (Janowicz *et al.*, 2015). In addition, Ratinier *et al.* (2016) showed that BTV NS4 favours replication in sheep and that knocking out NS4 (BTV8ΔNS4) results in attenuation of BTV8 in sheep. Therefore, NS4 is also a BTV virulence factor.

Knocking out NS3/NS3A leads to the attenuation of BTV8 (Feenstra *et al.*, 2014), while a 77 amino acid region in NS3/NS3A is essential for AHSV virulence and the deletion thereof results in an attenuated virus (van Rijn *et al.*, 2018). A decrease in the amount of NS1 tubules in an infected cell changes the pathogenesis of BTV. Instead of cell rounding, apoptosis and lytic release there is a shift to budding of virions from the plasma membrane accompanied by a decrease in CPE and an increase in release of infectious virions. The ratio of NS1 tubules to NS3 is also thought to influence this (Owens *et al.*, 2004). Some proteins also influence virulence in other ways *e.g.,* BTV NS3 and NS4 act as IFN antagonists and work together to target STAT1 (Chauveau *et al.*, 2013; Ratinier *et al.*, 2016; Li *et al.*, 2021). Furthermore, NS3 is a viroporin and plays a role in membrane permeability (Han and Harty, 2004; Meiring *et al.*, 2009).

In naturally and experimentally infected horses, AHSV NS4 is observed in the cytoplasm and nucleus of microvascular endothelial cells and mononuclear phagocytes of the heart and lung, and in stellate-shaped dendritic macrophage-like cells with long cytoplasmic processes in the red pulp of the spleen (Zwart *et al.*, 2015). It is possible that these cells are dendritic macrophage-like antigen-presenting cells. If so, AHSV NS4 could play an important role in interactions with the host immune system (Zwart *et al.*, 2015). Therefore, based on what has been observed for other non-structural proteins and for BTV NS4 it was proposed that AHSV NS4 be added to the list of candidates for influencing viral virulence.

Studies in horses are expensive, time-consuming and raise ethical concerns, therefore one of the factors that impedes AHSV research is the lack of a suitable small animal model in which to study the virus (Maartens *et al.*, 2011). Strains of AHSV that are attenuated in horses kill IFNAR$^{-/-}$ mice, therefore the use of mice as a small animal model in the study of AHSV virulence and pathogenesis is not suitable (Prof. PA van Rijn, personal communication). A small animal model that has proved useful in a wide array of studies is the embryonated chicken egg (ECE) model. This small animal model is particularly advantageous as embryonated eggs are available all year round, are inexpensive, do not require major infrastructure for incubation and can be easily manipulated *in ovo* (Darnell and Schoenwolf, 2000; Bahr, 2008; Bednarczyk *et al.*, 2021). Furthermore, compared to mammalian animal models, chicken embryos develop quickly (Bednarczyk *et al.*, 2021) and are more ethically acceptable, allowing for more research to be performed in a shorter periods of time. As a result, the ECE model has been used widely in many research areas, including vascular permeability, virology, embryology, epigenetics, development, reproduction and ovarian cancer (Flamme *et al.*, 1995; Darnell and Schoenwolf, 2000; Dauber *et al.*, 2004; Bahr, 2008; Pink *et al.*, 2012; Bednarczyk *et al.*, 2021).

Although few studies have been done thus far, the ECE model has proved useful in studies involving AHSV. The first study was part of an MSc dissertation (Maartens, 2009), parts of which were later published (Maartens *et al.*, 2011). This work aimed to investigate tissue tropism of AHSV in ECEs. Virulent AHSV5 was

shown to kill ECEs within 60 hours of infection (Maartens, 2009; Maartens *et al.*, 2011). These embryos appeared cherry-red in colour due to hyperaemia. Also observed were petechial or ecchymotic haemorrhages on the head, neck, trunk, limbs, or feather follicles (Maartens, 2009). As in horses, endothelial damage was a key contributor to the pathogenesis of AHSV in ECEs. Positive immunolabelling was detected in the microvascular endothelial cells, and in some cases mononuclear-like cells, within tissues such as the dermis and feather pulp, liver, lung, spleen, cardiac and skeletal muscle (Maartens *et al.*, 2011). Therefore, similar tissue tropism to that observed in AHSV-infected horses was seen in infected ECEs (Maartens, 2009; Maartens *et al.*, 2011). This study also showed that the selective tropism of AHSV for certain endothelial cells in horses was also observed in ECEs (Maartens *et al.*, 2011). In preliminary work done at Deltamune (Pty) Ltd, ECEs infected with a recombinant virulent AHSV5 virus (rFR) died within 3 to 4 days of infection and showed typical lesions of AHSV infection such as full body hyperaemia and oedema. In contrast, the same virus lacking NS4 expression did not kill any ECEs and none of the embryos showed signs of infection. Therefore, rFR was deemed virulent in ECEs and the NS4 knockout was attenuated. This resulted in a patent for the knockout virus due to its vaccine potential (Potgieter *et al.*, 2017). Also investigated was rAHSV4LP, which was rescued based on the attenuated strain of AHSV4 described by Erasmus (1974), and the same virus lacking NS4 expression. Both viruses were attenuated in ECEs. The same results were observed in horses infected with these viruses, further suggesting that the ECE model is a good small animal model in which to study AHSV.

The aim of this chapter was to investigate the role of NS4 in AHSV viral replication, virulence, and pathogenesis. To do this, reverse genetics was used to generate wild-type, NS4 knockout and reassortant viruses based on virulent AHSV5 and attenuated AHSV4LP. All reverse genetics-derived viruses were assayed *in vitro* to assess the expression and intracellular localisation of NS4, as well as the replication kinetics of the viruses in BSR cells. Pathogenicity and virulence were then assayed *in vivo* using an ECE model.

## 3.2. MATERIALS AND METHODS

### 3.2.1. Cells and viruses

BSR-T7/5 cells (Section 2.2.1.), BSR cells (a clone of BHK-21 cells and a gift from Prof. PA van Rijn) and BSR-T7/5-Clone 16 cells [BSR-T7/5 cells with a biallelic STAT1 knockout, obtained from Prof. AC Potgieter, Deltamune (Pty) Ltd] were maintained as monolayers in Dulbecco's Modified Eagle's Medium (DMEM, HyClone™) supplemented with 10% FBS, 1.2% Fungizone and 1% Pen/Strep at 37°C, with $CO_2$ and 90% humidity. The AHSV4 and AHSV5 OIE reference strains have been described previously (Potgieter *et al.*, 2015). Here, they are referred to as AHSV4Ref and AHSV5Ref (Table 3.1.) and were obtained from Prof. AC Potgieter at Deltamune (Pty) Ltd. Virus titres were determined as described in Section 2.2.2.

**Table 3.1.** AHSV reference strains and recombinant wild type, knockout and reassortant viruses used or generated in Chapter 3.

| Virus | Details |
|---|---|
| AHSV5Ref | OIE reference strain received from Prof. AC Potgieter at Deltamune (Pty) Ltd.<br>Virulent AHSV5 isolate HS 30/62 (Fourie, FR). The isolation history has been described previously in Potgieter *et al.* (2015). |
| AHSV4Ref | OIE reference strain received from Prof. AC Potgieter at Deltamune (Pty) Ltd.<br>Virulent AHSV4 isolate HS 32/62. The isolation history has been described previously in Potgieter *et al.* (2015). |
| rAHSV5 | Rescued by RG to represent the virulent reference strain AHSV5 isolate HS 30/62. |
| rAHSV5ΔNS4 | Rescued by RG using transcription plasmids containing AHSV5 Seg-1 to -8 and Seg-10 plus the plasmid containing AHSV5 Seg-9ΔNS4 ($S9_{5\Delta NS4}$). |
| rAHSV4LP | Rescued by RG to represent attenuated AHSV4LP. This virus represents virulent AHSV4 HS 32/62 that was attenuated by passage in cell culture and the selection of large plaques in Vero cells, official passage number is HS32/62-10S-10BHK-3LP-7Vero (Erasmus, 1973). |
| rAHSV4LPΔNS4 | Rescued by RG using transcription plasmids containing AHSV4LP Seg-1 to -8 and Seg-10 plus the plasmid containing AHSV4LP Seg-9ΔNS4 ($S9_{4LP\Delta NS4}$). |
| rAHSV5+$S9_{4LP}$ | Reassortant containing the AHSV5 backbone with Seg-9 from AHSV4LP ($S9_{4LP}$). Rescued by RG. |
| rAHSV5+$S9_{4LP\Delta NS4}$ | Reassortant containing AHSV5 backbone rAHSV4LP Seg-9ΔNS4 ($S9_{4LP\Delta NS4}$). Rescued by RG. |
| rAHSV4LP+$S9_5$ | Reassortant containing the AHSV4LP backbone with Seg-9 from AHSV5 ($S9_5$). Rescued by RG. |
| rAHSV4LP+$S9_{5\Delta NS4}$ | Reassortant containing AHSV4LP backbone with rAHSV5 Seg-9ΔNS4 ($S9_{5\Delta NS4}$). Rescued by RG. |

RG = reverse genetics.
S9 = Seg-9.

### 3.2.2. Rescue of recombinant wild-type, knockout and reassortant viruses

In this study two virus backbones were used to assess the contribution of NS4 to virulence and pathogenicity. The first, AHSV5, represents wild-type virulent AHSV and the second, AHSV4LP, represents attenuated AHSV. The pathogenicity of both these viruses have been tested in horses to confirm their phenotypes (Potgieter *et al.*, 2017; van Rijn *et al.*, 2018). The plasmid-based reverse genetics protocol was used to rescue the viruses used in this chapter, as described in Section 2.2.2. The recombinant viruses, rAHSV4LP and rAHSV5 are described in Section 2.2.2. A full list of viruses used or generated in this chapter is provided in Table 3.1.

An AHSV5 NS4 knockout, rAHSV5ΔNS4, was rescued using the AHSV5 Seg-9ΔNS4 plasmid ($S9_{5\Delta NS4}$) obtained from Dr S Boughan (University of Pretoria). This transcription plasmid included the nucleotide substitutions detailed in Section 2.2.2., as well as two additional modifications, G209A and T332A, which introduced two stop codons at amino acids positions 6 and 47 respectively in the NS4 ORF, effectively abolishing AHSV5 NS4 expression (Figure 3.1A). The stop codon-generating mutations were introduced due to the low levels of leaky NS4 expression detected from rAHSV5minNS4 in Chapter 2 of this study.

The AHSV4 NS4 knockout mutant, rAHSV4LPΔNS4, was rescued using the AHSV4LP Seg-9ΔNS4 plasmid ($S9_{4LP\Delta NS4}$) obtained from Prof. AC Potgieter which was synthesised at GenScript Corporation. This plasmid included the nucleotide substitutions detailed in Section 2.2.2., as well as two additional modifications G338A and G347A, that introduced two stop codons at amino acid positions 42 and 45 respectively in the NS4 ORF to ensure AHSV4 NS4 expression was abolished (Figure 3.1B). The stop codons and modifications were introduced based on results with rAHSV5minNS4 where it was shown that both changes of start codons and inclusion of stop codons are needed to completely abolish detectable NS4 expression (Chapter 2 of this study).

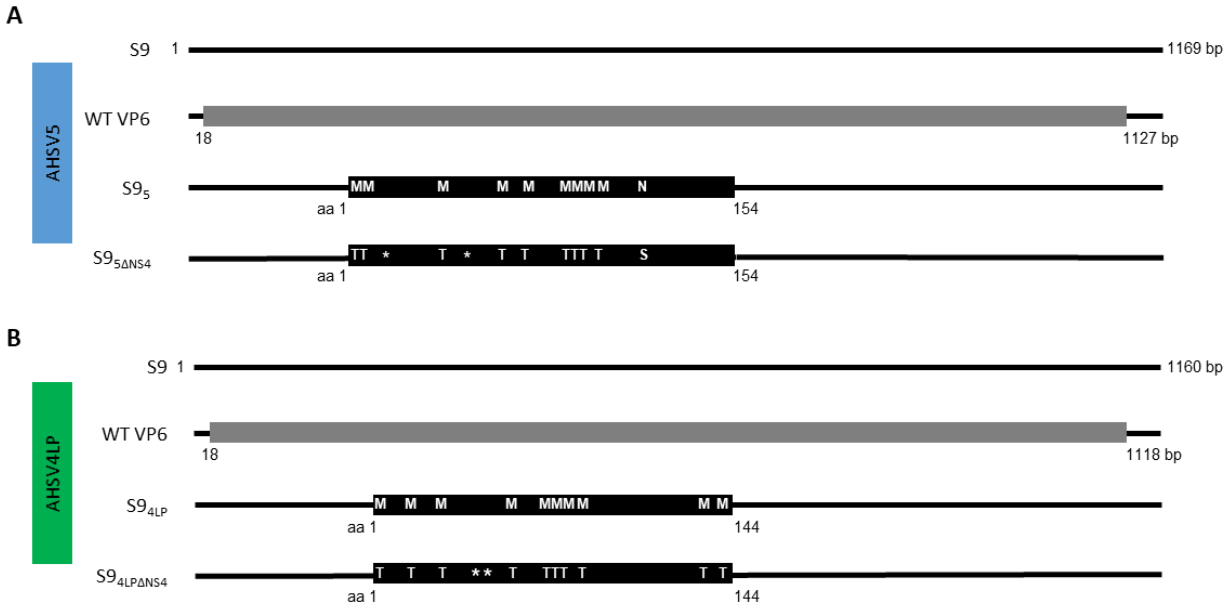


**Figure 3.1. Schematic representation of AHSV5 and AHSV4LP Seg-9 (S9) and the positions of the wild type (WT) VP6 and NS4 ORFs.** Specific amino acid changes to $S9_5$ and $S9_{4LP}$ are shown in $S9_{5\Delta NS4}$ (A) and $S9_{4LP\Delta NS4}$ (B) and the introduction of stop codons are illustrated by an *.

Genomic reassortants between rAHSV4LP and rAHSV5 were also rescued and are denoted with the name of the virus forming the backbone, followed by the substituted segment marked with a “4” or “5” subscript to indicate the serotype of the virus of origin. For example, rAHSV4LP+$S9_5$ is a reassortant containing the AHSV4LP backbone (Seg-1 to Seg-8 and Seg-10) and Seg-9 from AHSV5.

### 3.2.3. Isolation of dsRNA

BSR cells seeded in 6 well plates ($3.8x10^6$ cells) were infected with the recombinant wild-type, knockout or reassortant viruses (Table 3.1) at an MOI of 0.1 and harvested when full CPE was observed. The cells were then collected via low-speed centrifugation at 1 180 x g for 10 min at 4°C. The supernatant was discarded, and the pellet resuspended in 1 ml TRI Reagent™ solution (Invitrogen™) to lyse the cells. After 5 min at RT, 200 µl chloroform (Merck) was added and the tube was shaken vigorously for 15 seconds (s) and incubated for 3 min at RT. To allow for phase separation the solution was centrifuged at 10 625 x g for 15 min at 4°C. The upper aqueous phase containing RNA was collected and 500 µl isopropanol was added to precipitate the RNA. After 10 min incubation at RT, the solution was centrifuged at 10 625 x g for 10 min at 4°C to pellet the RNA. The pellet was then rinsed once with 75% ethanol (4 150 x g, 10 min, 4°C), air-dried and resuspended in 100 µl LiChlorosolv® Water (Merck). Thereafter, lithium chloride was added to a final concentration of 2 M and the sample incubated for at least 18 h at 4°C to precipitate ssRNA. ssRNA was pelleted via centrifugation at 16 602 x g for 30 min at 4°C and the dsRNA-containing supernatant was kept. The dsRNA was precipitated by adding 20 µl 1M sodium chloride and 350 µl 96% ethanol and incubating at -20°C for at least one h. The pellet was collected via centrifugation at 16 602 x g for 15 min at 4°C and then vortexed briefly with 1 ml 96% ethanol and centrifuged at 16 602 x g for 20 min at 4°C. The dsRNA pellet was airdried and resuspended in 40 µl of LiChlorosolv® Water before being quantified using NanoDrop™ ND-1000 spectrophotometry (Thermo Scientific™) and visualised via agarose gel electrophoresis.

### 3.2.4. Agarose gel electrophoresis

Samples were mixed with 6 x TriTrack DNA Loading Dye (Thermo Scientific™) and resolved using 1-1.5% agarose gels prepared with 1 × TAE (40 mM Tris-HCl, 20 mM acetic acid, 1 mM EDTA) and 0.5 µg/µl ethidium bromide. Gels were run in 1 x TAE at 90 V until adequate separation was observed.

### 3.2.5. First strand cDNA synthesis and polymerase chain reaction (PCR) of Seg-9

The dsRNA was denatured in the presence of DMSO (Thermo Scientific™) for 2 min at 95°C at a concentration of 1.6 µl/500 ng of dsRNA and used as a template for cDNA synthesis using the RevertAid First Strand cDNA synthesis kit (Thermo Scientific™). The reaction was then placed on ice and 1 µl random hexamer primers and nuclease-free water to a total volume of 12 µl were added. To this, 5X reaction buffer, RiboLock RNase Inhibitor (20 U/µl), 10 mM dNTP mix and RevertAid H Minus M-MuLV Reverse Transcriptase (200 U/µl) were added to a final volume of 20 µl. The reaction was mixed gently and centrifuged, followed by incubation at 25°C for 5 min and 60 min at 42°C. Incubation at 70°C for 5 min terminated the reaction. The resulting first strand cDNA was used for polymerase chain reaction (PCR) amplification of Seg-9. Seg-9 was amplified using DreamTaq PCR Master Mix (2X, Thermo Scientific™), containing DreamTaq DNA Polymerase, optimised DreamTaq buffer, MgCl2 and dNTPs. Each PCR reaction contained 12.5 µl DreamTaq Master Mix, 0.5 µM each

of NS4 all serotypes forward and reverse primers (Table 3.2.), 1 µl of the cDNA product (template) and nuclease-free water to a final volume of 20 µl. The PCR conditions included an initial denaturation step of 95°C for 2 min, followed by 30 cycles of denaturation at 95°C for 30 s, primer annealing at 54°C for 30 s and extension at 72°C for 1 min. Final extension was done at 72°C for 10 min. Following amplification, the PCR products were analysed via agarose gel electrophoresis and used as template for the sequencing of Seg-9.

**Table 3.2.** AHSV Seg-9 specific primers used for PCR and sequencing.

| Primer name | Primer type | NS4 type | Primer sequence (5'-3') |
|---|---|---|---|
| NS4 All serotypes For | Forward | All | CTCATGTCTTCGGCATTACTC |
| NS4 All serotypes Rev | Reverse | All | GCAAGCCCCTATCTACAGTAAATAAG |
| NS4-I For | Forward | NS4-I | ATAGGATCCGATGGAGGATTGGGATCAGC |
| NS4-I Rev | Reverse | NS4-I | CCAAGCTTCTAATCCCCCATCCCGTC |
| NS4-II For | Forward | NS4-II | AAGGATCCTATGATGATCGAAGAGTGGA |
| NS4-II Rev | Reverse | NS4-II | GGAAGCTTCTAATCCTCCAATCCGTCTA |

All primers were received from Dr S Boughan (Boughan *et al.*, 2020).
For = Forward.
Rev = Reverse.

### 3.2.6. Sequencing of Seg-9

The PCR products generated in Section 3.2.6. were used to sequence Seg-9. To do this, the ABI PRISM BigDye™ Terminator Cycle Sequencing kit (v3.1, Applied Biosystems) was used. Briefly, 1 µl BigDye™ reaction mix and 1 µl of 5 x sequencing buffer were added to 2.1 µM sequencing primer (Table 3.2), 50 ng of the DNA sample and LiChlorosolv® Water to a final volume of 10 µl. Cycle sequencing was done with an initial step of 96°C for 3 min, followed by 30 cycles of 96°C for 10 s, 60°C (NS4-I primers)/54°C (NS4-II primers) for 5 s and 60°C for 4 min before bring the reaction down to 4°C. Thereafter, each 10 µl reaction was added to 3 µl NaOAc (3M, pH 4.6), 62.6 µl absolute ethanol and 24.5 µl LiChlorosolv® Water in a 500 µl Eppendorf tube® to make a final volume of 100 µl. After vortexing briefly, the reactions were centrifuged at 16 100 x g for 45 min. The supernatant was removed and 250 µl of freshly prepared 70% ethanol was immediately added, and the reactions were vortexed briefly. Centrifugation was done at 16 100 x g for 10 min before repeating the 70% ethanol wash step. The supernatant was removed, and the pellets were allowed to dry on a heating block at 60°C for ±10 min. The dried pellets were then placed into an Applied Biosystems 3500xl genetic analyser (Life Technologies) at the DNA Sequencing Laboratory of the University of Pretoria. Sequences were aligned using BioEdit Sequence Alignment Editor (v7.2.5).

### 3.2.7. Harvesting infected cells for protein expression analysis

Monolayers of BSR-T7/5 cells ($3.8x10^6$ cells) were infected with the viruses listed in Table 3.1 and harvested as described in Section 2.2.3 at 24 hpi.

### 3.2.8. Protein expression analysis via SDS-PAGE and Western blot

Samples were subjected to SDS-PAGE (15% separating gel, 5% stacking gel) and Western blot as described in Sections 2.2.7 and 2.2.8. The anti-NS4(GS), anti-NS1(786) and anti-NS2 primary antibodies were used in conjunction with protein A HRP conjugate (Section 2.2.8).

### 3.2.9. Immunofluorescence and confocal microscopy

BSR-T7/5 cells grown on sterile coverslips in 24-well plates were infected at an MOI of 0.1 and at 24 hpi were processed for immunofluorescence and CLSM as described in Section 2.2.9. For dual labelling of NS4 and VP7, anti-NS4(E3F) primary and AF 633 conjugated goat anti-rabbit IgY secondary antibody (Table 2.2) were used to label NS4. Guinea pig anti-VP7 (Rutkowska *et al.*, 2011) and Alexa Flour® 488 goat anti-guinea pig IgG (H+L) (Invitrogen™, A11073) were used to label VP7. All slides were viewed using a Zeiss LSM 880 CLSM coupled to an Airyscan detector.

### 3.2.10. Virus growth curves

Virus growth curves were carried out in BSR cells. Cell monolayers in 24-well plates were infected with the appropriate virus (Table 3.1.) at a MOI of 0.1. After 1 h, the virus was removed, and the cells rinsed with clean DMEM to remove any unbound virus. Complete DMEM was then added to each well and the plates were incubated at 37°C, with $CO_2$ and 90% humidity. At 12, 24, 36, 48 and 72 hpi cells were harvested by scraping and total virus was collected and resuspended with a 22G needle. Virus titre was determined by endpoint dilution in BSR cells followed by immunoperoxidase monolayer assay (IPMA) after 72 h, according to standard procedures (Wensvoort *et al.*, 1986). Cells were fixed with ice-cold 50% methanol:50% acetone and incubated at -20°C for 30 min. Thereafter, blocking was done with 1% tryptone (Merck) and 0.05% Tween-20 (Sigma-Aldrich®) in 1 x PBS. Primary antibody labelling was done with anti-NS2 (Table 2.2) diluted in blocking solution at 37°C, with $CO_2$ and 90% humidity. Cells were then washed three times with wash buffer (Section 2.2.8) and incubated with protein A HRP conjugate (Section 2.2.8) diluted in blocking solution (1 hr, 37°C, with $CO_2$ and 90% humidity). Cells were washed three times with wash buffer and chromagen development was done using the AEC staining kit (Sigma-Aldrich®). Titres were expressed as $\log_{10}TCID_{50}$/ml and each experiment was performed independently in triplicate from two different virus stocks. Statistical analyses were done using one-way ANOVA and Dunnett's T3 test ($P < 0.05$) in IBM® SPSS® Statistics Software (v26).

### 3.2.11. Infection of embryonated chicken eggs (ECEs)

Embryonated chicken egg experiments were performed at Deltamune (Pty) Ltd (DEC approval number O-15-25). ECEs were obtained from the specific pathogen–free White Leghorn flock managed by Avifarms (Pty) Ltd (Lyttelton, South Africa). Thirteen days after incubation the ECEs were injected intravenously with ~100 µl each of the recombinant wild-type, knockout and reassortant viruses listed in Table 3.1. Briefly, an ECE was candled and a hobby drill was used to create a small window in the eggshell above a suitable chorio-allantoic

blood vessel. ECEs were injected with 100 µl virus or MEM using an insulin syringe with a fixed 27G needle. The windows were then sealed with a drop of wood and paper glue and the ECEs incubated at 32°C with humidity. Thereafter, the ECEs were candled once a day and mortalities recorded. ECEs showing movement of the embryo and intact chorio-allantoic vasculature were considered viable. Death was indicated by lack of movement of the embryo and collapse of the chorio-allantoic blood vessels. Embryos that died within 12 h of inoculation were considered non-specific deaths. In the case of death, the ECE was placed at 4°C until harvesting. Any embryos that were still alive on day 6 post inoculation were euthanised by hypothermia (4°C for at least 5 h).

### 3.2.12. Harvesting ECEs

Each embryo was removed from the egg using sterile tweezers and separated from the allantoic, amniotic and yolk sacs by severing the umbilical cord. The embryos were placed on sterile petri dishes and examined for any lesions typical of AHSV infection. Photographs were taken using a Huawei P30 lite phone (Huawei Device Co., Ltd). The head, wings and legs were then removed and discarded, and the remaining tissue was homogenised using grit and a mortar and pestle. Before pouring into a sterile Falcon tube, 1.5 ml 1 x PBS per embryo was added the homogenate.

### 3.2.13. Total RNA isolation from ECEs

The initial steps of RNA isolation were done using a MagNA Lyser Instrument (Roche Diagnostics) as it homogenises tissues and cells. Therefore, the initial steps were done in 2 ml screw-capped tubes containing ceramic beads 1.4 mm in diameter (MagNA Lyser Green Beads, Roche Diagnostics). To each tube 750 µl TRI Reagent™ solution, 50 µl LiChlorosolv® Water and 200 µl of the homogenate were added. Shaking was then done in the MagNA Lyser Instrument at 7 000 rpm for 1 min. Thereafter, 200 µl chloroform was added and shaking was done in the MagNA Lyser Instrument for 30 s before the tubes were incubated at RT for 3 min. The tubes were then centrifuged at 13 539 x g for 15 min at 4°C to allow for phase separation. The RNA containing aqueous phase was transferred to a new tube containing 500 µl of isopropanol and mixed well. After incubation at RT for 10 min, the solution was centrifuged at 13 539 x g for 10 min at 4°C to pellet the RNA. The supernatant was removed, and the pellet washed with 1 ml freshly prepared 75% ethanol made with LiChlorosolv® Water (5 289 x g, 10 min, 4°C). The supernatant was removed and the pellet airdried before being dissolved in 100 µl LiChlorosolv® Water.

### 3.2.14. Real-time reverse transcriptase polymerase chain reaction (RT-PCR)

RT-PCR targeting Seg-4 (VP4), or Seg-5 (NS1) was done using the LightCycler® 480 RNA Master Hydrolysis Probes kit (Roche Diagnostics). The primers and probes were designed by Olfert Landt (TIB MolBiol, Seg-4) or Prof. AC Potgieter (Seg-5) and synthesised by TIB Molbiol and are listed in Table 3.3. The probes were labelled with the fluorescent dye 6-carboxyfluorescein (FAM) and had a black hole quencher (BHQ) on the 3’ end.

Reactions consisted of 2.1 µl LiChlorosolv® Water, 0.65 µl Activator, 200 nM of each primer, 100 nM of hydrolysis probe, 3.75 µl of 2.7 x LightCycler® 480 RNA Master Hydrolysis Probes mix and 3 µl sample RNA. The reactions were placed into a LightCycler® Nano Real-Time PCR System (Roche Diagnostics) and cycled at 98°C for 20 s to denature dsRNA, 61°C for 5 min for reverse transcription, followed by 40 cycles of 95°C for 10 s and 61°C for 20 s for target amplification and detection. LightCycler® Nano Software (v1.1.0, Roche Diagnostics) and Microsoft Excel were used to analyse the amplification data.

**Table 3.3.** Primers and probes used for RT-PCR.

| | Primer type | Primer sequence (5'-3') | Probe sequence (5'-3') |
|---|---|---|---|
| Seg-4 (VP4) | Forward | TTAGGATGGAACCTTACGC | FAM-CTTTGAGTAGGTATTCGATCTCCTGCG-BHQ |
| | Reverse | ATTCTGCCCCTCTCTAACCA | |
| Seg-5 (NS1) | Forward | CGCAATCTTCGGATGTAAGC | FAM-TCGCCA+TCC+TCA+TCATCG-BHQ |
| | Reverse | GCACACTACCTTGGATCTCTG | |

+ plus indicates position of locked nucleic acids in the probe.

## 3.3. RESULTS

### 3.3.1. Rescue of recombinant wild-type, knockout and reassortant viruses

Little is currently known about the potential role of NS4 in AHSV replication and virulence. Therefore, the aim of this chapter was to investigate these aspects using reverse genetics-derived wild-type, knockout and reassortant viruses (Table 3.1). Rescue was done using a plasmid-based reverse genetics system, and all viruses used the virulent AHSV5 and attenuated AHSV4LP backbones. AHSV5Ref and AHSV5 express NS4-II, whereas AHSV4Ref and AHSV4LP expresses NS4-I (Boughan *et al.*, 2020).

Overall, AHSV5Ref and AHSV4Ref were available for use in this chapter and eight wild-type, NS4 knockout or reassortant viruses were generated via reverse genetics (Table 3.1). rAHSV5 and rAHSV4LP represented AHSV5Ref and AHSV4LP respectively and therefore served as the wild-type serotype 5 and attenuated serotype 4 recombinant viruses. rAHSV5ΔNS4 and rAHSV4LPΔNS4 represented the NS4 knockout mutants, and the reassortant viruses rAHSV5+$S9_{4LP}$, rAHSV4LP+$S9_{5}$, rAHSV5+$S9_{4LP\Delta NS4}$ and rAHSV4LP+$S9_{5\Delta NS4}$ allowed S9 and Seg9ΔNS4 to be assessed in the context of the different backbones. The first sign of successful virus rescue is the appearance of CPE. CPE was observed in all cases and the viruses were harvested when 100% CPE was reached. To confirm the presence of virus, dsRNA isolations were performed and subjected to agarose gel electrophoresis (Figure 3.2). In all cases, dsRNA was recovered, and resembled the known migration pattern of the 10 dsRNA segments of AHSV (Figure 3.2A and C).

Next, to confirm that the viruses contained the correct version of Seg-9 the segment was amplified using the appropriate primers and the resulting PCR products are shown in Figure 3.2B and D. Some background amplification was observed on the agarose gels but was not deemed enough to influence sequencing. Therefore, these PCR products were used for the nucleotide sequencing of Seg-9. Sequencing confirmed that the correct Seg-9 was incorporated into each virus (Appendix A). Sequencing also confirmed the presence of one nucleotide substitution, C254G, that results in a one amino acid difference, P85R, between AHSV4Ref and AHSV4LP NS4 (Figures A3 and A4, Appendix A).

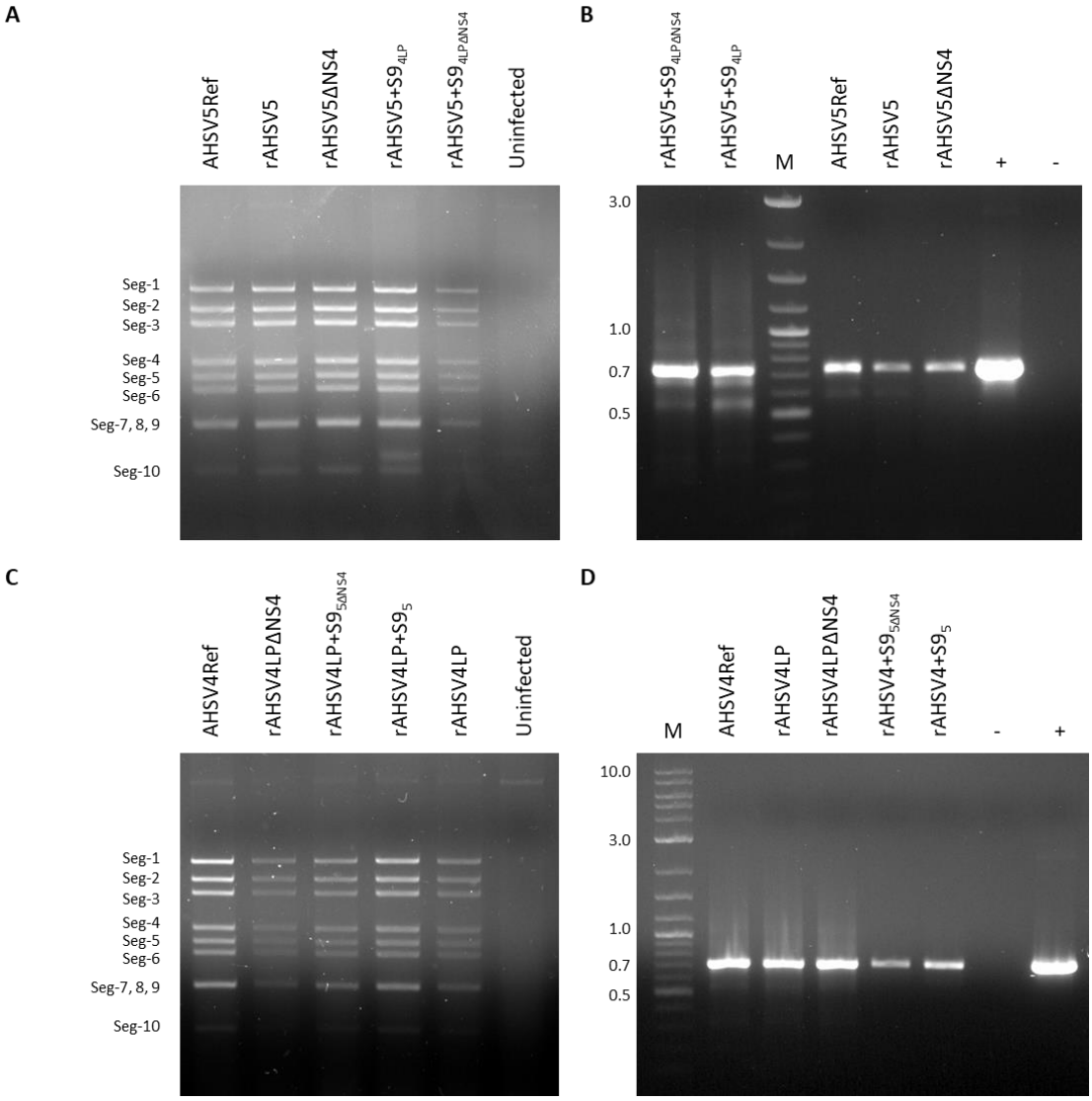


**Figure 3.2. Agarose gel electrophoresis of purified dsRNA and PCR amplification of Seg-9.** BSR cells were infected with AHSV5Ref, rAHSV5, rAHSV5ΔNS4, rAHSV5+S9$_{4LP}$, rAHSV5+S9$_{4LPΔNS4}$, AHSV4Ref, rAHSV4LP, rAHSV4LPΔNS4, rAHSV4LP+S9$_5$ or rAHSV4LP+S9$_{5ΔNS4}$ after which dsRNA was isolated. The positions of segments 1-10 are as indicated on the left (A and C). PCR amplification of Seg-9 is shown in B and D. M = Quick-Load 1 kb Plus DNA Ladder, sizes of fragments are as indicated (kb); + = positive control, pJET-Seg-9; - = negative control, dH$_2$O.

Therefore, the wild-type, knockout and reassortant viruses had been rescued successfully, each containing the correct Seg-9 or Seg-9ΔNS4, and could be characterised in more detail.

### 3.3.2. Characterisation of the expression and intracellular localisation of NS4

Western blot analysis was then used to test for NS4 expression. The viruses containing Seg-9 from AHSV5 (S9$_5$) were expected to express NS4-II (~23 kDa), and those containing AHSV4LP Seg-9 (S9$_{4LP}$) were expected to express NS4-I (~20 kDa), whereas those containing the Seg-9 NS4 knockouts should show no NS4 expression. BSR-T7/5 cells were infected with each of the viruses listed in Table 3.1 and were processed for

Western blot at 24 hpi. The results are shown in Figure 3.3, with the viruses containing the AHSV5 backbone in Figure 3.3A and those containing the AHSV4LP backbone in Figure 3.3B.

A ~23 kDa sized band corresponding to that observed in AHSV5Ref-infected cells was detected in rAHSV5-infected cells, confirming that this virus expressed NS4-II (Figure 3.3A). Faint bands of a smaller size were also observed in these two lanes and may have been due some protein degradation. As expected, a protein corresponding to NS4-I (~20 kDa) was observed in rAHSV5+S9$_{4LP}$-infected cells and no NS4 was observed in cells infected with rAHSV5ΔNS4 or rAHSV5+S9$_{4LPΔNS4}$ (Figure 3.3A). A faint band corresponding to the size of NS4-I (~20 kDa) was observed in rAHSV4LP-infected cells and corresponded to that observed in AHSV4Ref-infected cells (Figure 3.3B). As expected, rAHSV4LP+S9$_5$ expressed a protein corresponding to the size of NS4-II (~23 kDa), and no NS4 expression was observed in rAHSV4LPΔNS4- or AHSV4LP+S9$_{5ΔNS4}$-infected cells. Labelling with anti-NS2 (41 kDa) or anti-VP7 (38 kDa) was done as an infection control and showed that all viruses were replicating. Thus, all viruses showed the expected pattern of NS4 expression via Western blot.

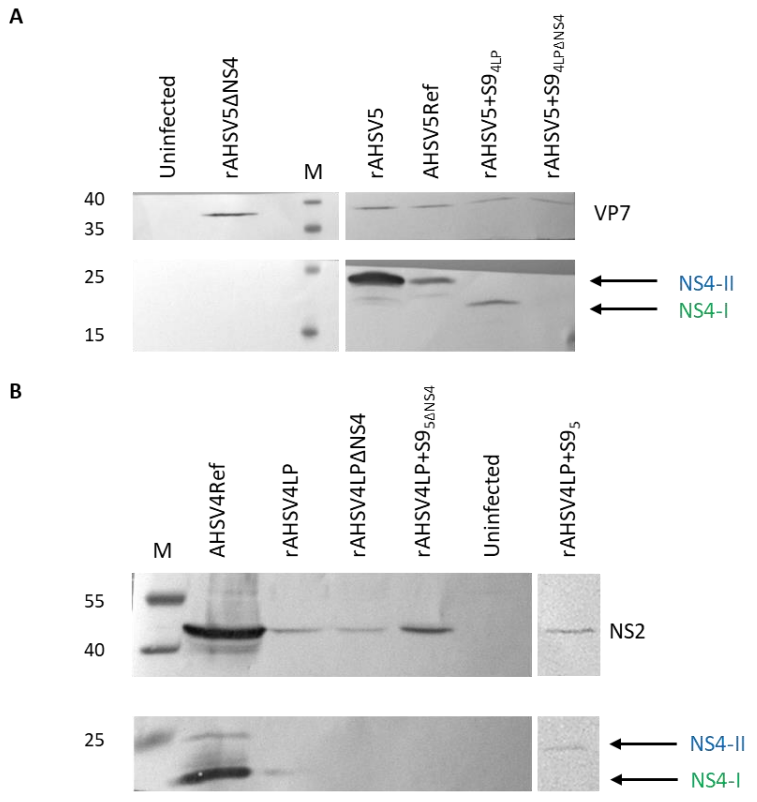


**Figure 3.3. Western blot analysis of NS4 expression.** BSR-T7/5 cells were infected with AHSV5Ref, rAHSV5, rAHSV5ΔNS4, rAHSV5+S9$_{4LP}$, rAHSV5+S9$_{4LPΔNS4}$, AHSV4Ref, rAHSV4LP, rAHSV4LPΔNS4, rAHSV4LP+S9$_5$ or rAHSV4LP+S9$_{5ΔNS4}$ and at 24 hpi were harvested for Western blot analysis using anti-NS4(GS), anti-VP7 or anti-NS2 and protein A peroxidase conjugate. (A) NS4 expression in viruses containing the AHSV5 backbone. (B) NS4 expression in viruses containing the AHSV4LP backbone. The expected sizes of NS4-I (green, ~20 kDa), NS4-II (blue, ~23 kDa), VP7 (~38 kDa) and NS2 (~41 kDa) are indicated. M = PageRuler$^{TM}$ Prestained Protein Ladder, sizes of molecular weight markers are indicated on the left (kDa).

Next, CLSM was used to investigate the intracellular localisation of NS4. BSR-T7/5 cells were infected with the viruses listed in Table 3.1 and were processed for immunofluorescence and CLSM at 24 hpi. The cells were dual labelled for VP7 (as an infection control) and NS4 and the results are shown in Figure 3.4. Little to no background labelling of NS4 or VP7 was observed in uninfected cells (Figure 3.4). NS4 as expressed by AHSV5Ref, rAHSV5 and rAHSV4LP+S9$_5$ was found throughout infected cells but with more NS4 observed in the cytoplasm. This was the expected localisation pattern for NS4-II. In contrast, NS4 as expressed by AHSV4Ref, rAHSV4LP and rAHSV5+S9$_{4LP}$ was found throughout infected cells but with a stronger signal in the nucleus, corresponding to what was expected for NS4-I (Figure 3.4). No NS4 was observed in cells infected with the NS4 knockout and reassortant viruses rAHSV5ΔNS4, rAHSV4LPΔNS4, rAHSV5+S9$_{4ΔNS4}$ or rAHSV4LP+S9$_{5ΔNS4}$. This is what was expected, as in all cases Seg-9 had been engineered to lack NS4 expression and no protein was observed via Western blot (Figure 3.4).

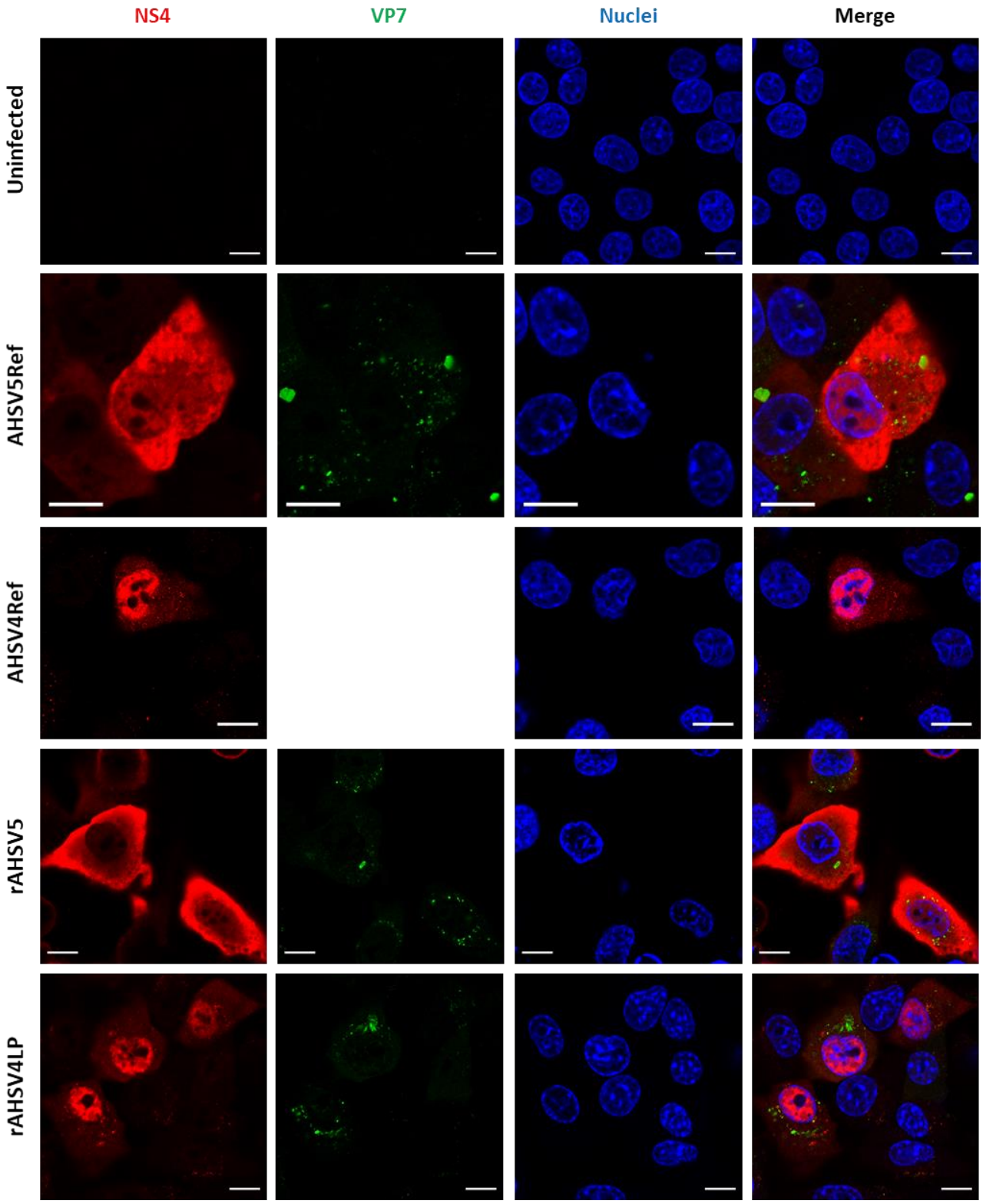

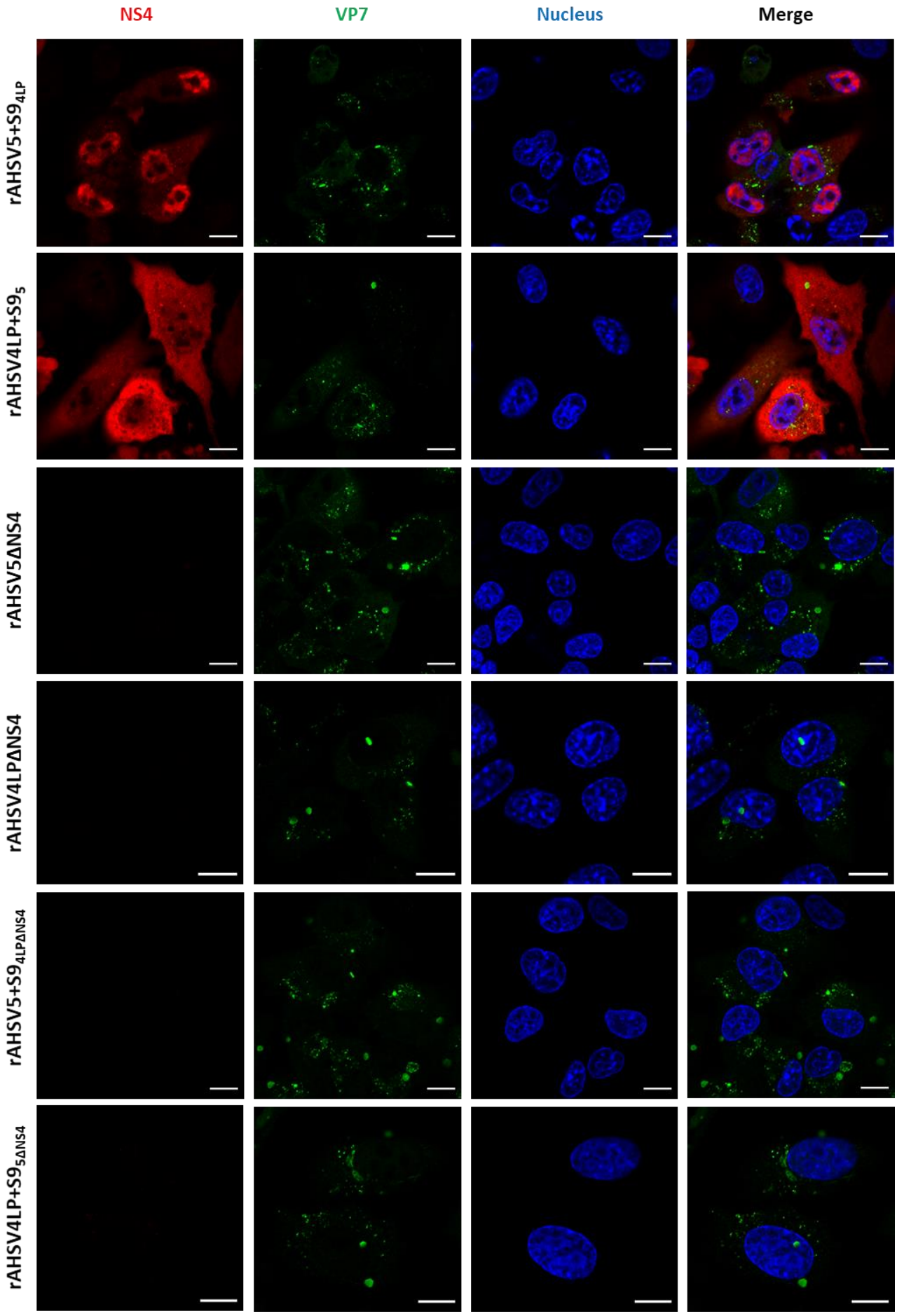

**Figure 3.4. CLSM micrographs showing the localisation of NS4 in BSR-T7/5 cells.** Cells infected with AHSV5Ref, AHSV4Ref, rAHSV5, rAHSV4LP, rAHSV5+$9_{4LP}$, rAHSV4LP+$S9_5$, rAHSV5ΔNS4, rAHSV4LPΔNS4, rAHSV5+$S9_{4LPΔNS4}$, or AHSV4LP+$S9_{5ΔNS4}$ were fixed at 24 hpi and processed for immunofluorescence and CLSM. Dual labelling was performed using anti-NS4(E3F) and anti-VP7 primary, and AF 633 conjugated goat anti-rabbit IgG and AF 488 goat anti-guinea pig IgG. In the case of AHSV4Ref only, NS4 was labelled with anti-NS4(E3F) primary and AF 488 conjugated goat anti-rabbit IgG (shown here in red). Nuclei were stained with DAPI. Scale bar = 10 µm.

Therefore, these results showed that all viruses expressed the expected variant of NS4 and that the intracellular localisation thereof is dependent on Seg-9 itself, and not the backbone of the virus.

### 3.3.3. Replication kinetics of wild-type, knockout and reassortant viruses

Next, the replication kinetics of all the viruses were assessed in BSR cells. Cells were infected at an MOI of 0.1 with the viruses listed in Table 3.1 and total virus titres were determined using a combination of endpoint dilution (expressed as $TCID_{50}$/ml) and IPMA at 12, 24, 36, 48 and 72 hpi. Firstly, the replication of rAHSV5 was compared to that of AHSV5Ref in order to see if the rescued virus replicated similarly to the reference strain *in vitro*. Figure 3.5A shows that the replication of rAHSV5 was comparable to that of AHSV5Ref. In the case of rAHSV5ΔNS4, knocking out NS4 did not change the overall replication kinetics compared to rAHSV5 in BSR cells. Furthermore, rAHSV5+$S9_{4LPΔNS4}$ showed replication that was comparable to both rAHSV5 and rAHSV5ΔNS4. Interestingly, rAHSV5+$S9_{4LP}$ showed a higher titre than all other viruses containing the rAHSV5 backbone at 12 hpi, and was statistically significantly different to rAHSV5 at this time point. This virus however showed no replication over the 72-hour period and was statistically significantly lower than rAHSV5 at 48 hpi.

The replication of rAHSV4LP was statistically significantly different than AHSV4Ref at 12, 48 and 72 hpi and clustered with rAHSV4LPΔNS4 and rAHSV4LP+$S9_{5ΔNS4}$, both of which lack NS4 expression (Figure 3.5B). rAHSV4LP+$S9_5$ showed replication that was comparable to AHSV4Ref, but was statistically significant different from rAHSV4LP at 36, 48 and 72 hpi. The strain rAHSV4LP+$S9_5$ showed the best replication overall.

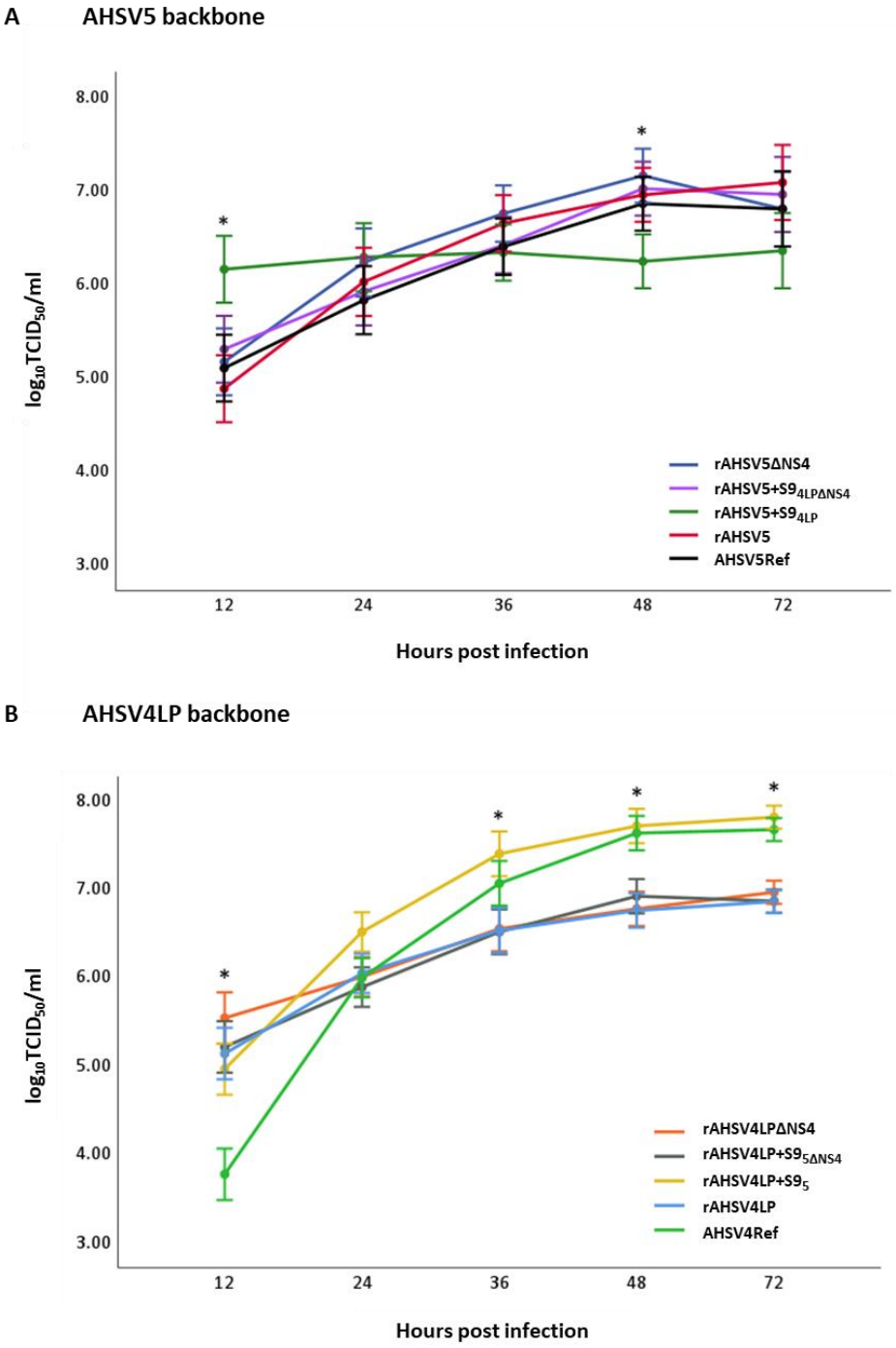


**Figure 3.5. *In vitro* replication kinetics of all reference, wildtype, knockout and reassortant viruses in BSR cells.** Cells were infected with (A) AHSV5Ref, rAHSV5, rAHSV5ΔNS4, rAHSV5+S9$_{4LP}$, rAHSV5+S9$_{4LPΔNS4}$ or (B) AHSV4Ref, rAHSV4LP, rAHSV4LPΔNS4, rAHSV4LP+S9$_5$, AHSV4LP+S9$_{5ΔNS4}$ at an MOI of 0.1, and viral titres determined from 12 to 72 hpi by endpoint dilution analysis and expressed as $log_{10}TCID_{50}$/ml. Experiments were performed twice independently, each time in triplicate. Statistical analyses were done using one-way ANOVA and Dunnett's T3 test ($P < 0.05$). Statistically significance differences to rAHSV5 or rAHSV4LP are indicated by a *. The error bars represent 95% confidence interval.

Taken together these results indicate that S9$_5$ gives AHSV a replication advantage in BSR cells.

### 3.3.4. Analysis of pathogenicity and virulence in embryonated chicken eggs (ECEs)

Next, the pathogenesis and virulence of the wild-type, knockout and reassortant viruses were investigated in embryonated chicken eggs (ECEs). Four different experiments were done and will be presented as such. In all cases, ECEs were infected with the viruses generated by reverse genetics thirteen days after incubation. Upon harvesting, the ECEs were examined for lesions that are typical of AHSV infection. Such lesions included hyperaemia, petechial haemorrhaging, ecchymotic haemorrhaging and oedema, and could be observed separately or together. Table 3.4 summarises each experiment and shows the survival rate in each case, along with the $C_q$ value obtained via RT-PCR where possible.

In experiment 1, viruses were rescued in BSR-T7/5-Clone 16 cells and were then inoculated into ECEs three days later. The day on which embryos died was not recorded in this experiment. Embryos that were mock-infected did not die, showed development of feathers, and showed no signs of disease (Figure 3.6A). This is hereafter referred to as the normal phenotype. A 50% survival rate was observed in rAHSV5-infected ECEs (Table 3.4). This was unexpected due to preliminary (Potgieter *et al.*, 2017) and subsequent studies (Prof. AC Potgieter, personal communication) studies showing that rAHSV5 is highly virulent in ECEs and routinely results in 0% survival rates. This virus is therefore often used as a positive control for virulence. Of the three embryos that were killed by rAHSV5 (Table 3.4), two showed full body hyperaemia and oedema (Figure 3.6A), and the third displayed oedema, scattered petechial haemorrhaging and less hyperaemia than in the other embryos. The NS4 knockout, rAHSV5ΔNS4, showed a survival rate of 100%, as did the rAHSV5+S9$_{4LP\Delta NS4}$ reassortant containing S9ΔNS4 from AHSV4LP. Five of the six embryos infected with rAHSV5ΔNS4 and rAHSV5+S9$_{4LP\Delta NS4}$ showed no lesions and displayed the normal phenotype. The remaining embryo infected with rAHSV5ΔNS4 had oedema under the chin (yellow arrow, Figure 3.6A) and the remaining embryo infected with rAHSV5+S9$_{4LP\Delta NS4}$ had petechial haemorrhaging and oedema (blue and green arrows, Figure 3.6A). These lesions are mild and did not hamper the development of the embryos, nor did they cause death. RT-PCR confirmed that virus was present in infected embryos (Table 3.4). While it appears that knocking out NS4 causes attenuation of rAHSV5, one cannot fully deduce that from this data set because the control (rAHSV5) was not fully virulent as expected.

**Table 3.4.** Summary of the experiments done in the embryonated chicken egg (ECE) model.

| Experiment | Virus | Titre/100 µl inoculum | Total # of ECE | Dead | Alive | Survival rate | Day of death (dpi) | RT-PCR $C_q$ value | |
|---|---|---|---|---|---|---|---|---|---|
| | | | | | | | | NS1 | VP4 |
| 1 | rAHSV5 | 7.97E+05 | 6 | 3 | | 50% | NR | 26.43 | 23.23 |
| | | | | | 3 | | | 26.89 | 27.86 |
| | rAHSV5ΔNS4 | 1.12E+06 | 6 | | 6 | 100% | | 32.54 | 31.78 |
| | rAHSV5+S9$_{4LPΔNS4}$ | 3.56E+06 | 6 | | 6 | 100% | | | 33.41 |
| | Mock infected | | 2 | | 2 | 100% | | | |
| 2 | rAHSV5 | 6.32E+03 | 4 | 1 | | 75% | NR | | |
| | | | | | 3 | | | | |
| | rAHSV5ΔNS4 | 1.12E+06 | 5 | 1 | | 80% | NR | | |
| | | | | | 4 | | | | |
| | rAHSV5+S9$_{4LP}$ | 1.00E+05 | 5 | 1 | | 80% | NR | | |
| | | | | | 4 | | | | |
| | rAHSV5+S9$_{4LPΔNS4}$ | 8.66E+04 | 4 | 1 | | 75% | NR | | |
| | | | | | 3 | | | | |
| | rAHSV4LP | 5.02E+05 | 5 | 2 | | 60% | NR | | |
| | | | | | 3 | | | | |
| | rAHSV4LPΔNS4 | 2.00E+05 | 5 | | 5 | 100% | | | |
| | rAHSV4LP+S9$_5$ | 2.00E+05 | 5 | 5 | | 0% | NR | | |
| | rAHSV4LP+S9$_{5ΔNS4}$ | 3.56E+05 | 5 | | 5 | 100% | | | |
| | Mock infected | | 2 | | 2 | 100% | | | |
| 3 | rAHSV5 | 1.12E+04 | 12 | 10 | | 8% | 2 | 28.95 | 28.87 |
| | | | | 1 | | | 5 | | |
| | | | | | 1 | | | | 29.73 |
| | rAHSV5ΔNS4 | 4.62E+05 | 12 | 2 | | 75% | 3 | 34.74 | 27.95 |
| | | | | 1 | | | 5 | 27.89 | 23.02 |
| | | | | | 9 | | | 36.84 | 35.47 |
| | rAHSV5+S9$_{4LP}$ | 7.97E+05 | 12 | 4 | | 42% | 3 | 24.98 | 24.77 |
| | | | | 3 | | | 5 | 32.92 | 28.32 |
| | | | | | 5 | | | 36.47 | 32.50 |
| | rAHSV5+S9$_{4LPΔNS4}$ | 6.32E+05 | 12 | 1 | | 17% | 1 | 27.60 | 23.09 |
| | | | | 1 | | | 2 | | |
| | | | | 3 | | | 3 | 31.40 | 26.54 |
| | | | | 2 | | | 4 | 34.12 | 26.20 |
| | | | | 2 | | | 5 | 35.50 | 28.46 |
| | | | | 1 | | | 5 SE | 35.54 | 30.06 |
| | | | | | 2 | | | 35.60 | 30.02 |
| | Mock infected | | 3 | | 3 | 100% | | | |
| 4 | rAHSV5 | 1.12E+04 | 11 | 4 | | 45% | 3 | 32.53 | 22.72 |
| | | | | 1 | | | 4 | 27.25 | 22.43 |
| | | | | 1 | | | 5 | 22.55 | 21.24 |
| | | | | | 5 | | | 35.59 | 33.88 |
| | rAHSV5ΔNS4 | 4.62E+05 | 11 | 1 | | 91% | 5 | | 33.40 |
| | | | | | 10 | | | 16.10 | 36.16 |
| | rAHSV5+S9$_{4LP}$ | 7.97E+05 | 12 | 2 | | 58% | 3 | 35.4 | 26.61 |
| | | | | 1 | | | 5 | 35.97 | 32.13 |
| | | | | 2 | | | 6 | 34.87 | 29.00 |
| | | | | | 7 | | | | 35.18 |
| | rAHSV5+S9$_{4LPΔNS4}$ | 6.32E+05 | 12 | 3 | | 58% | 5 | 32.40 | 26.42 |
| | | | | 2 | | | 6 | 35.15 | 31.48 |
| | | | | | 7 | | | 36.51 | 35.12 |
| | Mock infected | | 6 | | 6 | 100% | | | |

S9 = Seg-9.
NR = Not recorded.
SE = Small embryo.

The recombinant viruses used in preliminary studies were rescued in BSR-T7/5 cells. Therefore, it was decided to rescue fresh viruses in BSR-T7/5 cells instead of BSR-T7/5-Clone 16 cells and then repeat the experiment in ECEs (Experiment 2, Table 3.4). After rescue the viruses were stored at 4°C for at least 9 days before injection into embryos. In this experiment between 4 and 5 embryos were infected per virus. Compared to experiment 1, titres of rAHSV5 and rAHSV5+S9$_{4LP\Delta NS4}$ were lower in experiment 2 and the titre of rAHSV5ΔNS4 was the same. The survival rate for rAHSV5 was 75% in this experiment, higher than in experiment 1 (50%). The embryo that died as a result from rAHSV5 infection did not display the typical diseased phenotype (Figure 3.6B). Although some hyperaemia was observed it was not as severe as that described by Maartens *et al.* (2009) or Potgieter *et al.* (2017). Some petechial haemorrhages on the feather follicles were also observed. The survival rates for embryos infected with rAHSV5ΔNS4, rAHSV5+S9$_{4LP}$ and rAHSV5+S9$_{4LP\Delta NS4}$ ranged from 75% - 80%. In all three instances it was one embryo that died, all of which are shown in Figure 3.6B. The embryos that died as a result of rAHSV5ΔNS4 and rAHSV5+S9$_4$ infection displayed hyperaemia and an ecchymotic haemorrhage was observed in the embryo that died as a result of rAHSV5+S9$_{4LP\Delta NS4}$ infection (white arrow, Figure 3.6B). One of the embryos that survived infection with rAHSV5ΔNS4 displayed some oedema and one of the embryos that survived infection with rAHSV5+S9$_{4LP\Delta NS4}$ showed slight hyperaemia but it was not enough to kill the embryos. All other embryos that survived infection with those three viruses displayed the normal phenotype (not shown). Experiment 2 also included ECEs that were infected with viruses containing the AHSV4LP backbone (Experiment 2, Table 3.4). rAHSV4LP was expected to show a 100% survival rate based on preliminary work (Potgieter *et al.*, 2017). However, in this instance only 60% survival was observed (Table 3.4) therefore this virus was more virulent than anticipated. Hyperaemia and some oedema were observed in the two embryos that died as a result of infection with rAHSV4LP (Figure 3.6C). Of those that survived only one presented with clinical lesions: hyperaemia and oedema under the chin (Figure 3.6C). The NS4 knockout, rAHSV4LPΔNS4, showed a survival rate of 100% and only one of the five embryos showed oedema under the chin (Figure 3.6C). Infection with the rAHSV4LP+S9$_5$ reassortant resulted in a 0% survival rate (Table 3.4) and all embryos showed hyperaemia reminiscent of infection with rAHSV5 (Potgieter *et al.*, 2017). Oedema was also present in two of the embryos and one embryo presented with petechial haemorrhaging. Infection with the rAHSV4LP+S9$_{5\Delta NS4}$ reassortant virus showed a 100% survival rate (Table 3.4). No clinical lesions were observed in the embryos infected with this virus (Figure 3.6C). RT-PCR was unsuccessful for experiment 2 and is therefore not shown.

Due to the high survival rate for rAHSV5 in experiment 2, viruses were rescued a third time and injected into ECEs immediately (Experiment 3, Table 3.4). In addition to this, the number of embryos that were infected with each virus was increased to 12 in this experiment and day of embryo death was recorded. The titres of rAHSV5, rAHSV5+S9$_{4LP}$ and rAHSV5+S9$_{4LP\Delta NS4}$ were higher in experiment 3 than in experiment 2, while that of rAHSV5ΔNS4 was lower. Unfortunately, infection with the viruses containing the AHSV4LP backbone could not be repeated due to time and financial constraints. In this experiment an 8% survival rate was observed

in ECEs infected with rAHSV5, and ten of the eleven embryos that died succumbed to the disease within 2 days of infection (Table 3.4). The images in Figure 3.6D show 8 of the embryos that died. All embryos, including those not shown, showed lesions typical of infection with virulent rAHSV5. These lesions included full body hyperaemia that was accompanied by oedema in some embryos, either under the chin or throughout the whole body. Several embryos had scattered petechial haemorrhages on the trunk or ecchymotic haemorrhages behind the head or both. The embryo that survived infection displayed oedema under the chin (Figure 3.6D). A survival rate of 75% was observed in rAHSV5ΔNS4-infected ECEs (Experiment 3, Table 3.4). The embryos that died had less severe lesions than those that died from rAHSV5. Only some hyperaemia was seen in these embryos and oedema under the chin was observed. Full body oedema and some petechial haemorrhages were observed in one of the embryos that survived (Figure 3.6D). All other embryos displayed the normal phenotype. ECEs infected with the reassortant viruses rAHSV5+S9$_{4LP}$ and rAHSV5+S9$_{4LP\Delta NS4}$, showed lower rates of survival than in the previous experiments (Table 3.4). Seven of the twelve embryos infected with rAHSV5+S9$_{4LP}$ died and displayed variable phenotypes (Figure 3.6D). For example, two of the embryos that died from rAHSV5+S9$_{4LP}$ showed oedema but no hyperaemia or haemorrhaging of any kind. The remaining embryos that died showed signs of hyperaemia, petechial haemorrhaging, oedema and some showed ecchymotic haemorrhaging behind the head. Two of the embryos that survived infection with rAHSV5+S9$_{4LP}$ are shown in Figure 3.6D. One embryo showed signs of full body oedema and ecchymotic haemorrhaging behind the head and one had oedema under the chin. The remaining embryos displayed the normal phenotype or oedema under the chin (not shown). Ten of the twelve embryos infected with rAHSV5+S9$_{4LP\Delta NS4}$ died (Experiment 3, Table 3.4). The embryo that died on day 1 showed lesions comparable to that observed with rAHSV5 infection: full body hyperaemia and some petechial haemorrhaging. Eight of the embryos that died between days 2 and 5 showed variable diseased phenotypes: seven showed some level of hyperaemia with or without oedema and petechial haemorrhaging. The remaining two embryos that died showed development of feathers but one showed full body oedema and one showed a severe ecchymotic haemorrhage on the back of its head. The embryo designated SE, or small embryo to distinguish it from other embryos that died on day 5, was very small and did not appear to have been an embryo that was 13 days post incubation at the time of infection. The embryos that survived appeared normal (Figure 3.6D). RT-PCR confirmed that virus was present in the infected ECEs (Experiment 3, Table 3.4).

A fourth experiment was then done using the same virus stocks but two weeks after rescue (Experiment 4, Table 3.4). The viruses were stored at 4°C prior to use. In this experiment rAHSV5 was less virulent than in experiment 3, with a survival rate of 45% versus 8%. Also, the embryos started dying a day later in experiment 4 (day 3 vs day 2). Although some hyperaemia and oedema were observed in the embryos that died from infection with rAHSV5 it was not as severe as those seen in experiment 3 (Figure 3.6D and E). ECEs injected with the remaining viruses, rAHSV5ΔNS4, rAHSV5+S9$_{4LP}$ and rAHSV5+S9$_{4LP\Delta NS4}$, also showed an increase in

survival rate compared to experiment 3 (Experiment 4, Table 3.4), suggesting that the viruses became more attenuated over the two-week period. The lesions observed in the embryos that died after infection with these three viruses were variable but were not as severe as those seen in experiment 3, and were also not as severe as those seen in rAHSV5-infected ECEs in experiment 4 (Figure 3.6). All embryos that survived infection with rAHSV5ΔNS4 and rAHSV5+S9$_{4LP\Delta NS4}$ showed the normal phenotype and had no clinical lesions and only one of the embryos that survived infection with rAHSV5+S9$_{4LP}$ had oedema under the chin (not shown). RT-PCR showed that virus was present in the infected embryos (Table 3.4).

**A** **Experiment 1**

Mock infected

rAHSV5 - Dead

rAHSV5 - Alive

rAHSV5ΔNS4 - Alive

rAHSV5+S9$_{4LP\Delta NS4}$ - Alive

**B** **Experiment 2**

rAHSV5 - Dead

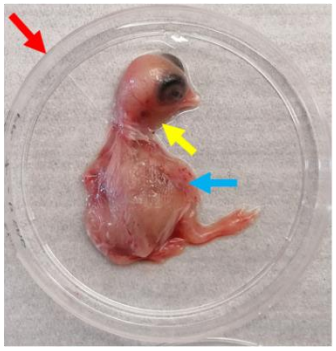

rAHSV5ΔNS4 - Dead

rAHSV5+S9$_{4LP}$ - Dead

rAHSV5+S9$_{4LP\Delta NS4}$ - Dead

C

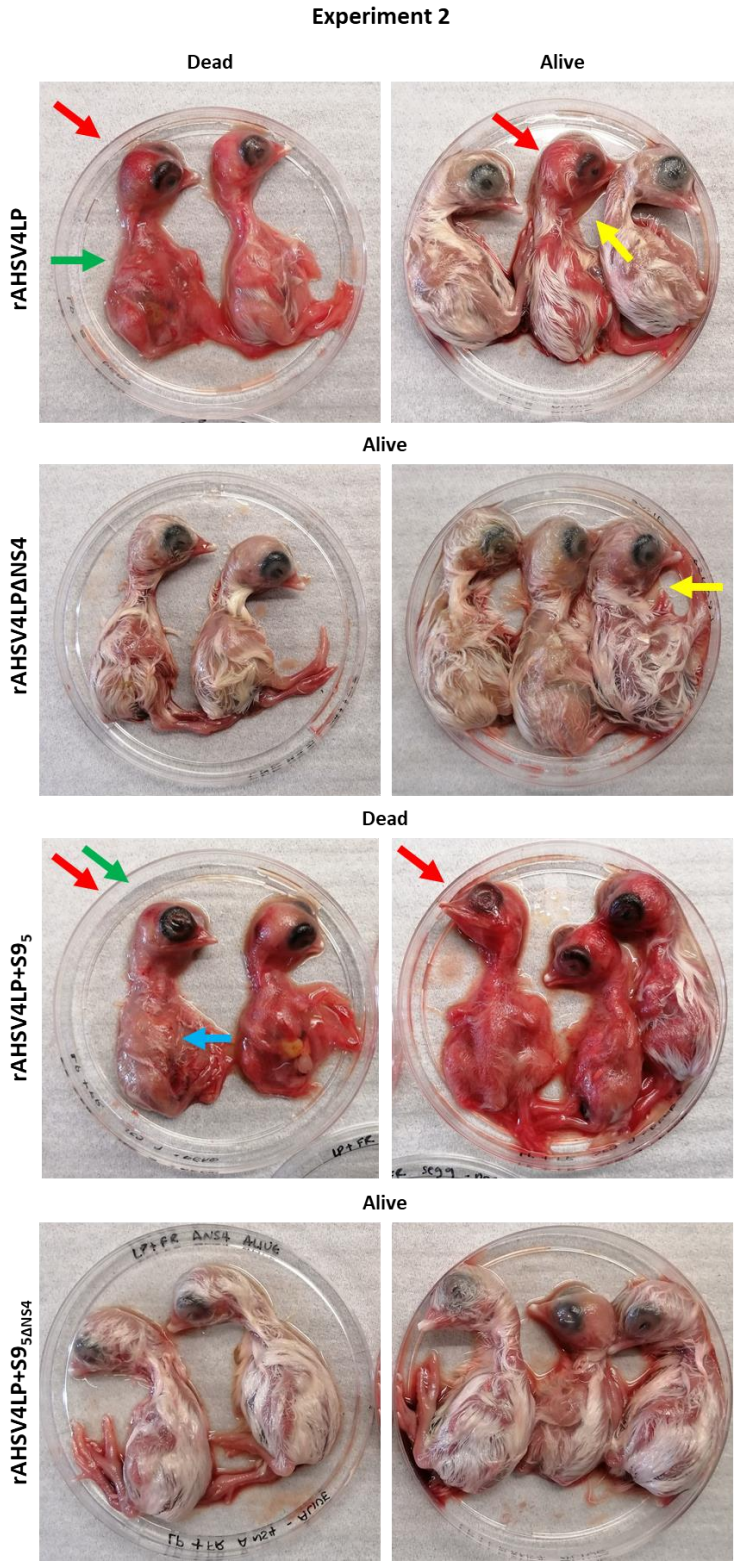

D

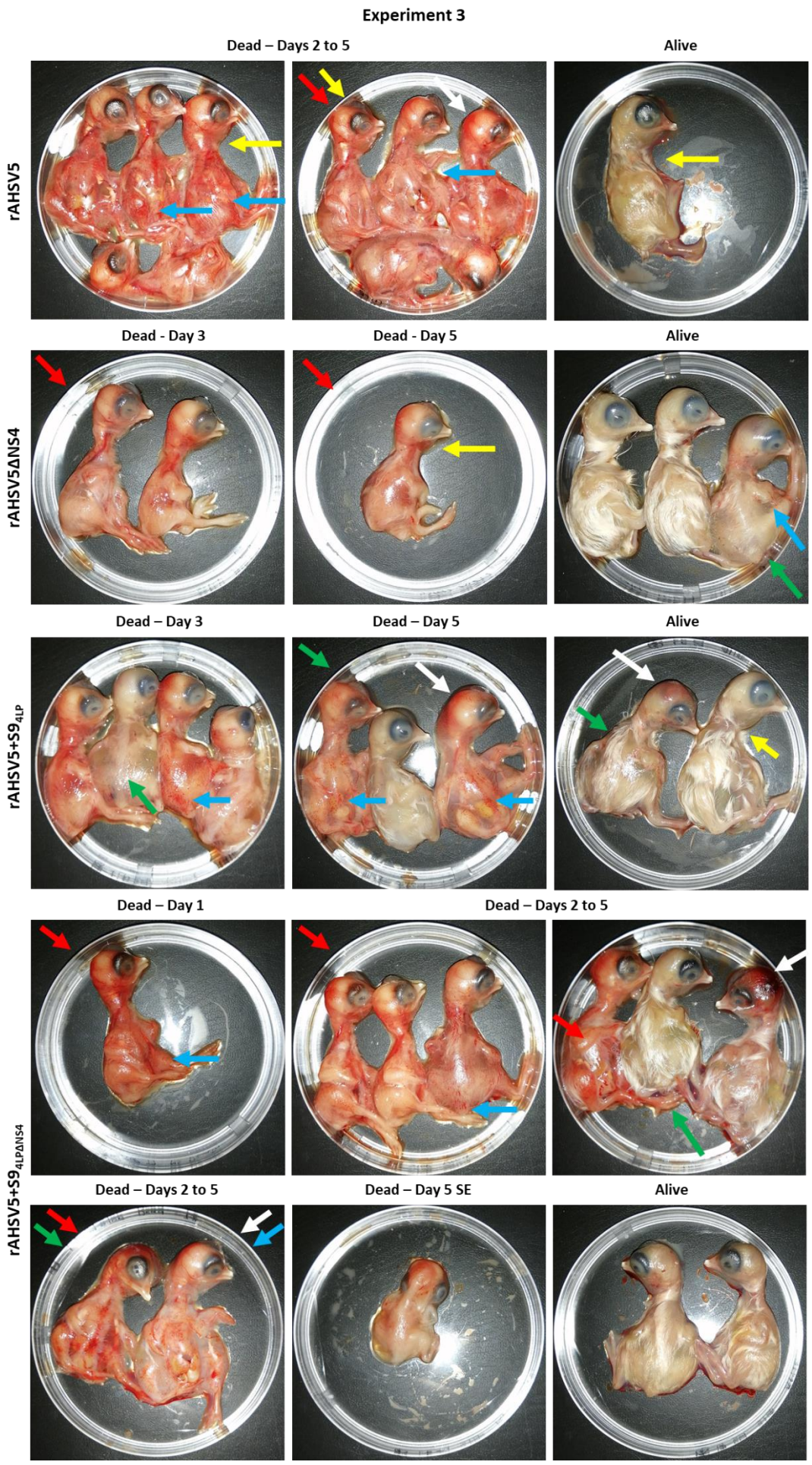

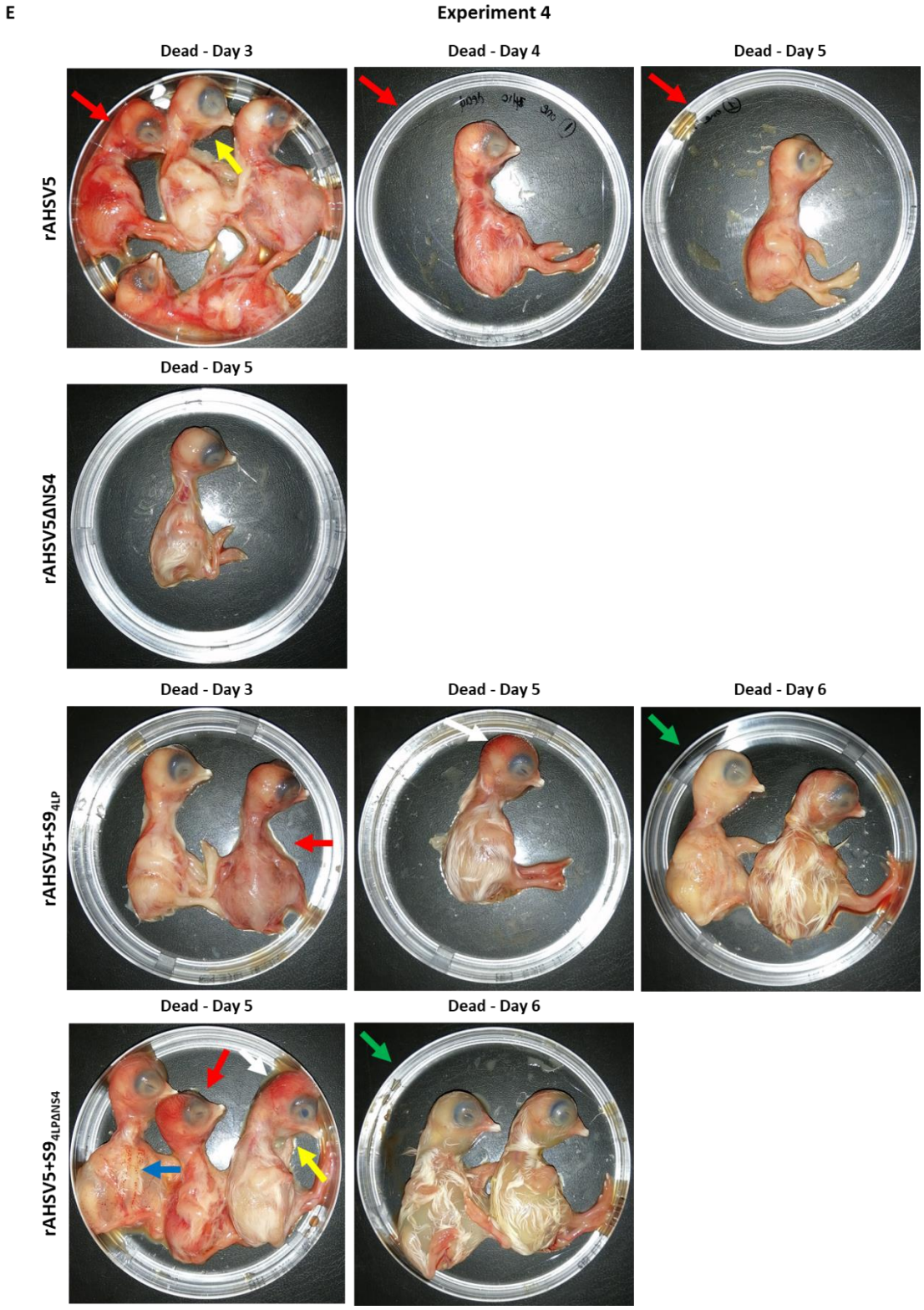


**Figure 3.6. Clinical lesions observed in embryos harvested from mock-infected and rAHSV-infected embryonated chicken eggs (ECEs).** Thirteen days after incubation ECEs were mock infected or were infected with rAHSV5, rAHSV5ΔNS4, rAHSV5+S9$_{4LP}$, rAHSV5+S9$_{4LPΔNS4}$, rAHSV4LP, rAHSV4LPΔNS4, rAHSV4LP+S9$_{5}$ or rAHSV4LP+S9$_{5ΔNS4}$ and incubated at 32°C until death or euthanasia. The embryos were then harvested and examined for clinical lesions common to AHSV infection. Four experiments were done. (A) Experiment 1, viruses were rescued in BSR-T7/5-Clone 16 cells; (B and C) Experiment 2, viruses were rescued in BSR-T7/5 cells, (B) rAHSV5 backbone, (C) rAHSV4LP backbone; (D) Experiment 3, new viruses were rescued and were injected into ECEs immediately; (E) Experiment 4, the same viruses as in Experiment 3 were used but two weeks later after being stored at 4°C. Arrows = Red indicates

hyperemia, yellow indicates oedema under the chin, green indicates oedema of the whole body, blue indicates petechial haemorrhages, white indicates ecchymotic haemorrhages.

Overall, while it is not possible to make conclusive deductions from these experiments the phenotypes observed in experiment 3 most closely matched those observed previously for rAHSV5. Therefore, it appears that infecting ECEs immediately after virus rescue is the best way to obtain reliable results in this small animal model. Also, the increased number of eggs infected per virus allows for more complete results.

### 3.4. DISCUSSION

While research has shown that BTV NS4 is a virulence factor in the host (Ratinier *et al.*, 2016) little is known about the role of AHSV NS4 in virulence and pathogenesis. Therefore, this chapter aimed to investigate the role of AHSV NS4 in virus replication, virulence, and pathogenesis. This was done by generating several wild-type, NS4 knockout and reassortant viruses using reverse genetics and then using them to assess the *in vitro* expression and localisation of NS4 as well as the replication kinetics of the viruses. Virulence and pathogenesis were then investigated *in vivo* using an ECE model.

The viruses generated by reverse genetics were compared to the virulent OIE reference strains of AHSV5 and AHSV4 with regard to NS4 expression, localisation and replication kinetics. In this chapter, rAHSV5 represented the wild-type virus for serotype 5. The rescue of this virus has been described previously (Boughan *et al.*, 2020) and is virulent in horses and in embryonated chicken eggs (Potgieter *et al.*, 2017). While AHSV4Ref is a virulent virus, rAHSV4LP was based on AHSV4LP, which was attenuated from the OIE reference strain of AHSV4 by Erasmus (1974). Seg-9 of AHSV4LP contains a one nucleotide substitution at position 254 (C254G) and is the only difference between the Seg-9 of AHSV4Ref and AHSV4LP. This mutation does not change the amino acid sequence of VP6 but results in a P85R change in NS4. Comparisons were made with AHSV4Ref to see if the one amino acid change in AHSV4LP NS4 has any functional significance *in vitro*. To address the low levels of leaky NS4 expression observed in rAHSV5minNS4-infected cells in Chapter 2, two NS4 knockout viruses were rescued here using Seg-9 plasmids containing two additional stop codons compared to the Seg-9 plasmids used to rescue rAHSV5minNS4 and rAHSV4minNS4. Additionally, four reassortant viruses were generated to investigate $S9_5$ and $S9_{5\Delta NS4}$ in the context of the AHSV4LP backbone, and $S9_{4LP}$ and $S9_{4LP\Delta NS4}$ in the context of the AHSV5 backbone. After rescue, all viruses were viable and replicating, and sequencing of Seg-9 confirmed that each virus contained the correct version of the wild-type ($S9_5$ or $S9_{4LP}$) or mutated forms of Seg-9 ($S9_{5\Delta NS4}$ or $S9_{4LP\Delta NS4}$). Sequencing also confirmed that all viruses containing $S9_{4LP}$ contained the P85R amino acid change in NS4.

AHSV4LP and AHSV5 express NS4-I and NS4-II respectively which differ in size and intracellular localisation, making it possible to visualise any differences in NS4 protein expression and intracellular localisation between the reverse genetics-derived viruses. Western blotting showed that rAHSV5 and rAHSV4LP+$S9_5$ express NS4-II, and rAHSV4LP and rAHSV5+$S9_{4LP}$ express NS4-I, with all other viruses lacking NS4 expression. Also observed was the expression of VP7 or NS2 in all infected samples indicating that infectious viruses had successfully been rescued. A homogenous but predominantly cytoplasmic distribution of NS4-II was observed in rAHSV5 and rAHSV4LP+$S9_5$ infected cells, corresponding to what has previously been described for AHSV NS4-II (Zwart *et al.*, 2015; Boughan *et al.*, 2020). NS4-I, as expressed by rAHSV4LP and rAHSV5+$S9_{4LP}$, showed the localisation pattern described for NS4-I, predominantly nuclear with some protein also being found in the cytoplasm (Zwart *et al.*, 2015; Boughan *et al.*, 2020). No difference in the expression or localisation of

NS4 was observed between AHSV4Ref and rAHSV4LP indicating that the one amino acid difference did not affect these aspects of NS4. No NS4 was detected in cells infected with rAHSV5ΔNS4, rAHSV4LPΔNS4, rAHSV5+S9$_{4LP\Delta NS4}$ or rAHSV4LP+S9$_{5\Delta NS4}$. Therefore, NS4 expression had successfully been abolished by the mutations to Seg-9. Together, these results showed that the expression and intracellular localisation of NS4-I and NS4-II is not influenced by the backbone into which Seg-9 is incorporated. Important to note is that Seg-9 also encodes VP6. VP6 clusters with NS4 in Clades I and II and the protein encoded also differs with regard to length and sequence (Zwart *et al.*, 2015). Therefore, it is possible that NS4 or VP6, or both, are responsible for the results seen here.

The replication kinetics of the reverse-genetics derived viruses were examined over 72 h in BSR cells. Knocking out NS4 did not change the overall replication kinetics of rAHSV5 or rAHSV4LP, no matter the origin of S9ΔNS4. Therefore, AHSV NS4 was shown to be dispensable for AHSV replication. A similar result was seen for BTV8 and BTV8ΔNS4 in BSR cells (Ratinier *et al.*, 2011) but NS4 was observed to give a replication advantage to BTV8 in cells with an intact IFN response (Ratinier *et al.*, 2016). It is possible that this is what occurred here too and that the titres of the NS4 knockouts would be lower than rAHSV5 and rAHSV4LP in cells that are capable of initiating an antiviral response. Overall, rAHSV5 replicated better than rAHSV5+S9$_{4LP}$, which did not show much replication over the 72-hour period. Incorporating S9$_5$ into the rAHSV4LP backbone resulted in a reassort that replicated to higher titres than rAHSV4LP, and significantly so from 36 to 72 hpi. Therefore, it is possible that NS4-II or VP6 (or both) as encoded by S9$_5$ are important for enhanced replication of AHSV. Also observed was that the replication of rAHSV4LP was statistically significantly lower than AHSV4Ref at 12, 48 and 72hpi and may be due to the P85R change in NS4.

Based on previous results obtained by Maartens *et al.* (2009, 2011) and in the patent by Potgieter *et al*. (2017) the virulence and pathogenicity of each reverse genetics-derived virus generated here were investigated in embryonated chicken eggs. The ECE model has been used in a variety of research areas over the years and is cost-effective, available all year round and more ethically acceptable than large animal models. The lesions of AHS disease are related to vascular permeability (Zientara *et al.*, 2015; Dennis *et al.*, 2019). The greater the vascular permeability, the more severe the lesion. Full body hyperaemia is the most severe lesion in the ECE model and, in most cases, causes death. In this instance the vascular damage is so severe that erythrocytes can extravasate out of the blood vessels into the surrounding areas of the body. When there is less bleeding, the embryos may still die but death will come at a later stage than when full body hyperaemia is observed. Oedema is the least severe lesion and embryos can survive with oedema under the chin and even with full body oedema.

In the experiments done by Potgieter *et al.* (2017) and in experiments done thereafter, rAHSV5 routinely killed all embryos and mostly within 48 hpi (Prof. AC Potgieter, personal communication). That was however

not the case here. The results for infection with rAHSV5 were variable over the four experiments, with the results of experiment 3 most closely resembling those obtained by Potgieter and colleagues. The survival rate of rAHSV5-infected embryos ranged from 45-75%, in experiments 1, 2 and 4. It was only experiment 3 that showed a survival rate as low as 8%. Phenotypically, the embryos also reflected the range in virulence of the virus. The lesions observed in experiment 3 were the most severe and most of the embryos died within 48 hpi. The disease was so severe in these embryos that feathers had not yet begun to develop. In this experiment viruses were rescued and then immediately injected into ECEs.

All other viruses including rAHSV5+S9$_{4LP}$ and except for rAHSV4LP+S9$_5$, appear attenuated compared to rAHSV5 based on the survival rates obtained across the experiments. The low survival rate obtained in experiment 3 for ECEs infected with rAHSV5+S9$_{4LP\Delta NS4}$ could be due to several non-specific deaths. For example, one of the embryos that died on day 5 was very small and did not show typical lesions of the disease, another embryo had a severe ecchymotic haemorrhage on the back of its head and a third showed signs of oedema but this does not lead to death in most cases. If these three embryos did indeed represent non-specific deaths the survival rate would be 42%, which is the same as that observed for rAHSV4LP in experiment 3. The survival rates for rAHSV5ΔNS4, rAHSV5+S9$_{4LP}$ and rAHSV5+S9$_{4LP\Delta NS4}$ may have been lower in experiment 3 compared to experiments 1 and 2 due to the number of embryos infected increasing to 12 per virus. It is possible that the survival rates in experiments 1 and 2 would have been lower had more embryos been included in the experiments. The phenotypes of embryos infected with these viruses also indicated that the viruses were attenuated compared to virulent rAHSV5. rAHSV4LP was expected to give a survival rate of 100% based on the results obtained by Potgieter *et al.* (2017) where the virus was shown to be completely attenuated in both horses and chicken embryos. Here, the survival rate was 60% and the embryos that died displayed signs of bleeding. One embryo showed some signs of bleeding and had oedema under the chin but survived. As infection with rAHSV5 was used as a control for virulence and did not give consistent results across the experiments it is not possible to make proper conclusions from these results. It does however appear that the incorporation of S9$_5$ into the rAHSV4LP backbone resulted in a virulent virus causing severe lesions in infected embryos that resembled those caused by virulent rAHSV5. Even though only one experiment was done with this virus, this result is interesting as rAHSV5+S9$_{4LP}$ appears attenuated in infected embryos across the different experiments.

There are several reasons why these experiments may not have worked. Firstly, it appeared that not all embryos were at the same stage of embryonic development. Some were very small in size, and some were larger than the others, therefore not all embryos used across the experiments were at the 13 days post incubation stage. This could be rectified by weighing the eggs before infection. This is important as the IFN inducibility of chicken embryo cells and intact embryos increases with age and corresponds to the maturation of the innate immune response (Isaacs and Baron, 1960; Sekellick and Marcus, 1985). Therefore, certain

viruses are able to grow well in younger embryos but at later stages of embryonic development embryos are able to limit viral infection (Isaacs and Baron, 1960). This has been seen in several studies on influenza A and B. Similar to what was done here, an influenza B virus non-structural NS1 knockout (ΔNS1-B) was generated via reverse genetics (Dauber *et al.*, 2004). The replication kinetics of this virus were then compared to the wild-type virus in 6-, 8- and 11-day old embryos over 72 h. The wild-type virus grew to high titres over the 72 h regardless of the age of the embryo but the ability of ΔNS1-B to grow decreased as the age of the embryo increased (Dauber *et al.*, 2004). This was similar to what was observed with influenza A lacking NS1 expression (Talon *et al.*, 2000). Talon *et al.* (2000) used embryos between 6 and 12 days old and Influenza A lacking NS1 expression grew badly in embryos older than 7 days due to the maturation of the innate immune response, while the wild-type grew well regardless (Talon *et al.*, 2000). Both studies therefore indicated that the NS1 protein of influenza A and B had some IFN-antagonistic properties, which was later confirmed in the same studies. Therefore, it is possible that the viruses generated here, especially those lacking NS4 expression, were able to replicate better in the younger embryos, which may have increased embryo deaths and skewed the results.

These experiments did not involve the same number of embryos per infection. It would be a good idea to keep this consistent in future experiments. It is also possible that the blood vessel was missed when infecting the embryos. In these experiments some of the viruses had low titres and infecting the embryos with the same initial inoculum would account for these differences. In Talon *et al.* (2000) and Dauber *et al.* (2004) all embryos were infected with 100 pfu of virus. In most of the experiments the viruses were not used immediately, therefore it is also possible that the titre of the viruses had dropped to even lower than what was recorded. This would influence the fitness of the viral population as dead virus particles would still be detected by the innate immune response, leading to an antiviral state. The RT-PCR did not work for experiment 2 and was not done for all embryos in the experiment, therefore it is not possible to have a definitive answer for these experiments. In the future it would be a good idea to use a commercially available kit or robots when isolating the RNA for the RT-PCR as was done in Potgieter *et al.* (2017). This would ensure that the RNA was not lost in the process. It would also be advantageous to do semi-quantitative PCR, with a standard curve using dsRNA of known quantity.

These results also showed that storing the viruses at 4°C for two weeks after rescue influences virulence. When injected into embryos immediately rAHSV5 was highly virulent but became partly attenuated after storage, as did all other viruses containing the AHSV5 backbone. Previous studies have suggested that the outer capsid proteins VP2 and VP5 play a role in virulence due to their involvement in virus attachment and entry and the triggering of apoptosis (Hassan and Roy, 1999; Mortola *et al.*, 2004; Potgieter *et al.*, 2009). AHSV virulence is influenced by the affinity of the virus for certain tissues (tissue tropism) (Erasmus, 1973). Based on this, virus particles that infect vital organs, such as the heart or lung, will be highly virulent, leading

to a severely diseased phenotype. Attenuation would represent subset of viruses that do not have selective affinity for vital organs (Erasmus, 1973; Potgieter *et al.*, 2009). VP2 detaches from the virion upon a drop in pH to 6.0-6.5 (Zhang *et al.*, 2016), therefore a drop in pH of the medium over time could have caused the detachment of VP2 from some virus particles. This could then have influenced the ability of those viruses to attach to and infect certain tissues, causing attenuation. While VP2 is dispensable for AHSV replication in BSR cells, VP5 is not (van Gennip *et al.*, 2017), therefore the viruses used in this study still contained VP5 as they were still able to replicate. It would be a good idea to freeze dry newly rescued viruses immediately to circumvent this problem. Alternatively, viruses could be passed in the brains of suckling mice (Erasmus, 1973) and then stored at -70°C. Twenty four-hour old mice are still in the embryonic state, therefore innate immunity is low. Virulent viruses store well in mouse brain (Prof. AC Potgieter and Mrs IM Wright, personal communication) therefore this is a viable option for future experiments.

Maartens *et al*. (2011) observed that in most instances, tissues that showed prominent haemorrhaging contained large amounts of positive immunolabeling for AHSV in the microvascular endothelium. The opposite, however, was not always true. One explanation for this is that blood does not always extravasate from damaged capillaries unless exposed to a certain amount of pressure. Thus, some of the tissues that contained haemorrhages were exposed to prehatching movement or were located next to structures that are actively moving. Examples include the back of the head, the dermis, the feathers and the cardiac muscles (Maartens *et al.*, 2011). Therefore, while viral infection can cause haemorrhaging it is possible that some of the petechial and ecchymotic haemorrhaging observed here was caused by the prehatching movement within the egg (Maartens, 2009; Maartens *et al.*, 2011).

This chapter shows that the expression and intracellular localisation of NS4 is dependent on Seg-9 itself and not the backbone into which it is incorporated. Seg-9 encodes both VP6 and NS4 therefore this could be due to one of the proteins or both. $S9_5$, which encodes NS4-II, in particular appears to give the virus an *in vitro* replication advantage. To date, not much research on AHSV has been done in an ECE model, therefore this was a preliminary investigation before testing these viruses in horses. While the control (rAHSV5) did not work consistently here it does appear that viruses containing $S9_5$ were virulent, independent of the AHSV backbone and age of the virus and caused severe lesions and death. Furthermore, viruses lacking NS4 expression appeared attenuated compared to rAHSV5. This suggests that NS4-II, encoded by $S9_5$, is a virulence factor in ECEs. Due to time and financial constraints the ECE model experiments could not be repeated therefore further studies need to be done to determine if this is the case. The limitations of the ECE model have been discussed and if repeated it would be best to rescue fresh viruses and inject them immediately into embryos that are at 13 days of incubation. The results in horses after infection with two reverse genetics-derived viruses are described in the next chapter.

# CHAPTER 4

## AHSV NS4 DELAYS HOST INNATE IMMUNITY AND INTERFERES WITH THE JAK-STAT SIGNALLING PATHWAY

## 4.1. INTRODUCTION

To establish successful infection a virus must overcome host immunity. Therefore, cytoplasmic viruses often encode nuclear proteins that act to suppress the host immune response (Zakaryan and Stamminger, 2011; Chen *et al.*, 2016). Innate immunity is the first line of defence against an invading pathogen. Upon infection with an RNA virus, innate immunity is initiated when dsRNA or ssRNA is recognised by host PRRs (Kell and Gale, 2015) ultimately leading to the production of type I IFN α and β (Randall and Goodbourn, 2008). The IFN response, which is central to innate immunity and the fight against viral infections, is mediated by the JAK-STAT signalling pathway. While some viruses encode proteins that act as direct IFN antagonists, others counteract the action of type I and type II IFNs. BTV modulates the IFN-I response by interfering with the JAK-STAT signalling pathway (Doceul *et al.*, 2014). BTV NS4 has subsequently been shown to modulate the IFN-response by downregulating mRNA levels of IFN-I and ISGs and downregulating the activities of certain promoters (Ratinier *et al.*, 2016). NS4 is not required for BTV replication in insect cells, mammalian cells, or $IFNAR^{-/-}$ mice (Ratinier *et al.*, 2011). It does, however, confer a replication advantage to BTV in mammalian cells in an IFN-induced state as well as *in vivo* in the host (Ratinier *et al.*, 2011; Ratinier *et al.*, 2016). BTV NS4 was therefore concluded to be an IFN antagonist and a key virulence factor in the host (Ratinier *et al.*, 2016).

Like BTV NS4, AHSV NS4 is found in both the nucleus and cytoplasm of infected cells (Zwart *et al.*, 2015) and binds dsDNA and not dsRNA (Belhouchet *et al.*, 2011; Zwart *et al.*, 2015). Thus, it has been suggested that AHSV NS4 may also play a role in virus-host interactions and in counteracting the host innate immune response. Furthermore, the results of Chapter 3 suggested that viruses containing $S9_5$ were virulent and those lacking NS4 expression were attenuated, therefore AHSV NS4 may be a virulence factor.

To determine the role of AHSV NS4 in virulence in the natural host, horses were inoculated with the recombinant viruses rAHSV5 or rAHSV5minNS4 described in Chapters 2 and 3 as part of vaccine trials at Deltamune (Pty) Ltd. These trials showed that knockdown of NS4 results in a highly attenuated virus, confirming what was suggested in Chapter 3. Therefore, the aim of this chapter was to compare the transcriptional response in a subset of these horses, to see how the lack of NS4 potentially mediates the transition of the virus from virulent to attenuated, and to see if the protein plays a role in the host immune response.

## 4.2. MATERIALS AND METHODS

### 4.2.1. Cells and viruses

Vero cells (ATCC CCL-81) were maintained as monolayers in DMEM supplemented with 5% FBS, 1.2% Fungizone and 1% Pen/Strep and were grown at 37°C, with $CO_2$ and 90% humidity. Alternatively, Vero cells were maintained as monolayers in VP-SFM (1X, Gibco®) or OptiPRO™ SFM (Gibco®) serum free medium supplemented with 1.2% Fungizone and 1% Pen/Strep and were grown at 37°C, with $CO_2$ and 90% humidity. The recombinant viruses rAHSV5, rAHSV5minNS4 and rAHSV5ΔNS4 described in Sections 2.2.2 and 3.2.2 were used in this chapter, as was rAHSV5 rescued from expression plasmids and synthetic ssRNA as described previously (van de Water *et al.*, 2015; Potgieter *et al.*, 2017).

### 4.2.2. Horse trials

Horse trials were conducted at the insect-free animal facilities of Deltamune (Pty) Ltd (Roodeplaat, South Africa) which are approved by the South African Department of Agriculture, Land Reform and Rural Development (DALRRD). DALRRD Section 20 approval, as well as approval by the Deltamune Ethical Committee (DEC, PD14-16, PD15-11, PD15-18, PD16-27, PD17-23) was obtained for all animal experimentation. All work was done by qualified veterinarians and researchers at Deltamune (Pty) Ltd. Table 4.1 provides a summary of the trials that were undertaken. Susceptibility of horses to AHS was determined using a commercial blocking ELISA (Eurofins Technologies Ingenasa). After inoculation, rectal temperatures were taken daily by and viraemia was tested from daily EDTA bleeds using RT-PCR targeting Seg-4 (VP4) or Seg-5 (NS1) (Section 3.2.14). Clinical signs were monitored daily.

### 4.2.3. Collection of blood and PBMC isolation

Blood was collected aseptically from the jugular vein of the horses involved in vaccine trial 2 (Table 4.1) using EDTA containing vacutainers on days 0 (before viral inoculation), 1 and 2 for all animals, and on day 4 for the horse inoculated with rAHSV5. This was done at Deltamune Pty (Ltd), and the vials were then transferred to the laboratory at the University of Pretoria immediately (<2 h) and peripheral blood mononuclear cells (PBMCs) were isolated via density gradient centrifugation. Blood samples were layered over Histopaque-1077® (Sigma-Aldrich) and centrifuged at 900 x g for 30 minutes (min) at room temperature (RT). The opaque interface containing PMBCs was collected, rinsed, resuspended in sterile 1 x PBS and centrifuged at 250 x g for 10 min at RT. The PBMC pellet was resuspended in a 1:3 mixture of sterile 1 x PBS and TRI reagent® (Sigma-Aldrich). Cells were stored at -70°C until RNA isolation.

**Table 4.1.** Summary of vaccine trials carried out at Deltamune (Pty) Ltd.

| Horse number | Trial number | Virus | Virus titre determined on BSR cells ($log_{10}TCID_{50}$/ml) | Infection route |
|---|---|---|---|---|
| 794 | 1 | rAHSV5 | 5.80 | IV |
| 16# | 2 | rAHSV5 | 5.80 | IV |
| 12 | 4 | rAHSV5 (pl) | 6.66 | IV |
| 15 | 5 | rAHSV5 (pl) | 6.66 | IV |
| B14 | 1 | rAHSV5minNS4 | 6.80 | IV |
| 453 | 1 | rAHSV5minNS4 | 6.80 | IV |
| 9 | 3 | rAHSV5minNS4 | 5.67 | IV |
| 14 | 3 | rAHSV5minNS4 | 5.67 | IV |
| 2# | 2 | rAHSV5minNS4 | 5.67 | IM |
| 4 | 2 | rAHSV5minNS4 | 5.67 | IM |
| 5# | 2 | rAHSV5minNS4 | 5.67 | IM |
| 6 | 2 | rAHSV5minNS4 | 5.67 | IM |
| 7# | 2 | rAHSV5minNS4 | 5.67 | IM |
| 2 | 3 | rAHSV5minNS4 | 5.67 | SC |
| 4 | 3 | rAHSV5minNS4 | 5.67 | SC |
| 5 | 3 | rAHSV5minNS4 | 5.67 | SC |
| 6 | 3 | rAHSV5minNS4 | 5.67 | SC |

rAHSV5 (pl) = recombinant AHSV5 rescued from plasmids only.
IV = intravenous, IM = intramuscular, SC = subcutaneous.
# Total RNA sent for RNA-seq.

### 4.2.4. Total RNA isolation

Total RNA was isolated according to the TRI reagent® protocol and resuspended in LiChlorosolv® Water (Merck). Additional RNA purification was done using the RNeasy® Mini kit (Qiagen), with the inclusion of the DNase digestion step, and the RNA eluted in LiChlorosolv® Water. Samples of the eluate were analysed via 1% agarose gel electrophoresis (0.5 x TBE, 180V, stained with ethidium bromide) and NanoDrop™ ND-1000 spectrophotometry (Thermo Fisher Scientific Inc.). RNA integrity and concentration were then assessed more stringently using the Experion™ Automated Electrophoresis System (BioRad Laboratories) at the ACGT Microarray Facility and Ion Torrent Sequencing Facility of the University of Pretoria.

### 4.2.5. Library preparation, transcriptome sequencing and mapping to the reference genome

Total RNA from four of the horses involved in vaccine trial 2 was used for transcriptome sequencing; namely from horse 16 inoculated with rAHSV5 which served as the control horse, and from horses 2, 5 and 7 inoculated with rAHSV5minNS4 (Table 4.1). This resulted in 3 biological replicates per day in the case of horses inoculated with rAHSV5minNS4 and one sample per day for rAHSV5 (Table 4.2). Between 2.3 and 4.6 µg total RNA of each sample was sent to Novogene (Hong Kong) for Illumina transcriptome sequencing with the Illumina HiSeq (Illumina, USA). Sequencing libraries were generated using the NEBNext® Ultra™ RNA Library Prep Kit for Illumina® (NEB, USA) as per the manufacturer's instructions. Index codes were added in

order to attribute sequences to each sample. The index-coded samples were clustered on a cBOT Cluster Generation System using TruSeq PE Cluster Kit v3-cBot-HS (Illumina) according to the manufacturer's instructions. Thereafter, library preparations were sequenced with Illumina HiSeq (Illumina, USA) resulting in 150 bp paired-end reads. Raw reads were filtered by in-house perl scripts (Novogene) in order to obtain clean reads. Data quality was then assessed according to error rate and GC distribution. The clean paired-end reads were mapped to ensemble release 84 of the *Equus caballus* reference genome EquCab2, using TopHat v2.0.12 with the mismatch parameter set to 2.

**Table 4.2.** Summary of samples and comparisons in the transcriptome analysis.

| Day (D) | Number of horses | Virus injected | Sample name | | Comparisons done (referred to as) |
|---|---|---|---|---|---|
| | | | Individual | Combined | |
| **0** | 1 | rAHSV5 | NS4_D0 | - | - |
| **1** | 1 | rAHSV5 | NS4_D1 | - | NS4_D1 vs NS4_D0 (NS4_D1) |
| **2** | 1 | rAHSV5 | NS4_D2 | - | NS4_D2 vs NS4_D0 (NS4_D2) |
| **4** | 1 | rAHSV5 | NS4_D4 | - | NS4_D4 vs NS4_D0 (NS4_D4) |
| **0** | 3 | rAHSV5minNS4 | minNS4_D0_1 | minNS4_D0 | - |
| | | rAHSV5minNS4 | minNS4_D0_2 | | |
| | | rAHSV5minNS4 | minNS4_D0_3 | | |
| **1** | 3 | rAHSV5minNS4 | minNS4_D1_1 | minNS4_D1 | minNS4_D1 vs minNS4_D0 (minNS4_D1) |
| | | rAHSV5minNS4 | minNS4_D1_2 | | |
| | | rAHSV5minNS4 | minNS4_D1_3 | | |
| **2** | 3 | rAHSV5minNS4 | minNS4_D2_1 | minNS4_D2 | minNS4_D2 vs minNS4_D0 (minNS4_D2) |
| | | rAHSV5minNS4 | minNS4_D2_2 | | |
| | | rAHSV5minNS4 | minNS4_D2_3 | | |

### 4.2.6. Expression quantification and differential gene expression

Two different approaches were used to analyse the same data from the point of mapping to the genome onwards, *i.e.*, for the quantification of gene expression and the downstream analysis of differential gene expression. Figure 4.1 illustrates the different analyses done on the same alignments to the genome (Section 4.2.5). Dataset 1 was done at Novogene (Hong Kong), and dataset 2 was analysed at the Centre for Bioinformatics and Computational Biology at the University of Pretoria (South Africa), as well as at the Centre for High Performance Computing (Cape Town, South Africa). For dataset 1, the number of reads mapped to each gene were counted using HTSeq software (v0.6.1, -m union). The read count values were then used as input data for differential gene expression analysis. At this point, the data for the three biological replicates of rAHSV5minNS4 was combined for each day (Table 4.2). Differential gene expression of the samples with biological replicates (rAHSV5minNS4) was analysed using DESeq (v1.10.1, padj<0.05) and used its inherent normalisation method. Samples without biological replicates (rAHSV5) were normalised using trimmed mean of M values (TMM) and then analysed using DEGSeq (v1.12.0, $\log_2$FoldChange>1 & qval<0.005). Gene expression levels and differential gene expression of dataset 2 were analysed with Cuffdiff which was run through Cufflinks (v2.1.1), part of the Tuxedo suite, followed by CummeRbund in RStudio (Version 1.0.136).

Differentially expressed genes were compared to the list of innate immunity-related genes in InnateDB v5.4 (Breuer *et al.*, 2013). Venn diagrams were drawn using the "Calculate and draw custom Venn diagrams" tool on the Bioinformatics and Evolutionary Genomics page of the Ghent University website (http://bioinformatics.psb.ugent.be/webtools/Venn).

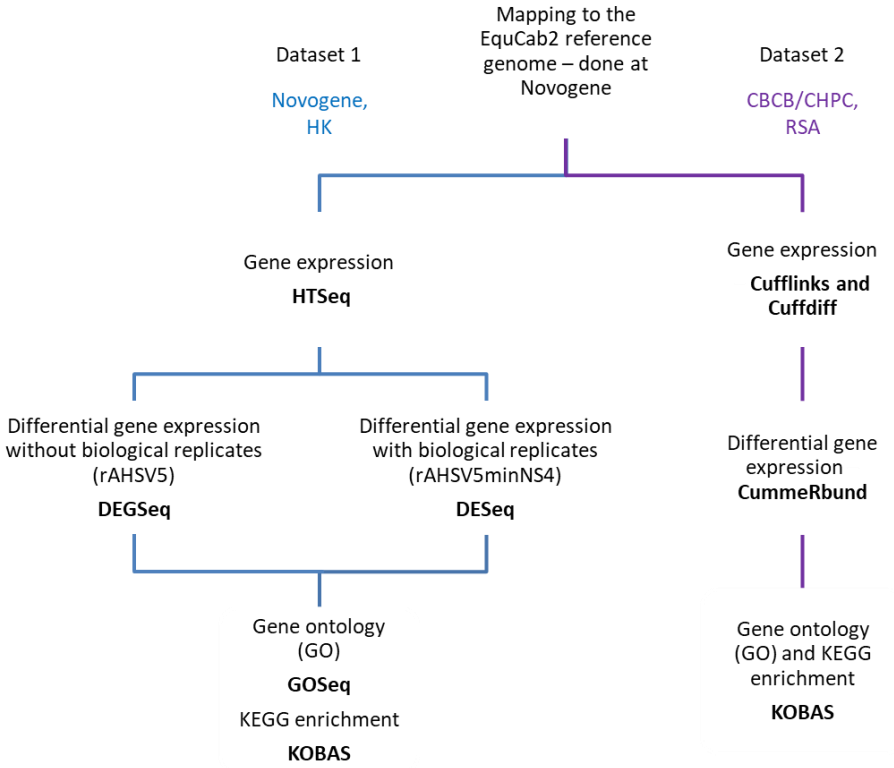


**Figure 4.1.** The two approaches used to quantify expression, and analyse differential gene expression, GO term and KEGG enrichment in this study. Dataset 1 was carried out at Novogene (Hong Kong) and Dataset 2 was carried out at the Centre for Bioinformatics and Computational Biology (CBCB) at the University of Pretoria (South Africa), as well as at the Centre for High Performance Computing (CHPC) in Cape Town (South Africa).

### 4.2.7. Gene ontology (GO) and KEGG enrichment analyses of differentially expressed genes

Gene ontology (GO) enrichment analysis of differentially expressed genes (DEGs) in Dataset 1 was done with GOSeq (v2.12). Length bias was corrected and GO terms with a corrected pval<0.05 were considered significantly enriched by DEGs. KEGG (Kyoto Encyclopedia of Genes and Genomes) enrichment analysis of DEGs in KEGG pathways was done with KOBAS (v2.0). KEGG pathways with corrected pval<0.05 were considered significantly enriched. GO enrichment and KEGG pathway enrichment analyses of Dataset 2 were done through KOBAS. In both cases, GO terms and KEGG pathways with corrected pval<0.05 were considered significantly enriched. KEGG pathways were filtered to include membrane transport, signal transduction, signalling molecules and interaction, as well as immune system pathways.

### 4.2.8. Harvesting of whole cell Vero lysates and Western blotting

Vero cells were cultured in 6-well plates and incubated at 37°C for 24 h. Thereafter, cells were harvested via low-speed centrifugation at 1 500 x g for 10 min. The pellet was rinsed twice with 1 x PBS at 800 x g for 5 min, and then resuspended in 100 µl RIPA buffer [150 mM NaCl, 1.0% TX-100, 0.5% sodium deoxycholate, 0.1% SDS (sodium dodecyl sulphate), 50 mM Tris, pH 8.0]. The resuspended pellets were then incubated on ice with shaking for 30 min and stored at -20°C. All lysates were subjected to 12% SDS-PAGE and Western blot (Section 2.6). The primary antibodies listed in Table 4.3 were used and detection was done using recombinant protein G-HRP (Invitrogen™, 10-1223). Labelling of NS1 was done with anti-NS1(786) (Table 2.2) as an infection control. Labelling of β-actin using a β-actin monoclonal (Elabscience®, E-AB-20031) or polyclonal (Elabscience®, E-AB-20058) antibody was done as a cytoplasmic loading control.

**Table 4.3.** Primary antibodies targeting STAT1, STAT2 or pSTAT1.

| Manufacturer | Catalog number | Host species | Targets | Immunogen |
|---|---|---|---|---|
| Sigma-Aldrich | AV38933 | Rabbit | STAT1 | Peptide with the sequence: MSQWYELQQLDSKFLEQVHQLYDDSFPMEIRQYLAQWLEKQDWEHAANDV |
| LSBio | LS-B4583 | Rabbit | STAT1 | Synthetic peptide from the N-terminal of human STAT1 |
| Abcam# | ab109320 | Rabbit | STAT1 | Synthetic peptide corresponding to the N-terminal of human STAT1 |
| Abcam | ab155933 | Mouse | STAT1 | Protein expressed in 293T cells transfected with human STAT1 expression vector |
| LSBio# | LS-C352894/67027 | Rabbit | pSTAT1 | KLH-conjugated peptide within the C-terminus of human STAT1, Phospho-Ser-727 (pSer727) |
| Merck | 07-140 | Rabbit | STAT2 | GST-fusion protein corresponding to residues 672-925 of STAT2 |
| Abcam | ab32367 | Rabbit | STAT2 | Synthetic peptide from the N-terminal of human STAT2 |
| Abcam | ab227312 | Rabbit | STAT2 | Recombinant fragment within STAT2 C-terminal |
| GenScript* | αSTAT2 #1 | Rabbit | STAT2 | KLH-conjugated peptide with sequence QKKKTPSLDPHQNQC |
| GenScript* | αSTAT2 #2 | Rabbit | STAT2 | KLH-conjugated peptide with sequence CEQRSVGTGKGTNKG |
| GenScript* | αSTAT2 #3 | Rabbit | STAT2 | KLH-conjugated peptide with sequence SQEVQASPAPEAAVC |

*Designed by Prof. AC Potgieter, Deltamune (Pty) Ltd.
#Antibodies used after optimisation.

### 4.2.9. Immunofluorescence and confocal microscopy

Vero cells were seeded on sterile coverslips in 24-well plates, or for cells grown in VP-SFM or OptiPRO™ SFM, coverslips were pre-treated with medium containing NEAA to promote cell attachment before the addition of cells. Cells were either left uninfected or were infected at a MOI of 0.1-1. At 24 hpi cells were left untreated, or were treated with 200 ng/ml of IFN-γ, (GenScript USA, Human Z02915-100 or CHO expressed Z02986-50) for 30 min to 5 h at 37°C, with $CO_2$ and 90% humidity. Thereafter, cells were fixed with 4% PFA for 30 min at RT and permeabilised with 0.2% TX-100 for 10 min at RT. Blocking was done with 5% blocking solution for 30 min at RT. Primary labelling was done with Abcam anti-STAT1 N-term, LSBio anti-pSTAT1 or Abcam anti-STAT2 C-term (Table 4.3), followed by secondary labelling with AF 488-conjugated goat anti-rabbit IgG (H+L) (Invitrogen™, A11034). Dual primary labelling was done using anti-NS1 (Eurofins Technologies Ingenasa) in conjunction with anti-STAT1 or anti-pSTAT1. Simultaneous secondary labelling was done using Alexa Fluor®

594-conjugated goat anti-mouse IgG (H + L, Invitrogen™, A11005) and Alexa Fluor® 488-conjugated goat anti-rabbit IgG (H+L, Table 2.2). Nuclei were stained with DAPI, and coverslips were mounted to glass slides using VECTASHIELD Mounting Medium. In all cases immunofluorescence was visualized using a Zeiss LSM 880 CLSM coupled to an Airyscan detector.

### 4.2.10. Cellular fractionation

Vero cells were cultured in 6-well plates (using complete DMEM) and AHSV-infected at a MOI of 0.5. At 24 hpi, cells were left untreated or treated with IFN-γ as detailed above. Cells were harvested, pelleted via low-speed centrifugation, and rinsed with 1 x PBS. Cell pellets were then resuspended in hypotonic buffer (10 mM Tris, 0.2 mM $MgCl_2$, pH 7.4), incubated on ice, lysed with a 22G needle, and subjected to low-speed centrifugation after which the supernatant was retained as the cytoplasmic fraction. The nuclear pellet was rinsed with 1 x PBS and resuspended in RIPA buffer (150 mM NaCl, 1.0% TX-100, 0.5% sodium deoxycholate, 0.1% SDS, 50 mM Tris, pH 8.0). Both the cytoplasmic and nuclear fractions were incubated on ice with shaking and stored at -20°C for Western blot analysis. All samples were subjected to 12% SDS-PAGE and Western blotting as in Section 4.2.8.

## 4.3. RESULTS

### 4.3.1. rAHSV5minNS4 is attenuated in experimentally infected horses

The recombinant viruses rAHSV5 or rAHSV5minNS4 were inoculated into horses at Deltamune (Pty) Ltd to compare the virulence of the viruses in the natural host. While these studies were not all part of the work done for this thesis, a summary of the safety data obtained from 5 vaccine trials conducted over several years is shown in Table 4.4 to provide the background to the rest of the data presented in this chapter. All control horses exposed to rAHSV5 showed clinical symptoms and died, or had to be euthanised, six to eight days after inoculation, independent of the method of virus rescue. Post-mortem examination showed that all four horses had classical lesions of the disease such as interstitial lung oedema, alveolar oedema (froth in the trachea), and that some, but not all, had hydropericardium (Figure 4.2). In contrast, despite evidence of virus replication, none of the thirteen horses inoculated with rAHSV5minNS4 showed any clinical signs of AHS, independent of the route of inoculation. These results, obtained by veterinarians and researchers at Deltamune (Pty) Ltd, showed that rAHSV5 is virulent in experimentally infected horses, whereas rAHSV5minNS4 is fully attenuated.

**Table 4.4.** Safety data obtained from 5 vaccine trials carried out at Deltamune (Pty) Ltd.

| Horse number | Trial number | Virus | Lowest Cq value | AHS clinical signs | Died / Euthanised | Neutralisation titre (day 28) | Alveolar oedema |
|---|---|---|---|---|---|---|---|
| 794 | 1 | rAHSV5 | 24.8 | Yes | Yes | - | Yes |
| 16 | 2 | rAHSV5 | 19.5 | Yes | Yes | - | Yes |
| 12 | 4 | rAHSV5 (pl) | 26.8 | Yes | Yes | - | Yes |
| 15 | 5 | rAHSV5 (pl) | 21.8 | Yes | Yes | - | Yes |
| B14 | 1 | rAHSV5minNS4 | 35.2* | No | - | 1024 | - |
| 453 | 1 | rAHSV5minNS4 | 30.3 | MR | - | >4096 | - |
| 9 | 3 | rAHSV5minNS4 | 35.2* | No | - | 128 | - |
| 14 | 3 | rAHSV5minNS4 | 36.8* | No | - | 128 | - |
| 2 | 2 | rAHSV5minNS4 | 34.5* | No | - | 32 | - |
| 4 | 2 | rAHSV5minNS4 | 34.1* | No | - | 32 | - |
| 5 | 2 | rAHSV5minNS4 | 34.3* | No | - | 64 | - |
| 6 | 2 | rAHSV5minNS4 | 36.3* | No | - | 16 | - |
| 7 | 2 | rAHSV5minNS4 | 34.7* | No | - | 32 | - |
| 2 | 3 | rAHSV5minNS4 | ND | No | - | 64 | - |
| 4 | 3 | rAHSV5minNS4 | ND | No | - | 128 | - |
| 5 | 3 | rAHSV5minNS4 | ND | No | - | 128 | - |
| 6 | 3 | rAHSV5minNS4 | ND | No | - | 16 | - |

rAHSV5 (pl) = recombinant AHSV5 rescued from plasmids (pl) only.
MR = mild reaction, ND = no data.
*Horse tested positive only two or three times during a 14-day period.

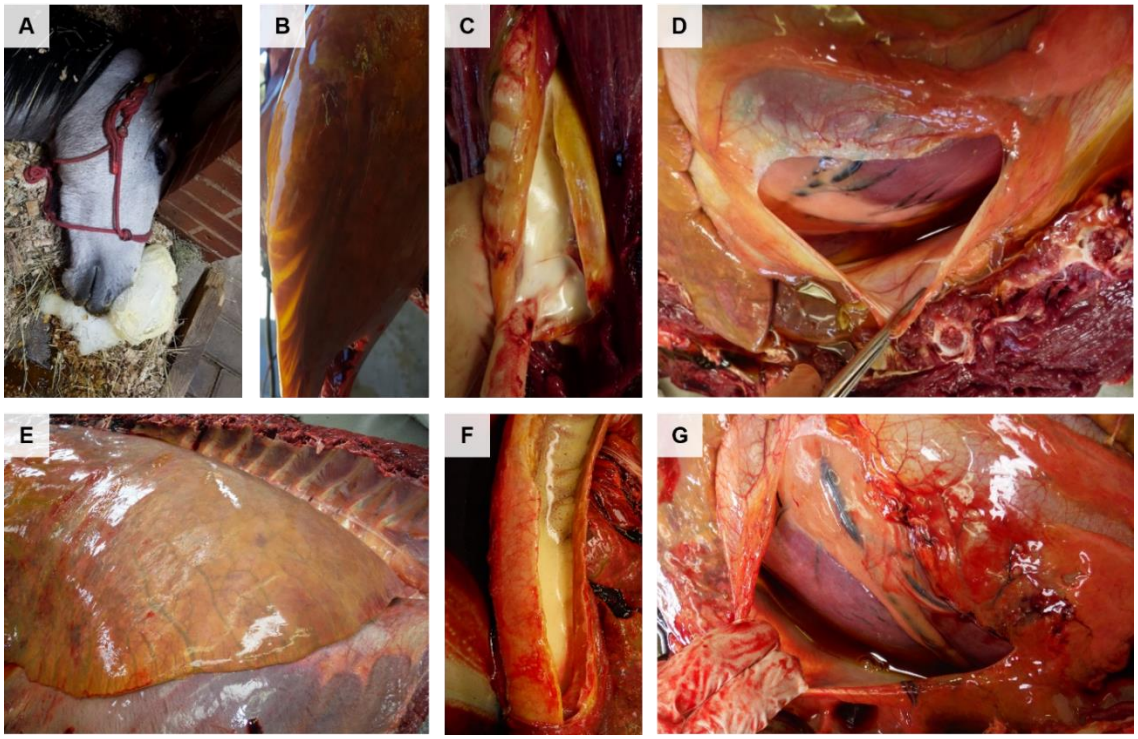


**Figure 4.2.** Images obtained from post-mortem examination of horses inoculated with rAHSV5. Classical lesions of disease such as frothing from the nostrils (A), interstitial and subpleural lung oedema (B, E), alveolar oedema (C, F) and hydropericardium (D, G) were observed.

### 4.3.2. PBMC collection and total RNA isolation

RNA-seq was subsequently used in order to compare the transcriptional responses in horses following inoculation with rAHSV5 or rAHSV5minNS4. The horses involved in vaccine trial 2 (Tables 4.1 and 4.4) were used in this part of the study. Blood was taken on days 0 (before inoculation), 1 and 2 for all horses, and day 4 for the horse inoculated with rAHSV5. Total RNA was then isolated from the PBMCs and analysed via agarose gel electrophoresis and NanoDrop™ spectrophotometry (Figure 4.3).

As seen in Figure 4.3, sufficient total RNA was isolated to be visualised on an agarose gel. Bands corresponding to 18S and 28S ribosomal RNA (rRNA) were seen on all gels, and the larger 28S band was of higher intensity than the smaller 18S band. Furthermore, there appeared to be no evidence of contamination or RNA degradation on the agarose gels. The OD260/280 ratios ranged from 1.97 to 2.13, and as a ratio of ~2.0 is generally regarded as pure in the case of RNA, these samples were regarded as pure RNA (NanoDrop Technical Support Bulletin, 2007). The RNA concentrations ranged from 20.50 ng/µl to 304.74 ng/µl, with the lowest concentrations of RNA observed for the samples obtained from the control horse inoculated with rAHSV5, as well as horse #6.

**rAHSV5 – Horse #16 – Control**

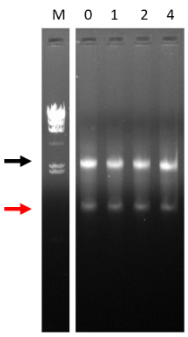


| | OD 260/280 | Concentration (ng/µl) |
|---|---|---|
| Day 0 (NS4_D0) | 2.01 | 149.84 |
| Day 1 (NS4_D1) | 2.10 | 72.85 |
| Day 2 (NS4_D2) | 2.03 | 78.71 |
| Day 4 (NS4_D4) | 1.99 | 63.49 |

**rAHSV5minNS4 – Horse #2**

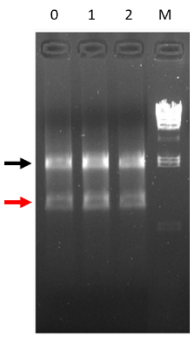


| | OD 260/280 | Concentration (ng/µl) |
|---|---|---|
| Day 0 (minNS4_D0_1) | 2.08 | 280.31 |
| Day 1 (minNS4_D1_1) | 2.06 | 304.74 |
| Day 2 (minNS4_D2_1) | 2.10 | 247.98 |

**rAHSV5minNS4 – Horse #4**

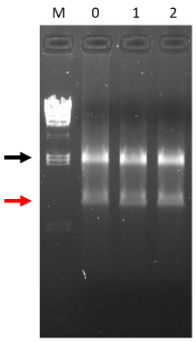


| | OD 260/280 | Concentration (ng/µl) |
|---|---|---|
| Day 0 (minNS4_D0_2) | 2.08 | 125.37 |
| Day 1 (minNS4_D1_2) | 2.12 | 148.21 |
| Day 2 (minNS4_D2_2) | 2.07 | 89.11 |

**rAHSV5minNS4 – Horse #5**

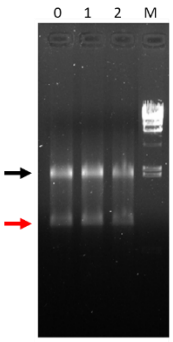


| | OD 260/280 | Concentration (ng/µl) |
|---|---|---|
| Day 0 (minNS4_D0_2) | 2.10 | 281.30 |
| Day 1 (minNS4_D1_2) | 2.11 | 165.46 |
| Day 2 (minNS4_D2_2) | 2.13 | 203.61 |

**rAHSV5minNS4 – Horse #6**

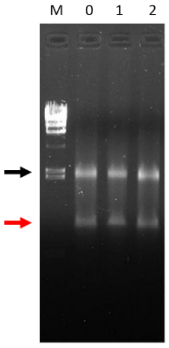


| | OD 260/280 | Concentration (ng/µl) |
|---|---|---|
| Day 0 (minNS4_D0_2) | 1.97 | 94.65 |
| Day 1 (minNS4_D1_2) | 2.02 | 20.50 |
| Day 2 (minNS4_D2_2) | 2.00 | 97.17 |

**rAHSV5minNS4 – Horse #7**

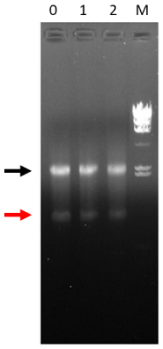


| | OD 260/280 | Concentration (ng/µl) |
|---|---|---|
| Day 0 (minNS4_D0_3) | 2.08 | 237.55 |
| Day 1 (minNS4_D1_3) | 2.09 | 172.81 |
| Day 2 (minNS4_D2_3) | 2.10 | 291.88 |

**Figure 4.3.** Agarose gel electrophoresis and NanoDrop™ spectrophotometry readings of total RNA isolated from PBMCs for six horses from vaccine trial 2. The agarose gels show 18S (red arrow) and 28S (black arrow) rRNA. M = Molecular weight marker II. The tables show the OD 260/280 reading and RNA concentration of each sample.

The electropherograms and graph in Figure 4.4 are representative of the results obtained from the Experion™ system. Two distinctive bands corresponding to 18S and 28S rRNA were seen on the electropherograms and correspond to the peaks seen in the graph. The Experion™ system also analysed the RQI value and classification, and the concentration of each total RNA sample (Table 4.5). This system returns RQI values between 1 and 10, with 1 being highly degraded RNA and 10 intact RNA (tech note 5761, Bio-Rad). Overall, the RQI values ranged from 9.2 to 9.9 and all had a classification of green, indicating that the total RNA was of high integrity. The RNA concentrations measured by the Experion™ system were somewhat higher than those obtained via NanoDrop™ spectrophotometry (Figure 4.3), and the concentration of the total RNA isolated from horse #6, as well as from the control horse inoculated with rAHSV5, was the lowest. These results indicated that the RNA samples appeared to be of high enough integrity to be used in RNA-seq.

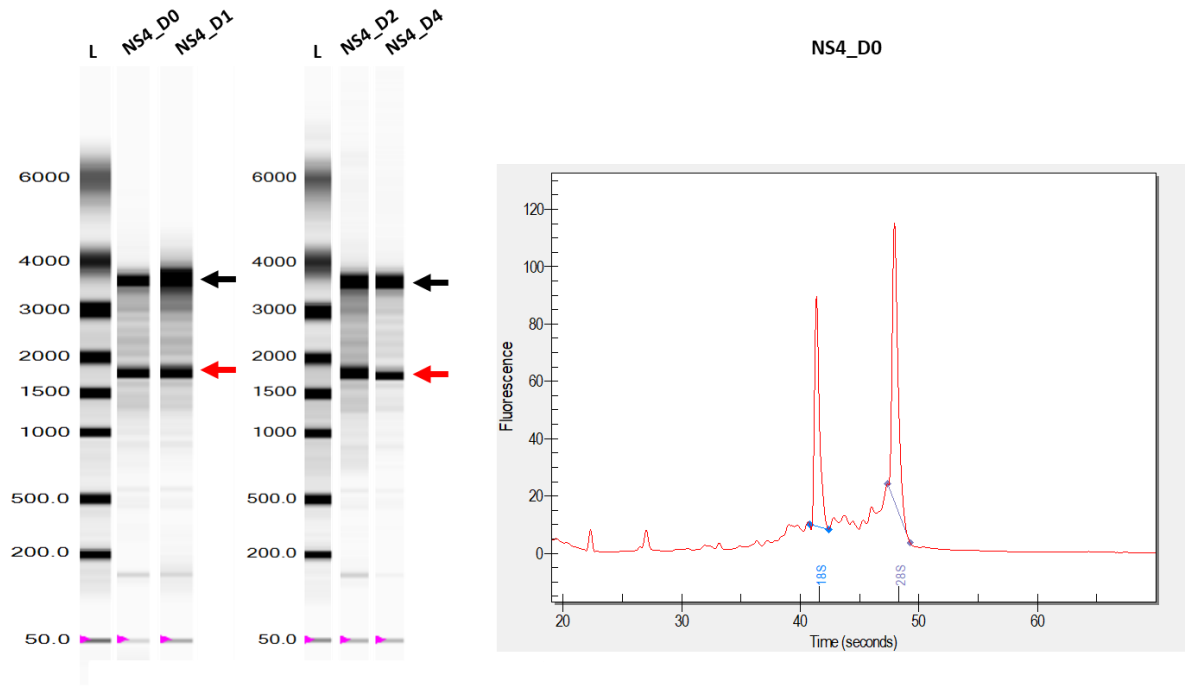


**Figure 4.4.** Electropherogram and graph obtained using the Experion™ Automated Electrophoresis System (BioRad Laboratories). Shown here are the results for the control horse inoculated with rAHSV5. The electropherograms on the left show 18S (red arrow) and 28S rRNA (black arrow). NS4_D0, NS4_D1, NS4_D2 and NS4_D4 represent the samples taken on Days 0, 1, 2 and 4 respectively for this horse. The graph shows fluorescence peaks obtained for NS4_D0. L = ladder, sizes are indicated on the left (bp).

**Table 4.5.** RNA quality control per horse, per day, as obtained from the Experion™ system.

| Horse | Day | RQI | RQI Classification | Concentration (ng/µl) |
|---|---|---|---|---|
| rAHSV5 – Horse #16 – Control | 0 | 9.4 | Green | 165.45 |
| | 1 | 9.9 | Green | 106.69 |
| | 2 | 9.6 | Green | 103.31 |
| | 4 | 9.9 | Green | 65.8 |
| rAHSV5minNS4 – Horse #2 | 0 | 9.6 | Green | 414.49 |
| | 1 | 9.8 | Green | 409.14 |
| | 2 | 9.9 | Green | 385.26 |
| rAHSV5minNS4 – Horse #4 | 0 | 9.2 | Green | 188.56 |
| | 1 | 9.7 | Green | 224.38 |
| | 2 | 9.8 | Green | 135.88 |
| rAHSV5minNS4 – Horse #5 | 0 | 9.7 | Green | 432.92 |
| | 1 | 9.8 | Green | 215.36 |
| | 2 | 9.8 | Green | 365.53 |
| rAHSV5minNS4 – Horse #6 | 0 | 9.5 | Green | 135.72 |
| | 1 | 9.8 | Green | 27.15 |
| | 2 | 9.8 | Green | 126.55 |
| rAHSV5minNS4 – Horse #7 | 0 | 9.3 | Green | 342.84 |
| | 1 | 9.7 | Green | 213.41 |
| | 2 | 9.3 | Green | 482.23 |

While the results of this section showed that total RNA was successfully isolated on all days and from all horses, it was decided that RNA from horses 16, 2, 5 and 7 should be used for transcriptome sequencing. In addition to high integrity, the total RNA quantity isolated from these horses was of a high enough yield to be used in such an experiment.

### 4.3.3. Transcriptome sequencing and mapping to the reference genome

RNA-seq of the total RNA with the Illumina HiSeq (Illumina, USA) generated on average 39.7 million paired-end raw reads per library (Table 4.6). After filtering the raw reads to remove poly-N reads, low quality reads and reads containing adapter contamination, 38.2 million reads per library, on average, were left as clean reads, accounting for 96% of the total number (Table 4.6). The error rate of the sequencing was 0.01% in the case of all the libraries. Therefore, there was a base call accuracy of 99.99% with a 0.01% chance of error during the sequencing protocol. Also, there was no indication of GC bias. Thus, the clean paired-end reads were suitable for mapping to the *Equus caballus* genome.

In general, the total number of clean reads mapped to the reference genome should be greater than 70% if the reference genome was appropriate and the study is contamination free (Novogene). In addition to this, the percentage of clean reads mapped to multiple regions should be less than 10% (Novogene). In all cases, higher than 72% of the total number of clean reads mapped to the reference genome (Table 4.6) and a low percentage (average of 1.03%) of clean reads mapped to multiple regions in the reference genome. In all cases, more than 71% of the reads could be uniquely mapped to the genome. Thus, the mapping of the clean paired-end reads to the reference genome was successful with little contamination. Therefore, the alignments were deemed suitable to use for downstream analyses.

**Table 4.6.** Transcriptome sequencing and mapping to the *Equus caballus* genome.

| Horse | Sample name | Raw reads | Clean reads | Error rate (%) | GC content (%) | Total mapped reads or fragments | Multiple mapped reads or fragments | Uniquely mapped reads |
|---|---|---|---|---|---|---|---|---|
| rAHSV5 Control Horse | Day 0 (NS4_D0) | 39830774 | 38467246 | 0.01 | 54.66 | 29580884 (76.9%) | 361040 (0.94%) | 29219844 (75.96%) |
| | Day 1 (NS4_D1) | 36659956 | 35397902 | 0.01 | 55.55 | 27078669 (76.5%) | 324815 (0.92%) | 26753854 (75.58%) |
| | Day 2 (NS4_D2) | 34237730 | 32875560 | 0.01 | 52.58 | 26092784 (79.37%) | 336959 (1.02%) | 25755825 (78.34%) |
| | Day 4 (NS4_D4) | 44152246 | 42304090 | 0.01 | 56.4 | 32524104 (76.88%) | 446958 (1.06%) | 32077146 (75.83%) |
| rAHSV5minNS4 – Horse 1 | Day 0 (minNS4_D0_1) | 45655520 | 43962406 | 0.01 | 57.53 | 31927718 (72.63%) | 448967 (1.02%) | 31478751 (71.6%) |
| | Day 1 (minNS4_D1_1) | 39145934 | 37610512 | 0.01 | 58.35 | 27999426 (74.45%) | 476235 (1.27%) | 27523191 (73.18%) |
| | Day 2 (minNS4_D2_1) | 40605156 | 39052694 | 0.01 | 57.36 | 29068361 (74.43%) | 396087 (1.01%) | 28672274 (73.42%) |
| rAHSV5minNS4 – Horse 2 | Day 0 (minNS4_D0_2) | 43988322 | 42433850 | 0.01 | 57.61 | 31523011 (74.29%) | 438725 (1.03%) | 31084286 (73.25%) |
| | Day 1 (minNS4_D1_2) | 37297402 | 35998836 | 0.01 | 54.58 | 27851707 (77.37%) | 341783 (0.95%) | 27509924 (76.42%) |
| | Day 2 (minNS4_D2_2) | 35244214 | 34029198 | 0.01 | 54.45 | 26324381 (77.36%) | 338356 (0.99%) | 25986025 (76.36%) |
| rAHSV5minNS4 – Horse 3 | Day 0 (minNS4_D0_3) | 39801798 | 37987734 | 0.01 | 57.34 | 28151124 (74.11%) | 425461 (1.12%) | 27725663 (72.99%) |
| | Day 1 (minNS4_D1_3) | 39015462 | 37459996 | 0.01 | 57.24 | 27819455 (74.26%) | 368309 (0.98%) | 27451146 (73.28%) |
| | Day 2 (minNS4_D2_3) | 40641056 | 39048980 | 0.01 | 57.45 | 29012402 (74.3%) | 401043 (1.03%) | 28611359 (73.27%) |
| Average | - | 39713505 | 38202231 | 0.01 | 56.24 | - | - | - |

### 4.3.4. Gene expression quantification and differential gene expression

As described in materials and methods two different approaches were used to analyse the data from the point of mapping onwards (Figure 4.1). Not only was this done to analyse differential gene expression but also to compare the results obtained when using different approaches on the same alignments.

On day 1, dataset 1, 28 genes were identified as being differentially expressed (DE) in the presence of NS4 (rAHSV5) (Figure 4.5A). Of these, 6 were upregulated and 22 were downregulated. The number of DE genes increased over time from 28 (day 1) to 191 on day 2, largely due to an increase in the number of upregulated genes, and finally to 750 on day 4. In contrast, 44 genes were DE on day 1 in the absence of NS4 (rAHSV5minNS4), 40 of which were upregulated and 4 downregulated and the number of DEGs decreased from day 1 (44) to day 2 (12) (Figure 4.5A). As seen in the Venn diagram, 3 genes were DE in both the presence (rAHSV5), and absence, of NS4 (rAHSV5minNS4), while the remaining genes were unique to each on day 1 (Figure 4.5A). On day 2, 9 genes were commonly differentially expressed.

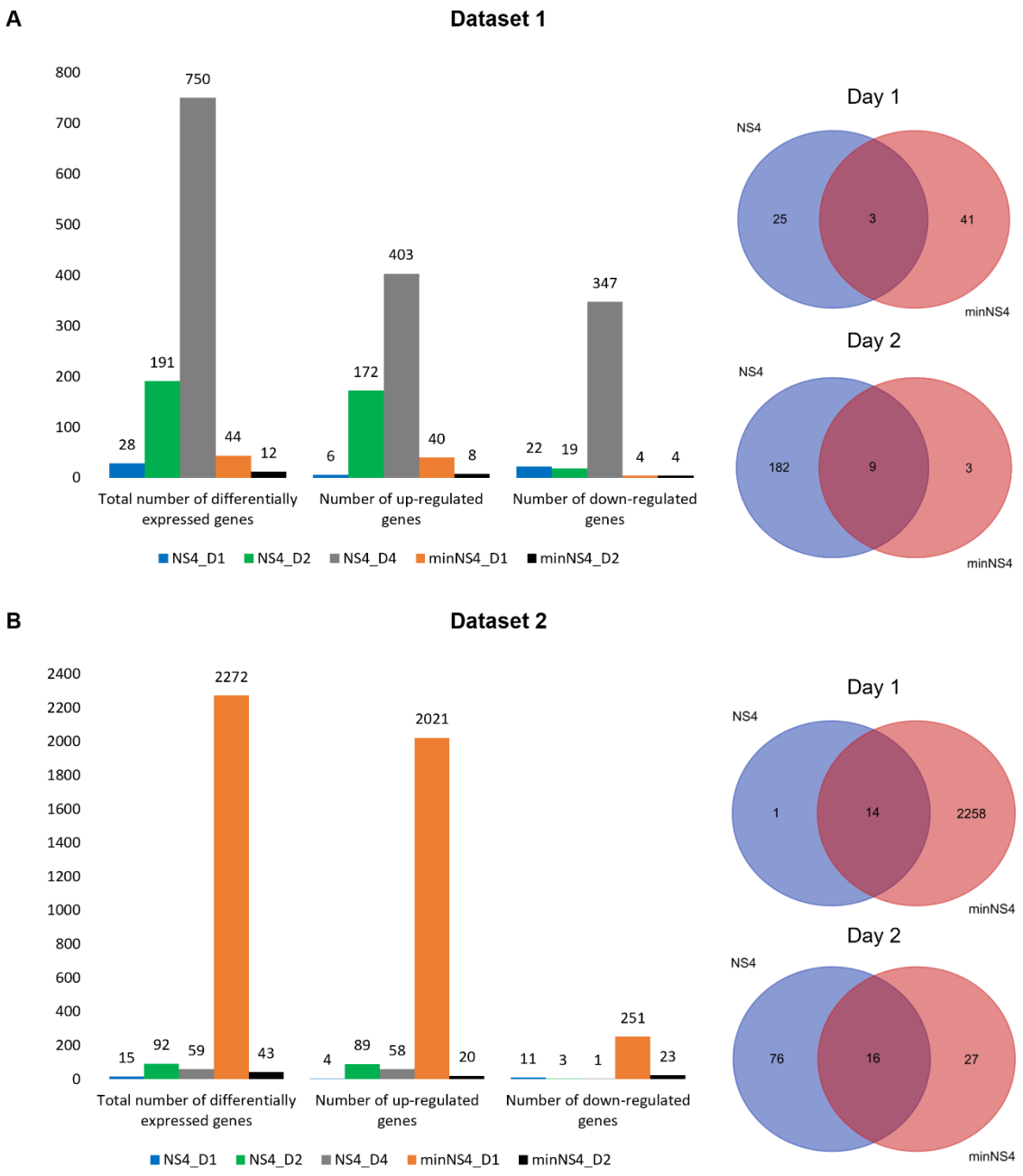


**Figure 4.5. Overview of the differentially expressed genes in dataset 1 (A) and dataset 2 (B).** The bar graphs show the number of total, up- and down-regulated differentially expressed genes on days 1, 2 and 4 for the horse inoculated with rAHSV5 (designated NS4) and days 1 and 2 for the horses infected with rAHSV5minNS4 (designated minNS4). In all cases the data was normalised to day 0. Differentially expressed genes that are unique or shared are shown in Venn diagrams comparing the total number of genes on days 1 and 2 in the presence (NS4) or absence (minNS4) of NS4.

The number of genes identified as being DE in dataset 2 (Figure 4.5B) differed somewhat from the dataset 1 results. On day 1 in dataset 2, a total of 15 genes were DE in the presence of NS4, 13 genes fewer than in dataset 1. Of the 15 DE genes, 4 were upregulated and 11 were downregulated. The number of DE genes increased from 15 to 92 on day 2 and then decreased to 59 on day 4. In contrast, 2272 genes were DE on day 1 in the absence of NS4 (rAHSV5minNS4), almost 52 times as many as in dataset 1 on the same day. Of the 2272 DE genes, 2021 were upregulated and 251 were down regulated. The number of DE genes decreased

from day 1 (2272) to day 2 (43). As seen in the Venn diagram, 14 genes were DE in both the presence (rAHSV5), and absence, of NS4 (rAHSV5minNS4) on day 1 and on day 2, 16 genes were commonly DE (Figure 4.5B). Thus, overall, in the presence of NS4 (rAHSV5) fewer genes were DE in dataset 2 than in dataset 1. In contrast, more were DE in dataset 2 than in dataset 1 in the absence of NS4 (rAHSV5minNS4).

Next, both the up- and down-regulated genes were examined in more detail. As the innate immune response is the first line of anti-viral defense, DE genes were compared to the immunity-related genes listed in InnateDB to determine if NS4 plays a role in immunity. The top ranked up- or down-regulated genes are shown in Tables 4.7-4.10, and the complete lists can be found in Appendices B (dataset 1) and C (dataset 2). Those DE genes predicted to be involved in innate immunity according to InnateDB are marked with an *. Figures 4.6 and 4.7 show the number of DEGs that were commonly up- or down-regulated between the two datasets, as well as those that were unique to each.

In dataset 1, six genes were upregulated on day 1 in the horse inoculated with rAHSV5 (Table 4.8, NS4_D1). Of these genes, three (OAS3, MX1 and OAS2) are known ISGs with OAS3 being the most upregulated on this day. In this horse, the number of upregulated genes increased considerably from day 1 to day 2, with 172 genes upregulated by day 2 (Figure 4.5, Table 4.7, NS4_D2). Of the 172 genes, at least 48 were involved in innate immunity (Appendix B). These genes included MX1, MX2 and PML; interferon-induced protein with tetratricopeptide repeats 1 (IFIT1), -3 and -5; OAS1, -2 and -3, as well as other well-characterised ISGs. Important regulators of immunity such as IRF7 (Table 4.7) and STAT1 and STAT2 were upregulated on day 2 (Appendix B). Four of the genes that were upregulated on day 1 were also upregulated on day 2 (OAS3, ENSECAG00000021220, MX1 and OAS2) and more strongly so on day 2 as indicated by the $\log_2$Fold change values (Table 4.7). The number of upregulated genes increased further to 403 by day 4, with the number of innate immunity-related genes also increasing (>82, Appendix B). This indicated that this immune response was activated by day 2 and continued to day 4. Sixty-three of the genes upregulated on day 2 were also upregulated on day 4 (Table 4.7 and Appendix B), and based on $\log_2$Fold change values most were upregulated to a greater extent on day 4.

For the horses infected with rAHSV5minNS4, more genes were upregulated on day 1 than in the control horse (40 vs 6), with at least 16 of these genes involved in innate immunity (Table 4.7, minNS4_D1, dataset 1). Among the top upregulated genes were the ISGs MX1 and MX2, IFIT5, IFI44, HERC5 and -6 as well as two novel genes Novel00397 and Novel02003. Furthermore, DDX58, one of the pattern recognition receptors of the RIG-I-like receptor signalling pathway, as well as STAT1 and IRF7, were upregulated on day 1 in these horses. As indicated in blue highlighting, three of the genes upregulated on day 1 (MX1, OAS3 and OAS2) were also upregulated on the same day in the control horse, where they were upregulated to a lower extent as indicated by the $\log_2$Fold change values. Only 8 genes were upregulated on day 2 in these horses (Table

4.7, minNS4_D2). All of these genes had also been upregulated on day 1, but their expression levels decreased from day 1 to day 2. The green highlighting in Table 4.7 shows that all of the upregulated genes on day 2 (minNS4_D2) were also upregulated on day 2 in the control horse (NS4_D2), where they were upregulated to a greater extent on the whole.

Table 4.8 shows the most upregulated genes in dataset 2. In the control horse, four genes were upregulated on day 1. Of these, two (OAS3 and MX1) were also upregulated in dataset 1 and to a comparable level as indicated by the $log_2$Fold change values (Figure 4.6, Tables 4.7 and 4.8). As in dataset 1, the number of upregulated genes increased from day 1 to day 2, in this case from 4 to 89. Of these, 81 were upregulated in both datasets (Figure 4.6) and to a comparable level (Tables 4.7 and 4.8, Appendices B and C), while the remaining eight genes (four novel, the as yet uncharacterised ENSECAG00000000968 and CXCL17, CCDC40, SYNE4) were unique to this dataset. Unlike what was seen in dataset 1, the number of upregulated genes in the control horse decreased from day 2 to day 4 (Figure 4.5B). Of the 58 genes upregulated on day 4, 53 were also upregulated on day 4 in dataset 1 (Figure 4.6). Once again, based on $log_2$Fold change values, the level of upregulation was comparable between datasets 1 and 2 (Tables 4.7 and 4.8). The 5 genes that were unique to dataset 2 on day 4 were novel genes.

In the horses inoculated with rAHSV5minNS4, many more genes were upregulated on day 1 in dataset 2 than in dataset 1 (2021 vs 40). Thirty-eight of the genes were upregulated in both datasets, with 1983 unique to dataset 2 (Figure 4.6). The genes Novel02003 and SPHK1 were unique to dataset 1. At least 185 of the 2021 genes upregulated on day 1 were predicted to be involved in innate immunity (Table 4.8, dataset 2 and Appendix C). As indicated in blue highlighting, three of the 4 upregulated genes were also upregulated on day 1 in the control horse, and like in dataset 1, the genes were upregulated to a greater extent in the horses inoculated with rAHSV5minNS4 (Table 4.8 and Appendix C). As observed in dataset 1, the number of upregulated genes decreased from day 1 (2021) to day 2 (20), in this case a considerable decrease. At least 8 of the 20 were predicted to be involved in innate immunity, and 7 genes (MX2, OAS2, OAS3, SIGLEC1, CMPK2, Novel00397 and ENSECAG00000000284) were upregulated in both datasets (Figure 4.6). The green highlighting in Table 4.8 and Appendix C shows that 16 genes were also upregulated in the control horse on day 2. Similar to what was observed in dataset 1, the genes were upregulated to a greater extent in the control horse on day 2.

**Table 4.7.** Dataset 1 – Top upregulated differentially expressed genes on days 1, 2 and/or 4 as compared to day 0 for the horse infected with rAHSV5 (designated NS4) and for the horses infected with rAHSV5minNS4 (designated minNS4). Genes differentially expressed on the same day for both NS4 and minNS4 are highlighted in blue (day 1) or green (day 2).

| Gene | NS4_D1 | | NS4_D2 | | NS4_D4 | | Gene | minNS4_D1 | | minNS4_D2 | |
|---|---|---|---|---|---|---|---|---|---|---|---|
| | Rank[a] | $log_2FC$[b] | Rank[a] | $log_2FC$[b] | Rank[a] | $log_2FC$[b] | | Rank[a] | $log_2FC$[b] | Rank | $log_2FC$ |
| OAS3* | U1 | 1.62 | U16 | 4.4304 | U11 | 6.4897 | Novel02004 | U1 | 5.6909 | - | - |
| ENSECAG00000021220 | U2 | 1.5197 | U23 | 4.1436 | U64 | 3.5219 | MX2* | U2 | 5.5855 | U2 | 3.4715 |
| MX1* | U3 | 1.3585 | U8 | 5.9236 | U10 | 6.6216 | Novel00397 | U3 | 5.3207 | U1 | 4.0086 |
| STAB1 | U4 | 1.2245 | - | - | - | - | Novel02003 | U4 | 5.189 | - | - |
| TGM3 | U5 | 1.1218 | - | - | - | - | IFIT5* | U5 | 4.3476 | - | - |
| OAS2* | U6 | 1.0924 | U25 | 4.0317 | U24 | 5.0045 | IFI44 | U6 | 4.2385 | U3 | 1.9847 |
| APOBEC3Z1B | - | - | U1 | 8.0631 | U2 | 9.007 | MX1* | U7 | 3.7577 | - | - |
| Novel00397 | - | - | U2 | 7.7817 | U1 | 11.001 | HERC5* | U8 | 3.4031 | - | - |
| MX2* | - | - | U3 | 7.5321 | U3 | 8.5137 | ENSECAG00000000284 | U9 | 3.2036 | U4 | 1.6982 |
| Novel02003 | - | - | U4 | 7.2867 | U5 | 7.4986 | HERC6 | U10 | 3.1709 | - | - |
| Novel00818 | - | - | U5 | 7.2274 | U4 | 7.5143 | Novel01303 | U11 | 3.0508 | - | - |
| DDX60 | - | - | U6 | 6.9685 | U7 | 7.3932 | DDX58* | U12 | 2.8417 | - | - |
| Novel01228 | - | - | U7 | 6.3226 | U22 | 5.0633 | SPHK1* | U13 | 2.8402 | - | - |
| CCL2* | - | - | U9 | 5.7699 | U12 | 6.2304 | OASL | U14 | 2.8347 | - | - |
| Novel02081 | - | - | U10 | 5.4359 | U19 | 5.241 | Novel01876 | U15 | 2.825 | - | - |
| IFIT5* | - | - | U11 | 5.3356 | U21 | 5.1826 | OAS3* | U16 | 2.8087 | U6 | 1.5056 |
| ISG15* | - | - | U12 | 5.2103 | U8 | 7.0132 | C1R* | U17 | 2.7992 | - | - |
| ENSECAG00000000284 | - | - | U13 | 4.788 | U17 | 5.5516 | RTP4 | U18 | 2.7486 | - | - |
| HERC5* | - | - | U14 | 4.4969 | U44 | 4.0961 | FBXO39 | U19 | 2.7377 | - | - |
| IFIT1* | - | - | U15 | 4.459 | U45 | 4.0605 | IRF7* | U20 | 2.6988 | - | - |
| HSD11B1 | - | - | U17 | 4.4046 | U13 | 5.9152 | GBP2* | U21 | 2.6869 | - | - |
| IFI44 | - | - | U18 | 4.344 | U48 | 3.9876 | C2* | U22 | 2.65 | - | - |
| CXCL10* | - | - | U19 | 4.2425 | U26 | 4.8572 | ITSN1 | U23 | 2.6337 | - | - |
| ETV7 | - | - | U20 | 4.2387 | U20 | 5.2229 | CMPK2 | U24 | 2.6184 | U5 | 1.6838 |
| Novel02002 | - | - | U21 | 4.2387 | U55 | 3.7706 | ENSECAG00000005126 | U25 | 2.6017 | - | - |
| IFI6* | - | - | U22 | 4.162 | U15 | 5.7488 | ENSECAG00000012132 | U26 | 2.5958 | - | - |
| IFIH1* | - | - | U24 | 4.103 | U37 | 4.3226 | IFI6* | U27 | 2.558 | - | - |
| HERC6 | - | - | U26 | 4.0114 | U56 | 3.7248 | OAS2* | U28 | 2.5476 | U7 | 1.3382 |
| Novel01303 | - | - | U27 | 3.9936 | U38 | 4.313 | XAF1 | U29 | 2.5432 | - | - |
| IRG1 | - | - | U28 | 3.9694 | U47 | 4.0036 | HSD11B1 | U30 | 2.4699 | - | - |
| OAS1* | - | - | U29 | 3.9188 | U29 | 4.7622 | OAS1* | U31 | 2.4688 | - | - |
| IFIT3* | - | - | U30 | 3.8494 | U67 | 3.4453 | Novel02081 | U32 | 2.381 | - | - |
| ENSECAG00000010185 | - | - | U31 | 3.8455 | U73 | 3.2855 | IRG1 | U33 | 2.3481 | - | - |
| IFI44L | - | - | U32 | 3.794 | U79 | 3.1244 | Novel00654 | U34 | 2.317 | - | - |
| IRF7* | - | - | U33 | 3.7091 | U16 | 5.6167 | SPATS2L | U35 | 2.2573 | - | - |
| XAF1 | - | - | U34 | 3.693 | U35 | 4.4591 | STAT1* | U36 | 2.2151 | - | - |
| FBXO39 | - | - | U35 | 3.6748 | U53 | 3.803 | ZCCHC2 | U37 | 2.1628 | - | - |
| RTP4 | - | - | U36 | 3.67 | U36 | 4.4495 | ENSECAG00000024875 | U38 | 2.1312 | - | - |
| EIF2AK2* | - | - | U37 | 3.5122 | U102 | 2.6891 | SIGLEC1* | U39 | 2.1219 | U8 | 1.3016 |
| CMPK2 | - | - | U38 | 3.495 | U31 | 4.6301 | DTX3L | U40 | 1.9868 | - | - |
| SAMD9L | - | - | U39 | 3.4872 | U113 | 2.4844 | | | | | |
| EPSTI1 | - | - | U40 | 3.4791 | U80 | 3.0907 | | | | | |
| RSAD2* | - | - | U41 | 3.3533 | U23 | 5.0315 | | | | | |
| RNF213 | - | - | U42 | 3.1751 | U39 | 4.2855 | | | | | |
| OASL | - | - | U43 | 3.1098 | U34 | 4.5074 | | | | | |
| GBP5 | - | - | U44 | 3.0003 | U204 | 1.7655 | | | | | |
| DDX58* | - | - | U45 | 2.9652 | U76 | 3.2151 | | | | | |
| CD274* | - | - | U46 | 2.8545 | - | - | | | | | |
| ISG20* | - | - | U47 | 2.8413 | U52 | 3.8241 | | | | | |

[a]Ranks of upregulated (U) genes in each comparison, [b]$Log_2$Fold change, *Involved in innate immunity according to InnateDB.

**Table 4.8.** Dataset 2 – Top upregulated differentially expressed genes on days 1, 2 and/or 4 as compared to day 0 for the horse infected with rAHSV5 (designated NS4) and for the horses infected with rAHSV5minNS4 (designated minNS4). Genes differentially expressed on the same day for both NS4 and minNS4 are highlighted in blue (day 1) or green (day 2).

| Gene | NS4_D1 | | NS4_D2 | | NS4_D4 | | Gene | minNS4_D1 | | minNS4_D2 | |
|---|---|---|---|---|---|---|---|---|---|---|---|
| | Rank[a] | log$_2$FC[b] | Rank[a] | log$_2$FC[b] | Rank[a] | log$_2$FC[b] | | Rank[a] | log$_2$FC[b] | Rank | log$_2$FC |
| Novel02003 | - | Undef | - | Undef | | Undef | Novel02004 | - | Undef | - | - |
| IRG1 | U1 | 1.78038 | U20 | 3.95674 | U19 | 4.06152 | CXCL9* | - | Undef | - | - |
| OAS3* | U2 | 1.70758 | U7 | 4.59276 | U3 | 6.67791 | DDX60 | U1 | 7.76127 | - | - |
| MX1* | U3 | 1.43006 | U1 | 5.9795 | U2 | 6.71257 | SAMD9L | U2 | 7.2139 | - | - |
| SYNE4 | - | - | - | Undef | - | - | IFIH1* | U3 | 6.88652 | - | - |
| CXCL17 | - | - | - | Undef | - | - | MX2* | U4 | 6.1096 | U2 | 3.92648 |
| CCDC40 | - | - | - | Undef | - | - | SAMD9 | U5 | 5.48854 | - | - |
| Novel01869 | - | - | - | Undef | - | Undef | IFI44L | U6 | 5.47037 | - | - |
| CCL2* | - | - | U2 | 5.93223 | U4 | 6.33303 | KIF20B | U7 | 5.45109 | - | - |
| IFIT5* | - | - | U3 | 5.37026 | U6 | 5.22627 | FAM111B | U8 | 5.41364 | - | - |
| ISG15* | - | - | U4 | 5.32708 | U1 | 7.13139 | IFIT1* | U9 | 5.32705 | - | - |
| Novel02081 | - | - | U5 | 4.95343 | - | - | Novel00356 | U10 | 5.30045 | - | - |
| ENSECAG00000000284 | - | - | U6 | 4.77232 | - | - | Novel00397 | U11 | 5.29999 | U1 | 3.9838 |
| HERC5* | - | - | U8 | 4.52517 | U18 | 4.14351 | ENSECAG00000020878 | U12 | 4.89565 | - | - |
| IFIT1* | - | - | U9 | 4.43136 | U22 | 4.02971 | CCDC88A* | U13 | 4.81612 | - | - |
| IFI44 | - | - | U10 | 4.4244 | U23 | 4.02718 | Novel02002 | U14 | 4.71482 | - | - |
| IFI6* | - | - | U11 | 4.2432 | U5 | 5.65853 | ENSECAG00000016018 | U15 | 4.61517 | - | - |
| CXCL10* | - | - | U12 | 4.2025 | - | - | ENSECAG00000021220 | U16 | 4.55573 | - | - |
| Novel02002 | - | - | U13 | 4.19221 | - | - | ANKRD12 | U17 | 4.55263 | - | - |
| IFIH1* | - | - | U14 | 4.12434 | U16 | 4.34981 | ENSECAG00000002575 | U18 | 4.53576 | - | - |
| ENSECAG00000021220 | - | - | U15 | 4.07858 | U33 | 3.48704 | ESCO2 | U19 | 4.44709 | - | - |
| HERC6 | - | - | U16 | 4.01083 | U26 | 3.77151 | CXCL10* | U20 | 4.41577 | - | - |
| OAS2* | - | - | U17 | 4.00705 | U8 | 4.98493 | AIM2* | U21 | 4.37787 | - | - |
| Novel01303 | - | - | U18 | 4.00373 | - | - | IFIT5* | U22 | 4.34644 | U6 | 1.83905 |
| OAS1* | - | - | U19 | 3.99001 | U9 | 4.86412 | EIF2AK2* | U23 | 4.33529 | - | - |
| IFIT3* | - | - | U21 | 3.9316 | U34 | 3.48491 | GBP6* | U24 | 4.31724 | - | - |
| ENSECAG00000010185 | - | - | U22 | 3.92946 | U38 | 3.37124 | EPSTI1 | U25 | 4.28133 | - | - |
| RTP4 | - | - | U23 | 3.69225 | U14 | 4.52351 | RAD50 | U26 | 4.27369 | - | - |
| IFI44L | - | - | U24 | 3.66716 | U42 | 3.14015 | ENSECAG00000002739 | U27 | 4.22871 | - | - |
| XAF1 | - | - | U25 | 3.58324 | U15 | 4.50495 | SMC2 | U28 | 4.2155 | - | - |
| SAMD9L | - | - | U26 | 3.5408 | - | - | NUCB2 | U29 | 4.1437 | - | - |
| EPSTI1 | - | - | U27 | 3.4789 | U44 | 3.07193 | IFI44 | U30 | 4.12668 | - | - |
| CMPK2 | - | - | U28 | 3.46771 | U12 | 4.65578 | LRRCC1 | U31 | 4.12394 | - | - |
| RSAD2* | - | - | U29 | 3.21431 | U11 | 4.85189 | ENSECAG00000010185 | U32 | 4.06331 | - | - |
| RNF213 | - | - | U30 | 3.18575 | - | - | CENPF | U33 | 4.03891 | - | - |
| OASL | - | - | U31 | 3.15699 | U13 | 4.62919 | N4BP2L2 | U34 | 4.00261 | - | - |
| ENSECAG00000001514 | - | - | U32 | 3.15524 | U7 | 5.00288 | Novel01228 | U35 | 3.98765 | - | - |
| EIF2AK2* | - | - | U33 | 3.1203 | - | - | FGFR1OP2 | U36 | 3.98607 | - | - |
| DDX58* | - | - | U34 | 3.09424 | U37 | 3.39395 | RBM41 | U37 | 3.94759 | - | - |
| GBP5 | - | - | U35 | 3.03315 | - | - | KIAA1551 | U38 | 3.92944 | - | - |
| ISG20* | - | - | U36 | 2.82766 | U25 | 3.77316 | SPG20 | U39 | 3.9073 | - | - |
| ENSECAG00000005126 | - | - | U37 | 2.78084 | - | - | TLR3* | U40 | 3.90019 | - | - |
| CD274* | - | - | U38 | 2.74992 | - | - | IFT74 | U41 | 3.88342 | - | - |
| DHX58* | - | - | U39 | 2.72386 | U17 | 4.15229 | MSR1* | U42 | 3.87422 | - | - |
| GBP6* | - | - | U40 | 2.70781 | - | - | EIF5B | U43 | 3.87031 | - | - |
| GBP2* | - | - | U41 | 2.66273 | - | - | AKAP9 | U44 | 3.86293 | - | - |
| MB21D1* | - | - | U42 | 2.62115 | - | - | EEA1 | U45 | 3.85209 | - | - |
| SIGLEC1* | - | - | U43 | 2.59662 | U10 | 4.86155 | CCDC91 | U46 | 3.84654 | - | - |
| PARP15 | - | - | U44 | 2.57423 | - | - | TNFSF10* | U47 | 3.84207 | - | - |

[a]Ranks of upregulated (U) genes in each comparison, [b]Log$_2$Fold change, *Involved in innate immunity according to InnateDB, Undef = undefined.

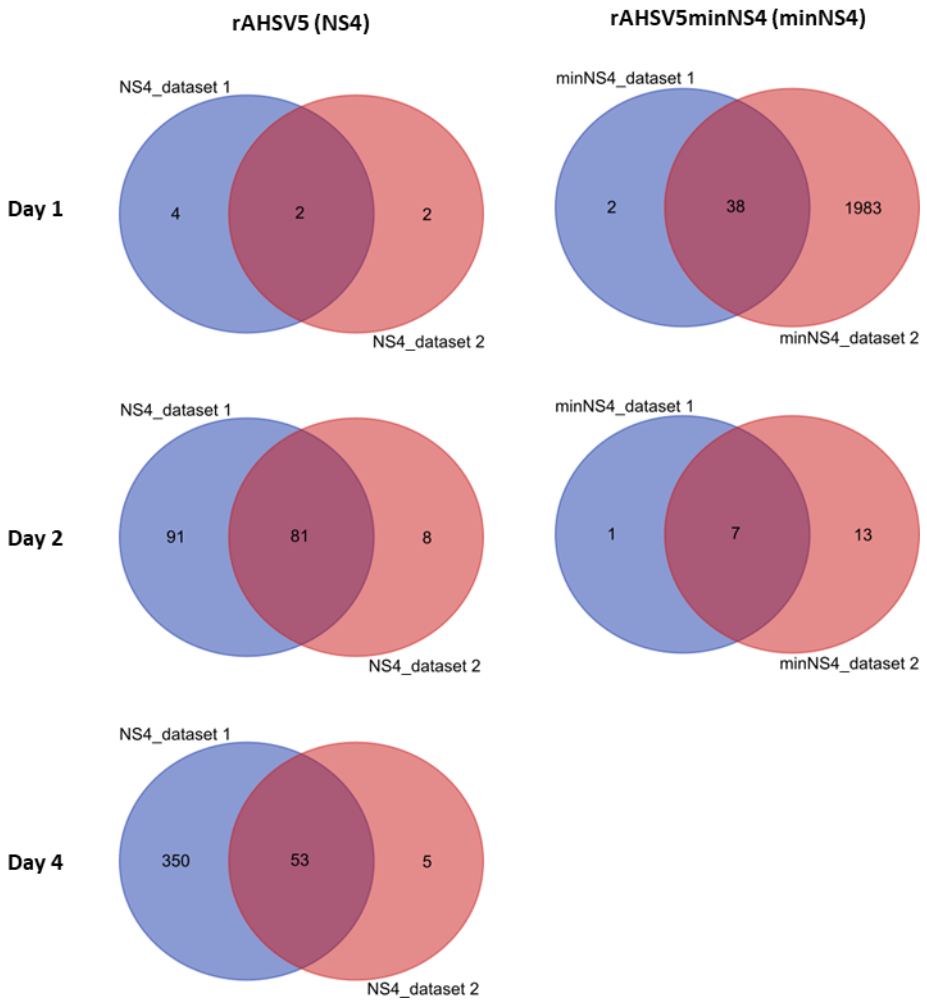


**Figure 4.6.** Upregulated genes that are unique or shared between dataset 1 and dataset 2 are shown in Venn diagrams comparing the upregulated genes on days 1, 2 and 4 in the presence (NS4) or absence (minNS4) of NS4.

The top downregulated genes are shown in Tables 4.9 and 4.10 and the full lists can be found in Appendices B and C. In dataset 1, 22 genes were downregulated in the control horse on day 1 (Table 4.9, NS4_D1). Three (CCDC88A, TRAT1 and TAX1BP1) of these genes are predicted to be involved in innate immunity. The number of downregulated genes decreased to 19 on day 2 (NS4_D2), none of which were downregulated on day 1. Two of the genes, MMP9 and IRF2BP1, are involved in innate immunity. The number of downregulated genes increased considerably from 19 on day 2 to 347 on day 4. Of the 347, at least 25 were innate immunity-related genes (Table 4.9 and Appendix B). Eight genes that were downregulated on day 2 were still downregulated on day 4.

Very few genes were downregulated in the horses infected with rAHSV5minNS4 (Table 4.9, minNS4_D1 and D2), none of which were common to both days. Two genes (DUSP1 and MMP9) involved in innate immunity were downregulated on day 2. As indicated in green highlighting, one gene, MMP9, was downregulated on day 2 in both the control horse and in the horses inoculated with rAHSV5minNS4.

Table 4.11 shows the most downregulated genes identified in dataset 2. On day 1, 11 genes were downregulated in the control horse (Table 4.10, NS4_D1), half of what was observed on the same day in dataset 1 (Table 4.9, NS4_D1). Nine of the genes were downregulated in both datasets and to comparable levels (Figure 4.7, Table 4.10). The remaining two genes, EEA1 and DNAJC2, were unique to dataset 2 (Figure 4.7). Only one gene, CCDC88A, was predicted to be involved in innate immunity. The number of downregulated genes decreased to 3 on day 2, also considerably less than the 19 downregulated genes in dataset 1 on the same day, none of which were downregulated on day 1. All three genes (FN1, SEPP1 and GAS2L1) were also downregulated in dataset 1 on the same day (Figure 4.7). Only one gene (Novel00408) was downregulated on day 4 in the control horse, and it was unique to this dataset. None of the downregulated genes in the control horse on days 2 and 4 were involve in innate immunity.

In the horses inoculated with rAHSV5minNS4, more genes were downregulated on day 1 in dataset 2 than in dataset 1 (251 vs 4) (Tables 4.9 and 4.10, Appendices B and C). At least 24 of these genes were involved in innate immunity and included MMP9, IL1B and CXCR4. Three genes (U3, FN1 and SCARNA2) were also downregulated on day 1 in dataset 1 (Figure 4.7 and Table 4.9). The number of downregulated genes decreased to 23 on day 2 in the horses inoculated with rAHSV5minNS4. Of these, 7 genes had also been downregulated on day 1 and at least 6 genes (MMP9, IL1B, CXCL2, DUSP1, S100A12 and TREM1) were involved in innate immunity. Three genes (DUSP1, MMP9 and MMP1) were also downregulated on day 2 in dataset 1. None of the genes downregulated on days 1 and 2 of the horses inoculated with rAHSV5minNS4 were downregulated on the same day in dataset 1.

**Table 4.9.** Dataset 1 - Top downregulated differentially expressed genes on days 1, 2 and/or 4 as compared to day 0 for the horse infected with rAHSV5 (designated NS4) and for the horses infected with rAHSV5minNS4 (designated minNS4). Genes differentially expressed on the same day for both NS4 and minNS4 are highlighted in green (day 2).

| Gene | NS4_D1 | | NS4_D2 | | NS4_D4 | | Gene | minNS4_D1 | | minNS4_D2 | |
|---|---|---|---|---|---|---|---|---|---|---|---|
| | Rank[a] | $log_2FC$[b] | Rank[a] | $log_2FC$[b] | Rank[a] | $log_2FC$[b] | | Rank[a] | $log_2FC$[b] | Rank[a] | $log_2FC$[b] |
| ANKRD12 | D1 | -2.95 | - | - | D287 | -1.0903 | U3 | D1 | -2.993 | NA | - |
| KIF20B | D2 | -2.793 | - | - | - | - | SCARNA2 | D2 | -2.5864 | NA | - |
| SMC4 | D3 | -2.549 | - | - | D30 | -1.6915 | 5_8S_rRNA | D3 | -2.4694 | NA | - |
| CCDC88A* | D4 | -2.2886 | - | - | - | - | FN1 | D4 | -2.407 | NA | - |
| JCHAIN | D5 | -2.2698 | - | - | D302 | -1.0696 | RETN | NA | - | D1 | -3.5695 |
| FGL2 | D6 | -1.9536 | - | - | D175 | -1.2734 | MMP1 | NA | - | D2 | -1.8825 |
| SSB | D7 | -1.9388 | - | - | D188 | -1.2502 | DUSP1* | NA | - | D3 | -1.5657 |
| PPIG | D8 | -1.8348 | - | - | D190 | -1.2466 | MMP9* | NA | - | D4 | -1.3939 |
| AKAP9 | D9 | -1.5708 | - | - | D35 | -1.6584 | | | | | |
| RAD50 | D10 | -1.4676 | - | - | D71 | -1.5008 | | | | | |
| CIR1 | D11 | -1.4044 | - | - | D97 | -1.4272 | | | | | |
| DEK | D12 | -1.3508 | - | - | D67 | -1.5134 | | | | | |
| EIF5B | D13 | -1.2612 | - | - | D285 | -1.0931 | | | | | |
| ENSECAG00000007621 | D14 | -1.1675 | - | - | D47 | -1.5644 | | | | | |
| TRAT1* | D15 | -1.1375 | - | - | D163 | -1.2897 | | | | | |
| CCAR1 | D16 | -1.1033 | - | - | D187 | -1.2502 | | | | | |
| ROCK1 | D17 | -1.0914 | - | - | D240 | -1.1531 | | | | | |
| ENSECAG00000020878 | D18 | -1.0788 | - | - | - | - | | | | | |
| KTN1 | D19 | -1.0587 | - | - | D41 | -1.595 | | | | | |
| SEC62 | D20 | -1.0497 | - | - | D26 | -1.7396 | | | | | |
| TAX1BP1* | D21 | -1.0428 | - | - | D279 | -1.1015 | | | | | |
| ITGA4 | D22 | -1.0419 | - | - | - | - | | | | | |
| FN1 | - | - | D1 | -4.6842 | D1 | -4.2612 | | | | | |
| SEPP1 | - | - | D2 | -2.4215 | D7 | -2.136 | | | | | |
| ENSECAG00000007258 | - | - | D3 | -1.9357 | D33 | -1.6645 | | | | | |
| ALDH3A1 | - | - | D4 | -1.8954 | - | - | | | | | |
| GAS2L1 | - | - | D5 | -1.8869 | - | - | | | | | |
| DDIT4 | - | - | D6 | -1.6516 | - | - | | | | | |
| MMP9* | - | - | D7 | -1.4784 | D75 | -1.4914 | | | | | |
| ENSECAG00000008721 | - | - | D8 | -1.3927 | - | - | | | | | |
| ENSECAG00000009556 | - | - | D9 | -1.38 | D299 | -1.0721 | | | | | |
| VAT1 | - | - | D10 | -1.3546 | D212 | -1.2103 | | | | | |
| IRF2BP1* | - | - | D11 | -1.2827 | - | - | | | | | |
| FCGRT | - | - | D12 | -1.1567 | - | - | | | | | |
| ZNF683 | - | - | D13 | -1.137 | - | - | | | | | |
| CHST2 | - | - | D14 | -1.127 | D50 | -1.5565 | | | | | |
| LRRC4B | - | - | D15 | -1.0873 | - | - | | | | | |
| GSN | - | - | D16 | -1.0166 | - | - | | | | | |
| ZFP36L1 | - | - | D17 | -1.0132 | D116 | -1.3927 | | | | | |
| MED25 | - | - | D18 | -1.0061 | - | - | | | | | |
| Novel02103 | - | - | D19 | -1.0036 | - | - | | | | | |
| MS4A2 | - | - | - | - | D2 | -2.6698 | | | | | |
| LRRCC1 | - | - | - | - | D3 | -2.3101 | | | | | |
| ALDH1A1 | - | - | - | - | D4 | -2.2793 | | | | | |
| MMP1 | - | - | - | - | D5 | -2.2367 | | | | | |
| KIAA1551 | - | - | - | - | D6 | -2.1409 | | | | | |
| CCNG1 | - | - | - | - | D8 | -2.0402 | | | | | |
| Novel01276 | - | - | - | - | D9 | -1.9883 | | | | | |
| SIRT1* | - | - | - | - | D10 | -1.9774 | | | | | |

[a]Ranks of downregulated (D) genes in each comparison, [b]$Log_2$Fold change, *Involved in innate immunity according to InnateDB.

**Table 4.10.** Dataset 2 - Top downregulated differentially expressed genes on days 1, 2 and/or 4 as compared to day 0 for the horse infected with rAHSV5 (designated NS4) and for the horses infected with rAHSV5minNS4 (designated minNS4).

| Gene | NS4_D1 | | NS4_D2 | | NS4_D4 | | Gene | minNS4_D1 | | minNS4_D2 | |
|---|---|---|---|---|---|---|---|---|---|---|---|
| | Rank[a] | $log_2FC$[b] | Rank[a] | $log_2FC$[b] | Rank[a] | $log_2FC$[b] | | Rank[a] | $log_2FC$[b] | Rank[a] | $log_2FC$[b] |
| ANKRD12 | D1 | -2.98087 | - | - | - | - | GPR84 | D1 | -3.63744 | - | - |
| KIF20B | D2 | -2.82913 | - | - | - | - | FGFRL1 | D2 | -3.21611 | - | - |
| CCDC88A* | D3 | -2.48761 | - | - | - | - | Novel00916 | D3 | -3.21413 | - | - |
| JCHAIN | D4 | -2.20732 | - | - | - | - | U3 | D4 | -2.91903 | - | - |
| SSB | D5 | -2.08218 | - | - | - | - | SCARNA2 | D5 | -2.57241 | - | - |
| FGL2 | D6 | -1.91539 | - | - | - | - | HIST2H2AA3 | D6 | -2.52548 | - | - |
| PPIG | D7 | -1.90072 | - | - | - | - | FN1 | D7 | -2.44518 | - | - |
| EEA1 | D8 | -1.79453 | - | - | - | - | RNase_MRP | D8 | -2.26601 | - | - |
| AKAP9 | D9 | -1.61592 | - | - | - | - | NPAS1 | D9 | -2.13005 | - | - |
| DNAJC2 | D10 | -1.59258 | - | - | - | - | ENSECAG00000016810 | D10 | -2.01847 | - | - |
| DEK | D11 | -1.35471 | - | - | - | - | CXCL8 | D11 | -1.96896 | D1 | -3.55308 |
| FN1 | - | - | D1 | -4.67968 | - | - | MEFV* | D12 | -1.69336 | - | - |
| SEPP1 | - | - | D2 | -2.49073 | - | - | 7SK | D13 | -1.64559 | - | - |
| GAS2L1 | - | - | D3 | -1.90977 | - | - | GFI1B | D14 | -1.60256 | - | - |
| Novel00408 | - | - | - | - | - | Undef | HOMER3 | D15 | -1.5952 | - | - |
| | | | | | | | UBXN11 | D16 | -1.56032 | - | - |
| | | | | | | | VAT1 | D17 | -1.55506 | - | - |
| | | | | | | | MMP9* | D18 | -1.5223 | D11 | -1.39906 |
| | | | | | | | CCNE1 | D19 | -1.49379 | - | - |
| | | | | | | | CRISPLD2 | D20 | -1.4499 | - | - |
| | | | | | | | ENSECAG00000000051 | D21 | -1.42804 | D5 | -1.95542 |
| | | | | | | | SMOX | D22 | -1.4099 | - | - |
| | | | | | | | ENSECAG00000024563 | D23 | -1.40285 | - | - |
| | | | | | | | Novel01719 | D24 | -1.40115 | - | - |
| | | | | | | | IL1B* | D25 | -1.39469 | D4 | -2.15462 |
| | | | | | | | Novel01087 | D26 | -1.39356 | - | - |
| | | | | | | | EPHB3 | D27 | -1.39305 | - | - |
| | | | | | | | CXCR4* | D28 | -1.39241 | - | - |
| | | | | | | | IGSF3 | D29 | -1.38492 | - | - |
| | | | | | | | CALY | D30 | -1.38411 | - | - |
| | | | | | | | GALR2 | D31 | -1.3804 | - | - |
| | | | | | | | Novel01940 | D32 | -1.38022 | - | - |
| | | | | | | | Novel00900 | D33 | -1.34704 | - | - |
| | | | | | | | Novel01995 | D34 | -1.32488 | - | - |
| | | | | | | | PER1 | D35 | -1.32429 | - | - |
| | | | | | | | ENO2 | D36 | -1.31734 | - | - |
| | | | | | | | FCER2 | D37 | -1.30249 | - | - |
| | | | | | | | SEPT5 | D38 | -1.29697 | - | - |
| | | | | | | | ENSECAG00000008721 | D39 | -1.2725 | - | - |
| | | | | | | | OSGIN1 | D40 | -1.27176 | - | - |
| | | | | | | | ENSECAG00000020640 | D41 | -1.2704 | - | - |
| | | | | | | | PRF1 | D42 | -1.26376 | - | - |
| | | | | | | | ADGRG3 | D43 | -1.24116 | - | - |
| | | | | | | | MFGE8* | D44 | -1.23708 | - | - |
| | | | | | | | GZMH | D45 | -1.23645 | - | - |
| | | | | | | | RNF122 | D46 | -1.22866 | - | - |
| | | | | | | | ALDH3A1 | D47 | -1.22475 | - | - |
| | | | | | | | ADGRG1 | D48 | -1.21981 | - | - |
| | | | | | | | AVPI1 | D49 | -1.18634 | - | - |

[a]Ranks of downregulated (D) genes in each comparison, [b]$Log_2$Fold change, *Involved in innate immunity according to InnateDB, Undef = Undefined.

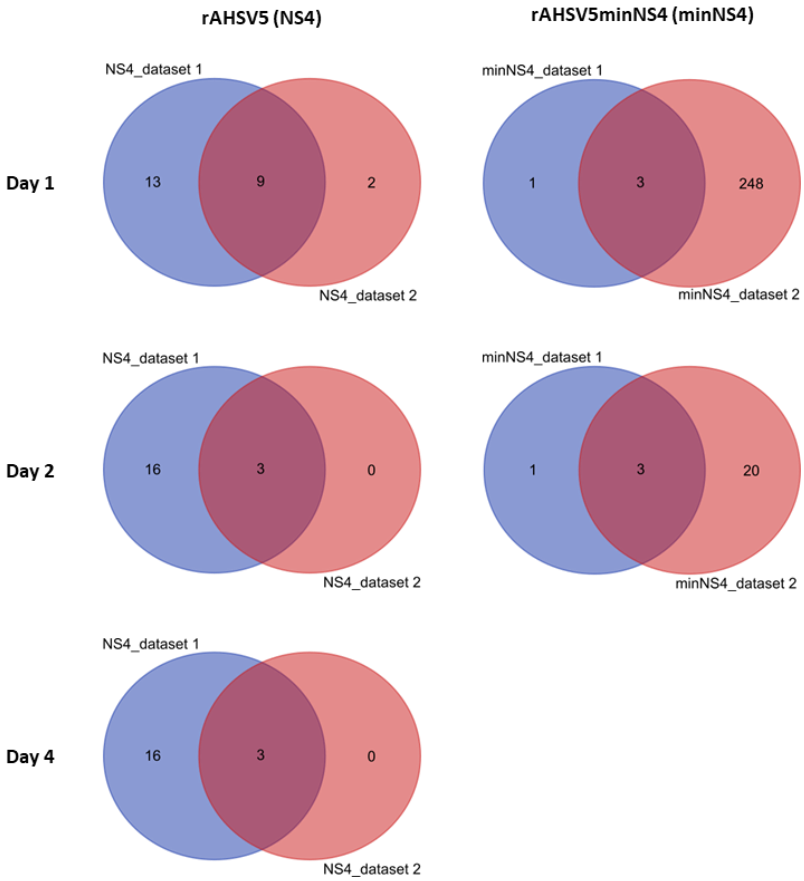


**Figure 4.7.** Downregulated genes that are unique or shared between dataset 1 and dataset 2 are shown in Venn diagrams comparing the upregulated genes on days 1, 2 and 4 in the presence (NS4) or absence (minNS4) of NS4.

Thus, the DEGs in dataset 1 showed upregulation of genes involved in innate immunity of day 1 in the absence of NS4 (horses inoculated with rAHSV5minNS4). Similar upregulation was only observed on day 2 in the presence of NS4 (horses inoculated with rAHSV5). Dataset 2 largely confirmed these results.

### 4.3.5. Gene Ontology (GO) enrichment analyses

Gene ontology (GO) term enrichment analyses were then performed to classify the DEGs in terms of their biological function. The terms belong to three established categories: biological process, molecular function or cellular component (Ashburner *et al.*, 2000). The GO terms were sorted based on the corrected p-value, with values <0.05 being significantly enriched. The top 30 most significantly enriched GO terms are shown in Figures 4.8 (dataset 1) and 4.9 (dataset 2) and are grouped according to the three categories mentioned above. The full lists can be found in Appendices D and E.

In the control horse (rAHSV5), 1033 GO terms were enriched across the three categories: biological processes (745 terms), molecular function (150 terms) and cellular component (138 terms) on day 1, dataset 1 (Appendix D). The most enriched GO terms on this day were 2'-5'-oligoadenylate synthetase activity, leukocyte tethering or rolling, RNA binding and regulation of establishment of cell polarity (Appendix D).

Although several terms were related to the host defense response and the presence of a virus none of the terms were significantly enriched on this day (Figure 4.8, Appendix D).

On day 2, dataset 1, 3026 GO terms across the three categories, biological processes (2377 terms), molecular function (404 terms) and cellular component (245 terms) were enriched in the control horse (rAHSV5, Appendix D). Ninety-nine (99) GO terms were significantly enriched. The most significantly enriched terms were response to virus, defense response to virus, immune system process and defense response (Appendix D). More GO terms alluding to the presence of a virus were enriched in DEGs on day 2 than on day 1. A notable difference between day 1 and day 2 was that terms referring to immunity and innate immunity were among the top enriched terms on day 2 (Figure 4.8). These included immune system process, immune response, innate immune response, regulation of immune system process, response to cytokine, regulation of innate immune response, response to interferon-alpha. There were also 36 GO terms that contained reference to “interferon” on this day (Appendix D).

By day 4, dataset 1, 6916 GO terms were enriched, 433 of which significantly so (Appendix D). Again, the majority of GO terms fell under the biological processes category (5263), with 1050 in the molecular function category and 603 in the cellular component category. The most significantly enriched terms on day 4 were immune system process, defense response, response to biotic stimulus and negative regulation of multi-organism process (Figure 4.8, Appendix D). In the biological processes category 18 of the terms that were enriched on day 2 were still enriched on day 4 and included terms alluding to innate immunity and the presence of a virus. On this day 7 terms containing “innate”, 38 containing “interferon”, 72 containing “immunity” and 14 containing “virus” were enriched (Appendix D).

In the horses inoculated with rAHSV5minNS4, 1176 GO terms were enriched on day 1, dataset 1 (Figure 4.8, Appendix D). Of these 927 fell under the biological process category, 155 under molecular function and 94 under cellular component. In contrast to day 1 in the control horse (rAHSV5), 30 of the terms were significantly enriched (Figure 4.8). Twenty-two terms containing “interferon” and 5 containing “innate” were enriched (minNS4_D1, Appendix D). Furthermore, immune system process and immune response were in the top 30 most enriched GO terms on this day.

On day 2, dataset 1, 566 GO terms in total were enriched in the horses inoculated with rAHSV5minNS4, almost half of those enriched on day 1 (Appendix D). Across the three categories 446 terms belonged to biological processes, 76 belonged to molecular function and 44 belonged to cellular component. This was also much less than the 3026 terms enriched on day 2 in the control horse. Only one term, 2'-5'-oligoadenylate synthetase activity, was significantly enriched (Figure 4.8). In contrast to day 1, no terms referring to immunity were among the 30 most enriched terms based on significance (Figure 4.8) and only

three containing “immune” were enriched overall. Also, the number of terms containing “interferon” dropped to 1 and no terms containing “innate” were enriched on day 2.

**Figure 4.8.** GO enrichment analysis of the differentially expressed genes in rAHSV5 (NS4) or rAHSV5minNS4 (minNS4) infected horses on days 1, 2 and/or 4 in dataset 1. GO terms were sorted according to according to statistical significance (* = corrected pval<0.05) and the 30 most significantly enriched GO terms are shown.

In dataset 2, only 4 GO terms were enriched on day 1 in the control horse (rAHSV5), all of which belonged to the cellular component category (NS4_D1, Figure 4.9). This is considerably less than the 1033 GO terms observed for the same day in dataset 1 (Appendix D).

By day 2, 241 GO terms were enriched across the three categories: biological processes (203 terms), molecular function (23 terms) and cellular component (15 terms) (Appendix E, Dataset 2). In contrast to dataset 1, no GO terms were significantly enriched on this day. Among the most enriched terms were a few that alluded to the host immune response (*e.g.,* cytokine-mediated signalling pathway, chemokine-mediated signalling pathway, immune system process and inflammatory response). Only one term alluding to the presence of a virus was among the 30 most enriched GO terms, as opposed to 44 on day 2 in dataset 1 (Appendices D and E). Only 2 terms containing the word “interferon”, 1 containing the word “innate” and 6 terms containing “immune” were enriched on day 2 in this dataset. The lower numbers observed in this dataset may be due to fewer GO terms being enriched overall in dataset 2 as a result of fewer DEGs (Figure 4.5).

Only 214 terms were enriched in the control horse (rAHSV5) on day 4 in dataset 2, whereas 6916 terms were enriched by 750 DEGs on day 4 in dataset 1 (Appendices D and E). No GO terms were significantly enriched, and the top 53 GO terms had the same corrected p-value (Appendix E). Of the 214 terms, 179 fell under the biological process category, 20 under molecular function and the remaining 15 under cellular component. The term “viral process” was the only term referring to the presence of a virus (Figure 4.9, Appendix E). On this day fewer terms referring to innate immunity were enriched in dataset 2. Only 1 term containing “innate’, 2 containing “interferon” and 4 containing “immune” were enriched. Several other terms alluding to immunity and the “inflammatory response” were, however, enriched on this day in dataset 2 and included the words “cytokine” and “chemokine”.

In the horses inoculated with rAHSV5minNS4, 1725 GO terms across the three categories: biological processes (1198), molecular function (284) and cellular component (243) were enriched on day 1 (Appendix E, dataset 2). Of these, 192 were significantly enriched. In contrast to dataset 1, the top enriched terms belonged to the cellular components category no terms referring to immunity or to the presence of a virus were in the top 30 most enriched terms (Figure 4.9, Appendix E). In this dataset only two terms containing “interferon” and 5 containing “innate” were enriched on day 1. Furthermore, only one term, viral process” alluding to the presence of a virus was enriched on this day in dataset 2, compared to 10 in dataset 1.

Although not in the top 30 most enriched GO terms, 32 terms containing “immune” were enriched on day 1 in dataset 2, 11 of which significantly so (Appendix E). In addition to this, 3 terms containing “immunity” and 4 containing “adaptive” were enriched on this day in dataset 2.

The differentially expressed genes on day 2, dataset 2, in the horses inoculated with rAHSV5minNS4 were enriched in 417 GO terms across the three categories, 250 of which were significantly enriched. Thus, almost double the amount of GO terms were enriched in these horses than in the control horse on day 2, dataset 2. As in dataset 1, most of the terms (360) fell under the biological process category. Of the remaining terms 42 fell under the molecular function category and 15 fell under cellular component. In contrast to day 1, only one term containing “innate” was enriched on day 2. Also, the number of terms containing “immune” dropped considerably from 32 to 10. Two terms containing “interferon” and two containing “immunity” were enriched. This is similar to what was observed in dataset 1 on the same day.


**Figure 4.9.** GO enrichment analysis of the differentially expressed genes in rAHSV5 (NS4) or rAHSV5minNS4 (minNS4) infected horses on days 1, 2 and/or 4 in dataset 2. GO terms were sorted according to according to statistical significance (* = corrected pval<0.05) and the 30 most significantly enriched GO terms are shown.

Overall, although fewer GO terms were enriched in dataset 2, the results from both datasets suggested that an immune response had been initiated by day 2 in the control horse inoculated with rAHSV5 but had already been initiated on day 1 in the horses inoculated with rAHSV5minNS4.

### 4.3.6. KEGG enrichment analyses

To further define the function of the DE genes, they were mapped to canonical pathways in KEGG. As described in materials and methods, pathways were filtered to include membrane transport, signal transduction, signalling molecules and interaction, and immune system pathways, of which there were 3, 33, 5 and 21 pathways respectively, resulting in a total of 62 pathways that were investigated in more detail. These results are summarized in Figure 4.10 and 4.11, and the full lists of enriched KEGG pathways can be found in Appendices E and F.

In the control horse immunized with rAHSV5, 12 of the 62 KEGG pathways mentioned above were enriched on day 1 in dataset 1 (Figure 4.10, blue bars, NS4_D1). All 12 pathways were enriched by the downregulated genes ROCK1 and ITGA4, except for the notch signalling pathway that was downregulated by CIR1 (Appendix E). Five of the 12 pathways (platelet activation, leukocyte transendothelial migration, intestinal immune network for IgA production, hematopoietic cell lineage and the chemokine signalling pathway) were immune system pathways (Figure 4.10). For the horses inoculated with rAHSV5minNS4, 14 of the 62 KEGG pathways were enriched on day 1 (blue bars, minNS4_D1, dataset 1), of which 12 were enriched by upregulated genes. Six of the enriched pathways were immune system pathways (the Toll-like and RIG-I-like receptor signalling pathways, Fc gamma R-mediated phagocytosis, cytosolic DNA-sensing pathway, complement and coagulation cascades and the chemokine signalling pathway). The Toll-like receptor and RIG-I-like receptor signalling pathways are hallmarks of innate immunity. The VEGF, NF-kappa B, JAK-STAT and calcium signalling pathways involved in signal transduction were also enriched on day 1 in these horses (Figure 4.10, blue bars, minNS4_D1). Such pathways are important in the regulation of several processes, many of which are involved in immunity. Among the DE genes enriching the pathways on day 1 (rAHSV5minNS4) were STAT1, IRF7, DDX58, SIGLEC1, C1R, C2, and SPHK1 (Appendix E). These pathways were not enriched on day 1 in the control horse.

In the control horse the number of enriched pathways increased from day 1 to day 2 (dataset 1, Figure 4.10, green bars, NS4_D2). Of these pathways, 12 were immune system pathways including the chemokine signalling pathway and complement and coagulation cascades. The Toll-like receptor and RIG-I-like receptor signalling pathways were activated on day 2 by upregulated genes only, and 24 h (1 day) later than in the horses infected with rAHSV5minNS4. Among the DE genes enriching these two pathways were CXCL10, IFIH1, ISG15, IRF7, DDX58, DHX58, TLR2, STAT1 and CD86. The RIG-I-like receptor signalling pathway and the cytosolic DNA sensing pathway were significantly enriched. More signal transduction pathways were

enriched on day 2, and included the JAK-STAT, MAPK, NF-kappa B signalling pathways. All were enriched by upregulated genes except for NF-kappa B which was enriched by both up-and down-regulated genes. B-cell receptor signalling, and natural killer cell mediated cytotoxicity that were enriched on day 2 are involved in adaptive immunity. Overall, more immune system processes were enriched on day 2 for rAHSV5, indicating a 24-hour delay in the onset of a strong immune response in this horse. In the horses inoculated with rAHSV5minNS4, only a few pathways were enriched on day 2 (Figure 4.10, green bars, minNS4_D2). None of the pathways identified on day 1 were still enriched on day 2, save for cell adhesion molecules (CAMs) due to SIGLEC1, which was still upregulated on day 2 (Appendix E). Instead, pathways such as the MAPK and TNF signalling pathways, leukocyte transendothelial migration were enriched due to the downregulation of MMP1, MMP9 or DUSP1.

The results on day 4, dataset 1, showed an increase in the overall number of enriched pathways for rAHSV5, with the numbers of immune system pathways and signal transduction pathways required by them increasing from day 2 to day 4 (Figure 4.10, red bars, NS4_D4). All processes that were enriched on day 2 were still enriched on day 4, to a greater extent. Immune system pathways enriched on day 4 included both innate and adaptive immune system processes. All pathways enriched on day 4 were enriched by upregulated genes.

The above indicated that the presence of NS4 (rAHSV5) results in many immune response pathways to be transcriptionally activated 24 h later than when the protein is absent (rAHSV5minNS4). Furthermore, this appears to be due to a delay in the innate immune response specifically.


**Figure 4.10.** KEGG pathways enriched in dataset 1 by the differentially expressed genes on days 1, 2 and 4 in horses that were infected with rAHSV5 or rAHSV5minNS4. Pathways involved in membrane transport are listed in orange, signaling molecules and interaction in purple, signal transduction in black and the immune system in gold. * = corrected pval<0.05.

In dataset 2, none of the 62 pathways investigated in more detail were enriched on day 1 in the control horse (NS4_D1, Figure 4.11, Appendix F). This contrasts with the 12 that were observed in dataset 1 on the same day (NS4_D1, Figure 4.10). For the horses inoculated with rAHSV5minNS4, 45 of the 62 KEGG pathways were enriched on day 1 in dataset 2, 15 of which significantly so (Figure 4.11, blue bars, minNS4_D1). This is considerably more than the 14 enriched in dataset 1 on day 1. All 45 pathways, which include 16 immune system pathways such as the Toll-like and RIG-I-like receptor signalling pathways were not enriched on day 1 in the control horse. As seen in Appendix F, most of the pathways were enriched by a combination of up- and down-regulated genes, with the majority of genes being upregulated. The high number of enriched pathways may be due to the high number of DEGs on this day in dataset 2 (2272, Figure 4.5).

On day 2, dataset 2, 13 of the 62 pathways were enriched in the control horse, half of the number of those that were enriched on the same day in dataset 1 (Figure 4.11, green bars, NS4_D2). All of the pathways enriched on day 2 in the control horse in dataset 2 were enriched by upregulated genes indicating activation of the pathways (Appendix F). Of the pathways enriched on this day, 6 were immune system pathways (the Toll-like receptor, RIG-I-like receptor, chemokine signalling pathways, the cytosolic DNA sensing pathway, natural killer cell mediated cytotoxicity and complement and coagulation cascades, Figure 4.11, green bars, NS4_D2), and were enriched 24 h later than in the horses inoculated with rAHSV5minNS4 (Figure 4.11, blue bars, minNS4_D1). Five signal transduction pathways were enriched in this horse on day 2 and included the JAK-STAT, TNF and NF-kappa B signalling pathways, in comparison to the 11 signal transduction pathways enriched on day 2 in dataset 1 (Figures 4.10 and 4.11). All pathways enriched on day 2 were also enriched on day 2 in dataset 1, and the RIG-I-like receptor signalling, and cytosolic DNA sensing pathways were significantly enriched in both datasets on day 2. Fewer KEGG pathways were enriched on day 2 (19) than on day 1 (45) in the horses inoculated with rAHSV5minNS4 (Figure 4.11, green bars, minNS4_D2). In contrast to day 2 in the control horse, these pathways were enriched by downregulated genes only, indicating pathway suppression (Appendix F). Thus, while several immune system processes were still enriched, they were no longer activated. Essentially, this confirms what was seen in dataset 1: a tapering off of the immune response.

The results on day 4, dataset 2, showed a decrease in the number of enriched KEGG pathways for rAHAVS-5 from day 2 (13) to day 4 (7) (Figure 4.11, red bars, NS4_D4). This contrasts with dataset 1, where an increase was observed from day 2 to day 4. As with day 2, all KEGG pathways were enriched by upregulated genes on day 4 (Appendix F). Four immune system processes were still enriched on day 4, namely the chemokine, RIG-I-like receptor signalling (padj<0.05) and cytosolic DNA sensing pathways as well as complement and coagulation cascades. This is less than the 16 immune system pathways enriched on day 4 in dataset 1. The only signal transduction pathway that was enriched on this day was the NF-kappa B signalling pathway.


**Figure 4.11.** KEGG pathways enriched in dataset 2 by the differentially expressed genes on days 1, 2 and 4 in horses that were infected with rAHSV5 or rAHSV5minNS4. Pathways involved in membrane transport are listed in orange, signaling molecules and interaction in purple, signal transduction in black and the immune system in gold. * = corrected pval<0.05.

Overall, fewer KEGG pathways were enriched in the control horse in dataset 2 when compared to dataset 1, thus while this dataset shows that an innate immune response is initiated by day 2, and continues somewhat to day 4, it does not show the progression from day 1 to day 4 that was seen in dataset 1. Both datasets give

a similar result with regard to the horses inoculated with rAHSV5minNS4 in that a strong immune response, particularly innate immunity, was initiated within 24 h of infection and that this tapered somewhat from day 1 to day 2.

### 4.3.7. AHSV NS4 affects the translocation of STAT1 into the nucleus

The IFN response is a critical element of innate immunity and results in the expression of ISGs that ultimately lead to an antiviral state. The JAK-STAT signalling pathway is an important mediator of this response. As such, this pathway is often targeted by viruses in an attempt to counteract or evade the IFN-response (Samuel, 2001). As an example, Chikungunya virus (CHIKV) non-structural protein 2 (nsP2) blocks the nuclear translocation of STAT1 thereby acting as an inhibitor of IFN-induced JAK-STAT signalling (Fros *et al.*, 2010; Fros *et al.*, 2013). It is also known that BTV inhibits JAK-STAT signalling pathway by blocking the phosphorylation and nuclear translocation of STAT1 early in infection or by downregulating the expression of JAK1 and TYK2 later in the infection cycle (Doceul *et al.*, 2014). Also, BTV NS4 acts as an IFN antagonist and downregulates the transcription of ISGs (Ratinier *et al.*, 2016). Here, the JAK-STAT signalling pathway itself was enriched on day 1 in the case of the horses inoculated with rAHSV5minNS4, but only on days 2 and 4 (not day 1) in the horse inoculated with rAHSV5. The JAK-STAT signalling pathway was also activated on day 1 in horses inoculated with rAHSV5minNS4 in dataset 2, and on day 2 it was enriched by the downregulated CSF3R gene. Based on the above, the aim of this section was to investigate whether AHSV NS4 affects the innate immune response on a protein level by interfering with the JAK-STAT signalling pathway specifically.

The synthetic viruses rAHSV5 and rAHSV5ΔNS4 (which does not have NS4 expression) described in Chapter 3 were used to investigate this. In essence, Vero cells were to be infected, treated with IFN and processed for immunofluorescence and CLSM. Under normal circumstances, treatment with IFN should result in phosphorylation, dimerisation and the subsequent nuclear translocation of STAT1 and/or STAT2 (Fleming, 2016). Vero cells have a ~9 Mb deletion in the genome which caused the loss of the IFN-I gene cluster, therefore IFN alpha and beta cannot be produced (Osada *et al.*, 2014). The cells do however have an intact IFN-signalling pathway and can respond to interferon treatment (Desmyter *et al.*, 1968; Osada *et al.*, 2014) . Any differences between the intracellular localisation of STAT1, STAT2 or pSTAT1 in rAHSV5 versus rAHSV5ΔNS4 infected Vero cells treated with IFN would be due to NS4 or the lack thereof.

Several antibodies against STAT1, STAT2 and pSTAT1 were obtained (Table 4.3), and tested to see if they were suitable for detection of these target proteins in Vero cells. Whole cell lysates were subjected to Western blot analyses with the various primary antibodies (Figure 4.12). The only anti-STAT1 antibody that gave a positive signal was the Abcam antibody directed against the N-terminal of STAT1. The anti-pSTAT1 labelling did not yield any signal on the Western blot, and STAT2 was only faintly detected with the Abcam antibody against the C-terminal of STAT2. The two antibodies that gave a positive signal on the Western blots,

plus the LSBio anti-pSTAT1 antibody, were subsequently also tested in indirect immunofluorescence and confocal microscopy. Figure 4.13 shows uninfected, untreated Vero cells that were labelled for STAT1, pSTAT1 or STAT2. As expected, STAT1 staining was observed in the cytoplasm but it was also observed in the nucleus (Figure 4.13A). In the case of cells labelled with anti-pSTAT1, signal was observed in the nucleus (Figure 4.13B). In uninfected, untreated Vero cells STAT1 should be cytoplasmic and pSTAT1 should not be observed, thus the nuclear staining posed a problem as any nuclear translocation of STAT1 in response to IFN-signalling would be difficult to track. Figure 4.13C shows the results obtained with using anti-STAT2. This antibody was expected to give a distribution pattern similar to that of STAT1, mainly cytoplasmic. Instead, STAT2 was only observed in the nucleus, causing this antibody to be excluded from the rest of the work.

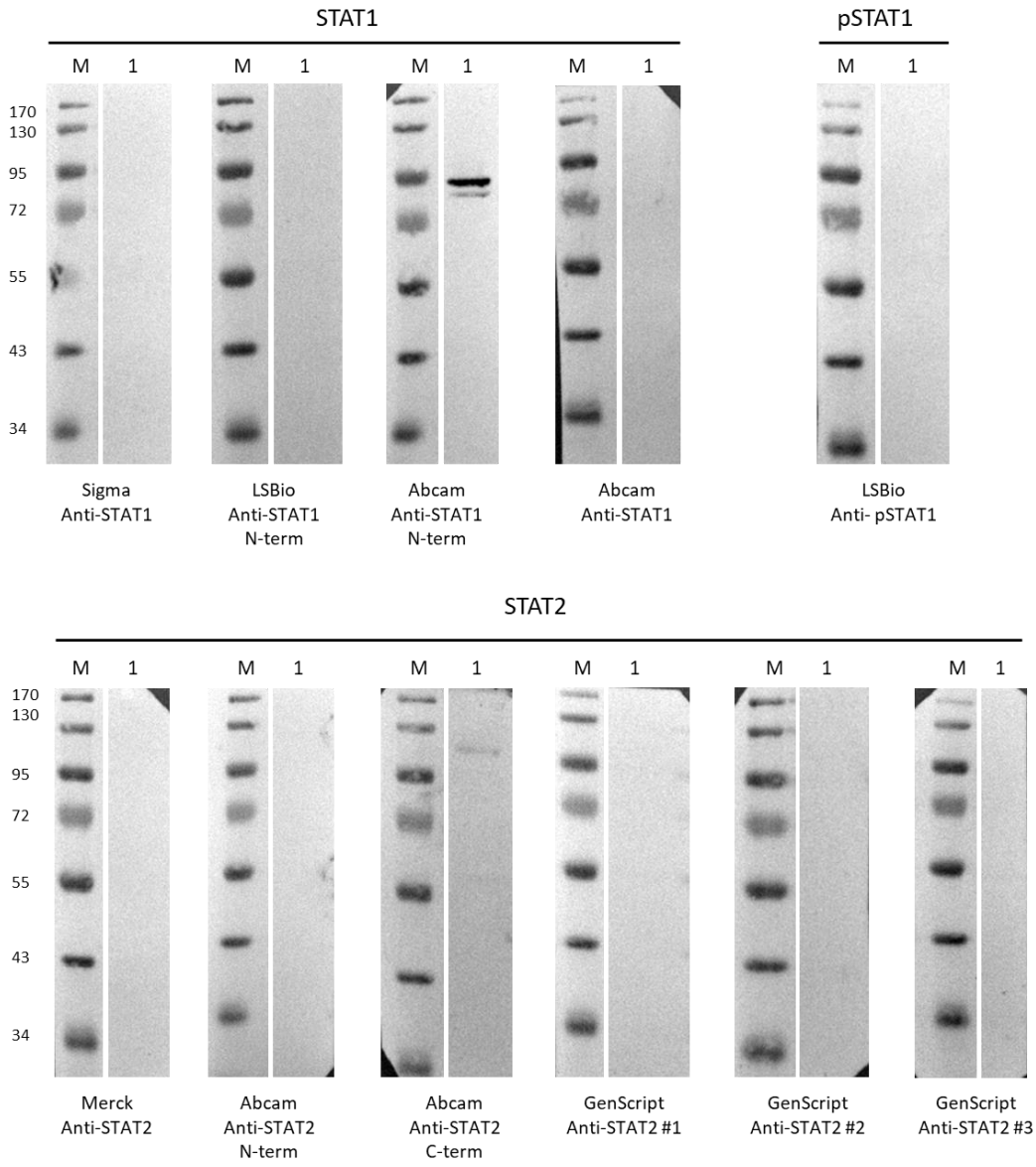


**Figure 4.12. Preliminary tests of primary antibodies against STAT1, STAT2 and pSTAT1 in immunoblot.** Whole cell lysates of Vero cells were subjected to 12% SDS-PAGE and Western blot analysis with the indicated primary antibody and recombinant protein G-HRP. M = PageRuler™ Prestained Protein Ladder, sizes of molecular weight markers are indicated on the left (kDa); Lane 1, Vero cell lysate.

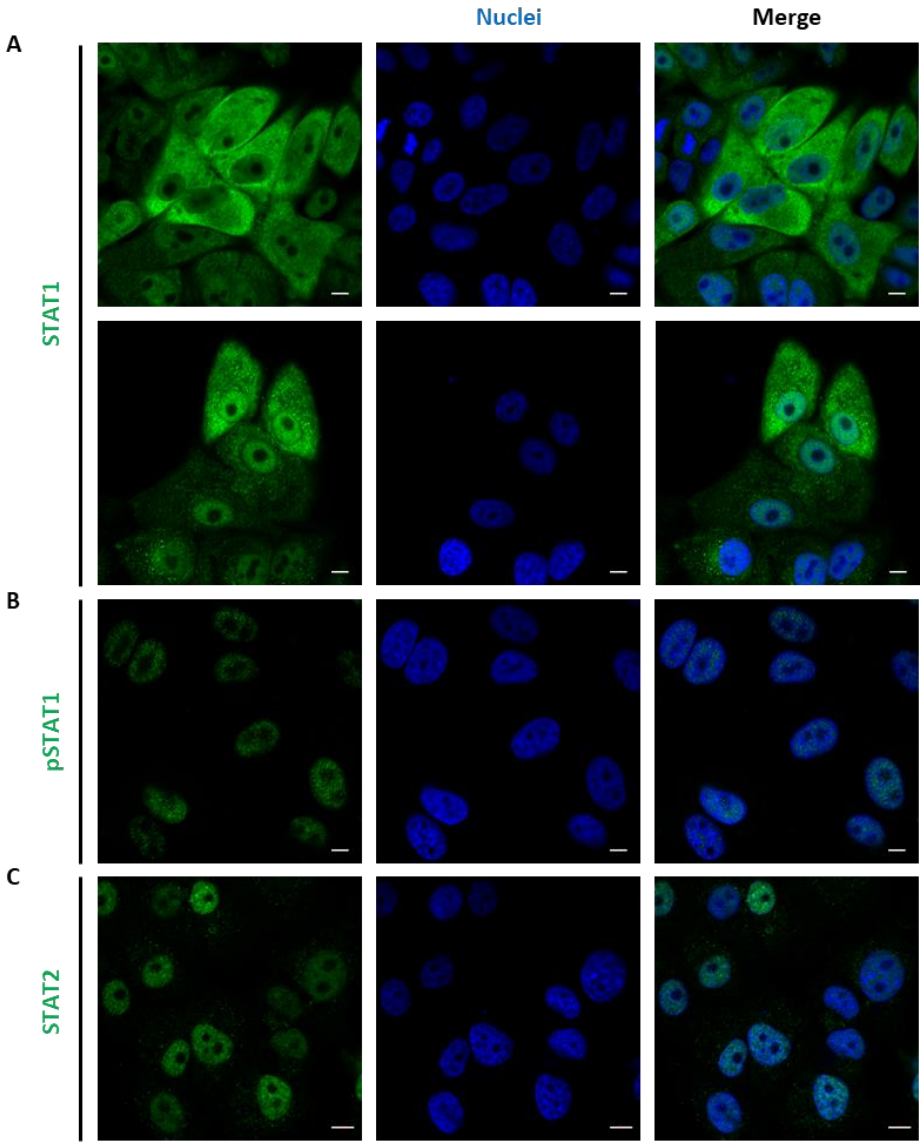


**Figure 4.13. Preliminary tests of primary antibodies against STAT1, pSTAT1 and STAT2 in confocal microscopy.** Uninfected Vero cells were fixed at 24 hours post seeding and prepared for immunofluorescence and CLSM using the Abcam anti-STAT1 N-term (A), LSBio anti-pSTAT1 (B) or Abcam anti-STAT2 C-term (C) primary antibody and the AF 488 conjugated goat anti-rabbit IgG secondary antibody. Nuclei were stained with DAPI. Scale bars = 10 µm.

Complete DMEM supplemented with serum was used for the initial experimental work. Therefore, it was possible that the small amount of IFN known to be present in the serum could have initiated JAK-STAT signalling and caused the phosphorylation and translocation of STAT1 into the nucleus. To test if serum was the cause of the nuclear STAT1 labelling, Vero cells were adapted to VP-SFM serum-free medium and the immunofluorescence and confocal microscopy repeated. As seen in Figure 4.14A, nuclear labelling of STAT1 was still observed, and in most instances cytoplasmic labelling was somewhat diminished. The pSTAT1 labelling was somewhat better, but still not at an acceptable level (Figure 4.14B). Furthermore, the cells did not grow optimally in the VP-SFM. OptiPRO™ SFM was also tested to see if this would improve the growth of the cells and allow for less nuclear signalling. Labelling for STAT1 and pSTAT1 yielded similar results to

those observed with VP-SFM (not shown). Thus, it appeared that the serum was not the cause of the nuclear signal.

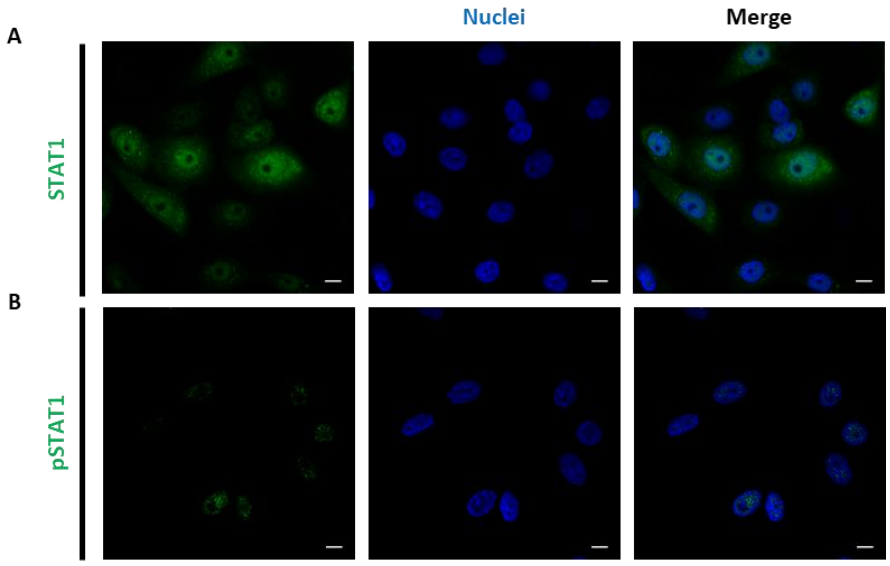


**Figure 4.14. Testing Abcam anti-STAT1 N-term and LSBio anti-pSTAT1 on Vero cells grown in VP-SFM.** Cells were adapted to VP-SFM, seeded onto coverslips, fixed at 24 hours post seeding and prepared for immunofluorescence and CLSM using Abcam anti-STAT1 N-term (A) or LSBio anti-pSTAT1 (B) primary and AF 488 conjugated goat anti-rabbit IgG secondary antibodies. Nuclei were stained with DAPI. Scale bars = 10 µm.

Different dilutions of the primary and secondary antibodies were subsequently tested to see if the nuclear signal was a technical issue resulting from labelling conditions. The results of this are shown in Figure 4.15. The 1:100 and 1:500 dilutions of anti-STAT1 showed nuclear signal (Figure 4.15A). The nuclear signal was lower in the case of the 1:1000 dilution but it was still present. Keeping the dilution of the primary antibody at 1:100 and changing the secondary antibody dilution gave better results. Much less nuclear signal was seen with a dilution of 1:1000 and even less was seen at a dilution of 1:1500. Furthermore, the cytoplasmic signal remained strong (Figure 4.15A). Figure 4.15B shows what was obtained when the same was done for the anti-pSTAT1 antibody. In this instance, the combination of primary antibody at 1:100 and secondary antibody at 1:1000 gave the least among of nuclear background overall. This showed that the nuclear signal was in large part background labelling resulting from insufficient dilution of the antibodies. The following combinations of antibody dilutions were decided on for the remainder of the experiments, 1:100 Abcam anti-STAT1 N-term + 1:1500 AF 488 conjugated goat anti-rabbit IgG and 1:100 LSBio anti-pSTAT1 + 1:1000 AF 488 conjugated goat anti-rabbit IgG.

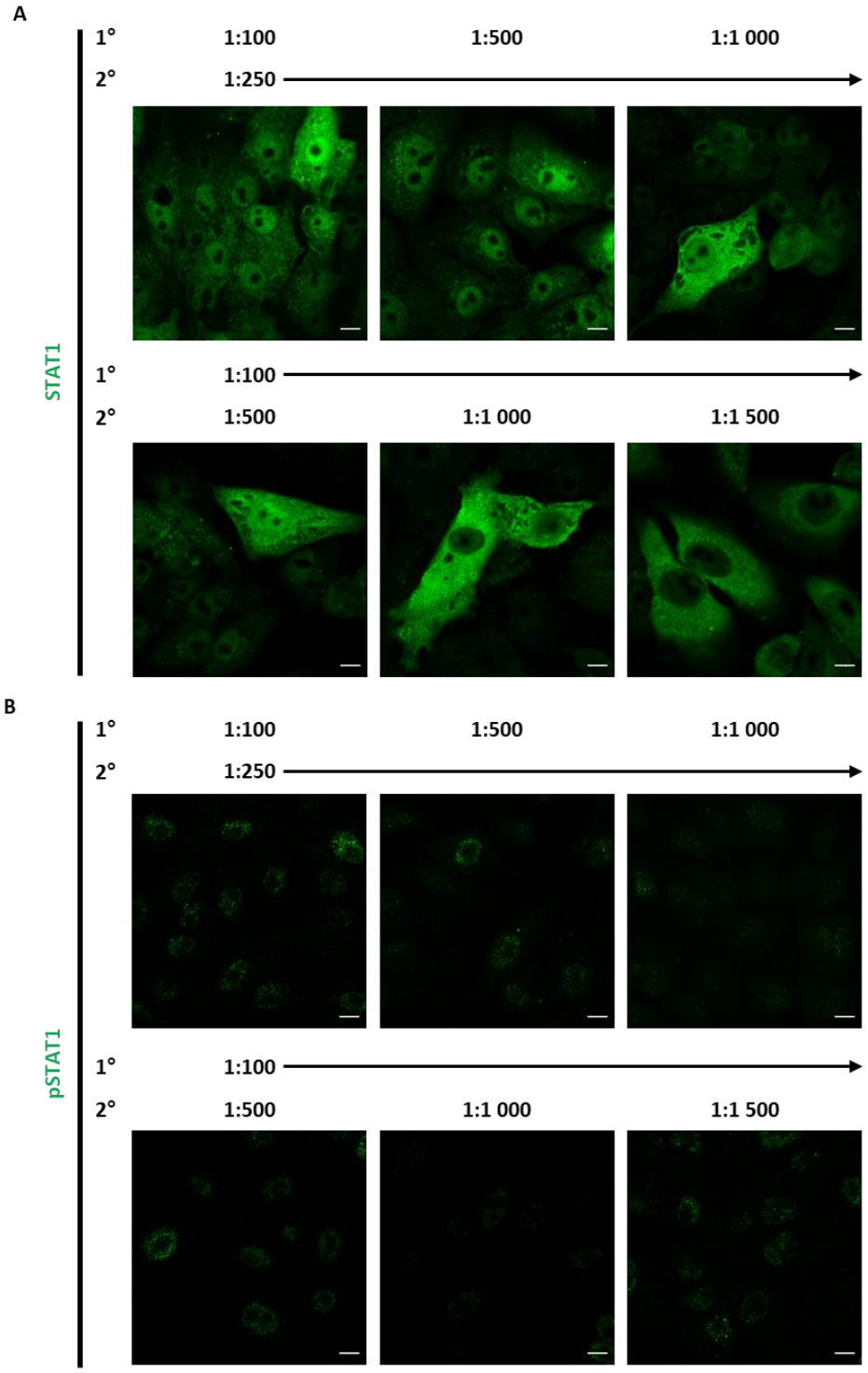


**Figure 4.15. Optimisation of primary and secondary antibody dilutions.** Uninfected Vero cells were fixed at 24 hours post seeding and prepared for immunofluorescence and CLSM with Abcam anti-STAT1 N-term (A) or LSBio anti-pSTAT1 (B) primary and AF 488 conjugated goat anti-rabbit IgG secondary antibodies. Different dilutions of the primary (1°) and secondary (2°) antibodies were used as indicated. Scale bars, 10 µm.

Treatment with IFN-alpha and beta can be used in the investigation of both STAT1 and STAT2, whereas IFN-gamma can only be used in the investigation of STAT1 (Lin and Young, 2014). Therefore, it was decided that IFN-gamma (IFN-γ) should be used in the remainder of the experiments due to the anti-STAT1 and anti-pSTAT1 antibodies that worked well in CLSM. Some optimisation was done regarding the duration of IFN-γ

treatment, and the translocation of STAT1 into the nucleus could be observed equally well with treatment lasting anywhere from 30 min to 5 h (not shown).

Once the optimisation of the various steps of the experiment was finalised, Vero cells were infected with rAHSV5 or rAHSV5ΔNS4 and left untreated or were treated with IFN-γ at 24 hpi. rAHSV5ΔNS4 was used in these experiments as no expression of NS4 was observed in cells infected with this virus in Chapter 3, in contrast to the leaky expression observed in rAHSV5minNS4-infected cells in Chapter 2. Following IFN treatment, the cells were processed for CLSM and labelled for STAT1 and AHSV NS1 (Figure 4.16). The cellular localisation of STAT1 was predominantly cytoplasmic in both uninfected and virus-infected cells. Upon treatment with IFN-γ, STAT1 translocated into the nucleus of uninfected cells as expected. In contrast, STAT1 remained cytoplasmic in the majority of rAHSV5-infected cells. Labelling of non-structural protein NS1, which is highly expressed following AHSV infection and forms tubular aggregates in the cytoplasm, allowed infected cells to be distinguished from uninfected cells in the same field. This clearly illustrated the difference in the STAT1 localisation following IFN-γ treatment in the presence versus absence of rAHSV5 replication, and allowed us to deduce that viral infection resulted in no nuclear detection of STAT1 in interferon-treated cells. However, in rAHSV5ΔNS4-infected cells, which would sustain normal viral replication just lacking NS4 expression, the interferon treatment resulted in nuclear translocation of STAT1 (Figure 4.16). This indicated that the presence of NS4 results in the cytoplasmic retention of STAT1.

Anti-STAT1 detects unphosphorylated STAT1 as well as the phosphorylated form that dimerises and enters the nucleus. Therefore, to verify these results the experiments were repeated with the antibody specific to pSTAT1 (Figure 4.17). Prior to the IFN treatment, little to no pSTAT1 could be detected in the nuclei of uninfected or virus-infected cells (Figure 4.17). This was to be expected, as the presence of IFN is required to activate the phosphorylation of STAT1. After treatment with IFN-γ a strong nuclear signal was observed for pSTAT1 in uninfected cells, as well as in rAHSV5ΔNS4-infected cells. No nuclear pSTAT1 was however observed in rAHSV5-infected cells (Figure 4.17). Taken together, these results suggest that AHSV NS4 interferes with the phosphorylation and/or translocation of STAT1 and pSTAT1 into the nucleus.

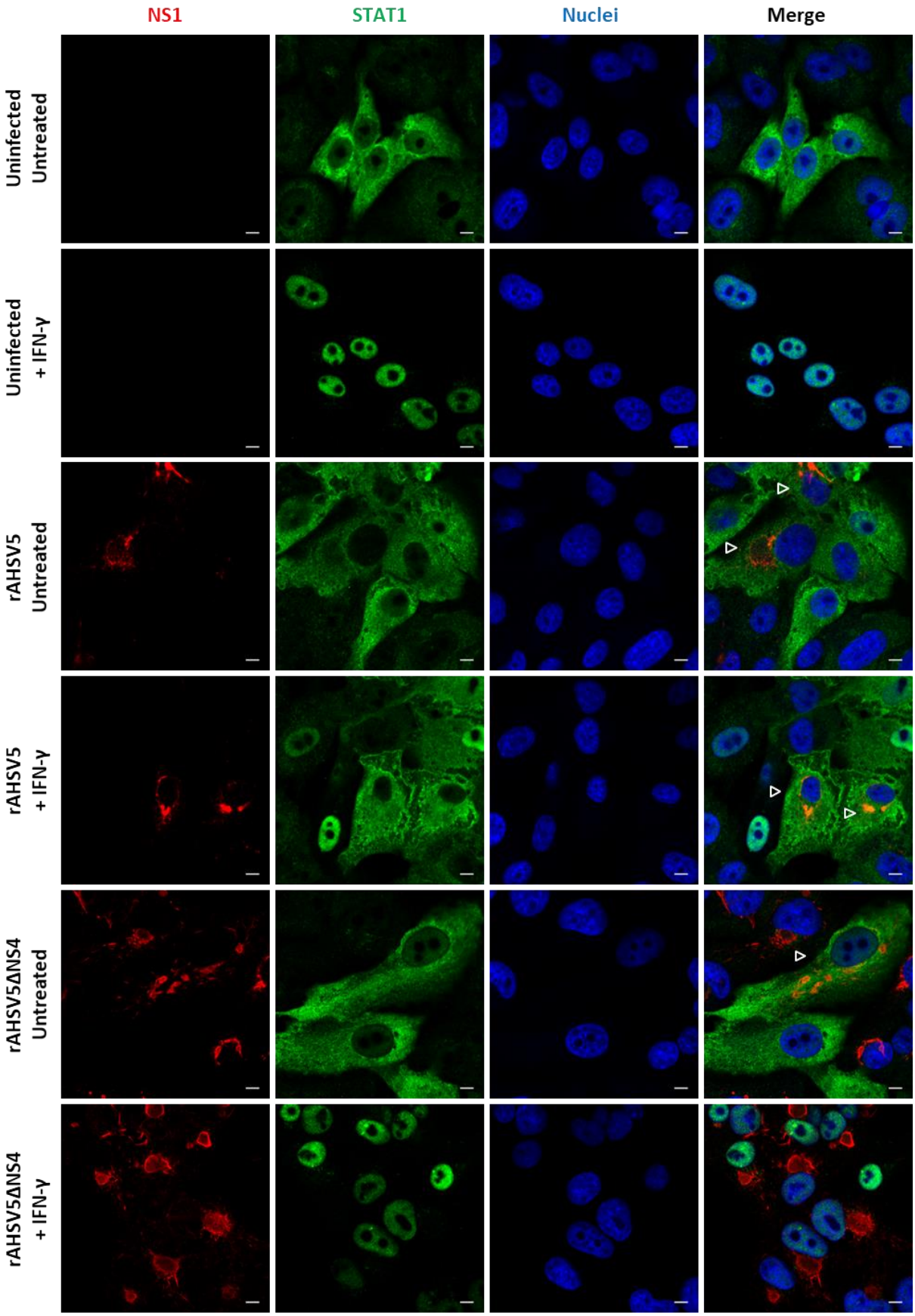


**Figure 4.16. NS4 interferes with nuclear translocation of STAT1.** Vero cells were infected with rAHSV5 or rAHSV5ΔNS4 and then treated with IFN-γ, fixed and processed for immunofluorescence and CLSM using anti-NS1 and Abcam anti-STAT1 N-term primary, and AF 594-conjugated goat anti-mouse IgG and AF 488-conjugated goat anti-rabbit IgG secondary antibodies. Nuclei were stained with DAPI. Open arrow heads indicate AHSV-infected cells lacking nuclear STAT1. Scale bars = 10 µm.

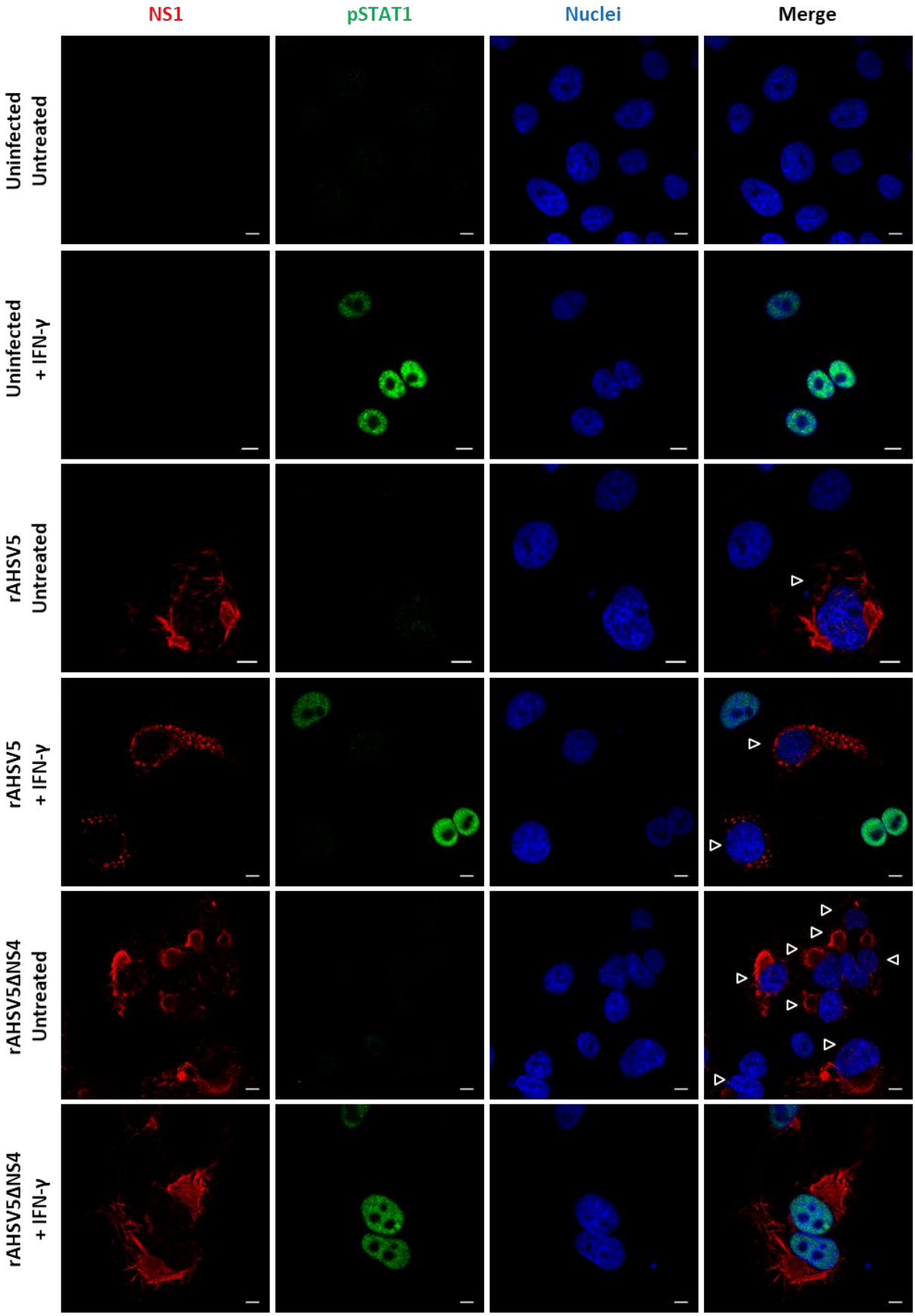


**Figure 4.17. NS4 interferes with nuclear translocation of pSTAT1.** Vero cells were infected with rAHSV5 or rAHSV5ΔNS4 and then treated with IFN-γ, fixed and processed for immunofluorescence and CLSM using anti-NS1 and LSBio anti-pSTAT1 primary, and AF 594-conjugated goat anti-mouse IgG and AF 488-conjugated goat anti-rabbit IgG secondary antibodies. Nuclei were stained with DAPI. Open arrow heads indicate AHSV-infected cells lacking nuclear STAT1. Scale bars = 10 µm.

To confirm what was observed in confocal microscopy it was decided that Western blots on nuclear and cytoplasmic fractions should be performed. Vero cells were infected with rAHSV5 or rAHSV5ΔNS4 and treated with IFN-γ at 24 hpi before being fractionated into nuclear and cytoplasmic fractions. The fractions were then exposed to SDS-PAGE and Western blot analysis using anti-NS1(786), β-actin, STAT1 or pSTAT1 antibodies. Several challenges were met with this experimental work and Figure 4.18 gives a summary of the results obtained. Unlike what was observed in CLSM, the anti-STAT1 and anti-pSTAT1 antibodies gave inconsistent results on the Western blots performed on nuclear and cytoplasmic fractions. Also, inconsistent was the labelling of β-actin (Figure 4.18A). This was determined to be due to the antibody itself and once replaced, β-actin was labelled successfully (Figure 4.18B) and consistently. Labelling against AHSV NS1 gave consistent results and NS1 was only detected in AHSV-infected fractions (both untreated and treated). As expected, the amount of NS1 observed was greater in the cytoplasm. AHSV NS1 and β-actin labelling suggested that the fractionation protocol is successful. A nuclear control would also be necessary for these experiments. This was attempted with an antibody directed against lamin B1, but was unsuccessful due to incorrect shipping conditions of the antibody. These final Western blots form the basis of future work on the elucidation of the mechanism in which NS4 interferes with the phosphorylation and/or translocation of the phosphorylated, dimerised version of STAT1 into the nucleus.

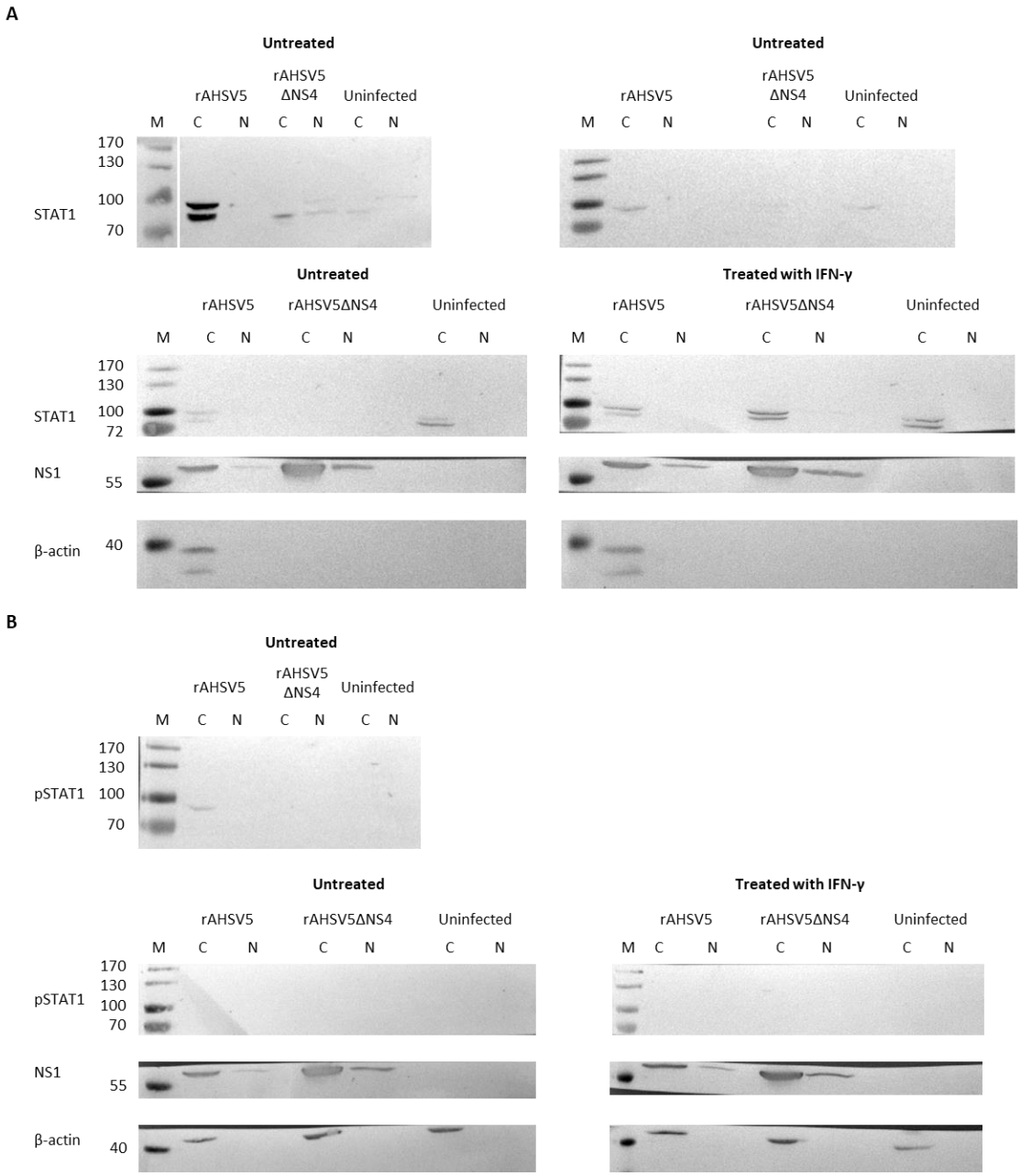


**Figure 4.18. Nuclear and cytoplasmic fractionation of untreated or IFN-γ-treated infected and uninfected Vero cells.** Vero cells were infected with rAHSV5 or rAHSV5ΔNS4 and treated with IFN-γ at 24 hpi prior to fractionation into cytoplasmic (C) or nuclear (N) fractions. The fractions were then assayed for STAT1 using Abcam anti-STAT1 N-term (A) or pSTAT1 using LSBio anti-pSTAT1 (B) and recombinant protein G-HRP. AHSV NS1(~63 kDa) was assayed as an infection control and β-actin (~42 kDa) was assayed as a control for the cytoplasmic fractions. M = PageRuler™ Prestained Protein Ladder, sizes of molecular weight markers are indicated on the left (kDa).

## 4.4. DISCUSSION

The recombinant viruses rAHSV5 and rAHSV5minNS4 described in Chapter 3 were inoculated into separate horses in vaccine trials undertaken at Deltamune (Pty) Ltd. These trials showed that rAHSV5 was highly pathogenic in horses, irrespective of whether the viruses were rescued using a plasmid only approach, or from expression plasmids plus ssRNA. In contrast, despite signs of viral replication, all horses inoculated with rAHSV5minNS4 survived and showed no clinical signs of disease, no matter the route of inoculation. These results confirmed that like BTV NS4 (Ratinier *et al.*, 2016), AHSV NS4 is a virulence factor in the host and the absence thereof (or very low expression of NS4 from rAHSV5minNS4, see Chapter 2), results in a safe, highly attenuated virus.

Based on the similarities observed to date for BTV NS4 and AHSV NS4, the aim here was to investigate if the lack of NS4 mediates the transition from virulence to attenuation, and to see if the protein interferes with host innate immunity. This was done using RNA-seq. RNA-seq has allowed many advances in the characterisation of transcriptomes (Ozsolak and Milos, 2011) and is ever evolving to provide more complete and well-analysed datasets. Due to financial constraints, total RNA of only one of the horses inoculated with rAHSV5 and three inoculated with rAHSV5minNS4 could be sent to Novogene (Hong Kong) for RNA-seq. This resulted in three biological replicates for rAHSV5minNS4 and one for rAHSV5. While several software packages exist for detecting differential gene expression, no single method is optimal under all conditions (Rapaport *et al.*, 2013; Soneson and Delorenzi, 2013; Zhang *et al.*, 2014; Seyednasrollah *et al.*, 2015). Therefore, it is recommended that two different software packages be used in the testing of differential gene expression (DGE) (Robles *et al.*, 2012; Zhang *et al.*, 2014; Seyednasrollah *et al.*, 2015). Therefore, two bioinformatics approaches were used from the point of mapping onwards to assess if the same results are obtained when using different software.

Overall, more genes were identified as differentially expressed in dataset 1 than in dataset 2 in the control horse, while the opposite was true for the horses inoculated with rAHSV5minNS4. These differences may be due to the software packages used to analyse differential gene expression. DEGSeq was used in dataset 1 for the control horse and DESeq was used to analyse DGE in the horses inoculated with rAHSV5minNS4, while Cuffdiff was used across the board in dataset 2. The use of TMM vs inherent normalisation was not expected to influence the results, as both have been seen to give similar results previously (Seyednasrollah *et al.*, 2015). Multiple studies have shown that DESeq is conservative when it comes to calling DEGs, especially when using default settings or with low transcript counts (≤100) (Robles *et al.*, 2012; Soneson and Delorenzi, 2013; Seyednasrollah *et al.*, 2015). This could account for the lower number of DEGs observed in dataset 1 compared to 2 (rAHSV5minNS4). Another possibility is that the difference is due to the number of biological replicates. DESeq is more reliable than Cuffdiff overall, especially when the number of replicates starts increasing (Seyednasrollah *et al.*, 2015). DESeq has a low false discovery rate with three replicates or more,

whereas Cuffdiff gives increased false positives, which would inflate DEG detection (Rapaport *et al.*, 2013; Soneson and Delorenzi, 2013). Therefore, it is possible that the considerably higher number of DEGs on day 1 (rAHSV5minNS4) in dataset 2 was due to this. Although three to four biological repeats appear to be sufficient for the analysis of DGE, biological variation also needs to be considered, in this case, the biological variation between the horses. More replicates are needed in experiments involving animal or human tissue than cell lines (Zhang *et al.*, 2014). Therefore, it would have been ideal to have more repeats for rAHSV5 as increasing the number of biological replicates can increase the quality and reliability of DEG detection (Robles *et al.*, 2012; Rapaport *et al.*, 2013).

Although there were differences in the number of DEGs between the datasets, the genes of both datasets suggested the innate IFN response had been activated within 24 h (1 day) of inoculation with rAHSV5minNS4. This was evidenced by the rapid upregulation of important regulators of immunity, as well as many ISGs and genes found to be involved in innate immunity. GO term enrichment analyses echoed this, especially in the case of dataset 1. Fewer GO terms were enriched overall in dataset 2, perhaps due to the lower number of DEGs on certain days or the use of KOBAS as opposed to GOSeq which was used in dataset 1. Further confirmation of the initiation of innate immunity was the activation of pathways such as the Toll-like and RIG-I-like receptor signalling pathways, which play an important role in innate immunity, which were observed on day 1 in the horses inoculated with rAHSV5minNS4. Similar to what was observed on day 1 in horses inoculated with attenuated AHSV4 (Pretorius *et al.*, 2016), several other immune system and signal transduction pathways, including JAK-STAT signalling, were also activated on day 1 (both datasets) in the horses inoculated with rAHSV5minNS4. More KEGG pathways were enriched in dataset 2 on this day, perhaps due to the high number of genes (2272) found to be DE.

Although several ISGs were also upregulated on day 1 in the presence of NS4 (rAHSV5) they were upregulated to a lower level than was seen in the absence of NS4 (both datasets). No immune system pathways were enriched on day 1 in the case of dataset 2 (rAHSV5), but several were enriched in dataset 1. The immune system pathways enriched on day 1, in dataset 1, in the presence of NS4 (rAHSV5) were enriched by down-regulated genes and importantly did not include the immune system pathways that were activated on day 1 in the horses inoculated with rAHSV5minNS4. Therefore, although innate immunity had been activated (dataset 1), it was not as strong an activation as in the absence of NS4. Thus, the expression of NS4 or its presence in the context of viral infection is unable to entirely inhibit mRNA expression of the host IFN response. These findings are similar to what has been observed in RNA-seq analyses done on nascent RNA isolated from BTV8ΔNS4 and BTV8wt infected and uninfected A549 cells at 12 hpi (Ratinier *et al.*, 2016).

An immune transcriptional response was observed on day 2 in the horse exposed to rAHSV5, with the activation of immune system and signal transduction pathways such as the RIG-I-like receptor, Toll-like

receptor, and JAK-STAT signalling. These pathways were already activated on day 1 in the absence of NS4 (rAHSV5minNS4). This was also observed in dataset 2, albeit to a lower extent. Overall, the RNA-seq results indicated that the presence of NS4 (rAHSV5) results in several immune response pathways only being transcriptionally activated 24 h later than when exposed to rAHSV5minNS4. Furthermore, this appears to be due to a delay in upregulation of innate immunity mRNAs specifically. This data also showed that both bioinformatics approaches led to the same conclusions overall, although literature suggests that Cuffdiff is not as reliable as other software when analysing DGE (Seyednasrollah *et al.*, 2015). Similar results were observed by Faber *et al*. (2021) where the authors compared the attenuated AHSV4 (*in vivo*) and virulent AHSV4 (*in vitro*) primary and secondary immune responses in horse PBMCs after 24 hours. Virulent AHSV4 was shown to impair innate immunity on an mRNA level by interfering with type I and III IFN responses and PBMCs survived during the virAHSV4 primary immune response. Although upregulation on an mRNA level does not mean there will be upregulation of the protein products of the same gene, the authors suggest that it may result in an inflammatory response that could cause immunopathology and therefore contribute to pathogenesis in naïve horses (Faber *et al.*, 2021). No expression of proinflammatory cytokines has been found *in vivo* in any of ten horses infected with different serotypes of AHSV (Prof. AC Potgieter, personal communication). A follow up study by the same group showed that oxidative stress in conjunction with IRE1α proapoptotic signalling played a role in the activation of the intrinsic apoptotic pathway, whilst cytotoxic lymphocytes induced extrinsic apoptotic pathway leading to the cell death during attenuated AHSV4 *in vivo* primary and secondary immune responses (Faber *et al.*, 2022). In contrast, by interfering with type I and II IFN responses, virulent AHSV4 lead to impaired NK cell responses and delayed immunity, and together with antioxidant defense, promoted survival (Faber *et al.*, 2022).

After the innate immune response has been initiated following the recognition of an RNA virus, the newly secreted type I IFNs bind to the IFN-α/β receptor IFNAR (Randall and Goodbourn, 2008; Fros *et al.*, 2010), leading to the phosphorylation of the tyrosine kinases, TYK1 and JAK1. This leads to the phosphorylation of the cytoplasmic transcription factors STAT1 and STAT2, which dimerise, bind to importin-α and together with IFN regulatory factor 9 (IRF9), form the IFN-stimulated gene factor 3 (ISGF3) complex (Randall and Goodbourn, 2008). This complex translocates into the nucleus where it binds to IFN-stimulated response elements (ISREs) present in promoters of ISGs leading to their expression. In contrast to type I IFNs which are induced by viral infection, type II IFN (IFN-γ) is induced by mitogenic or antigenic stimuli and only by certain types of cells (Samuel, 2001; Randall and Goodbourn, 2008). The IFN-γ response is also mediated by the JAK-STAT pathway and IFN-γ binds to the IFNGR receptor, activating JAK1 and JAK2 which leads to the phosphorylation of two STAT1 molecules which homodimerize into the γ activation factor. This factor translocates into the nucleus and binds to the gamma-activation sequence on ISGs, stimulating their transcription (Fleming, 2016). Several hundred ISGs can be expressed as a result of the IFN response and together they lead to a potent antiviral state (Randall and Goodbourn, 2008).

To promote their replication and spread, many viruses have evolved countermeasures against innate immunity, particularly the IFN response. One such measure involves encoding IFN antagonizing proteins (Randall and Goodbourn, 2008). These proteins are often multifunctional, especially in the case of RNA viruses, with roles that vary in importance depending on the stage of the virus replication cycle (Randall and Goodbourn, 2008). Examples of innate immune system antagonists include rotavirus VP3 and NSP1, Ebola virus protein VP35, Newcastle disease virus (NDV) V protein, rabies virus phosphoprotein, and several non-structural proteins within the arboviruses (Basler *et al.*, 2000; Huang *et al.*, 2003; Hollidge *et al.*, 2011; Oksayan *et al.*, 2012; Morelli *et al.*, 2015). Within the orbiviruses BTV NS3 and NS4 are known IFN antagonists, and like the NDV V protein, BTV NS4 is an important virulence factor (Huang *et al.*, 2003; Chauveau *et al.*, 2013; Ratinier *et al.*, 2016).

Another way of counteracting IFN-mediated innate immunity is by disrupting the normal functioning of the JAK-STAT signalling pathway (Fleming, 2016). For example, many viral proteins prevent the nuclear translocation of STAT1/2, STAT1/2 phosphorylation or the promotion of their nuclear export to antagonize IFN-mediated innate immunity (Melén *et al.*, 2004; Fros *et al.*, 2010; Fros *et al.*, 2013; Feng *et al.*, 2019; Mitra *et al.*, 2019). Canine distemper virus non-structural V protein, the hepatitis C virus core protein C and the hepatitis B virus precore protein p22 for example all inhibit the nuclear translocation of one or both proteins (Melén *et al.*, 2004; Röthlisberger *et al.*, 2010; Mitra *et al.*, 2019). Dengue virus non-structural protein NS5 prevents the phosphorylation of STAT2, which in turn prevents STAT1-STAT2 heterodimer formation thereby effectively blocking the nuclear translocation of STAT1 (Ashour *et al.*, 2009; Mazzon *et al.*, 2009). The nsP2 protein of Chikungunya virus inhibits type I/II IFN-stimulated JAK-STAT signalling by promoting the nuclear export of STAT1 (Fros *et al.*, 2010; Fros *et al.*, 2013; Goertz *et al.*, 2018). It is also possible for viruses to inhibit nuclear translocation after STAT has already been activated and bound to importin-α, as is the case in rotavirus infection (Holloway *et al.*, 2009; Holloway *et al.*, 2014). BTV inhibits the effect of IFN by inhibiting the phosphorylation and nuclear translocation of STAT1, and also inhibits the expression of other members of the JAK-STAT signalling pathway such as JAK1 and TYK2 (Doceul *et al.*, 2014).

Due to the JAK-STAT signalling pathway playing an important role in the first line of defense to viral infection, the abundance of literature demonstrating how viruses target this pathway to evade innate immunity, and what has been observed for BTV, it was decided to investigate if AHSV NS4 affects the innate immune response by interfering with the JAK-STAT signalling pathway specifically. Here, the JAK-STAT signalling pathway was activated on day 1 in the absence of NS4 (rAHSV5minNS4) but only on days 2 and 4 in the presence of NS4 (rAHSV5). Upon treatment with IFN-γ, STAT1 was generally retained in the cytoplasm in rAHSV5-infected cells but translocated into the nucleus in cells infected with rAHSV5ΔNS4. The rAHSV5ΔNS4 virus sustains normal replication, just lacks NS4. Therefore, the presence of NS4 during rAHSV5 infection

results in the cytoplasmic retardation of STAT1, effectively blocking type II IFN-induced JAK-STAT signalling. The mechanism by which AHSV NS4 interferes with STAT1 nuclear translocation requires further investigation, but the absence of pSTAT1 in rAHSV5 infected cells suggest that NS4 could inhibit phosphorylation of STAT1. AHSV NS4 is found in both the nucleus and the cytoplasm therefore it is possible that the protein may act at the stage of STAT1 import into, or export out of, the nucleus.

It was recently shown that within the nucleus AHSV NS4 colocalises with PML-NBs (Boughan *et al.*, 2020) which are found as distinct foci and are involved in a diverse range of cellular processes including antiviral defense against DNA and RNA viruses (Bernardi and Pandolfi, 2007; Scherer and Stamminger, 2016). By associating with NF-κB, STAT1, STAT2 and ISG promoters, PML regulates type I IFN signalling by regulating the ISGF3 complex and promoting ISG expression (Chen *et al.*, 2015; Kim and Ahn, 2015). The PML protein is also involved in type II IFN signalling by affecting STAT1 DNA binding and upregulating STAT1 phosphorylation (Choi *et al.*, 2006; El Bougrini *et al.*, 2011). As a result of its antiviral function, viruses have developed several ways to antagonize PML-NBs (Scherer and Stamminger, 2016). A well-studied PML-NB antagonist is the human cytomegalovirus (HCMV) immediate early protein 1 (IE1), a structural analogue of NS4-II (Boughan *et al.*, 2020). IE1 downregulates ISG transcription by interacting with STAT1 and STAT2 and by binding to PML, effectively sequestering ISGF3 (Paulus *et al.*, 2006; Huh *et al.*, 2008; Krauss *et al.*, 2009; Scherer *et al.*, 2014; Kim and Ahn, 2015; Scherer *et al.*, 2016). Due to its ability to bind dsDNA it is possible that AHSV NS4 prevents STAT1 binding to ISG promoters in cells in which STAT1 translocates into the nucleus, and in that way inhibits ISG expression (Belhouchet *et al.*, 2011; Zwart *et al.*, 2015). Furthermore, due to predicted structural similarities of AHSV NS4 and HCMV IE1 and the colocalisation of NS4 with PML-NBs it is possible that NS4 may act in a similar manner to IE1 and bind to PML and/or STAT1 in the nucleus. If this is the case, it is possible that AHSV NS4 would be able to sequester these proteins away from ISG promoters and inhibit ISG expression, effectively providing another way for NS4 to antagonize the IFN response via the JAK-STAT signalling pathway. Recent studies have shown that it is BTV NS3 that is responsible for inhibitory effects on IFN observed by Doceul *et al*. (2014) (Avia *et al.*, 2019). Furthermore, BTV NS3 uses its ubiquitination to target STAT2 for degradation through autophagy by degrading STAT2 (Avia *et al.*, 2019). A recent study found that BTV NS3 and NS4 target the SH2 domain of STAT1, together reducing the phosphorylation, heterodimerisation and nuclear translocation of STAT1, thereby interfering with IFN signalling (Li *et al.*, 2021). Chapter 2 showed that AHSV NS3 and NS4 do not colocalise extensively, but it is still possible that they work together in a manner similar to that observed for BTV NS3 and NS4 (Li *et al.*, 2021).

Many RNA viruses that replicate in the cytoplasm make use of nucleocytoplasmic trafficking of viral proteins to carry out various roles in viral replication and pathogenesis, as well as in the modulation of the immune response. In this Chapter results obtained from Deltamune (Pty) Ltd showed that knocking down AHSV NS4 expression from rAHSV5 results in virus attenuation. Thus, AHSV NS4 is a determinant of virus virulence. It

appears that the lack of NS4 mediates the transition of AHSV from virulent to attenuated in horses and that the protein interferes with innate immunity. One way in which AHSV NS4 interferes with the IFN response, can be via interfering with the nuclear accumulation of STAT1 during JAK-STAT signalling. As NS4 is found in both the nucleus and the cytoplasm it is possible that the protein may interact directly with STAT1 in either compartment, essentially inhibiting nuclear import or promoting nuclear export of STAT1. Further studies need to be carried out to determine the mechanism by which AHSV NS4 acts and whether other viral proteins are involved.

# CHAPTER 5

## CONCLUDING REMARKS

Although it has been known for many years that the AHSV genome encodes seven structural and three non-structural proteins, a fourth non-structural protein was recently identified. This protein, designated NS4, has been the subject of several studies over the past decade, most of which have centred on the NS4 protein of the related BTV. At the start of this study only one paper on AHSV NS4 had been published (Zwart *et al.*, 2015), therefore little was known about AHSV NS4 aside from its ability to bind dsDNA and its intracellular nucleocytoplasmic localisation. Research has since shown that BTV NS4 is an IFN antagonist and important virulence factor (Ratinier *et al.*, 2016) but the role of AHSV NS4 in the viral replication cycle, virulence and pathogenesis remains largely unknown.

The present study aimed to investigate the role of AHSV NS4 in virulence and host immunity, and formed part of a larger aim focused on investigating the function of NS4. The work described here includes an assessment of the intracellular colocalisation of AHSV NS4 with other non-structural proteins or mitochondria during the replication cycle. AHSV NS4 knockout and reassortant viruses were generated using reverse genetics and allowed the role of AHSV NS4 in viral replication to be investigated *in vitro,* and the role in virulence and pathogenesis to be investigated *in vivo* in ECEs. RNA-seq was then used to compare the transcriptional response in horses inoculated with the recombinant virulent wild-type virus rAHSV5 versus that of the NS4 knockout strain rAHSV5minNS4 with a focus on immune-related genes.

The non-structural proteins expressed by AHSV and BTV play key roles in the replication cycle therefore the colocalisation of NS4 with any, or all, of the proteins would help to elucidate the function of AHSV NS4. Some of the early research done on NS4 suggested that that BTV NS4 may be involved in the early stages of the infection cycle, or in virus release (Belhouchet *et al.*, 2011; Ratinier *et al.*, 2011) which also prompted colocalisation analyses to be performed in this study. The results obtained showed limited colocalisation of NS4 with the perimeter of NS1 tubule bundles. While the function of AHSV NS1 is unclear, BTV NS1 is a regulator of viral protein synthesis and may also play a role in release, pathogenesis, and disruption of the cell cycle (Owens *et al.*, 2004; Boyce *et al.*, 2012; Kerviel *et al.*, 2019). A recent study in our laboratory showed that both AHSV NS1 and NS4 colocalise with PML-NBs in the nucleus (Boughan *et al.*, 2020). These nuclear bodies are involved in antiviral defence; therefore, many viruses have developed ways of antagonising them (Bernardi and Pandolfi, 2007; Scherer and Stamminger, 2016). Based on what was observed here, and by Boughan *et al.* (2020), it is possible that both NS1 and NS4 act as PML-NB antagonists. NS2 forms VIBs which are the sites of virus replication and assembly (Thomas *et al.*, 1990; Brookes *et al.*, 1993; Uitenweerde *et al.*, 1995; Kar *et al.*, 2007). While some colocalisation of NS4 and NS2 was observed at the periphery of VIBs, none was observed in the VIB matrix. Therefore, it is unlikely that NS4 is involved in virus replication or assembly. NS3/A is involved in virus trafficking and release and is also an IFN antagonist (Beaton *et al.*, 2002; Celma and Roy, 2009; Meiring *et al.*, 2009; Celma and Roy, 2011; Chauveau *et al.*, 2013; Ferreira-Venter *et al.*, 2019). Although BTV NS4 is found at the plasma membrane (Belhouchet *et al.*, 2011), no colocalisation

of AHSV NS4 and NS3/A was observed at the plasma membrane, therefore it is unlikely that AHSV NS4 is involved in virus release and thereby cannot impact virulence through this mechanism.

BTV NS4 has structural relatedness to membrane associated proteins and in particular to the fzo-mitofusin protein (Belhouchet *et al.*, 2011) which has the mammalian homologues MFN1 and MFN2 (Santel and Fuller, 2001; Eura *et al.*, 2003) that are involved in mitochondrial membrane fusion. Based on this it was suggested that NS4 may localise to mitochondria, and if observed would suggest an array of possible functions for NS4. Amongst their many functions, mitochondria are involved in innate immunity and the regulation of antiviral signalling (West *et al.*, 2011) and several non-structural proteins localise to mitochondria to cause intrinsic apoptosis. Although limited, some colocalisation of NS4-II and NLS-NS4-II at the perimeter of a cluster of mitochondria was observed in this study, therefore it is possible that NS4 may be involved in the membrane depolarisation and intrinsic apoptosis caused by AHSV infection (Stassen *et al.*, 2012). MFN2 tethers mitochondria to the ER (de Brito and Scorrano, 2008) and can also cause the clustering of active mitochondria at the perinuclear region (Rojo *et al.*, 2002). Due to its structural relatedness to MFN2, and the limited colocalisation of AHSV NS4 and mitochondria observed here it is possible that AHSV NS4 could compete for the position of MFN2. If so, this would cause a break in the tethering of mitochondria and the ER and would disrupt mitochondrial distribution in the cytoplasm, effectively hampering the proper functioning of the organelles. Additionally, like BTV VP3, NS4 may associate with MAVS on the outer mitochondrial membrane (Pourcelot *et al.*, 2021). MAVS are essential for the correct activation of RLR-mediated antiviral immunity (Weinberg *et al.*, 2015) and the downstream induction of IFN (Chow *et al.*, 2015; Weinberg *et al.*, 2015). Therefore, an association between AHSV NS4 and MAVS may provide an avenue for immune system evasion by interfering with RIG-I-like signalling.

Although the results of the colocalisation analyses did not give conclusive results as to the function of AHSV NS4, evidence in the literature suggested that AHSV NS4 may be involved in virulence. Virulence is complex and multifactorial, and the viral determinants and interplay between virulence and pathogenesis regarding AHSV infection are largely unknown. Research has shown that multiple genome segments, including those that encode VP1, VP2, VP4, VP5, VP6, VP7 and NS3 determine BTV8 pathogenesis and virulence (Janowicz *et al.*, 2015). Additionally, BTV NS3/A and NS4 are also important virulence factors in the host (Feenstra *et al.*, 2014; Ratinier *et al.*, 2016; van Rijn *et al.*, 2018). Based on this information recombinant AHSV NS4 knockout and reassortant viruses based on virulent AHSV5 (expressing NS4-II) and attenuated AHSV4LP (expressing NS4-I) were generated by reverse genetics to investigate the role of AHSV NS4 in viral replication, virulence and pathogenesis. The results showed that the expression and intracellular localisation of AHSV NS4 is not influenced by the backbone into which Seg-9 is incorporated but rather by Seg-9 itself, and that the mutations that were introduced into each Seg-9 successfully abolished the expression of NS4. Seg-9 also encodes VP6, which clusters together with NS4 into Clades I and II and each protein differs with regard to length and

sequence. Therefore, it is possible that one or both proteins is responsible for the patterns of expression and localisation of AHSV NS4 in mammalian cell culture. Viruses containing Seg-9 from AHSV5 replicated better than those with Seg-9 from AHSV4LP, or the same segment lacking NS4 expression. Therefore, NS4-II and/or VP6 as encoded for by Seg-9 from AHSV5 may enhance the replication of AHSV in BSR cells.

Work done by Maartens *et al.* (2009, 2011) and in the patent by Potgieter *et al*. (2017) suggested that the embryonated chicken eggs were suitable for use as a small animal model in AHSV research. This is particularly so as the tissue tropism in ECEs is comparable to that observed in AHSV-infected horses (Maartens, 2009; Maartens *et al.*, 2011) and endothelial damage was shown to be a key contributor to the pathogenesis in ECEs, just as in horses. Therefore, ECEs were infected with each of the recombinant viruses to investigate the role of AHSV NS4 in virulence and pathogenesis. rAHSV5 routinely kills embryos within 48 hpi and although this was not observed in this study several deductions could be made from the experiments that were done. All viruses containing $S9_{4LP}$ or lacking NS4 expression appeared attenuated compared to rAHSV5 based both on survival rates and the phenotypes of the embryos. Interestingly, it appeared that incorporating $S9_5$ into the rAHSV4LP backbone resulted in a virulent virus. Therefore, it appears that NS4-II (encoded by $S9_5$) is a virulence factor in ECEs. Also apparent was that in most cases full body hyperaemia caused death and embryos appeared cherry-red in colour. Some embryos were still able to survive with partial hyperaemia and petechial and/or ecchymotic haemorrhaging and if death did occur, it occurred later than when full body hyperaemia was observed. This confirmed that full body hyperaemia is the most severe lesion in ECEs, and oedema is the least severe lesion, all of which occur due to changes in vascular permeability.

The results obtained here for ECEs infected with the recombinant viruses suggest that while useful, the experimental method needs to be optimised to obtain consistent results in future studies. Overall, it appears that viruses should be rescued and then immediately injected into ECEs for comparable and reliable results. In this way, the viruses would not be subjected to pH changes that may be experienced when stored at 4°C. Alternatively, viruses should be freeze-dried, or passaged in the brains of suckling mice immediately and then stored at -70°C. Additionally, embryos that are at the same stage of embryonic development should be used across an experiment, with the same number of embryos being used per virus under investigation.

The inoculation of two recombinant viruses, rAHSV5 and rAHSV5minNS4, into horses as part of vaccine trials at Deltamune (Pty) Ltd showed that rAHSV5 was pathogenic in horses, whereas rAHSV5minNS4 was attenuated. Therefore, like BTV NS4 (Ratinier *et al.*, 2016), AHSV NS4 is a virulence factor in the host and confirmed what was suggested by the work done in ECEs. The transcriptional response in a subset of these horses was compared using RNA-seq to investigate if the lack of NS4 mediates the transition from virulence to attenuation and that the protein interferes with host innate immunity. Two bioinformatic approaches were used to investigate this, and both led to essentially the same results overall.

An immune transcriptional response was observed on day 1 in horses inoculated with rAHSV5minNS4. Importantly, pathways such as the Toll-like and RIG-I-like receptor signalling pathways important in innate immunity were activated on this day. Innate immunity had been activated in the presence of NS4 (rAHSV5) on day 1 but the activation was not as strong as that observed in the absence of NS4. Furthermore, the immune system pathways that were enriched were enriched by downregulated genes. Overall, this showed that the expression of NS4, or its presence in the context of viral infection, is unable to entirely inhibit mRNA expression of the host IFN response, highlighting the complex nature of the host immune response. The immune response pathways that were observed on day 1 in the absence of NS4 were only transcriptionally activated 24 h later (day 2) in the presence of NS4. Furthermore, this appears to be due to a delay in the upregulation of innate immunity mRNAs specifically.

There is an abundance of literature demonstrating that viruses often target the JAK-STAT signalling pathway as a way of evading host innate immunity. This is due to the importance of the pathway in innate immunity, and the development of an antiviral response. Many viral proteins can either prevent the nuclear translocation of STAT1/2, or prevent the phosphorylation of STAT1/2, or promote the nuclear export of STAT1/2 (Melén *et al.*, 2004; Ashour *et al.*, 2009; Mazzon *et al.*, 2009; Fros *et al.*, 2010; Röthlisberger *et al.*, 2010; Fros *et al.*, 2013; Goertz *et al.*, 2018; Feng *et al.*, 2019; Mitra *et al.*, 2019). This, as well as the interference of BTV with this pathway (Doceul *et al.*, 2014) prompted an investigation into whether AHSV NS4 affects innate immunity by interfering with the JAK-STAT signalling pathway specifically. The transcriptome data showed that this pathway was activated on days 2 and later in the presence of NS4 (rAHSV5) but already on day 1 in the absence of NS4 (rAHSV5minNS4). The results obtained here showed that after treatment with IFN-γ, STAT1 translocated into the nucleus in cells infected with rAHSV5ΔNS4 but was generally retained in the cytoplasm in the case of rAHSV5. Therefore, the presence of NS4 blocks type II IFN-induced JAK-STAT signalling by causing the cytoplasmic retardation of STAT1 and provides evidence of an AHSV protein directly interfering with the innate immune response. The mechanism by with this occurs needs further investigation, but due to the nucleocytoplasmic localisation of NS4 it is possible that the protein may interact with STAT1 in either compartment at the stage of import into, or export out of, the nucleus. Co-immunoprecipitation or pull-down assays could be used to see if AHSV NS4 affects the interaction of STAT1 and importin-α5. Additionally, CRM1-mediated nuclear export could be inhibited to see if AHSV NS4 does indeed promote the export of STAT1 from the nucleus. It is also possible that NS4 inhibits STAT1 phosphorylation. It has since been shown that BTV NS3 and NS4 interfere with JAK-STAT signalling by targeting the SH2 domain of STAT1, together reducing the phosphorylation, heterodimerisation and nuclear translocation of STAT1 (Li *et al.*, 2021). Even though the results obtained in this study showed that AHSV NS3 and NS4 do not colocalise extensively, it is still possible that the proteins work together in a manner similar to that observed for BTV NS3 and NS4 (Li *et al.*, 2021).

In this study it was shown that AHSV NS4 interferes with the nuclear accumulation of the STAT1 protein in the interferon-induced JAK-STAT signalling pathway, effectively allowing AHSV to overcome antiviral responses in the host to promote viral replication and spread. Mechanisms of immune system evasion are complex and multifactorial; therefore, this is proposed to be one way in which AHSV evades host immunity. Future work could focus on identifying the mechanism by which AHSV NS4 acts upon the JAK-STAT signalling. As a start CLSM could be used to investigate if there are direct interactions between AHSV NS4 and STAT1. Additionally, this study identified areas where the ECE model can be optimised, and the experiments herein can be expanded in order to determine if any of the reverse genetics-derived viruses are potential vaccine candidates. Overall, this study has provided insights into the function of AHSV NS4 and confirms that like BTV NS4, AHSV NS4 is an important virulence factor.

**ABBREVIATIONS**

| | |
|---|---|
| 5’ppp/pp | 5’ triphosphate/diphosphate |
| °C | degrees Celsius |
| nm | nanometer |
| nM | nanomolar |
| µg | microgram |
| µl | microliter |
| µm | micrometer |
| µM | micromolar |
| aa | amino acid |
| AF | Alexa Fluor® |
| AHS | African horse sickness |
| AHSV | African horse sickness virus |
| APCs | antigen-presenting cells |
| BFAE | bovine foetal aorta endothelial cells |
| BHK | baby hamster kidney cells |
| BHQ | black hole quencher |
| BTV | bluetongue virus |
| CAMs | cell adhesion molecules |
| CARDs | caspase activation and recruitment domains |
| CCHFV | Crimean-Congo haemorrhagic fever virus |
| cDNA | complementary DNA |
| cGAS | cGAMP synthase |
| cGAS-STING | cGAS-stimulator of interferon genes |
| Ch | Chicken |
| CLSM | confocal laser scanning microscopy |
| CMV | cytomegalovirus |
| CPE | cytopathic effect |
| D | downregulated |
| DALRRD | South African Department of Agriculture, Land Reform and Rural Development |
| DAPI | 4',6-diamidino-2-phenylindole |
| DE | differentially expressed |
| DEC | Deltamune Ethical Committee |
| DEG(s) | differentially expressed gene(s) |

| | |
|---|---|
| DGE | differential gene expression |
| DISC | Disabled Infectious Single Cycle |
| DISA | Disabled Infectious Single Animal |
| DIVA | Differentiate Infected from Vaccinated Animals |
| DMEM | Dulbecco's Modified Eagle's Medium |
| ds | double stranded |
| DUF | domain of unknown function |
| EBSS | Earle's Balanced Salt Solution |
| ECEs | embryonated chicken eggs |
| ECRA | Entry Competent Replication Abortive |
| EHDV | epizootic haemorrhagic disease virus |
| ENSO | El Niño/Southern Oscillation |
| ER | endoplasmic reticulum |
| FAM | 6-carboxyfluorescein |
| FBS | foetal bovine serum |
| FR | Fourie |
| g | gravitational force |
| G | gauge |
| GIV | Great Island Virus |
| GO | gene ontology |
| GS | GenScript |
| h | hour(s) |
| HCMV | human cytomegalovirus |
| hpi | hours post infection |
| HPV | human papillomavirus |
| HRP | horseradish peroxidase |
| HSV | herpes simplex virus |
| IAV | Influenza A virus |
| IE1 | HCMV immediate early protein 1 |
| IFN(s) | interferon(s) |
| $IFNAR^{-/-}$ | type I IFN $receptor^{-/-}$ |
| IL-1 | interleukin-1 |
| IM | intramuscular |
| IPMA | immunoperoxidase monolayer assay |
| IRF | IFN-regulatory factor |
| ISG(s) | interferon stimulated gene(s) |

| | |
|---|---|
| IV | intravenous |
| JAK-STAT | Janus kinase-signal transducers and activators of transcription |
| kDa | kilodalton |
| KEGG | Kyoto Encyclopedia of Genes and Genomes |
| LAV | live attenuated virus |
| LGP2 | laboratory of genetics and physiology gene 2 |
| LF2000 | Lipofectamine 2000 |
| LRRs | leucine-rich repeats |
| MAM | mitochondria-associated ER membranes |
| MAVS | mitochondrial antiviral signalling proteins |
| MDA5 | melanoma differentiation-associated gene 5 |
| MEM | Modified Eagle's Medium |
| MFN1/2 | mitofusin 1/2 |
| MHC | major histocompatibility complex |
| min | minute(s) |
| MOI | multiplicity of infection |
| mRNA | messenger RNA |
| MR | mild reaction |
| ND | no data |
| NEAA | non-essential amino acids |
| NEMO | NF-κB essential modulator |
| NF-κB | nuclear factor kappa B |
| NLR(s) | nucleotide oligomerization domain-like receptors |
| NLS(s) | nuclear localisation signal(s) |
| NR | not recorded |
| NS4A | Zika virus non-structural protein 4A |
| NSP1 | Rotavirus non-structural protein 1 |
| OBP | Onderstepoort Biological Products |
| OIE | Office International des Epizooties |
| ORF(s) | open reading frame(s) |
| PAMPs | pathogen-associated molecular patterns |
| PBS | phosphate buffered saline |
| Pen/Strep | Penicillin and Streptomycin |
| PFA | paraformaldehyde |
| Pfu(/ml) | plaque forming units (per millilitre) |
| PHSV | Peruvian horse sickness virus |

| | |
|---|---|
| pl | plasmids |
| PML-NB(s) | promyelocytic leukemia nuclear bodies |
| PRR(s) | Pathogen recognition receptor(s) |
| PSB | protein solvent buffer |
| RD | repressor domain |
| RG | reverse genetics |
| RIG-I | retinoic acid inducible gene-I |
| RLR(s) | RIG-I like receptors |
| RNA-seq | RNA sequencing |
| rpm | revolutions per minute |
| RSV | respiratory syncytial virus |
| RT | room temperature |
| S9 | Segment 9 |
| SC | subcutaneous |
| SCRV | Saint Croix River virus |
| SDS | sodium dodecyl sulphate |
| SDS-PAGE | sodium dodecyl sulphate-polyacrylamide gel electrophoresis |
| SE | small embryo |
| seconds | s |
| Seg | segment |
| Sf9 | *Spodoptera frugiperda* cells |
| ss | single stranded |
| STAT1 | signal transducer and activator of transcription 1 |
| TBK1 | TANK binding kinase 1 |
| $TCID_{50}$/ml | 50% tissue infective dose per millilitre |
| TCRs | T-cell receptors |
| TH/C/reg | T helper/cytotoxic/regulatory cells |
| TEMED | N,N,N',N' tetramethylethylene diamine |
| TIR | intracellular Toll/IL-1 receptor domain |
| TLRs | Toll-like receptors |
| TMM | trimmed mean of M values |
| TRAF | tumour necrosis factor receptor-associated factors |
| TRIF | Toll/IL-1R domain-containing adaptor inducing IFN-β |
| TX-100 | Triton X-100 |
| U | units |
| U | upregulated |

| | |
|---|---|
| Undef | undefined |
| VIB(s) | viral inclusion body(ies) |
| VLPs | virus-like particles |
| YUOV | Yunnan orbivirus |

**LIST OF BUFFERS**

| | |
|---|---|
| Blocking solution | 5% or 1% skimmed (nonfat) milk powder in 1 x PBS |
| Blocking solution for IPMA | 1% tryptone and 0.05% Tween-20 in 1 x PBS |
| Lysis buffer | 0.5% Triton-X 100<br>0.15 M STE (0.01 M Tris, 0.001 M EDTA, 0.15 M NaCl) |
| PBS (1x) | 137 mM NaCl<br>2.7 mM KCl<br>4.3 mM $Na_2HPO_4.2H_2O$<br>1.4 mM $KH_2PO_4$<br>[pH 7.3] |
| PSB (6x) | 15% mercaptoethanol<br>40% glycerol<br>12% SDS<br>0.375 M Tris<br>[pH 6.6] |
| RIPA buffer | 150 mM NaCl<br>1% Triton X-100<br>0.5% sodium deoxycholate<br>0.1% SDS<br>50 mM Tris<br>[pH 8] |
| TAE (1x) | 40 mM Tris-HCl<br>20 mM Na-acetate<br>1 mM EDTA |
| TGS (1x) | 25 mM Tris-HCl [pH 8.3]<br>192 mM glycine<br>0.1% SDS |

| | |
|---|---|
| Towbin's transfer buffer | 25 mM Tris<br>192 mM glycine<br>20% methanol<br>[pH 8.3] |
| Wash buffer | 0.05% Tween-20 in 1 x PBS |

**APPENDIX A**

Sequencing of Seg-9 (S9) was done to confirm that the correct segment had been used when generating wild type, mutant and reassortant viruses via reverse genetics.

```
                                10        20        30        40        50

                         ....|....|....|....|....|....|....|....|....|....|
AHSV5Ref GenBank         ATGATGATCGAAGAGTGGAGAGCCAGAAATCTGAGGGAGGCGGATCAGCC
AHSV5Ref                 ..................................................
rAHSV5                   ..................................................
rAHSV5ΔNS4               .C..C...........A..................................
rAHSV4LP+S9_5            ..................................................
rAHSV4LP+S9_5ΔNS4        .C..C...........A..................................

                                60        70        80        90       100

                         ....|....|....|....|....|....|....|....|....|....|
AHSV5Ref GenBank         GATTGTCAACGCGGCGCAGGAAGCGCAGGAGCAGATTGCGCAACATCAGC
AHSV5Ref                 ..................................................
rAHSV5                   ..................................................
rAHSV5ΔNS4               ..................................................
rAHSV4LP+S9_5            ..................................................
rAHSV4LP+S9_5ΔNS4        ..............Y...................................

                               110       120       130       140       150

                         ....|....|....|....|....|....|....|....|....|....|
AHSV5Ref GenBank         AGGAGGAGGAGATGGAGGTGCAGGAGCAAGGACCGGGATTGGAGGGGGAG
AHSV5Ref                 ..................................................
rAHSV5                   ..................................................
rAHSV5ΔNS4               ............C.........................A..........
rAHSV4LP+S9_5            ..................................................
rAHSV4LP+S9_5ΔNS4        ............C.........................A..........

                               160       170       180       190       200

                         ....|....|....|....|....|....|....|....|....|....|
AHSV5Ref GenBank         GAGTGGGAGGAGTGGATTCGAGATCTGGAGGACATGGAGGACAGGGTGCA
AHSV5Ref                 ..................................................
rAHSV5                   ..................................................
rAHSV5ΔNS4               ..................................C...............
rAHSV4LP+S9_5            ..................................................
rAHSV4LP+S9_5ΔNS4        ..................................C...............

                               210       220       230       240       250

                         ....|....|....|....|....|....|....|....|....|....|
AHSV5Ref GenBank         GCCTCGGATGGAAAGGGAGTGGGTAAATCTAAGACCGGAGCAGATCGTGT
AHSV5Ref                 ..................................................
rAHSV5                   ..................................................
rAHSV5ΔNS4               ........C.........................................
rAHSV4LP+S9_5            ..................................................
rAHSV4LP+S9_5ΔNS4        ........C.........S................................

                               260       270       280       290       300

                         ....|....|....|....|....|....|....|....|....|....|
AHSV5Ref GenBank         CGCTAATGATGATGCAACACGCGATGTTGGTTCCAGTGAGGTATCATCTG
AHSV5Ref                 ..................................................
rAHSV5                   ..................................................
rAHSV5ΔNS4               ......C..C..C...........C..........................
rAHSV4LP+S9_5            ..................................................
rAHSV4LP+S9_5ΔNS4        ......C..Y..C...........C..........................
```

```
                                  310        320        330        340        350
                         ....|....|....|....|....|....|....|....|....|....|....|
AHSV5Ref GenBank         GTGGAATCACTTCAGGAGGTCTTCAAGGCCGAGGAGGACTCGTTGCAAAG
AHSV5Ref                 ..............................K.....................
rAHSV5                   ..................................................
rAHSV5ΔNS4               ..................................................
rAHSV4LP+S9₅             ..................................................
rAHSV4LP+S9₅ΔNS4         ..................................................

                                  360        370        380        390        400
                         ....|....|....|....|....|....|....|....|....|....|....|
AHSV5Ref GenBank         AGTAGTGAATGTGGCGGGGAATCATTGGATAGGACAGGCGGCTGCAGCGG
AHSV5Ref                 ..................................................
rAHSV5                   ..................................................
rAHSV5ΔNS4               ........G.........................................
rAHSV4 + S9₅             ..................................................
rAHSV4 + S9₅ΔNS4         ........G.........................................

AHSV5Ref GenBank         AAATTCAAAAACTGAGGGAGAGGAGGCAAAGGTTGGAGGGGGCGATAGAC
AHSV5Ref                 ..................................................
rAHSV5                   ..................................................
rAHSV5ΔNS4               ..................
rAHSV4LP+S9₅             ..................................................
rAHSV4LP+S9₅ΔNS4         .......

                                  460
                         ....|....|....|

AHSV5Ref GenBank         GGATTGGAGGATTAG
AHSV5Ref                 ...............
rAHSV5                   ...............
rAHSV5ΔNS4
rAHSV4LP+S9₅             ...............
rAHSV4LP+S9₅ΔNS4
```

**Figure A1. Nucleotide sequence alignment of the NS4 ORF of all wild-type, mutant and recombinant viruses containing $S9_5$ or $S9_{5\Delta NS4}$.** In all cases the ORFs are aligned with the AHSV5Ref NS4 ORF. All mutations are indicated, and K and Y indicate unknown bases due to PCR or sequencing error. The G at position 359 was caused when synthesising the pSMART-T7 plasmid containing AHSV5 Seg-9ΔNS4.

```
                                10        20        30        40        50

                         ....|....|....|....|....|....|....|....|....|....|
AHSV5Ref GenBank         MMIEEWRARNLREADQPIVNAAQEAQEQIAQHQQEEEMEVQEQGPGLEGE
AHSV5Ref                 ..................................................
rAHSV5                   ..................................................
rAHSV5ΔNS4               TT...*.............................T........*...
rAHSV4LP+S9₅             ..................................................
rAHSV4LP+S9₅ΔNS4         TT...*................X.............T........*...

                                60        70        80        90       100

                         ....|....|....|....|....|....|....|....|....|....|
AHSV5Ref GenBank         EWEEWIRDLEDMEDRVQPRMEREWVNLRPEQIVSLMMMQHAMLVPVRYHL
AHSV5Ref                 ..................................................
rAHSV5                   ..................................................
rAHSV5ΔNS4               ...........T.......T...............TTT...T........
rAHSV4LP+S9₅             ..................................................
rAHSV4LP+S9₅ΔNS4         ...........T.......T..X............TXT...T........

                               110       120       130       140       150

                         ....|....|....|....|....|....|....|....|....|....|
AHSV5Ref GenBank         VESLQEVFKAEEDSLQRVVNVAGNHWIGQAAAAEIQKLRERRQRLEGAID
AHSV5Ref                 ..........X.......................................
rAHSV5                   ..................................................
rAHSV5ΔNS4               ...................S.....................X
rAHSV4LP+S9₅             ..................................................
rAHSV4LP+S9₅ΔNS4         ...................S...............X

                         ....|
AHSV5Ref GenBank         GLED*
AHSV5Ref                 ....*
rAHSV5                   ....*
rAHSV5ΔNS4
rAHSV4LP+S9₅             ....*
rAHSV4LP+S9₅ΔNS4
```

**Figure A2. AHSV NS4 amino acid sequence alignment of all wild-type, mutant and recombinant viruses containing $S9_5$ or $S9_{5\Delta NS4}$.** In all cases the amino acid sequences were aligned with AHSV5Ref NS4. All mutations are shown and stop codons are indicated by *. X represents an unknown amino acid due to the PCR or sequencing error shown in Figure A1. The S at position 120 was caused by the nucleotide substitution mentioned in Figure A1.

```
                                10        20        30        40        50

                          ....|....|....|....|....|....|....|....|....|....|
AHSV4Ref GenBank          ATGGAGGATTGGGATCAGCAAAATCAGCAGAACCAGAACCAGCGGATGGA
AHSV4Ref                  ..................................................
rAHSV4LP                  ..................................................
rAHSV4LPΔNS4              .C.............................................C...
rAHSV5+S9_4LP             ..................................................
rAHSV5+S9_4LPΔNS4         .C.............................................C...

                                60        70        80        90        100

                          ....|....|....|....|....|....|....|....|....|....|
AHSV4Ref GenBank          TCAGGAGAATCAGCAAAATCGACAGGAGGAGATGGAGGTGGAGGAGCAGG
AHSV4Ref                  ..................................................
rAHSV4LP                  ..................................................
rAHSV4LPΔNS4              ................................C.................
rAHSV5+S9_4LP             ..................................................
rAHSV5+S9_4LPΔNS4         ................................C.................

                               110       120       130       140       150

                          ....|....|....|....|....|....|....|....|....|....|
AHSV4Ref GenBank          GCGCGGGGCTGGAGGGAGAGGAGTGGGCGGAGTGGCTGGAGGGGCTGGAC
AHSV4Ref                  ..................................................
rAHSV4LP                  ..................................................
rAHSV4LPΔNS4              ......................A........A.................
rAHSV5+S9_4LP             ..................................................
rAHSV5+S9_4LPΔNS4         ......................A........A.................

                               160       170       180       190       200

                          ....|....|....|....|....|....|....|....|....|....|
AHSV4Ref GenBank          GACGTGGAGGATCACTTCGTGGGGGACGGGATGCAGGATTGGGCGAATCT
AHSV4Ref                  ..................................................
rAHSV4LP                  ..................................................
rAHSV4LPΔNS4              ................................C.................
rAHSV5+S9_4LP             ..................................................
rAHSV5+S9_4LPΔNS4         ................................C.................

                               210       220       230       240       250

                          ....|....|....|....|....|....|....|....|....|....|
AHSV4Ref GenBank          ACGTCCGGAACAAATCATATCACTAATGATGATGCAACACGCAATGCTGG
AHSV4Ref                  ..................................................
rAHSV4LP                  ..................................................
rAHSV4LPΔNS4              ......................C..C..C..........C.....
rAHSV5+S9_4LP             ..................................................
rAHSV5+S9_4LPΔNS4         ......................C..C..C..........C.....

                               260       270       280       290       300

                          ....|....|....|....|....|....|....|....|....|....|
AHSV4Ref GenBank          TTCCGGTGAGGTACCATCTGGTGGAGTCACTTCAGGAAGTTCTCAAGGCG
AHSV4Ref                  ..................................................
rAHSV4LP                  ...G..............................................
rAHSV4LPΔNS4              ...G..............................................
rAHSV5+S9_4LP             ...G..............................................
rAHSV5+S9_4LPΔNS4         ...G..............................................
```

```
                                  310       320       330       340       350
                         ....|....|....|....|....|....|....|....|....|....|
AHSV4Ref GenBank         GAGGAGGGGGCGCTACAACGAGTGGTGAATCTGGCGGGCAACCACTGGAT
AHSV4Ref                 ..................................................
rAHSV4LP                 ..................................................
rAHSV4LPΔNS4             ..................................................
rAHSV5+S9(4LP)           ..................................................
rAHSV5+S9(4LPΔNS4)       ..................................................

                                  360       370       380       390       400
                         ....|....|....|....|....|....|....|....|....|....|
AHSV4Ref GenBank         CGGAAGAGCGGCGCAAGCGGAGATACAAGATCTCCAAGCGAGAAGACAAA
AHSV4Ref                 ..................................................
rAHSV4LP                 ..................................................
rAHSV4LPΔNS4             ..................................................
rAHSV5+S9(4LP)           ..................................................
rAHSV5+S9(4LPΔNS4)       ..................................................

                                  410       420       430
                         ....|....|....|....|....|....|....|
AHSV4Ref GenBank         GGTTGATGGGGGCGATCGACGGGATGGGGGATTAG
AHSV4Ref                 .................................
rAHSV4LP                 .................................
rAHSV4LPΔNS4             ......C.................C..........
rAHSV5+S9(4LP)           .................................
rAHSV5+S9(4LPΔNS4)       ......C.................C..........
```

**Figure A3. Nucleotide sequence alignment of the NS4 ORF of all wild-type, mutant and recombinant viruses containing $S9_{4LP}$ or $S9_{4LP\Delta NS4}$.** In all cases the ORFs are aligned with the AHSV4Ref NS4 ORF. All mutations are indicated. The G at position 254 of all rescued viruses is known to exist in the AHSV4LP vaccine strain.

```
                                10        20        30        40        50

                          ....|....|....|....|....|....|....|....|....|....|
AHSV4Ref GenBank          MEDWDQQNQQNQNQRMDQENQQNRQEEMEVEEQGAGLEGEEWAEWLEGLD
AHSV4Ref                  ..................................................
rAHSV4LP                  ..................................................
rAHSV4LPΔNS4              T.............T...........T............*..*.....
rAHSV5+S9 4LP             ..................................................
rAHSV5+S9 4LPΔNS4         T.............T...........T............*..*.....

                                60        70        80        90       100

                          ....|....|....|....|....|....|....|....|....|....|
AHSV4Ref GenBank          DVEDHFVGDGMQDWANLRPEQIISLMMMQHAMLVPVRYHLVESLQEVLKA
AHSV4Ref                  ..................................................
rAHSV4LP                  ..................................R...............
rAHSV4LPΔNS4              ..........T.............TTT...T..R...............
rAHSV5+S9 4LP             ..................................R...............
rAHSV5+S9 4LPΔNS4         ..........T.............TTT...T..R...............

                                110       120       130       140

                          ....|....|....|....|....|....|....|....|....|

AHSV4Ref GenBank          EEGALQRVVNLAGNHWIGRAAQAEIQDLQARRQRLMGAIDGMGD*
AHSV4Ref                  ...........................................*
rAHSV4LP                  ...........................................*
rAHSV4LPΔNS4              ..................................T.....T..*
rAHSV5+S9 4LP             ...........................................*
rAHSV5+S9 4LPΔNS4         ..................................T.....T..*
```

**Figure A4. AHSV NS4 amino acid sequence alignment of all wild-type, mutant and recombinant viruses containing $S9_{4LP}$ and $S9_{4LP\Delta NS4}$.** In all cases the amino acid sequences were aligned with AHSV4Ref NS4. All mutations are shown and stop codons are indicated by *. The nucleotide substitution at position 254 (Figure A3) leads to a P to R change at position 85 of the amino acid sequence of $S9_{4LP}$ and $S9_{4LP\Delta NS4}$.

**APPENDICES B-H**

Appendix B – Full list of differentially expressed genes in the transcriptome analysis of Dataset 1.

Appendix C – Full list of differentially expressed genes in the transcriptome analysis of Dataset 2.

Appendix D – Full list of GO terms enriched by the differentially expressed genes in the transcriptome analysis in Dataset 1.

Appendix E – Full list of GO terms enriched by the differentially expressed genes in the transcriptome analysis in Dataset 2.

Appendix F – Full list of KEGG pathways enriched by the differentially expressed genes in the transcriptome analysis in Dataset 1.

Appendix G – Full list of KEGG pathways enriched by the differentially expressed genes in the transcriptome analysis in Dataset 2.

Appendix H – *Equus caballus* gene IDs, associated gene names and description of each.

These appendices can be found using the following link:

https://drive.google.com/drive/u/0/folders/0AJ72IoC8XK4JUk9PVA

**REFERENCES**

Alcami, A., Koszinowski, U.H., 2000. Viral mechanisms of immune evasion. Trends Microbiol 8, 410-418.

Alexander, R.A., Neitz, W.O., Du Toit, P.J., 1936. Horsesickness: Immunization of horses and mules in the field during the season 1934-1935 with a description of the technique of preparation of polyvalent mouse neurotropic vaccine. Onderstepoort J Vet 7, 17-30.

Alexopoulou, L., Holt, A.C., Medzhitov, R., Flavell, R.A., 2001. Recognition of double-stranded RNA and activation of NF-κB by Toll-like receptor 3. Nature 413, 732-738.

Ashburner, M., Ball, C.A., Blake, J.A., Botstein, D., Butler, H., Cherry, J.M., Davis, A.P., Dolinski, K., Dwight, S.S., Eppig, J.T., Harris, M.A., Hill, D.P., Issel-Tarver, L., Kasarskis, A., Lewis, S., Matese, J.C., Richardson, J.E., Ringwald, M., Rubin, G.M., Sherlock, G., 2000. Gene Ontology: tool for the unification of biology. Nat Genet 25, 25-29.

Ashour, J., Laurent-Rolle, M., Shi, P.-Y., García-Sastre, A., 2009. NS5 of Dengue virus Mediates STAT2 binding and degradation. J Virol 83, 5408-5418.

Avia, M., Rojas, J.M., Miorin, L., Pascual, E., Van Rijn, P.A., Martín, V., García-Sastre, A., Sevilla, N., 2019. Virus-induced autophagic degradation of STAT2 as a mechanism for interferon signaling blockade. EMBO Rep 20, e48766.

Bahr, J.M., 2008. The Chicken as a Model Organism, In: Sourcebook of Models for Biomedical Research. P.M. Conn (Ed.). Humana Press, Totowa, NJ, pp. 161-167.

Barnard, B.J., 1997. Some factors governing the entry of *Culicoides* spp. (Diptera: Ceratopogonidae) into stables. Onderstepoort J Vet 64, 227-233.

Barnwal, B., Karlberg, H., Mirazimi, A., Tan, Y.J., 2016. The non-structural protein of Crimean-Congo hemorrhagic fever virus disrupts the mitochondrial membrane potential and induces apoptosis. J Biol Chem 291, 582-592.

Basak, A.K., Gouet, P., Grimes, J.M., Roy, P., Stuart, D., 1996. Crystal structure of the top domain of African horse sickness virus VP7: comparisons with bluetongue virus VP7. J Virol 70, 3797-3806.

Basler, C.F., Wang, X., Muhlberger, E., Volchkov, V., Paragas, J., Klenk, H.D., Garcia-Sastre, A., Palese, P., 2000. The Ebola virus VP35 protein functions as a type I IFN antagonist. Proc Natl Acad Sci USA 97, 12289-12294.

Beachboard, D.C., Horner, S.M., 2016. Innate immune evasion strategies of DNA and RNA viruses. Curr Opin Microbiol 32, 113-119.

Beaton, A.R., Rodriguez, J., Reddy, Y.K., Roy, P., 2002. The membrane trafficking protein calpactin forms a complex with bluetongue virus protein NS3 and mediates virus release. Proc Natl Acad Sci USA 99, 13154-13159.

Bednarczyk, M., Dunislawska, A., Stadnicka, K., Grochowska, E., 2021. Chicken embryo as a model in epigenetic research. Poultry Sci 100, 101164.

Bekker, S., Huismans, H., van Staden, V., 2014. Factors that affect the intracellular localization and trafficking of African horse sickness virus core protein, VP7. Virology 456–457, 279-291.

Belhouchet, M., Mohd Jaafar, F., Tesh, R., Grimes, J., Maan, S., Mertens, P.P., Attoui, H., 2010. Complete sequence of Great Island virus and comparison with the T2 and outer-capsid proteins of Kemerovo, Lipovnik and Tribec viruses (genus Orbivirus, family Reoviridae). J Gen Virol 91, 2985-2993.

Belhouchet, M., Mohd Jaafar, F., Firth, A.E., Grimes, J.M., Mertens, P.P., Attoui, H., 2011. Detection of a fourth orbivirus non-structural protein. PLoS ONE 6, e25697.

Bernardi, R., Pandolfi, P.P., 2007. Structure, dynamics and functions of promyelocytic leukaemia nuclear bodies. Nat Rev Mol Cell Biol 8, 1006-1016.

Bolte, S., Cordelieres, F.P., 2006. A guided tour into subcellular colocalisation analysis in light microscopy. J Microsc-Oxford 224, 213-232.

Bonilla, F.A., Oettgen, H.C., 2010. Adaptive immunity. J Allergy Clin Immun 125, S33-S40.

Boone, J.D., Balasuriya, U.B., Karaca, K., Audonnet, J.C., Yao, J., He, L., Nordgren, R., Monaco, F., Savini, G., Gardner, I.A., Maclachlan, N.J., 2007. Recombinant canarypox virus vaccine co-expressing genes encoding the VP2 and VP5 outer capsid proteins of bluetongue virus induces high level protection in sheep. Vaccine 25, 672-678.

Boughan, S., Potgieter, A.C., van Staden, V., 2020. African horse sickness virus NS4 is a nucleocytoplasmic protein that localizes to PML nuclear bodies. J Gen Virol 101, 366-384.

Boyce, M., Wehrfritz, J., Noad, R., Roy, P., 2004. Purified recombinant bluetongue virus VP1 exhibits RNA replicase activity. J Virol 78, 3994-4002.

Boyce, M., Celma, C.C., Roy, P., 2012. Bluetongue virus non-structural protein 1 is a positive regulator of viral protein synthesis. Virol J 9, 178.

Bremer, C.W., 1976. A gel electrophoretic study of the protein and nucleic acid components of African horsesickness virus. Onderstepoort J Vet Res 43, 193-199.

Breuer, K., Foroushani, A.K., Laird, M.R., Chen, C., Sribnaia, A., Lo, R., Winsor, G.L., Hancock, R.E.W., Brinkman, F.S.L., Lynn, D.J., 2013. InnateDB: systems biology of innate immunity and beyond-recent updates and continuing curation. Nucleic Acids Res 41, D1228-D1233.

Broering, T.J., Kim, J., Miller, C.L., Piggott, C.D., Dinoso, J.B., Nibert, M.L., Parker, J.S., 2004. Reovirus nonstructural protein mu NS recruits viral core surface proteins and entering core particles to factory-like inclusions. J Virol 78, 1882-1892.

Brookes, S.M., Hyatt, A.D., Eaton, B.T., 1993. Characterization of virus inclusion bodies in bluetongue virus-infected cells. J Gen Virol 74, 525-530.

Brown, C.C., Meyer, R.F., Grubman, M.J., 1994. Presence of African horse sickness virus in equine tissues, as determined by *in situ* hybridization. Vet Pathol 31, 689-694.

Buchholz, U.J., Finke, S., Conzelmann, K.-K., 1999. Generation of bovine respiratory syncytial virus (BRSV) from cDNA: BRSV NS2 is not essential for virus replication in tissue culture, and the human RSV leader region acts as a functional BRSV genome promoter. J Virol 73, 251-259.

Burdette, D.L., Monroe, K.M., Sotelo-Troha, K., Iwig, J.S., Eckert, B., Hyodo, M., Hayakawa, Y., Vance, R.E., 2011. STING is a direct innate immune sensor of cyclic di-GMP. Nature 478, 515-518.

Burrage, T.G., Laegreid, W.W., 1994. African horsesickness: pathogenesis and immunity. Comp Immunol Microb 17, 275-285.

Buttafuoco, A., Michaelsen, K., Tobler, K., Ackermann, M., Fraefel, C., Eichwald, C., 2020. Conserved rotavirus NSP5 and VP2 domains interact and affect viroplasm. J Virol 94, e01965-01919.

Calvo-Pinilla, E., Marin-Lopez, A., Utrilla-Trigo, S., Jimenez-Cabello, L., Ortego, J., 2020. Reverse genetics approaches: a novel strategy for African horse sickness virus vaccine design. Curr Opin Virol 44, 49-56.

Carpenter, S., Mellor, P.S., Fall, A.G., Garros, C., Venter, G.J., 2017. African horse sickness virus: history, transmission, and current status. Annu Rev Entomol 62, 343-358.

Celma, C.C., Roy, P., 2009. A viral nonstructural protein regulates bluetongue virus trafficking and release. J Virol 83, 6806-6816.

Celma, C.C.P., Roy, P., 2011. Interaction of calpactin light chain (S100A10/p11) and a viral NS protein is essential for intracellular trafficking of nonenveloped bluetongue virus. J Virol 85, 4783-4791.

Chang, Y.E., Laimins, L.A., 2000. Microarray analysis identifies interferon-inducible genes and Stat-1 as major transcriptional targets of human papillomavirus type 31. J Virol 74, 4174-4182.

Chauveau, E., Doceul, V., Lara, E., Breard, E., Sailleau, C., Vidalain, P.-O., Meurs, E.F., Dabo, S., Schwartz-Cornil, I., Zientara, S., Vitour, D., 2013. NS3 of bluetongue virus interferes with the induction of type I interferon. J Virol 87, 8241-8246.

Chen, Y., Wright, J., Meng, X., Leppard, K.N., 2015. Promyelocytic leukemia protein isoform II promotes transcription factor recruitment to activate interferon beta and interferon-responsive gene expression. Mol Cell Biol 35, 1660-1672.

Chen, Z., Liu, S., Sun, W., Chen, L., Yoo, D., Li, F., Ren, S., Guo, L., Cong, X., Li, J., Zhou, S., Wu, J., Du, Y., Wang, J., 2016. Nuclear export signal of PRRSV NSP1α is necessary for type I IFN inhibition. Virology 499, 278-287.

Choi, Y.-H., Bernardi, R., Pandolfi, P.P., Benveniste, E.N., 2006. The promyelocytic leukemia protein functions as a negative regulator of IFN-γ signaling. Proc Natl Acad Sci USA 103, 18715-18720.

Chow, J., Franz, K.M., Kagan, J.C., 2015. PRRs are watching you: Localization of innate sensing and signaling regulators. Virology 479-480, 104-109.

Clift, S.J., Williams, M.C., Gerdes, T., Smit, M.M., 2009. Standardization and validation of an immunoperoxidase assay for the detection of African horse sickness virus in formalin-fixed, paraffin-embedded tissues. J Vet Diagn Invest 21, 655-667.

Clift, S.J., Penrith, M.L., 2010. Tissue and cell tropism of African horse sickness virus demonstrated by immunoperoxidase labeling in natural and experimental infection in horses in South Africa. Vet Pathol 47, 690-697.

Coetzee, P., Van Vuuren, M., Stokstad, M., Myrmel, M., Venter, E.H., 2012. Bluetongue virus genetic and phenotypic diversity: Towards identifying the molecular determinants that influence virulence and transmission potential. Vet Microbiol 161, 1-12.

Coetzer, J.A.W., Guthrie, A.J., 2004. African horsesickness. In: Infectious Diseases Of Livestock With Special Reference To Southern Africa. J.A.W. Coetzer, G.R. Thomson, R.C. Tustin (Eds.); N.P.J. Kriek (Ass Ed.). Oxford University Press, Cape Town, pp 1231-1246.

Crawford, S.E., Criglar, J.M., Liu, Z., Broughman, J.R., Estes, M.K., 2020. COPII vesicle transport is required for rotavirus NSP4 interaction with the autophagy protein LC3 II and trafficking to viroplasms. J Virol 94, e01341-01319.

Darnell, D.K., Schoenwolf, G.C., 2000. The chick embryo as a model system for analyzing mechanisms of development, In: Developmental Biology Protocols: Volume I. J.M. Walker, R.S. Tuan, C.W. Lo (Eds.). Humana Press, Totowa, NJ, pp. 25-29.

Dauber, B., Heins, G., Wolff, T., 2004. The influenza B virus nonstructural NS1 protein is essential for efficient viral growth and antagonizes beta interferon induction. J Virol 78, 1865-1872.

de Brito, O.M., Scorrano, L., 2008. Mitofusin 2 tethers endoplasmic reticulum to mitochondria. Nature 456, 605-610.

Dempsey , E.W., 1956. Variations in the structure of mitochondria. J Biophys Biochem Cy 2, 305-312.

Dennis, S.J., Meyers, A.E., Guthrie, A.J., Hitzeroth, I.I., Rybicki, E.P., 2018a. Immunogenicity of plant-produced African horse sickness virus-like particles: implications for a novel vaccine. Plant Biotechnol J 16, 442-450.

Dennis, S.J., O'Kennedy, M.M., Rutkowska, D., Tsekoa, T., Lourens, C.W., Hitzeroth, I.I., Meyers, A.E., Rybicki, E.P., 2018b. Safety and immunogenicity of plant-produced African horse sickness virus-like particles in horses. Vet Res 49, 105.

Dennis, S.J., Meyers, A.E., Hitzeroth, II, Rybicki, E.P., 2019. African horse sickness: A review of current understanding and vaccine development. Viruses 11, 844.

Desmyter, J., Melnick, J.L., Rawls, W.E., 1968. Defectiveness of interferon production and of rubella virus interference in a line of African green monkey kidney cells (Vero). J Virol 2, 955-961.

Diprose, J.M., Grimes, J.M., Sutton, G.C., Burroughs, J.N., Meyer, A., Maan, S., Mertens, P.P., Stuart, D.I., 2002. The core of bluetongue virus binds double-stranded RNA. J Virol 76, 9533-9536.

Doceul, V., Chauveau, E., Lara, E., Breard, E., Sailleau, C., Zientara, S., Vitour, D., 2014. Dual modulation of type I interferon response by bluetongue virus. J Virol 88, 10792-10802.

Döring, M., Lessin, I., Frenz, T., Spanier, J., Kessler, A., Tegtmeyer, P., Dağ, F., Thiel, N., Trilling, M., Lienenklaus, S., Weiss, S., Scheu, S., Messerle, M., Cicin-Sain, L., Hengel, H., Kalinke, U., 2014. M27 expressed by cytomegalovirus counteracts effective type I interferon induction of myeloid cells but not of plasmacytoid dendritic cells. J Virol 88, 13638-13650.

du Plessis, M., Nel, L.H., 1997. Comparative sequence analysis and expression of the M6 gene, encoding the outer capsid protein VP5, of African horsesickness virus serotype nine. Virus Res 47, 41-49.

Eaton, B.T., Hyatt, A.D., White, J.R., 1987. Association of bluetongue virus with the cytoskeleton. Virology 157, 107-116.

Eaton, B.T., Hyatt, A.D., Brookes, S.M., 1990. The replication of bluetongue virus. Curr Top Microbiol 162, 89-118.

El Bougrini, J., Dianoux, L., Chelbi-Alix, M.K., 2011. PML positively regulates interferon gamma signaling. Biochimie 93, 389-398.

Els, H.J., Verwoerd, D.W., 1969. Morphology of bluetongue virus. Virology 38, 213-219.

Erasmus, B.J., 1963. Preliminary observations on the value of the guinea-pig in determining the innocuity and antigenicity of neurotropic attenuated horsesickness strains. Onderstepoort J Vet 30, 11-22.

Erasmus, B.J., 1973. The pathogenesis of African horsesickness, Proc 3rd Int Conf Equine Inf Dis, Paris, pp1-11.

Eura, Y., Ishihara, N., Yokota, S., Mihara, K., 2003. Two mitofusin proteins, mammalian homologues of FZO, with distinct functions are both required for mitochondrial fusion. J Biochem 134, 333-344.

Faber, E., Tshilwane, S.I., Kleef, M.V., Pretorius, A., 2021. Virulent African horse sickness virus serotype 4 interferes with the innate immune response in horse peripheral blood mononuclear cells *in vitro*. Infect Genet Evol 91, 104836.

Faber, E., Tshilwane, S.I., Van Kleef, M., Pretorius, A., 2022. Apoptosis versus survival of African horse sickness virus serotype 4-infected horse peripheral blood mononuclear cells. Virus Res 307, 198609.

Faber, F.E., van Kleef, M., Tshilwane, S.I., Pretorius, A., 2016. African horse sickness virus serotype 4 antigens, VP1-1, VP2-2, VP4, VP7 and NS3, induce cytotoxic T cell responses *in vitro*. Virus Res 220, 12-20.

Fasina, F., Potgieter, A.C., Ibironke, A., Bako, B., Bwala, D., Kumbish, P., 2008. First report of an outbreak of African horsesickness virus serotype 2 in the northern hemisphere. J Equine Vet Sci 28, 167-170.

Feenstra, F., van Gennip, R.G.P., Maris-Veldhuis, M., Verheij, E., van Rijn, P.A., 2014. Bluetongue virus without NS3/NS3a expression is not virulent and protects against virulent bluetongue virus challenge. J Gen Virol 95, 2019-2029.

Feng, K., Deng, F., Hu, Z., Wang, H., Ning, Y.-J., 2019. Heartland virus antagonizes type I and III interferon antiviral signaling by inhibiting phosphorylation and nuclear translocation of STAT2 and STAT1. J Biol Chem 294, 9503–9517.

Ferreira-Venter, L., Venter, E., Theron, J., van Staden, V., 2019. Targeted mutational analysis to unravel the complexity of African horse sickness virus NS3 function in mammalian cells. Virology 531, 149-161.

Firth, A.E., 2008. Bioinformatic analysis suggests that the Orbivirus VP6 cistron encodes an overlapping gene. Virol J 5, 48.

Flamme, I., von Reutern, M., Drexler, H.C.A., Syed-Ali, S., Risau, W., 1995. Overexpression of vascular endothelial growth factor in the avian embryo induces hypervascularization and increased vascular permeability without alterations of embryonic pattern formation. Dev Biol 171, 399-414.

Fleming, S.B., 2016. Viral inhibition of the IFN-induced JAK/STAT signalling pathway: development of live attenuated vaccines by mutation of viral-encoded IFN-antagonists. Vaccines 4, 23.

Forzan, M., Wirblich, C., Roy, P., 2004. A capsid protein of nonenveloped Bluetongue virus exhibits membrane fusion activity. Proc Natl Acad Sci USA 101, 2100-2105.

Forzan, M., Marsh, M., Roy, P., 2007. Bluetongue virus entry into cells. J Virol 81, 4819-4827.

Fros, J.J., Liu, W.J., Prow, N.A., Geertsema, C., Ligtenberg, M., Vanlandingham, D.L., Schnettler, E., Vlak, J.M., Suhrbier, A., Khromykh, A.A., Pijlman, G.P., 2010. Chikungunya virus nonstructural protein 2 inhibits type I/II interferon-stimulated JAK-STAT signaling. J Virol 84, 10877-10887.

Fros, J.J., van der Maten, E., Vlak, J.M., Pijlman, G.P., 2013. The C-terminal domain of chikungunya virus nsP2 independently governs viral RNA replication, cytopathicity, and inhibition of interferon signaling. J Virol 87, 10394-10400.

Gibbs, E.P., Tabachnick, W.J., Holt, T.J., Stallknecht, D.E., 2008. U.S. concerns over bluetongue. Science 320, 872.

Goertz, G.P., McNally, K.L., Robertson, S.J., Best, S.M., Pijlman, G.P., Fros, J.J., 2018. The methyltransferase-like domain of chikungunya virus nsP2 inhibits the interferon response by promoting the nuclear export of STAT1. J Virol 92, e01008-01018.

Gold, S., Monaghan, P., Mertens, P., Jackson, T., 2010. A clathrin independent macropinocytosis-like entry mechanism used by bluetongue virus-1 during infection of BHK cells. PLoS ONE 5, e11360.

Gomez-Villamandos, J.C., Sanchez, C., Carrasco, L., Laviada, M.M., Bautista, M.J., Martinez-Torrecuadrada, J., Sanchez-Vizcaino, J.M., Sierra, M.A., 1999. Pathogenesis of African horse sickness: ultrastructural study of the capillaries in experimental infection. J Comp Pathol 121, 101-116.

Goodbourn, S., Didcock, L., Randall, R.E., 2000. Interferons: cell signalling, immune modulation, antiviral response and virus countermeasures. J Gen Virol 81, 2341-2364.

Goubau, D., Schlee, M., Deddouche, S., Pruijssers, A.J., Zillinger, T., Goldeck, M., Schuberth, C., Van der Veen, A.G., Fujimura, T., Rehwinkel, J., Iskarpatyoti, J.A., Barchet, W., Ludwig, J., Dermody, T.S., Hartmann, G., Reis e Sousa, C., 2014. Antiviral immunity via RIG-I-mediated recognition of RNA bearing 5'-diphosphates. Nature 514, 372-375.

Gould, E.A., Higgs, S., 2009. Impact of climate change and other factors on emerging arbovirus diseases. T Roy Soc Trop Med H 103, 109-121.

Grewar, J.D., Weyer, C.T., Venter, G.J., van Helden, L.S., Burger, P., Guthrie, A.J., Coetzee, P., Labuschagne, K., Bührmann, G., Parker, B.J., Thompson, P.N., 2019. A field investigation of an African horse sickness outbreak in the controlled area of South Africa in 2016. Transbound Emerg Dis 66, 743-751.

Grimes, J., Basak, A.K., Roy, P., Stuart, D., 1995. The crystal structure of bluetongue virus VP7. Nature 373, 167-170.

Grimes, J.M., Burroughs, J.N., Gouet, P., Diprose, J.M., Malby, R., Zientara, S., Mertens, P.P., Stuart, D.I., 1998. The atomic structure of the bluetongue virus core. Nature 395, 470-478.

Groskreutz, D.J., Babor, E.C., Monick, M.M., Varga, S.M., Hunninghake, G.W., 2010. Respiratory syncytial virus limits α subunit of eukaryotic translation initiation factor 2 (eIF2α) phosphorylation to maintain translation and viral replication. J Biol Chem 285, 24023-24031.

Guthrie, A.J., Quan, M., Lourens, C.W., Audonnet, J.C., Minke, J.M., Yao, J., He, L., Nordgren, R., Gardner, I.A., Maclachlan, N.J., 2009. Protective immunization of horses with a recombinant canarypox virus vectored vaccine co-expressing genes encoding the outer capsid proteins of African horse sickness virus. Vaccine 27, 4434-4438.

Habjan, M., Andersson, I., Klingström, J., Schümann, M., Martin, A., Zimmermann, P., Wagner, V., Pichlmair, A., Schneider, U., Mühlberger, E., Mirazimi, A., Weber, F., 2008. Processing of Genome 5′ Termini as a Strategy of Negative-Strand RNA Viruses to Avoid RIG-I-Dependent Interferon Induction. PLoS ONE 3, e2032.

Hales, K.G., Fuller, M.T., 1997. Developmentally regulated mitochondrial fusion mediated by a conserved, novel, predicted GTPase. Cell 90, 121-129.

Han, Z., Harty, R.N., 2004. The NS3 protein of bluetongue virus exhibits viroporin-like properties. J Biol Chem 279, 43092-43097.

Hassan, S.H., Wirblich, C., Forzan, M., Roy, P., 2001. Expression and functional characterization of bluetongue virus VP5 protein: role in cellular permeabilization. J Virol 75, 8356-8367.

Hassan, S.S., Roy, P., 1999. Expression and functional characterization of bluetongue virus VP2 protein: role in cell entry. J Virol 73, 9832-9842.

Hazrati, A., 1967. Identification and typing of horse-sickness virus strains isolated in the recent epizootic of the disease in Morocco, Tunisia, and Algeria. Arch Inst Razi 19, 131–143.

Heise, M.T., Virgin, H.W., 2013. Pathogenesis of Viral Infection, In: Fields Virology. D.M. Knipe, P.M. Howley (Eds.), Sixth ed. Lippincott Williams & Wilkins, Philadelphia, pp. 254-285.

Hewat, E.A., Booth, T.F., Roy, P., 1992. Structure of bluetongue virus particles by cryoelectron microscopy. J Struct Biol 109, 61-69.

Hewat, E.A., Booth, T.F., Roy, P., 1994. Structure of correctly self-assembled bluetongue virus-like particles. J Struct Biol 112, 183-191.

Hill, A., Jugovic, P., York, I., Russ, G., Bennink, J., Yewdell, J., Ploegh, H., Johnson, D., 1995. Herpes simplex virus turns off the TAP to evade host immunity. Nature 375, 411-415.

Hollidge, B.S., Weiss, S.R., Soldan, S.S., 2011. The role of interferon antagonist, non-structural proteins in the pathogenesis and emergence of arboviruses. Viruses 3, 629-658.

Holloway, G., Truong, T.T., Coulson, B.S., 2009. Rotavirus antagonizes cellular antiviral responses by inhibiting the nuclear accumulation of STAT1, STAT2, and NF-κB. J Virol 83, 4942-4951.

Holloway, G., Dang, V.T., Jans, D.A., Coulson, B.S., 2014. Rotavirus inhibits IFN-induced STAT nuclear translocation by a mechanism that acts after STAT binding to importin-α. J Gen Virol 95, 1723-1733.

Holloway, G., Johnson, R.I., Kang, Y., Dang, V.T., Stojanovski, D., Coulson, B.S., 2015. Rotavirus NSP6 localizes to mitochondria via a predicted N-terminal α-helix. J Gen Virol 96, 3519-3524.

Howell, 1963. Observations on the occurrence of African horsesickness amongst immunised horses. Onderstepoort J Vet 30, 3-10.

Howell, P.G., 1962. The isolation and identification of further antigenic types of african horsesickness virus. Onderstepoort Journal of Veterinary Research 29, 139-149.

Huang, Z., Krishnamurthy, S., Panda, A., Samal, S.K., 2003. Newcastle disease virus V protein is associated with viral pathogenesis and functions as an alpha interferon antagonist. J Virol 77, 8676-8685.

Huh, Y.H., Kim, Y.E., Kim, E.T., Park, J.J., Song, M.J., Zhu, H., Hayward, G.S., Ahn, J.-H., 2008. Binding STAT2 by the acidic domain of human cytomegalovirus IE1 promotes viral growth and is negatively regulated by SUMO. J Virol 82, 10444-10454.

Huismans, H., Els, H.J., 1979. Characterization of the tubules associated with the replication of three different orbiviruses. Virology 92, 397-406.

Huismans, H., van Dijk, A.A., Bauskin, A.R., 1987a. In vitro phosphorylation and purification of a nonstructural protein of bluetongue virus with affinity for single-stranded RNA. J Virol 61, 3589-3595.

Huismans, H., van Dijk, A.A., Els, H.J., 1987b. Uncoating of parental bluetongue virus to core and subcore particles in infected L cells. Virology 157, 180-188.

Huismans, H., Vanderwalt, N.T., Cloete, M., Erasmus, B.J., 1987c. Isolation of a capsid protein of bluetongue virus that induces a protective immune response in sheep. Virology 157, 172-179.

Huismans, H.V., Van Staden, V., Fick, W.C., M. van Niekerk, M., 2004. A comparison of different orbivirus proteins that could affect virulence and pathogenesis. Vet Ital 40, 417-425.

Hyatt, A.D., Eaton, B.T., Brookes, S.M., 1989. The release of bluetongue virus from infected cells and their superinfection by progeny virus. Virology 173, 21-34.

Hyatt, A.D., Gould, A.R., Coupar, B., Eaton, B.T., 1991. Localization of the non-structural protein NS3 in bluetongue virus-infected cells. J Gen Virol 72, 2263-2267.

Hyatt, A.D., Zhao, Y., Roy, P., 1993. Release of bluetongue virus-like particles from insect cells is mediated by BTV nonstructural protein NS3/NS3A. Virology 193, 592-603.

Isaacs, A., Baron, S., 1960. Antiviral action of interferon in embryonic cells. The Lancet 276, 946-947.

Ishikawa, H., Barber, G.N., 2008. STING is an endoplasmic reticulum adaptor that facilitates innate immune signalling. Nature 455, 674-678.

Ishikawa, H., Ma, Z., Barber, G.N., 2009. STING regulates intracellular DNA-mediated, type I interferon-dependent innate immunity. Nature 461, 788-792.

Iwasaki, A., Medzhitov, R., 2015. Control of adaptive immunity by the innate immune system. Nat Immunol 16, 343-353.

Janowicz, A., Caporale, M., Shaw, A., Gulletta, S., Di Gialleonardo, L., Ratinier, M., Palmarini, M., 2015. Multiple genome segments determine virulence of bluetongue virus serotype 8. J Virol 89, 5238-5249.

Jassey, A., Liu, C.H., Changou, C.A., Richardson, C.D., Hsu, H.Y., Lin, L.T., 2019. Hepatitis C virus non-structural protein 5A (NS5A) disrupts mitochondrial dynamics and induces mitophagy. Cells 8, 290.

Javed, F., Manzoor, S., 2018. HCV non-structural NS4A protein of genotype 3a induces mitochondria mediated death by activating Bax and the caspase cascade. Microb Pathogenesis 124, 346-355.

Kanai, Y., van Rijn, P.A., Maris-Veldhuis, M., Kaname, Y., Athmaram, T.N., Roy, P., 2014. Immunogenicity of recombinant VP2 proteins of all nine serotypes of African horse sickness virus. Vaccine 32, 4932-4937.

Kar, A.K., Bhattacharya, B., Roy, P., 2007. Bluetongue virus RNA binding protein NS2 is a modulator of viral replication and assembly. BMC Mol Biol 8, 4.

Kell, A.M., Gale, M., Jr., 2015. RIG-I in RNA virus recognition. Virology 479-480, 110-121.

Kerviel, A., Ge, P., Lai, M., Jih, J., Boyce, M., Zhang, X., Zhou, Z.H., Roy, P., 2019. Atomic structure of the translation regulatory protein NS1 of bluetongue virus. Nat Microbiol 4, 837-845.

Kim, Y.E., Ahn, J.H., 2015. Positive role of promyelocytic leukemia protein in type I interferon response and its regulation by human cytomegalovirus. PLoS Pathog 11, e1004785.

Kindt, T.J., Goldsby, R.A., Osborne, B.A., 2007. Kuby Immunology, Sixth ed. W. H. Freeman and Company, New York.

King, S., Rajko-Nenow, P., Ashby, M., Frost, L., Carpenter, S., Batten, C., 2020. Outbreak of African horse sickness in Thailand, 2020. Transbound Emerg Dis 67, 1764-1767.

Koshiba, T., Detmer, S.A., Kaiser, J.T., Chen, H., McCaffery, J.M., Chan, D.C., 2004. Structural Basis of Mitochondrial Tethering by Mitofusin Complexes. Science 305, 858-862.

Krauss, S., Kaps, J., Czech, N., Paulus, C., Nevels, M., 2009. Physical requirements and functional consequences of complex formation between the cytomegalovirus IE1 protein and human STAT2. J Virol 83, 12854-12870.

Krug, R.M., 2015. Functions of the influenza A virus NS1 protein in antiviral defense. Curr Opin Virol 12, 1-6.

Kundlacz, C., Pourcelot, M., Fablet, A., Moraes, R.A.D.S., Léger, T., Morlet, B., Viarouge, C., Sailleau, C., Turpaud, M., Gorlier, A., Breard, E., Lecollinet, S., Rijn, P.A.v., Zientara, S., Vitour, D., Caignard, G., López, S., 2019. Novel function of bluetongue virus NS3 protein in regulation of the MAPK/ERK signaling pathway. J Virol 93, e00336-00319.

Kushnir, N., Streatfield, S.J., Yusibov, V., 2012. Virus-like particles as a highly efficient vaccine platform: Diversity of targets and production systems and advances in clinical development. Vaccine 31, 58-83.

Labadie, T., Jegouic, S., Roy, P., 2019. Bluetongue virus nonstructural protein 3 orchestrates virus maturation and drives non-lytic egress via two polybasic motifs. Viruses 11, 1107.

Labadie, T., Sullivan, E., Roy, P., 2020. Multiple routes of bluetongue virus egress. Microorganisms 8, 965.

Lacheiner, K., 2006. Tubules composed of non-structural protein NS1 of African horsesickness virus as a system for the immune display of foreign peptides, Department of Genetics. University of Pretoria, Pretoria, pp. 1-155.

Laegreid, W.W., Burrage, T.G., Stone-Marschat, M., Skowronek, A., 1992. Electron microscopic evidence for endothelial infection by African horsesickness virus. Vet Pathol 29, 554-556.

Laegreid, W.W., Skowronek, A., Stone-Marschat, M., Burrage, T., 1993. Characterization of virulence variants of African horsesickness virus. Virology 195, 836-839.

Li, Z., Lu, D., Yang, H., Li, Z., Zhu, P., Xie, J., Liao, D., Zheng, Y., Li, H., 2021. Bluetongue virus non-structural protein 3 (NS3) and NS4 coordinatively antagonize type I interferon signaling by targeting STAT1. Vet Microbiol 254, 108986.

Limn, C.K., Roy, P., 2003. Intermolecular interactions in a two-layered viral capsid that requires a complex symmetry mismatch. J Virol 77, 11114-11124.

Lin, F.-c., Young, H.A., 2014. Interferons: Success in anti-viral immunotherapy. Cytokine Growth F R 25, 369-376.

Liu, G., Park, H.-S., Pyo, H.-M., Liu, Q., Zhou, Y., 2015. Influenza A virus panhandle structure is directly involved in RIG-I activation and IFN induction. J Virol 89, 6067-6079.

Lorenzo, M.E., Ploegh, H.L., Tirabassi, R.S., 2001. Viral immune evasion strategies and the underlying cell biology. Semin Immunol 13, 1-9.

Lu, G., Pan, J., Ou, J., Shao, R., Hu, X., Wang, C., Li, S., 2020. African horse sickness: Its emergence in Thailand and potential threat to other Asian countries. Transbound Emerg Dis 67, 1751-1753.

Lulla, V., Lulla, A., Wernike, K., Aebischer, A., Beer, M., Roy, P., 2016. Assembly of Replication-Incompetent African Horse Sickness Virus Particles: Rational Design of Vaccines for All Serotypes. J Virol 90, 7405-7414.

Lulla, V., Losada, A., Lecollinet, S., Kerviel, A., Lilin, T., Sailleau, C., Beck, C., Zientara, S., Roy, P., 2017. Protective efficacy of multivalent replication-abortive vaccine strains in horses against African horse sickness virus challenge. Vaccine 35, 4262-4269.

Lymperopoulos, K., Wirblich, C., Brierley, I., Roy, P., 2003. Sequence specificity in the interaction of bluetongue virus non-structural protein 2 (NS2) with viral RNA. J Biol Chem 278, 31722-31730.

Ma, J., Ketkar, H., Geng, T., Lo, E., Wang, L., Xi, J., Sun, Q., Zhu, Z., Cui, Y., Yang, L., Wang, P., 2018. Zika virus non-structural protein 4A blocks the RLR-MAVS signaling. Front Microbiol 9, 1350.

Maartens, L.H., 2009. Tissue tropism of African horsesickness virus in the chicken embryo demonstrated with the avidin-biotin complex immunoperoxidase method, Department of Paraclinical Sciences. University of Pretoria, pp. 1-71.

Maartens, L.H., Erasmus, B.J., Clift, S.J., 2011. Tissue tropism of African horsesickness virus in the chicken embryo demonstrated with the avidin-biotin complex immunoperoxidase method. Vet Pathol 48, 1085-1093.

MacLachlan, N.J., Balasuriya, U.B., Davis, N.L., Collier, M., Johnston, R.E., Ferraro, G.L., Guthrie, A.J., 2007. Experiences with new generation vaccines against equine viral arteritis, West Nile disease and African horse sickness. Vaccine 25, 5577-5582.

Maclachlan, N.J., 2010. Global implications of the recent emergence of bluetongue virus in europe. Vet Clin N Am-Food A 26, 163-171.

Maclachlan, N.J., Guthrie, A.J., 2010. Re-emergence of bluetongue, African horse sickness, and other orbivirus diseases. Vet Res 41, 35.

Maclachlan, N.J., Zientara, S., Wilson, W.C., Richt, J.A., Savini, G., 2019. Bluetongue and epizootic hemorrhagic disease viruses: recent developments with these globally re-emerging arboviral infections of ruminants. Curr Opin Virol 34, 56-62.

Maggioni, C., Braakman, I., 2005. Synthesis and quality control of viral membrane proteins. Curr Top Microbiol 285, 175-198.

Manole, V., Laurinmaki, P., Van Wyngaardt, W., Potgieter, C.A., Wright, I.M., Venter, G.J., van Dijk, A.A., Sewell, B.T., Butcher, S.J., 2012. Structural insight into African horsesickness virus infection. J Virol 86, 7858-7866.

Maree, F.F., Huismans, H., 1997. Characterization of tubular structures composed of nonstructural protein NS1 of African horsesickness virus expressed in insect cells. J Gen Virol 78 1077-1082.

Maree, S., Durbach, S., Huismans, H., 1998. Intracellular production of African horsesickness virus core-like particles by expression of the two major core proteins, VP3 and VP7, in insect cells. J Gen Virol 79, 333-337.

Marq, J.-B., Kolakofsky, D., Garcin, D., 2010. Unpaired 5' ppp-nucleotides, as found in arenavirus dsRNA panhandles, are not recognized by RIG-I. J Biol Chem 285, 18208-18216.

Martin, L.A., Meyer, A.J., O'Hara, R.S., Fu, H., Mellor, P.S., Knowles, N.J., Mertens, P.P., 1998. Phylogenetic analysis of African horse sickness virus segment 10: sequence variation, virulence characteristics and cell exit. Arch Vir S 14, 281-293.

Martinez-Torrecuadrada, J.L., Diaz-Laviada, M., Roy, P., Sanchez, C., Vela, C., Sanchez-Vizcaino, J.M., Casal, J.I., 1996. Full protection against African horsesickness (AHS) in horses induced by baculovirus-derived AHS virus serotype 4 VP2, VP5 and VP7. J Gen Virol 77, 1211-1221.

Matsuo, E., Yamazaki, K., Tsuruta, H., Roy, P., 2018. Interaction between a unique minor protein and a major capsid protein of Bluetongue virus controls virus infectivity. J Virol 92, e01784-01717.

Mazzon, M., Jones, M., Davidson, A., Chain, B., Jacobs, M., 2009. Dengue virus NS5 inhibits interferon-α signaling by blocking signal transducer and activator of transcription 2 phosphorylation. J Infect Dis 200, 1261-1270.

McBride, H.M., Neuspiel, M., Wasiak, S., 2006. Mitochondria: More than just a powerhouse. Curr Biol 16, R551-R560.

Meiring, T.L., Huismans, H., van Staden, V., 2009. Genome segment reassortment identifies non-structural protein NS3 as a key protein in African horsesickness virus release and alteration of membrane permeability. Arch Virol 154, 263-271.

Meiswinkel, R., Baylis, M., Labuschagne, K., 2000. Stabling and the protection of horses from *Culicoides bolitinos* (Diptera: Ceratopogonidae), a recently identified vector of African horse sickness. B Entomol Res 90, 509-515.

Melén, K., Fagerlund, R., Nyqvist, M., Keskinen, P., Julkunen, I., 2004. Expression of hepatitis C virus core protein inhibits interferon-induced nuclear import of STATs. J Med Virol 73, 536-547.

Mellor, P.S., Boorman, J., Baylis, M., 2000. Culicoides biting midges: Their role as arbovirus vectors. Annu Rev Entomol 45, 307-340.

Mellor, P.S., Hamblin, C., 2004. African horse sickness. Vet Res 35, 445-466.

Mertens, P.P.C., Burroughs, J.N., Walton, A., Wellby, M.P., Fu, H., O'Hara, R.S., Brookes, S.M., Mellor, P.S., 1996. Enhanced infectivity of modified bluetongue virus particles for two insect cell lines and for two *Culicoides* vector species. Virology 217, 582-593.

Mitra, B., Wang, J., Kim, E.S., Mao, R., Dong, M., Liu, Y., Zhang, J., Guo, H., 2019. Hepatitis B virus precore protein p22 inhibits interferon-alpha signaling by blocking STAT nuclear translocation. J Virol 93, e00196-00119.

Mizukoshi, N., Sakamoto, K., Iwata, A., Tsuchiya, T., Ueda, S., Watanabe, T., Kamada, M., Fukusho, A., 1992. The complete sequence of African horsesickness virus serotype 4 (vaccine strain) RNA segment 5 and its predicted polypeptide compared with NS1 of bluetongue virus. J Gen Virol 73, 2425-2428.

Mizukoshi, N., Sakamoto, K., Iwata, A., Tsuchiya, T., Ueda, S., Apiwatnakorn, B., Kamada, M., Fukusho, A., 1993. The complete nucleotide sequence of African horsesickness virus serotype 4 (vaccine strain) segment 4, which encodes the minor core protein VP4. Virus Res 28, 299-306.

Modrof, J., Lymperopoulos, K., Roy, P., 2005. Phosphorylation of bluetongue virus nonstructural protein 2 is essential for formation of viral inclusion bodies. J Virol 79, 10023-10031.

Mohl, B.P., Kerviel, A., Labadie, T., Matsuo, E., Roy, P., 2020. Differential localization of structural and non-structural proteins during the bluetongue virus replication cycle. Viruses 12, 343.

Morelli, M., Ogden, K.M., Patton, J.T., 2015. Silencing the alarms: Innate immune antagonism by rotavirus NSP1 and VP3. Virology 479-480, 75-84.

Moresco, E.M.Y., LaVine, D., Beutler, B., 2011. Toll-like receptors. Curr Biol 21, R488-R493.

Mortola, E., Noad, R., Roy, P., 2004. Bluetongue virus outer capsid proteins are sufficient to trigger apoptosis in mammalian cells. J Virol 78, 2875-2883.

Muzio, M., Mantovani, A., 2000. Toll-like receptors. Microbes Infect 2, 251-255.

Nandi, S., Chanda, S., Bagchi, P., Nayak, M.K., Bhowmick, R., Chawla-Sarkar, M., 2014. MAVS protein is attenuated by rotavirus nonstructural protein 1. PLoS ONE 9, e92126.

Nason, E.L., Rothagel, R., Mukherjee, S.K., Kar, A.K., Forzan, M., Prasad, B.V., Roy, P., 2004. Interactions between the inner and outer capsids of bluetongue virus. J Virol 78, 8059-8067.

Nelemans, T., Kikkert, M., 2019. Viral innate immune evasion and the pathogenesis of emerging RNA virus infections. Viruses 11, 961.

Noad, R., Roy, P., 2003. Virus-like particles as immunogens. Trends Microbiol 11, 438-444.

Nomura-Takigawa, Y., Nagano-Fujii, M., Deng, L., Kitazawa, S., Ishido, S., Sada, K., Hotta, H., 2006. Non-structural protein 4A of Hepatitis C virus accumulates on mitochondria and renders the cells prone to undergoing mitochondria-mediated apoptosis. J Gen Virol 87, 1935-1945.

O'Hara, R.S., Meyer, A.J., Burroughs, J.N., Pullen, L., Martin, L.A., Mertens, P.P., 1998. Development of a mouse model system, coding assignments and identification of the genome segments controlling virulence of African horse sickness virus serotypes 3 and 8. Arch Vir S 14, 259-279.

Oellermann, R.A., 1970. Plaque formation by African horsesickness virus and characterization of its RNA. Onderstepoort J Vet 37, 137-143.

Oellermann, R.A., Els, H.J., Erasmus, B.J., 1970. Characterization of African horsesickness virus. Arch Gesamte Virusforsch 29, 163-174.

OIE, 2011. Terrestrial Animal Health Code. Paris, France: OIE.

Oksayan, S., Wiltzer, L., Rowe, C.L., Blondel, D., Jans, D.A., Moseley, G.W., 2012. A novel nuclear trafficking module regulates the nucleocytoplasmic localization of the rabies virus interferon antagonist, P protein. J Biol Chem 287, 28112-28121.

Osada, N., Kohara, A., Yamaji, T., Hirayama, N., Kasai, F., Sekizuka, T., Kuroda, M., Hanada, K., 2014. The genome landscape of the African green monkey kidney-derived Vero cell line. DNA Res 21, 673-683.

Owens, R.J., Limn, C., Roy, P., 2004. Role of an arbovirus nonstructural protein in cellular pathogenesis and virus release. J Virol 78, 6649-6656.

Ozsolak, F., Milos, P.M., 2011. RNA sequencing: advances, challenges and opportunities. Nat Rev Genet 12, 87-98.

Papa, G., Venditti, L., Arnoldi, F., Schraner, E.M., Potgieter, C., Borodavka, A., Eichwald, C., Burrone, O.R., 2019. Recombinant rotaviruses rescued by reverse genetics reveal the role of NSP5 hyperphosphorylation in the assembly of viral factories. J Virol 94, e01110-01119.

Patel, A., Roy, P., 2014. The molecular biology of Bluetongue virus replication. Virus Res 182, 5-20.

Paulus, C., Krauss, S., Nevels, M., 2006. A human cytomegalovirus antagonist of type I IFN-dependent signal transducer and activator of transcription signaling. Proc Natl Acad Sci USA 103, 3840-3845.

Pink, D.B.S., Schulte, W., Parseghian, M.H., Zijlstra, A., Lewis, J.D., 2012. Real-time visualization and quantitation of vascular permeability *in vivo*: Implications for drug delivery. PLoS ONE 7, e33760.

Potgieter, A.C., Cloete, M., Pretorius, P.J., van Dijk, A.A., 2003. A first full outer capsid protein sequence data-set in the *Orbivirus* genus (family *Reoviridae*): cloning, sequencing, expression and analysis of a complete set of full-length outer capsid VP2 genes of the nine African horsesickness virus serotypes. J Gen Virol 84, 1317-1326.

Potgieter, A.C., Page, N.A., Liebenberg, J., Wright, I.M., Landt, O., van Dijk, A.A., 2009. Improved strategies for sequence-independent amplification and sequencing of viral double-stranded RNA genomes. J Gen Virol 90, 1423-1432.

Potgieter, A.C., Wright, I.M., van Dijk, A.A., 2015. Consensus sequence of 27 African horse sickness virus genomes from viruses collected over a 76-year period (1933 to 2009). Genome Announcements 3, e00921-00915.

Potgieter, A.C., Wright, I.M., Erasmus, B.J., 2017. Inventors; live attenuated African horsesickness virus. *South Africa patent* WO 2016/071850;2017:10-11.

Pourcelot, M., Amaral Moraes, R., Fablet, A., Bréard, E., Sailleau, C., Viarouge, C., Postic, L., Zientara, S., Caignard, G., Vitour, D., 2021. The VP3 protein of bluetongue virus associates with the MAVS complex and interferes with the RIG-I-signaling pathway. Viruses 13, 230.

Prasad, B.V., Yamaguchi, S., Roy, P., 1992. Three-dimensional structure of single-shelled bluetongue virus. J Virol 66, 2135-2142.

Pretorius, A., Faber, F.E., van Kleef, M., 2016. Immune gene expression profiling of PBMC isolated from horses vaccinated with attenuated African horsesickness virus serotype 4. Immunobiology 221, 236-244.

Prins, K.C., Cárdenas, W.B., Basler, C.F., 2009. Ebola virus protein VP35 impairs the function of interferon regulatory factor-activating kinases IKKε and TBK-1. J Virol 83, 3069-3077.

Ramadevi, N., Burroughs, N.J., Mertens, P.P., Jones, I.M., Roy, P., 1998. Capping and methylation of mRNA by purified recombinant VP4 protein of bluetongue virus. Proc Natl Acad Sci USA 95, 13537-13542.

Randall, R.E., Goodbourn, S., 2008. Interferons and viruses: an interplay between induction, signalling, antiviral responses and virus countermeasures. J Gen Virol 89, 1-47.

Rapaport, F., Khanin, R., Liang, Y., Pirun, M., Krek, A., Zumbo, P., Mason, C.E., Socci, N.D., Betel, D., 2013. Comprehensive evaluation of differential gene expression analysis methods for RNA-seq data. Genome Biol 14, R95.

Ratinier, M., Caporale, M., Golder, M., Franzoni, G., Allan, K., Nunes, S.F., Armezzani, A., Bayoumy, A., Rixon, F., Shaw, A., Palmarini, M., 2011. Identification and characterization of a novel non-structural protein of bluetongue virus. PLoS Pathog 7, e1002477.

Ratinier, M., Shaw, A.E., Barry, G., Gu, Q., Di Gialleonardo, L., Janowicz, A., Varela, M., Randall, R.E., Caporale, M., Palmarini, M., 2016. Bluetongue virus NS4 protein is an interferon antagonist and a determinant of virus virulence. J Virol 90, 5427-5439.

Reed, L.J., Muench, H., 1938. A simple method of estimating fifty per cent endpoints. Am J Hyg 27, 493-497.

Riddin, M.A., Venter, G.J., Labuschagne, K., Villet, M.H., 2019. *Culicoides* species as potential vectors of African horse sickness virus in the southern regions of South Africa. Med Vet Entomol 33, 498-511.

Ries, C., Vögtlin, A., Hüssy, D., Jandt, T., Gobet, H., Hilbe, M., Burgener, C., Schweizer, L., Häfliger-Speiser, S., Beer, M., Hoffmann, B., 2021. Putative Novel Atypical BTV Serotype '36' Identified in Small Ruminants in Switzerland. Viruses 13, 721.

Robles, J.A., Qureshi, S.E., Stephen, S.J., Wilson, S.R., Burden, C.J., Taylor, J.M., 2012. Efficient experimental design and analysis strategies for the detection of differential expression using RNA-Sequencing. BMC Genomics 13, 484.

Rojas, J.M., Avia, M., Martín, V., Sevilla, N., 2021. Inhibition of the IFN response by bluetongue virus: The story so far. Front Microbiol 12, 692069.

Rojo, M., Legros, F.d.r., Chateau, D., Lombès, A., 2002. Membrane topology and mitochondrial targeting of mitofusins, ubiquitous mammalian homologs of the transmembrane GTPase Fzo. J Cell Sci 115, 1663-1674.

Röthlisberger, A., Wiener, D., Schweizer, M., Peterhans, E., Zurbriggen, A., Plattet, P., 2010. Two domains of the V protein of virulent canine distemper virus selectively inhibit STAT1 and STAT2 nuclear import. J Virol 84, 6328-6343.

Roy, P., Bishop, D.H., Howard, S., Aitchison, H., Erasmus, B., 1996. Recombinant baculovirus-synthesized African horsesickness virus (AHSV) outer-capsid protein VP2 provides protection against virulent AHSV challenge. J Gen Virol 77, 2053-2057.

Roy, P., 2001. Orbiviruses, In: Fields Virology. D.M. Knipe, P.M. Howley (Eds.), Sixth ed. Lippincott Williams and Wilkins, Philadelphia, pp. 1835-1865.

Roy, P., 2005. Bluetongue virus proteins and particles and their role in virus entry, assembly, and release. Adv Virus Res 64, 69-123.

Roy, P., 2020a. Bluetongue virus assembly and exit pathways. Adv Virus Res 108, 249-273.

Roy, P., 2020b. Highly efficient vaccines for Bluetongue virus and a related Orbivirus based on reverse genetics. Curr Opin Virol 44, 35-41.

Rutkowska, D.A., Meyer, Q.C., Maree, F., Vosloo, W., Fick, W., Huismans, H., 2011. The use of soluble African horse sickness viral protein 7 as an antigen delivery and presentation system. Virus Res 156, 35-48.

Rutkowska, D.A., Mokoena, N.B., Tsekoa, T.L., Dibakwane, V.S., O'Kennedy, M.M., 2019. Plant-produced chimeric virus-like particles - a new generation vaccine against African horse sickness. BMC Vet Res 15, 432.

Samuel, C.E., 2001. Antiviral actions of interferons. Clin Microbiol Rev 14, 778-809.

Santel, A., Fuller, M.T., 2001. Control of mitochondrial morphology by a human mitofusin. J Cell Sci 114, 867-874.

Schade-Weskott, M.L., van Schalkwyk, A., Koekemoer, J.J.O., 2018. A correlation between capsid protein VP2 and the plaque morphology of African horse sickness virus in cell culture. Virus Genes 54, 527-535.

Scherer, M., Klingl, S., Sevvana, M., Otto, V., Schilling, E.M., Stump, J.D., Muller, R., Reuter, N., Sticht, H., Muller, Y.A., Stamminger, T., 2014. Crystal structure of cytomegalovirus IE1 protein reveals targeting of TRIM family member PML via coiled-coil interactions. PLoS Pathog 10, e1004512.

Scherer, M., Otto, V., Stump, J.D., Klingl, S., Muller, R., Reuter, N., Muller, Y.A., Sticht, H., Stamminger, T., 2016. Characterization of recombinant human cytomegaloviruses encoding IE1 mutants L174P and 1-382 reveals that viral targeting of PML bodies perturbs both intrinsic and innate immune responses. J Virol 90, 1190-1205.

Scherer, M., Stamminger, T., 2016. Emerging role of PML nuclear bodies in innate immune signaling. J Virol 90, 5850-5854.

Schmidt, A., Schwerd, T., Hamm, W., Hellmuth, J.C., Cui, S., Wenzel, M., Hoffmann, F.S., Michallet, M.-C., Besch, R., Hopfner, K.-P., Endres, S., Rothenfusser, S., 2009. 5'-triphosphate RNA requires base-paired structures to activate antiviral signaling via RIG-I. Proc Natl Acad Sci USA 106, 12067-12072.

Sekellick, M.J., Marcus, P.I., 1985. Interferon induction by viruses. XIV. Development of interferon inducibility and its inhibition in chick embryo cells "aged" *in vitro*. J Interferon Res 5, 651-667.

Seyednasrollah, F., Laiho, A., Elo, L.L., 2015. Comparison of software packages for detecting differential expression in RNA-seq studies. Brief Bioinform 16, 59-70.

Shaw, A.E., Bruning-Richardson, A., Morrison, E.E., Bond, J., Simpson, J., Ross-Smith, N., Alpar, O., Mertens, P.P., Monaghan, P., 2013. Bluetongue virus infection induces aberrant mitosis in mammalian cells. Virol J 10, 319.

Shu, C., Yi, G., Watts, T., Kao, C.C., Li, P., 2012. Structure of STING bound to cyclic di-GMP reveals the mechanism of cyclic dinucleotide recognition by the immune system. Nat Struct Mol Biol 19, 722-724.

Soneson, C., Delorenzi, M., 2013. A comparison of methods for differential expression analysis of RNA-seq data. BMC Bioinformatics 14, 91.

Soubannier, V., McBride, H.M., 2009. Positioning mitochondrial plasticity within cellular signaling cascades. Biochim Biophys Acta 1793, 154-170.

Stassen, L., Huismans, H., Theron, J., 2012. African horse sickness virus induces apoptosis in cultured mammalian cells. Virus Res 163, 385-389.

Stauber, N., Martinez-Costas, J., Sutton, G., Monastyrskaya, K., Roy, P., 1997. Bluetongue virus VP6 protein binds ATP and exhibits an RNA-dependent ATPase function and a helicase activity that catalyze the unwinding of double-stranded RNA substrates. J Virol 71, 7220-7226.

Stevens, L.M., Moffat, K., Cooke, L., Nomikou, K., Mertens, P.P.C., Jackson, T., Darpel, K.E., 2019. A low-passage insect-cell isolate of bluetongue virus uses a macropinocytosis-like entry pathway to infect natural target cells derived from the bovine host. J Gen Virol 100, 568-582.

Stewart, M., Hardy, A., Barry, G., Pinto, R.M., Caporale, M., Melzi, E., Hughes, J., Taggart, A., Janowicz, A., Varela, M., Ratinier, M., Palmarini, M., 2015. Characterization of a second open reading frame in genome segment 10 of bluetongue virus. J Gen Virol 96, 3280-3293.

Stoltz, M.A., van der Merwe, C.F., Coetzee, J., Huismans, H., 1996. Subcellular localization of the nonstructural protein NS3 of African horsesickness virus. Onderstepoort J Vet 63, 57-61.

Sullivan, E., Lecollinet, S., Kerviel, A., Hue, E., Pronost, S., Beck, C., Dumarest, M., Zientara, S., Roy, P., 2021. Entry-competent-replication-abortive African horse sickness virus strains elicit robust immunity in ponies against all serotypes. Vaccine 39, 3161-3168.

Sun, L., Wu, J., Du, F., Chen, X., Chen, Z.J., 2013. Cyclic GMP-AMP synthase is a cytosolic DNA sensor that activates the type I interferon pathway. Science 339, 786-791.

Sung, P.-Y., Vaughan, R., Rahman, S.K., Yi, G., Kerviel, A., Kao, C.C., Roy, P., Gallagher, T., 2019. The interaction of bluetongue virus VP6 and genomic RNA is essential for genome packaging. J Virol 93, e02023-02018.

Tabachnick, W.J., Day, J.F., 2013. Impact of climate change on vector-borne arboviral episystems, In: Viral Infections and Global Change. S.K. Singh (Ed.). John Wiley & Sons, Inc, Hoboken, NJ, pp. 21-34.

Talon, J., Salvatore, M., O'Neill, R.E., Nakaya, Y., Zheng, H., Muster, T., García-Sastre, A., Palese, P., 2000. Influenza A and B viruses expressing altered NS1 proteins: A vaccine approach. Proc Natl Acad Sci USA 97, 4309-4314.

Thomas, C.P., Booth, T.F., Roy, P., 1990. Synthesis of bluetongue virus-encoded phosphoprotein and formation of inclusion bodies by recombinant baculovirus in insect cells: it binds the single-stranded RNA species. J Gen Virol 71, 2073-2083.

Toh, X., Wang, Y., Rajapakse, M.P., Lee, B., Songkasupa, T., Suwankitwat, N., Kamlangdee, A., Judith Fernandez, C., Huangfu, T., 2021. Use of nanopore sequencing to characterize african horse sickness virus (AHSV) from the African horse sickness outbreak in Thailand in 2020. Transbound Emerg Dis 00, 1-10.

Trevisan, T., Pendin, D., Montagna, A., Bova, S., Ghelli, A.M., Daga, A., 2018. Manipulation of mitochondria dynamics reveals separate roles for form and function in mitochondria distribution. Cell Rep 23, 1742-1753.

Turnbull, P.J., Cormack, S.B., Huismans, H., 1996. Characterization of the gene encoding core protein VP6 of two African horsesickness virus serotypes. J Gen Virol 77, 1421-1423.

Uchida, L., Espada-Murao, L.A., Takamatsu, Y., Okamoto, K., Hayasaka, D., Yu, F., Nabeshima, T., Buerano, C.C., Morita, K., 2014. The dengue virus conceals double-stranded RNA in the intracellular membrane to escape from an interferon response. Sci Rep 4, 7395-7395.

Uitenweerde, J.M., Theron, J., Stoltz, M.A., Huismans, H., 1995. The multimeric nonstructural NS2 proteins of bluetongue virus, African horsesickness virus, and epizootic hemorrhagic disease virus differ in their single-stranded RNA-binding ability. Virology 209, 624-632.

Urakawa, T., Ritter, D.G., Roy, P., 1989. Expression of largest RNA segment and synthesis of VP1 protein of bluetongue virus in insect cells by recombinant baculovirus: association of VP1 protein with RNA polymerase activity. Nucleic Acids Res 17, 7395-7401.

van de Water, S.G., van Gennip, R.G., Potgieter, C.A., Wright, I.M., van Rijn, P.A., 2015. VP2 exchange and NS3/NS3a deletion in African horse sickness virus (AHSV) in development of disabled infectious single animal vaccine candidates for AHSV. J Virol 89, 8764-8772.

van der Meyden, C.H., Erasmus, B.J., Swanepoel, R., Prozesky, O.W., 1992. Encephalitis and chorioretinitis associated with neurotropic African horsesickness virus infection in laboratory workers. Part I. Clinical and neurological observations. S Afr Med J 81, 451-454.

van Gennip, R.G.P., van de Water, S.G.P., Potgieter, C.A., van Rijn, P.A., 2017. Structural protein VP2 of African horse sickness virus is not essential for virus replication *in vitro*. J Virol 91, e01328-01316.

van Rijn, P.A., Maris-Veldhuis, M.A., Potgieter, C.A., van Gennip, R.G.P., 2018. African horse sickness virus (AHSV) with a deletion of 77 amino acids in NS3/NS3a protein is not virulent and a safe promising AHS Disabled Infectious Single Animal (DISA) vaccine platform. Vaccine 36, 1925-1933.

van Rijn, P.A., 2019. Prospects of next-generation vaccines for bluetongue. Front Vet Sci 6, 407.

van Rijn, P.A., Maris-Veldhuis, M.A., Grobler, M., Wright, I.M., Erasmus, B.J., Maartens, L.H., Potgieter, C.A., 2020. Safety and efficacy of inactivated African horse sickness (AHS) vaccine formulated with different adjuvants. Vaccine 38, 7108-7117.

van Staden, V., Huismans, H., 1991. A comparison of the genes which encode non-structural protein NS3 of different orbiviruses. J Gen Virol 72, 1073-1079.

van Staden, V., Theron, J., Greyling, B.J., Huismans, H., Nel, L.H., 1991. A comparison of the nucleotide sequences of cognate NS2 genes of three different orbiviruses. Virology 185, 500-504.

van Staden, V., Stoltz, M.A., Huismans, H., 1995. Expression of nonstructural protein NS3 of African horsesickness virus (AHSV): evidence for a cytotoxic effect of NS3 in insect cells, and characterization of the gene products in AHSV infected Vero cells. Arch Virol 140, 289-306.

Venter, E., van der Merwe, C.F., Buys, A.V., Huismans, H., van Staden, V., 2014. Comparative ultrastructural characterisation of African horse sickness virus-infected mammalian and insect cells reveals novel potential virus release mechanism from insect cells. J Gen Virol 95, 642-651.

Venter, G.J., Graham, S.D., Hamblin, C., 2000. African horse sickness epidemiology: vector competence of South African *Culicoides* species for virus serotypes 3, 5 and 8. Med Vet Entomol 14, 245-250.

Venter, G.J., Koekemoer, J.J., Paweska, J.T., 2006. Investigations on outbreaks of African horse sickness in the surveillance zone in South Africa. Rev Sci Tech OIE 25, 1097-1109.

Verhoef, F.A., Venter, G.J., Weldon, C.W., 2014. Thermal limits of two biting midges, *Culicoides imicola* Kieffer and *C. bolitinos* Meiswinkel (Diptera: Ceratopogonidae). Parasite Vector 7, 384.

Vermaak, E., Conradie, A.M., Maree, F.F., Theron, J., 2016. African horse sickness virus infects BSR cells through macropinocytosis. Virology 497, 217-232.

Verwoerd, D.W., 1969. Purification and characterization of bluetongue virus. Virology 38, 203-212.

Verwoerd, D.W., Louw, H., Oellermann, R.A., 1970. Characterization of bluetongue virus ribonucleic acid. J Virol 5, 1-7.

Verwoerd, D.W., Els, H.J., De Villiers, E.M., Huismans, H., 1972. Structure of the bluetongue virus capsid. J Virol 10, 783-794.

von Teichman, B.F., Dungu, B., Smit, T.K., 2010. *In vivo* cross-protection to African horse sickness serotypes 5 and 9 after vaccination with serotypes 8 and 6. Vaccine 28, 6505-6517.

Vreede, F.T., Huismans, H., 1998. Sequence analysis of the RNA polymerase gene of African horse sickness virus. Arch Virol 143, 413-419.

Weinberg, S.E., Sena, L.A., Chandel, N.S., 2015. Mitochondria in the regulation of innate and adaptive immunity. Immunity 42, 406-417.

Wensvoort, G., Terpstra, C., Boonstra, J., Bloemraad, M., Van Zaane, D., 1986. Production of monoclonal antibodies against swine fever virus and their use in laboratory diagnosis. Vet Microbiol 12, 101-108.

West, A.P., Shadel, G.S., Ghosh, S., 2011. Mitochondria in innate immune responses. Nat Rev Immunol 11, 389-402.

Weyer, C.T., Grewar, J.D., Burger, P., Rossouw, E., Lourens, C., Joone, C., le Grange, M., Coetzee, P., Venter, E., Martin, D.P., MacLachlan, N.J., Guthrie, A.J., 2016. African horse sickness caused by genome reassortment and reversion to virulence of live, attenuated vaccine viruses, South Africa, 2004-2014. Emerg Infect Dis 22, 2087-2096.

Wirblich, C., Bhattacharya, B., Roy, P., 2006. Nonstructural protein 3 of bluetongue virus assists virus release by recruiting ESCRT-I protein Tsg101. J Virol 80, 460-473.

Wisnovsky, S., Lei, Eric K., Jean, Sae R., Kelley, Shana O., 2016. Mitochondrial chemical biology: New probes elucidate the secrets of the powerhouse of the cell. Cell Chem Biol 23, 917-927.

Wohlsein, P., Pohlenz, J.F., Davidson, F.L., Salt, J.S., Hamblin, C., 1997. Immunohistochemical demonstration of African horse sickness viral antigen in formalin-fixed equine tissues. Vet Pathol 34, 568-574.

Wohlsein, P., Pohlenz, J.F., Salt, J.S., Hamblin, C., 1998. Immunohistochemical demonstration of African horse sickness viral antigen in tissues of experimentally infected equines. Arch Vir S 14, 57-65.

Wu, J., Sun, L., Chen, X., Du, F., Shi, H., Chen, C., Chen, Z.J., 2013. Cyclic GMP-AMP is an endogenous second messenger in innate immune signaling by cytosolic DNA. Science 339, 826-830.

Xia, X., Wu, W., Cui, Y., Roy, P., Zhou, Z.H., 2021. Bluetongue virus capsid protein VP5 perforates membranes at low endosomal pH during viral entry. Nat Microbiol 6, 1424-1432.

Xu, G., Wilson, W., Mecham, J., Murphy, K., Zhou, E.M., Tabachnick, W., 1997. VP7: an attachment protein of bluetongue virus for cellular receptors in *Culicoides variipennis*. J Gen Virol 78, 1617-1623.

Yssel, L., 2020. Interaction of African horse sickness virus inclusion bodies with cellular translation machinery to compartmentalise virus protein synthesis, Biochemistry, Genetics and Microbiology. University of Pretoria, pp. 1-95.

Zakaryan, H., Stamminger, T., 2011. Nuclear remodelling during viral infections. Cell Microbiol 13, 806-813.

Zhang, X., Boyce, M., Bhattacharya, B., Zhang, X., Schein, S., Roy, P., Zhou, Z.H., 2010. Bluetongue virus coat protein VP2 contains sialic acid-binding domains, and VP5 resembles enveloped virus fusion proteins. Proc Natl Acad Sci USA 107, 6292-6297.

Zhang, X., Patel, A., Celma, C.C., Yu, X., Roy, P., Zhou, Z.H., 2016. Atomic model of a nonenveloped virus reveals pH sensors for a coordinated process of cell entry. Nat Struct Mol Biol 23, 74-80.

Zhang, Z.H., Jhaveri, D.J., Marshall, V.M., Bauer, D.C., Edson, J., Narayanan, R.K., Robinson, G.J., Lundberg, A.E., Bartlett, P.F., Wray, N.R., Zhao, Q.-Y., 2014. A comparative study of techniques for differential expression analysis on RNA-Seq data. PLoS ONE 9, e103207.

Zientara, S., Sailleau, C., Viarouge, C., Höper, D., Beer, M., Jenckel, M., Hoffmann, B., Romey, A., Bakkali-Kassimi, L., Fablet, A., Vitour, D., Bréard, E., 2014. Novel bluetongue virus in goats, Corsica, France, 2014. Emerg Infect Dis 20, 2123-2125.

Zientara, S., Weyer, C., Lecollinet, S., 2015. African horse sickness. Rev Sci Tech OIE 34, 315-327.

Zwart, L., Potgieter, C.A., Clift, S.J., van Staden, V., 2015. Characterising non-structural protein NS4 of African horse sickness virus. PLoS ONE 10, e0124281.